REGULATION OF FUNCTIONAL CELL SURFACE EXPRESSION BY OLIGOMERIZATION AND N-LINKED GLYCOSYLATION OF MEMBRANE PROTEINS

by

Gina M Whitaker

A THESIS SUBMITTED IN PARTIAL FULFILLMENT OF THE REQUIREMENTS FOR THE DEGREE OF

DOCTOR OF PHILOSOPHY

in

The Faculty of Graduate Studies

(Physiology)

THE UNIVERSITY OF BRITISH COLUMBIA
(Vancouver)

October 2010

ABSTRACT

Oligomerization and N-linked glycosylation are processes thought to be initiated in the ER during translation and act to regulate the trafficking and functional surface expression of many ion channels and G protein-coupled receptors. HCN channels are known to form tetrameric channels from identical subunits as a prerequisite for functional cell surface expression. Different HCN subunits may also co-assemble to form heteromeric channels with unique properties. Using BRET and immunofluorescence analysis, along with electrophysiology, HCN2 and HCN4 were shown to form functional channels with current properties intermediate of those observed when either isoform is expressed. Furthermore, when expressed in equal amounts in CHO cells, HCN2 and HCN4 did not exhibit preference for homo- versus hetero-oligomerization. Many GPCRs are capable of associating as dimers or higher order oligomers. However the functional and physiological relevance of this type of interaction is not uniform for all GPCRs. The ability of both GIP and GLP-1 receptors to form oligomeric complexes was examined using BRET. The resulting saturation curves suggest that GIPR and GLP-1R are capable of forming receptor homomers and heteromers in CHO cells.

The effects of N-linked glycosylation on GPCR trafficking and function are diverse and depend on the receptor studied and whether or not this receptor contains one or more consensus sites for N-glycan binding. Like many family B GPCRs, both the GIP and GLP-1 receptors possess large extracellular N-terminal domains with multiple consensus sites for N-linked glycosylation. Each of these Asn residues was shown to be glycosylated when either human receptor was expressed in CHO cells. Complete removal of N-linked glycosylation severely impaired and completely abolished functional surface expression of GLP-1R and GIPR, respectively. Furthermore, tunicamycin treatment decreased GIPR cell surface number and impaired GIP-potentiated glucose-induced insulin release in an INS-1 pancreatic beta cell line. These results highlight the importance of N-linked glycosylation in regulating the amount of GIPR or GLP-1R at the cell surface.

Overall, these results expand upon the diverse roles of oligomerization and N-linked glycosylation in the regulation of membrane protein functional cell surface expression.

TABLE OF CONTENTS

ABSTRACT ii
TABLE OF CONTENTS iii
LIST OF TABLES vii
LIST OF FIGURES viii
LIST OF ABBREVIATIONS x
ACKNOWLEDGEMENTS xi
DEDICATION xii
CO-AUTHORSHIP STATEMENT xiii
1 INTRODUCTION 1
1.1 Membrane Protein Cell Surface Expression 1
1.1.1 From Translation to Functional Cell Surface Expression 1
1.1.2 Factors that Regulate Membrane Protein Cell Surface Expression 2
1.1.3 Membrane Protein Oligomerization 3
1.1.4 Homomeric and Heteromeric Membrane Protein Complexes 4
1.2 Assembly of Tetrameric Ion Channels 5
1.2.1 Early Evidence for Ion Channel Assembly Comes from Kv Channels 5
1.2.2 Structural Determinants of Kv Channel Assembly 6
1.2.3 Subunit Stoichiometry 7
1.3 HCN Channels 8
1.3.1 Overview of HCN Channel Structure and Function 8
1.3.2 Tissue Expression of HCN Channel Isoforms 9
1.3.3 Physiological Roles of HCN Channels *in vivo* 10
1.3.4 Tetrameric Assembly of HCN Channels 10
1.4 GPCR Structure and Function 13
1.4.1 Different Classes and Functions of GPCRs 13
1.4.2 Structural Organization of GPCRs 14
1.4.3 GPCR Dimerization 15
1.4.4 Dimers or Higher Order Oligomers? 17
1.4.5 The Structure of Rhodopsin as a Model for Other GPCRs 18
1.4.6 Functional Relevance of GPCR Dimerization 18
1.5 Regulation of GPCR Expression and Function by N-Glycosylation 19
1.5.1 Mechanism of N-Glycosylation 19

1.5.2 Differential Roles for N-Glycosylation of GPCRs 21
1.6 GIP and GLP-1 Receptors 22
1.6.1 GIP and GLP-1 Receptor Expression and Function 22
1.6.2 Structural Characteristics of GIPR and GLP-1R 24
1.6.3 Evidence for Formation of GIPR and GLP-1R Homomers and Heteromers. 26
1.6.4 N-glycosylation of GIPR and GLP-1R 27
1.7 Statement of Thesis Objectives and Hypotheses 28
1.8 References 34
2 HCN2 AND HCN4 ISOFORMS SELF-ASSEMBLE AND CO-ASSEMBLE WITH EQUAL PREFERENCE TO FORM FUNCTIONAL PACEMAKER CHANNELS 55
2.1 Introduction 55
2.2 Experimental Procedures 57
2.2.1 Molecular Biology 57
2.2.2 Cell Culture and Expression 58
2.2.3 Whole Cell Patch Clamp Electrophysiology and Analysis 58
2.2.4 Immunocytochemistry, Fluorescence Microscopy with Structured Illumination and Determination of Pearson Correlation Coefficients 59
2.2.5 Bioluminescence Resonance Energy Transfer (BRET) Analysis 60
2.2.6 Immunoprecipitation and Western Blotting of Rat Thalamus 61
2.2.7 Immunohistochemistry 61
2.3 Results 62
2.3.1 Tetrameric Assembly of HCN2 and HCN4 Isoforms 62
2.3.2 Homomeric and Heteromeric Combinations of HCN2 and HCN4 Produce Equally High Pearson Correlation Coefficients in CHO Cells 63
2.3.3 Homomeric and Heteromeric Combinations of HCN2 and HCN4 Produce Equally High BRET Ratios in CHO Cells 65
2.3.4 Functional Evidence for Co-Assembly of HCN2 and HCN4 in CHO Cells 66
2.3.5 Evidence Supporting Co-Assembly of HCN2 and HCN4 in Native Tissue 69
2.4 Discussion 70
2.5 References 79
3 REGULATION OF GIP AND GLP-1 RECEPTOR CELL SURFACE EXPRESSION BY N-LINKED GLYCOSYLATION AND RECEPTOR HETEROMERIZATION 83
3.1 Introduction 83
3.2 Experimental Procedures 84
3.2.1 Molecular Biology 84

3.2.2 Cell Culture and Expression **85**
3.2.3 Tunicamycin Treatment **85**
3.2.4 Cell Surface Biotinylation **86**
3.2.5 Western Blotting **86**
3.2.6 ELISA Assays **86**
3.2.7 TR-FRET cAMP Assays **87**
3.2.8 BRET Assays **87**
3.2.9 Culture of INS-1 Cells **88**
3.2.10 Saturation Binding Analysis in INS-1 Cells **88**
3.2.11 Insulin Release from INS-1 Cells **88**
3.3 Results **89**
3.3.1 Multiple N-Glycosylation Consensus Sites are Present and Utilized on the N-Termini of the Human GIPR and GLP-1R **89**
3.3.2 N-Glycosylation Faciliates Cell Surface Expression of the GIPR more than the GLP-1R **90**
3.3.3 Potency and Efficacy of the cAMP Response of the GIPR and GLP-1R to Their Natural Ligands are Augmented by N-Glycosylation at a Single Site **91**
3.3.4 Function and Cell Surface Expression of a GIPR Mutant Lacking N-Glycosylation is Rescued by Close Association with the Wild Type GLP-1R **92**
3.3.5 N-Glycosylation Maintains Cell Surface GIP Receptor Number and GIP-Potentiated Insulin Secretion in INS-1 Cells **93**
3.4 Discussion **94**
3.5 References **108**
4 CONCLUDING CHAPTER **113**
4.1 Overview **113**
4.2 Variable Stabilities of Membrane Protein Oligomeric Complexes **113**
4.3 Tetrameric Assembly of HCN2 and HCN4 Channels in CHO Cells **115**
4.4 Homomeric and Heteromeric Assembly of HCN2 and HCN4 *In Vivo* **117**
4.5 Functional Relevance of Potential GIPR and GLP-1R Oligomerization **120**
4.6 Regulation of GIPR and GLP-1R Cell Surface Expression by N-Glycosylation. **121**
4.7 Summary **123**
4.8 References **127**
APPENDIX A: HYPERPOLARIZATION-ACTIVATED CYCLIC NUCLEOTIDE-MODULATED 'HCN' CHANNELS CONFER REGULAR AND FASTER RHYTHMICITY TO BEATING MOUSE EMBRYONIC STEM CELLS [3] **130**

APPENDIX B: USING BIOLUMINESCENCE RESONANCE ENERGY TRANSFER TO MEASURE ION CHANNEL ASSEMBLY 147

APPENDIX C: BIOHAZARD APPROVAL CERTIFICATE.....158

LIST OF TABLES

Table 3.1 Mean EC_{50} values and amplitude of responses for cAMP concentration-response curves in figure 3.5 106

Table 3.2 Mean EC_{50} values and amplitude of response for cAMP concentration-response curves in figure 3.6A 107

LIST OF FIGURES

Figure 1.1 Crystal structure of Kv1.2 in complex with its β2 subunit from the side with the extracellular region above (left) or from the extracellular side of the pore (right) 29

Figure 1.2 Cartoon model of HCN channel topology, depicting one of four subunits 30

Figure 1.3 Model for packing arrangement of rhodopsin molecules within paracrystalline arrays of native disc membranes 31

Figure 1.4 Cartoon diagram of the core glycan added to protein nascent chains at their N-glycosylation consensus sequence 32

Figure 1.5 Cartoon depiction of a typical family B GPCR topology 33

Figure 2.1 Tetrameric assembly of Rluc- and GFP-tagged subunits 72

Figure 2.2 Correlation of fluorescent intensities in co-transfected CHO cells support similar levels of self-assembly and co-assembly of HCN2 and HCN4 73

Figure 2.3 BRET ratios support similar levels of self-assembly and co-assembly of HCN2 and HCN4 isoforms in live CHO cells 74

Figure 2.4 HCN4 rescues an HCN2 trafficking mutant to the cell surface and forms functional heteromeric channels 75

Figure 2.5 HCN2 and HCN4 co-immunoprecipitate from the rat thalamus 77

Figure 2.6 HCN2 and HCN4 colocalize within certain regions of the embryonic mouse heart 78

Figure 3.1 Consensus sites for N-glycosylation are found in the N-termini of the closely related human GIPR and GLP-1R 97

Figure 3.2 All putative N- glycosylation sites found on the N-termini of human GIPR and GLP-1R are used 98

Figure 3.3 N-glycosylation more strongly impacts cell surface expression of the GIPR than the GLP-1R 99

Figure 3.4 N-glycosylation increases levels of cell surface isoforms of GIPR and GLP-1R protein 100

Figure 3.5 Potency and efficacy of GIP and GLP-1 effects on cAMP production in CHO cells are enhanced by N-glycosylation of their receptors 101

Figure 3.6 Function but not cell surface expression of N62,77Q-GIPR is rescued by co-expression of wild type GLP-1R 102

Figure 3.7 Cell surface expression of N62,77Q-GIPR is not rescued by co-expression with the wild type GIPR 103

Figure 3.8 BRET values for cells expressing GIPR and GLP-1R suggest heteromeric and homomeric associations..... 104

Figure 3.9 N-glycosylation regulates GIP receptor number and GIP-potentiated insulin secretion in INS-1 cells..... 105

Figure 4.1 Variable stabilities of different membrane complexes..... 126

LIST OF ABBREVIATIONS

AC	Adenylyl Cyclase
β1-AR	Beta 1-Adrenergic Receptor
β2-AR	Beta 2-Adrenergic Receptor
BRET	Bioluminescence Resonance Energy Transfer
CHO	Chinese Hamster Ovary
CNBD	Cyclic Nucleotide Binding Domain
CNG	Cyclic Nucleotide-Gated
COP-II	Coat Protein Complex
D2R	Dopamine-2 Receptor
EGFP	Enhanced Green Fluorescent Protein
ELISA	Enzyme-Linked Immunosorbent Assay
ER	Endoplasmic Reticulum
FRAP	Fluorescence Recovery After Photobleaching
FRET	Fluorescence Resonance Energy Transfer
GFP	Green Fluorescent Protein
GIP(R)	Glucose-dependent Insulinotropic Polypeptide (Receptor)
GLP-1(R)	Glucagon-like Peptide-1 (Receptor)
GPCR	G Protein-Coupled Receptor
HA	Hemagglutinin
HCN	Hyperpolarization-activated Cyclic Nucleotide Modulated
HEK	Human Embryonic Kidney
I_f	Funny Current
KCR1	Potassium Channel Regulator Protein 1
Kir	Inward Rectifying Potassium
Kv	Voltage-Gated Potassium
LH	Leutinizing Hormone
MiRP1	MinK-Related Peptide 1
NT1	Neurotensin 1
PBS	Phosphate-Buffered Saline
PKA	Protein Kinase A
PNGaseF	Peptide: N-Glycosidase F
PVDF	Polyvinylidene Fluoride
RIPA	Radioimmunoprecipitation Assay
RLuc	Renilla Luciferase
SUR	Sulfonylurea Receptor
T2DM	Type-2 Diabetes Mellitus
TM	Transmembrane
VPAC	Vasoactive Intestinal Peptide Receptor

ACKNOWLEDGEMENTS

I would firstly like to thank my senior supervisor, Dr Eric Accili. Your advice, mentorship, encouragement and support have been invaluable to my graduate experience. The way you would get excited over even the simplest western blots gave me the motivation needed to get the work done! I would also like to thank my supervisory committee, Dr Chris McIntosh, Dr Edwin Moore and Dr Glen Tibbits. Thank you for your expert guidance and support along the way. I would also like to thank all of my labmates, who have become like family to me, making this experience so rich and full of great memories.

I would like to thank my parents, Filomena and Ron. You once gave me a quote that said, "Whatever your mind can conceive and believe, it can achieve." Thank you for always believing in me, and championing me through all of my endeavours. You have truly made me feel like I could live up to that quote. Thank you also to my sister Mara, for becoming such a great support and friend over these years.

Finally, to my little family: I would like to thank my daughter, Sofia. Your entry into this world gave me a renewed sense of purpose, and an incredible motivation to complete this thesis. Every time I felt you kick, it would be a pleasant reminder not to procrastinate. Lastly, thank you to the love of my life, Keith. Your encouragement, patience and support over these years have been limitless. You are truly an incredible man and husband and I look up to you and love you more for that.

"Whatever may be your task, work at it heartily, as something done for the Lord and not for men." Colossians 3:23

DEDICATION

To Keith

CO-AUTHORSHIP STATEMENT

- In Chapter 2 of this thesis, I performed all but the electrophysiological experiments to produce the published data shown. The rat thalamic tissue was isolated by J Cooke. H Nazzari assisted me in the mutagenesis and subcloning of various HCN constructs used for BRET assays. D Angoli collected and analyzed all electrophysiological data in figure 2-4. Dr Eric Accili and I collaboratively contributed to the manuscript preparation.
- In Chapter 3 of this thesis, I performed all the experiments, except those performed in INS-1 cells (Figure 3-9). FC Lynn collected and analyzed data as well as constructed the graphs shown in Figure 3-9. C Fulton, an undergraduate honors student assisted me in the collection and analysis of the BRET data in Figure 3-8, under my supervision. Dr Eric Accili and I collaboratively contributed to the manuscript preparation, with assistance and input from Dr CHS McIntosh.
- In Appendix A of this thesis, I performed the experiments required for Figure 3.
- I wrote the book chapter in Appendix B with assistance and editing from Dr Eric Accili, in response to an invitation to write a method-based description of the use of BRET to measure ion channel assembly.

1 INTRODUCTION

1.1 Membrane Protein Cell Surface Expression

1.1.1 From Translation to Functional Cell Surface Expression

As a membrane protein is synthesized, it begins its journey through a cell emerging N-terminus-first from a ribosome located on the cytosolic face of the ER membrane. The nascent peptide chain exits the ribosome, traveling through the Sec 61 translocon complex, which is an aqueous channel bound to the ribosome, and ultimately entering into the ER lumen. Signal sequences located near the N-terminal end of polypeptides are recognized by signal recognition particles, which couple the ribosome to the translocon complex, and ensure targeting of nascent chains to the ER for protein synthesis (Hebert and Molinari, 2007). While in the translocon, hydrophobic regions of the protein begin to be integrated into the membrane. The resultant membrane topology depends on specific amino acid sequences, as well as lipid-protein interactions that occur at this stage (Johnson and van Waes, 1999; McCormick et al., 2003).

As the nascent polypeptide chain enters the ER lumen, it becomes subject to various co-translational modifications such as cleavage of signal sequences, addition of N-linked glycans to consensus sites, disulfide bond formation, phosphorylation, and addition of lipid anchors, with the help of resident ER chaperones and folding enzymes (Hebert and Molinari, 2007). These modifications, along with direct interactions with various resident ER chaperones, all contribute to proper and efficient protein folding. Some membrane-bound proteins, for example many ion channels and G protein-coupled receptors (GPCRs), oligomerize to form both homomeric and/or heteromeric protein complexes, a process that is thought be co-translational thus contributing to proper folding, and will be further discussed shortly. Many proteins also associate with auxiliary subunits or form higher order protein complexes in the ER, which can regulate proper folding and downstream trafficking as well as function. For example, the $GABA_{R1}$ receptor, Gβγ subunit and Kir 3 channel form a signaling complex shortly after protein synthesis, likely in the ER (David et al., 2006).

Association of polypeptide chains with various ER chaperones, namely the family of heat-shock proteins, prevents aggregation, and plays a role in facilitating and maintaining proper folding. ER chaperones also dictate whether or not a protein is fit to traffic out of the

ER or if it is retained for further processing and/or destined for degradation. Unfolded or misfolded proteins are retained in the ER by chaperones and further attempts at proper folding continue. Terminally misfolded proteins are eventually targeted out of the ER for lysosomal degradation (Ellgaard and Helenius, 2003).

The presence of specific motifs located on many membrane proteins act as ER export or retention signals that also regulate trafficking out of the ER. For example, retention signals in both Kir6.2 and SUR subunits of the K_{ATP} channel must be masked in order for ER export and proper functional surface expression to occur (Zerangue et al., 1999). Another example is the Kir2.1 channel isoform, which contains a diacidic motif located on its C-terminus that is essential for ER export, regardless of proper folding and assembly (Ma et al., 2001).

Properly folded and assembled proteins disassociate from ER chaperones and are packaged into COP-II vesicles, likely through direct binding of COP-II components with C-terminal ER export motifs (Barlowe, 2003). From here, they are rapidly transported out of the ER and onto the ER-Golgi intermediate complex for further sorting, then through to the Golgi network.

Once in the Golgi network, membrane proteins undergo further maturation and post-translational processing such as O-glycosylation, and completion of N-linked (N-) glycosylation, an important and sometimes necessary step for proper surface expression of many (but not all) membrane proteins. From the Golgi, mature proteins are sorted into vesicles along with essential transport machinery and continue along the trafficking pathway to the plasma membrane. Defective proteins that have somehow escaped ER quality control may at this point be transported back to the ER or to endosomes for lysosomal degradation (Arvan et al., 2002).

1.1.2 Factors that Regulate Membrane Protein Cell Surface Expression

The array of events that take place within the ER in order to achieve a properly folded and mature functional protein all contribute to the amount of functional protein that is expressed at the cell surface. As discussed, these events include interactions with ER-resident chaperones, as well as co-translational modifications such as N-glycosylation, phosphorylation and disulfide bond formation. Assembly into oligomeric complexes as well as interactions with auxiliary and scaffolding proteins influence both the amount of protein expressed at the cell surface, as well as its functional profile (Deutsch, 2002). Various post-

translational modifications occurring in the ER and Golgi network, such as acetylation, ubiquitination, O-glycosylation, complex N-glycosylation, palmitoylation, and phosphorylation, also regulate functional cell surface expression (Murray et al., 2009). Finally, while at the cell surface, many membrane proteins can be internalized at variable rates and subsequently degraded or recycled back to the plasma membrane, often in a phosphorylation-dependent manner (Pongs, 2009; Tan et al., 2004). The interplay of all these events and interactions occurring during folding and assembly, trafficking (both anterograde and retrograde) and while the protein is expressed at the surface, act to regulate the amount of protein that is expressed at the cell surface at a given time, as well as a protein's functional characteristics.

For the purposes of this thesis, I will elaborate on two specific events that regulate function and surface expression of various membrane proteins. First I will introduce oligomerization of membrane proteins in the sections to follow, with particular relevance to Hyperpolarization-activated Cyclic Nucleotide-modulated (HCN) channels in section 1.2 and then specifically with respect to certain GPCRs in section 1.3. I will also elaborate on N-glycosylation as a potential regulator of functional cell surface expression of GPCRs in section 1.4.

1.1.3 Membrane Protein Oligomerization

Many membrane proteins associate as higher order complexes. For some, this type of association is essential for functional expression, and for others it may act to simply modulate expression and/or functional profiles. Certain ion channels, for example the mammalian voltage-gated potassium channels are composed of four subunits that oligomerize to form a tetrameric channel surrounding an ion-conducting pore (Deutsch, 2002; MacKinnon, 1991). Similarly, most 7-transmembrane receptors are capable of associating as oligomeric complexes, and for some the receptor dimer is considered to be the minimal functional unit. The $GABA_{B1}$ receptor, for example, is composed of R1 and R2 protomers that must dimerize in order to exit the ER and produce a functional receptor at the cell surface (Jones et al., 1998; White et al., 1998). Other 7-transmembrane receptors however are also functional as monomers, despite their ability to dimerize (for examples, see Meyer et al., 2006; Ernst et al., 2007; Whorton et al., 2007).

The dynamic interplay of three factors is thought to favour oligomerization of membrane proteins (Muller et al., 2008). The first is an intrinsic affinity that interacting proteins have for each other, through specific recognition domains. The second is the common dislike of transmembrane proteins for the surrounding aqueous environment, thereby favouring oligomerization. Thirdly, transmembrane protein movement is restricted within the plasma membrane and the organization of specific lipids surrounding them contributes to the affinity of two interacting partners for each other.

For many proteins, the formation of oligomeric complexes is thought to take place in the ER, early in biogenesis and is essential for proper folding and ER export (Bulenger et al., 2005; Deutsch, 2002). This theory has been supported by many studies that have shown the dominant negative effects of mutant ER-retained proteins when coexpressed with their wild type counterparts (reviewed in Milligan, 2007). Evidence for early oligomerization occurring simultaneously with protein folding in the ER comes from biochemical studies performed to characterize Kv channel assembly (Deal et al., 1994; Nagaya and Papazian, 1997; Schulteis et al., 1998; Shen et al., 1993). For some proteins, oligomerization in the ER is essential in order to mask specific retention signals or hydrophobic regions, which would otherwise prevent forward trafficking (Reddy and Corley, 1998). Furthermore, association of transmembrane segments between oligomeric partners is thought to facilitate correct folding in the ER by reducing the exposure of hydrophobic regions and thus preventing aggregation (Muller et al., 2008).

1.1.4 Homomeric and Heteromeric Membrane Protein Complexes

Many membrane proteins have a propensity to form both homomeric and heteromeric complexes. Homomeric proteins are composed of identical associating partners, whereas heteromeric proteins possess structurally similar partners, but the resulting protein displays unique function compared to if each interacting subunit were expressed on its own (Pin et al., 2007). Heteromeric protein formation thus has a potential to greatly increase the diversity of possible phenotypes for a given gene pool, depending on the functional consequences of such an interaction.

When determining the likelihood that two different proteins associate as heteromeric complexes, certain elements must be considered. Firstly, with the exception of gap junctions, the two interacting proteins of interest must be coexpressed in the same tissue. Second, the

temporal location of the expressing partners must coincide such that the two proteins actually meet within the cell at the appropriate time and space for interaction to occur, often within the ER and early on in the biogenic pathway (Panyi and Deutsch, 1996). Finally, interaction affinities, possibly due to structural similarities and/or the presence of specific recognition domains between two interacting partners, will determine the composition of the mature protein complex. For example, specific voltage-gated potassium channels encoded by the HERG gene are composed of HERG 1a and 1b alpha subunits with divergent N-termini. These N-termini specifically interact early in biogenesis to preferentially form heteromeric channels that produce native I_{Kr} *in vivo* (Phartiyal et al., 2007). Whereas expression of the HERG 1a subunit alone produces a homomeric channel with unique functional properties, expression of the 1b subunit yields a trafficking-deficient protein, trapped in the ER due to the presence of an unmasked ER retention motif (Phartiyal et al., 2008). On the other hand and in contrast to the well-studied GABA-B receptor, many other GPCRs that are able to form heterodimers do so with a slightly lower affinity than their corresponding ability to associate as homomeric receptors, as measured largely by saturation resonance energy transfer experiments (reviewed in Milligan and Bouvier, 2005; Milligan, 2007). The exact site(s) of interaction between GPCR protomers however is not clear, and likely not the same for all receptors.

1.2 Assembly of Tetrameric Ion Channels

1.2.1 Early Evidence for Ion Channel Assembly Comes from Kv Channels

In the case of tetrameric ion channels, the first evidence for channel assembly came from early studies in which two Kv channel subunits from the same family, which only differed slightly in sequence but significantly in function were co-expressed and current properties observed (Christie et al., 1990; Isacoff et al., 1990; MacKinnon, 1991; Ruppersberg et al., 1990). In each of these studies, the resulting functional profiles did not reflect a simple mathematical summation of two separate homomeric populations. As such, these channels were proposed to form functional heteromers, and presumably these cells expressed a mixture of homomeric and heteromeric channels.

1.2.2 Structural Determinants of Kv Channel Assembly

Voltage-gated K^+ channels are composed of four alpha subunits which form a central ion-conducting pore. Each subunit contains six transmembrane-spanning domains with intracellular N- and C-termini. This general topology and structure, originally predicted through functional, sequence and hydropathy analysis, has been confirmed and further elucidated through resolution of Kv channel crystal structures (Jiang et al., 2003; Long et al., 2005). Kv channels are classified into eleven subfamilies, named Kv1-Kv11, with multiple isoforms present within each group. Kv1-Kv4 subfamilies have been more widely studied in terms of assembly, and many members within subfamilies Kv5-Kv11 require heteromerization with other subunits in order to functionally express (Ottschytsch et al., 2002).

Kv1-Kv4 members within the same subgroups are able to both self-assemble and co-assemble to form functional channels, owing to the presence of a highly conserved domain that confers specificity of interaction between subunits (Covarrubias et al., 1991; Salkoff et al., 1992; Shen and Pfaffinger, 1995; Xu et al., 1995). Early studies using co-immunoprecipitation and sucrose density gradient analysis determined that a specific region on the N-terminus of a *Shaker*-type Kv channel was primarily responsible for subunit assembly, and was subsequently named the tetramerization- or T1-domain (Li et al., 1992; Shen et al., 1993). This highly conserved domain, located adjacent to the first transmembrane helix, has been identified as a critical site for tetramerization of most Kv channels. The crystal structure of the T1 domain as a tetramer reveals four identical subunits that assemble around a four-fold axis, containing a central pore, with the most highly conserved amino acids located within the core of the domain (Figure 1.1, Kreusch et al., 1998; Liu et al., 2005; Winklmeier et al., 2009). Tetramerization of the T1 domain is facilitated by hydrogen bond and salt bridge formation between 15 polar residues that are conserved within each Kv channel subfamily, thus conferring specificity of interaction between subunits. Studies have directly shown that assembly of subunits at this recognition domain occurs during translation, while the nascent chain is still attached to the ribosome (Kosolapov and Deutsch, 2003; Lu et al., 2001). Interestingly, when the T1 domain is missing, functional channels are still able to form, albeit with much lower efficiency and without specificity of interaction (Tu et al., 1996).

1.2.3 Subunit Stoichiometry

The subunit stoichiometry of mature heteromeric channels, as well as the proportion of homomeric to heteromeric channels formed can vary. Whereas in one extreme, preferential association can yield a strictly homomeric population, random association will on the other hand result in a binomial mixture of homomeric and heteromeric channels with variable stoichiometries (Deutsch, 2003; Hille, 2001; MacKinnon, 1991; Panyi and Deutsch, 1996). The direct measurement of subunit stoichiometry however is difficult, given the limitations of current methodology. Furthermore, variations in relative expression levels of two subunits of interest, as well as their surrounding cellular environment will likely dictate the subunit composition of a given tetrameric protein (Barrera et al., 2007). Nevertheless, subunit stoichiometries for various ion channels expressed in heterologous expression systems have been proposed. CNG channels, for example, preferentially form heterotetramers made up of A and B subunits and are thought to assemble in an 3A:1B stoichiometry. This asymmetric assembly is based on the presence of a C-terminal leucine zipper domain present on A subunits that mediates a trimeric interaction, followed by association with B subunit monomers (Zhong et al., 2002; Zhong et al., 2003). The unique 3:1 tetrameric stoichiometry has been confirmed *in vivo*, from CNG channels of rod photoreceptors (Weitz et al., 2002). A more recent study has used atomic force microscopy to determine that transient receptor potential channels, TRPP2 and TRPC1 associate as heteromers with a 2:2 stoichiometry, in a alternating subunit arrangement, to form functional channels in HEK cells (Kobori et al., 2009). Apart from these two different channels, the mechanism and proportion of homomeric versus heteromeric assembly *in vivo* remains elusive, and is likely unique to the membrane protein and/or cellular context.

In chapter 2 of this thesis, homomeric and heteromeric assembly of HCN channels will be investigated, with particular emphasis on the proportion of homomeric versus heteromeric channels present in Chinese Hamster Ovary (CHO) cells. Moreover, evidence supporting the formation of heteromeric HCN channels *in vivo* will be presented.

1.3 HCN Channels

1.3.1 Overview of HCN Channel Structure and Function

HCN channels are members of the superfamily of voltage-gated cation channels (Yu et al., 2005). They are similar in structure to the mammalian voltage-gated K^+ channels in that they are composed of four subunits that assemble to form a channel with a central ion-conducting pore. Each subunit contains intracellular N- and C-termini and a transmembrane core domain composed of six α-helical segments (S1-S6, Figure 1.2). The first four segments harbour the voltage-sensing domain, and the S5-S6 segment forms a large part of the pore domain with an extracellular pore loop located between S5 and S6 (Wahl-Schott and Biel, 2009). Furthermore, a highly conserved N-glycosylation recognition sequence is located between S5 and the pore loop. A characteristic unique to HCN channels is that they are activated upon membrane hyperpolarization. They are permeable to both Na^+ and K^+ with a ratio of about 1:4, but carry mainly an inward Na^+ current under physiological conditions since the channel is activated at negative potentials, close to the reversal potential of K^+ (Wahl-Schott and Biel, 2009). Furthermore, HCN channels are directly modulated by cAMP, owing to the presence of a cyclic nucleotide-binding domain (CNBD) located in the C-terminal domain. Modulation of these channels by cAMP is reflected by accelerated activation kinetics as well as a shift in their voltage-dependence of activation to more positive potentials (Wainger et al., 2001).

In mammals, there are four HCN channel isoforms, HCN1, HCN2, HCN3 and HCN4, which are variably expressed in numerous tissues. Each isoform is capable of assembling as a homotetramer to form functional channels with distinct characteristics in heterologous expression systems, yet all produce current with biological properties reflective of the native hyperpolarization-activated current, I_h, also known as the funny current, I_f (Moosmang, et al., 2001). Functional differences observed among the isoforms include variable activation kinetics and cAMP-dependent modulation. HCN1 current displays the fastest activation kinetics and activates at the most positive potentials among the isoforms, whereas HCN4-producing current possesses the slowest activation profile and activates at more negative potentials. Compared to both HCN2 and HCN4 current, which are strongly modulated by cAMP, HCN1-producing current displays a weak shift in cAMP-modulated activation and

interestingly, human HCN3 current is unaffected by cAMP, despite the presence of an apparently functional CNBD (Stieber et al., 2005).

1.3.2 Tissue Expression of HCN Channel Isoforms

The discovery and measurement of I_f in the heart in the late 1970s and in neurons in the early 1980s greatly preceded the characterization and cloning of the HCN gene, which did not begin to be elucidated until the late 1990s (Brown et al., 1977; Brown et al., 1979; Yanagihara and Irisawa, 1980; Halliwell and Adams, 1982; Maccaferri et al., 1993; Ludwig et al., 1998; Santoro et al., 1998; Seifert et al., 1999). Since then, all four isoforms of HCN channel protein have been detected throughout the nervous system and heart. Expression levels of individual isoforms however, vary greatly depending on the specific regions, and in some instances depend on the species studied.

All HCN channel isoforms have been detected at variable amounts in different regions of the brain (Abbas et al., 2006; Doan et al., 2004; Moosmang et al., 1999; Notomi and Shigemoto, 2004; Santoro et al., 2000). HCN1 expression is most prominent in the hippocampus, cerebellar cortex, neocortex and brain stem. HCN2 is highly expressed in the olfactory bulb, hippocampus, thalamus and brain stem, and at lower levels throughout most other studied regions of the brain. HCN3 expression can be detected at moderately high levels within the olfactory bulb along with HCN4, which is also abundantly expressed in the thalamus. In the heart, HCN2 and HCN4 are the dominant isoforms and expression is most prominent within the conduction systems (Ludwig et al., 1999). HCN4 is the main isoform expressed in the sinoatrial and atrioventricular nodes as well as the Purkinje fibers, and expression levels of other isoforms within these regions vary depending on the species (Marionneau et al., 2005; Moosmang et al., 2001; Shi et al., 1999). HCN2 is the dominantly-expressed isoform in atrial and ventricular myocytes with the other three isoforms detected at lower levels (Shi et al., 1999; Stillitano et al., 2008).

HCN channel expression has also been detected in other regions of the central nervous system, as well as the peripheral and enteric nervous systems, in pancreatic islet β cells, retina and testis (reviewed in (Biel et al., 2009)). Moreover, HCN2 and HCN3 isoforms are expressed in mouse embryonic stem cells (see appendix A, (Qu et al., 2008)).

Interestingly, HCN isoform expression in certain tissues appears to be dynamically regulated. Activity-dependent changes in isoform expression for example, have been

proposed in hippocampal neurons, thus modulating the properties of I_h in these cells (Santoro and Baram, 2003).

1.3.3 Physiological Roles of HCN Channels *in vivo*

HCN channels are most abundantly expressed in the heart and central nervous system, and their function in these tissues has been widely studied. In various neurons of the brain, I_h plays a role in setting and stabilizing the resting membrane potential (Biel et al., 2009). In CA1 hippocampal and neocortical pyramidal neurons, I_h is involved in regulating the integration of dendritic excitatory post-synaptic potentials (Magee, 1998; Magee, 1999). More recently, I_h has been implicated in the control of spatial working memory by regulating action potential firing in prefrontal cortical neurons (Wang et al., 2007). In the brain, I_h is also involved in motor learning, synaptic transmission and generation of thalamic rhythms (reviewed in Biel et al., 2009).

In the heart, I_h is primarily responsible for regulating rhythmicity. It plays a key role in the generation of rhythmic beating in the sinoatrial node by activation upon hyperpolarization, thus contributing to the diastolic depolarization phase of the action potential (Brown and DiFrancesco, 1980; DiFrancesco, 1991). It is also involved in autonomic regulation of heart rate via direct cAMP modulation of HCN channel function due to adrenergic or muscarinic stimulation (DiFrancesco and Tortora, 1991).

1.3.4 Tetrameric Assembly of HCN Channels

Although it is well known that HCN channels form tetrameric ion channels and that they closely resemble the quaternary structure of Kv channels, their precise mechanisms of assembly are unknown. Preliminary studies have suggested a role for the N-terminus in HCN channel assembly, similar to that of the T1 domains of Kv channels. The N-termini of both HCN1 and HCN2 were shown to directly interact using yeast-two hybrid analysis (in contrast to the C-termini) and removal of the HCN2 N-terminus abolished its trafficking to the cell surface (Proenza et al., 2002). Further sequence analysis of HCN channel N-termini revealed a highly conserved region immediately adjacent to the first transmembrane helix (Tran et al., 2002). Interestingly, this region was necessary for functional expression of HCN2 in CHO cells and was identified as the area of HCN2 N-terminal interaction using yeast two hybrid assays. These data suggest that HCN channels may contain a region similar to the Kv channel

T1 domain that is important for efficient and specific self-assembly and co-assembly of HCN channels.

The similarities in structure and function among HCN channel isoforms, combined with their overlapping patterns of expression throughout the brain and heart form the basis for the hypothesis that HCN channel isoforms are able to coassemble to form functional heteromeric channels *in vivo*. Indeed, when co-expressed in HEK 293 cells, all pairs of HCN isoforms except for HCN2 and HCN3 can be co-immunoprecipitated, suggesting that most combinations of isoforms are structurally capable of some form of physical interaction (Much et al., 2003).

The potential for heteromeric channel assembly *in vivo* is supported by the fact that native hyperpolarization-activated currents measured from both heart and brain possess variable voltage-dependent characteristics and cAMP modulation, and differ from the currents produced by heterologously-expressed homomeric HCN channels (Baruscotti et al., 2005; Santoro and Tibbs, 1999). For example, despite the fact that HCN4 is the most prominent isoform expressed in the SA node, its homomeric channel properties do not completely correlate to those of native I_f. Expression of an HCN4-HCN1 tandem construct in HEK cells, where the N-terminus of HCN1 was fused to the C-terminus of HCN4 indeed led to the formation of a channel with activation kinetics more similar to native I_f in rabbit SA node, than if either HCN1 or HCN4 were individually expressed (Altomare et al., 2003).

There is substantial evidence for the ability of HCN1 and HCN2 to co-assemble to form functional heteromeric channels in heterologous expression systems. Co-expression of HCN1 and HCN2 in *Xenopus* oocytes produces a current that activates with kinetics and voltage dependence intermediate to that resulting from individual subunit expression, but is not a reflection of the linear algebraic sum of individual populations of channels, thus supporting the notion of functional heteromeric assembly of HCN1 and HCN2 (Chen et al., 2001). Furthermore, when expression levels of HCN1 and HCN2 were varied, different current properties ensued, suggesting variable heteromerization depending on the amount of each isoform expressed (Chen et al., 2001). Expression of a concatenated HCN1-HCN2 construct in *Xenopus* oocytes produced currents with activation kinetics intermediate to when HCN1 or HCN2 were expressed alone, yet again not reflecting the mathematical average of the two individual currents (Ulens and Tytgat, 2001). Furthermore, the current properties were similar to those produced when equal amounts of HCN1 and HCN2 were coexpressed.

Together these data suggest that HCN1 and HCN2 can coassemble to form functional heteromeric channels in heterologous expression systems. A non-functional HCN1 pore mutant channel equally suppressed function of both wild type HCN1 and HCN2 in *Xenopus* oocytes, suggesting that HCN1 and HCN2 are able to self-assemble and co-assemble without discrimination between isoforms (Xue et al., 2002). As mentioned earlier, yeast two-hybrid experiments revealed a conserved domain within the N-terminus of HCN1 and HCN2 as the site of direct interaction between subunits and important for assembly of functional channels (Proenza et al., 2002; Tran et al., 2002). Furthermore, functional homomeric or heteromeric channels do not require the presence of the CNBD from all four co-assembling subunits, as shown by functional surface rescue of a CNBD-lacking HCN2 mutant, when coexpressed with either wild type HCN1 or HCN2 (Proenza et al., 2002).

Evidence for co-assembly of HCN1 and HCN2 *in vivo* are supported by the fact that they can be co-immunoprecipitated from mouse brain lysates (Much et al., 2003). Furthermore, hyperpolarization-activated currents measured from mouse globus pallidus neurons that co-express HCN1 and HCN2, displayed activation kinetics reflective of HCN1/2 heteromeric channels (Chan et al., 2004). HCN1 and HCN2 are also thought to form functional heteromeric channels in the rat hippocampus, and seizure-induced increases in co-assembly have been detected by co-immunoprecipitation (Brewster et al., 2005). This increase in heteromeric channel formation is thought to be due to downregulation of HCN1 protein and a corresponding doubling in HCN2/HCN1 expression ratio, increasing the probability that HCN1 will interact with HCN2 (Zha et al., 2008). Interestingly, an increase in the extent of HCN1 N-glycosylation following seizure activity has also been observed, and experimentally blocking N-glycosylation prevented activity-dependent increases in HCN1-HCN2 co-assembly, suggesting that this post-translational modification is important for heteromeric assembly, possibly by enhancing the stability and half-life of HCN1-HCN2 heteromers (Zha et al., 2008).

HCN2 and HCN4 expression overlaps in various regions of the heart and brain (Abbas et al., 2006; Ludwig et al., 1999; Notomi and Shigemoto, 2004). Moreover, single channel recordings of I_f in human atrial myocytes reveal currents with characteristics that resemble a combination of HCN2 and HCN4, suggesting that these two isoforms form functional heteromeric channels *in vivo* (Michels et al., 2005). Co-expression of a nonfunctional HCN2 channel with a mutation within the pore region suppressed HCN4 current in a dominant

negative manner in CHO cells. When this HCN2 channel mutant was expressed in neonatal rat ventricular myocytes, both native I_f density and spontaneous beating were significantly reduced (Er et al., 2003). More recently, HCN2 and HCN4 were co-immunoprecipitated from mouse heart lysates (Ye and Nerbonne, 2009). Further analysis of native HCN2 in these hearts revealed that this isoform undergoes proteolytic cleavage somewhere in the C-terminus. Co-expression of HCN4 with C-terminally-cleaved HCN2 produced currents with activation kinetics more reflective of native I_f than when the wild type isoforms are co-expressed. Together, these data provide evidence for a functional role for HCN2-HCN4 heteromer formation in the heart.

Direct evidence for the formation of functional HCN2-HCN4 heteromers remains elusive, although studies to date have certainly suggested a role for this type of assembly. The relative propensity for homomeric vs. heteromeric HCN channel assembly is also unknown, and as mentioned can be difficult to measure. In chapter 2 of this thesis, further support for the presence of HCN2-HCN4 heteromers in CHO cells and *in vivo* will be shown. Furthermore, novel techniques using both imaging and resonance energy transfer will be used to compare the extent to which HCN2 and HCN4 are able to co-assemble *vs.* self-assemble to form functional channels in CHO Cells.

1.4 GPCR Structure and Function

1.4.1 Different Classes and Functions of GPCRs

Human GPCRs comprise a large superfamily of transmembrane receptors (approximately 800 members) that, through coupling to G proteins, regulate downstream effectors, such as, among others, adenylyl cyclases, phospholipases, protein kinases and ion channels. The five main families within this superfamily, rhodopsin (family A), secretin (family B), glutamate (family C), adhesion, and frizzled/taste2, are grouped based on structural and ligand-binding similarity (Fredriksson et al., 2003; Lagerstrom and Schioth, 2008). The rhodopsin family is by far the largest of the families, containing approximately 670 of the 800 human GPCRs, which can be further divided into four subgroups, α, β, γ and δ.

The two main properties of a receptor are 1) responding to a stimulus, usually by binding a specific ligand and 2) activating intracellular effectors. Upon activation, a GPCR undergoes a conformational change, which renders it capable of productively coupling to a

specific G protein complex. This coupling allows the receptor to catalyze exchange of GDP for GTP, which in turn initiates a number of distinct intracellular signaling cascades. To date, four main classes of heterotrimeric G protein complexes (made up of an α, β and γ subunit) have been identified, based on sequence and functional similarities of the Gα subunits $G\alpha_s$, $G\alpha_i$, $G\alpha_q$ and $G\alpha_{12}$. The exact G protein complex that a receptor is able to bind to governs which signaling cascade is initiated. For example, the well-studied β_1-adrenergic receptor couples to $G\alpha_s$, which in turn stimulates adenylyl cyclase, thereby increasing intracellular cAMP, which then activates PKA. On the other hand, the M2-muscarinic receptor couples to $G\alpha_i$, resulting in adenylyl cyclase inhibition and thus an opposite response to the β_1-adrenergic receptor.

1.4.2 Structural Organization of GPCRs

There are two main characteristics common among all GPCRs. The first is that they consist of seven transmembrane-spanning domains with an extracellular N-terminus and an intracellular C-terminus. This general architecture was first confirmed from studies of two-dimensional crystals of rhodopsin (Krebs et al., 1998; Schertler et al., 1993). The second is that they are able to bind to specific heterotrimeric G protein complexes in order to initiate a signal transduction cascade within the cell. Additionally, most mammalian GPCRs are thought to contain sites on their extracellular regions for N-glycosylation, and many possess modulatory phosphorylation sites on their C-termini.

Until recently, little has been known regarding the structural biology of GPCRs, with only the crystal structure of the inactive state of rhodopsin resolved (Palczewski et al., 2000; Fotiadis et al., 2003; Liang et al., 2003). However, over the past few years, the structures for human β2-AR (Rasmussen et al., 2007), avian β1-AR (Warne et al., 2008), and human A2 adenosine receptor (Jaakola et al., 2008) have been obtained. These results have revealed that all four proteins of known 3D structure have relatively similar architecture, at least in their inactive states, with key differences in their extracellular loops and ligand binding regions, as well as some variation in transmembrane structure (Lagerstrom and Schioth, 2008; Rosenbaum et al., 2009). Although all crystal structures solved to date are from the rhodopsin family of GPCRs, these results have been used to infer structure of other families. Furthermore, ligand-bound extracellular domains of GPCRs from other families have been solved, for example for the Glucagon-Like Peptide-1 (GLP-1) and Glucose-dependent

Insulinotropic Polypeptide (GIP) receptors, which are both members of the secretin family (Parthier et al., 2007; Runge et al., 2008).

1.4.3 GPCR Dimerization

Although GPCRs were traditionally thought to function as monomeric entities, complexing in a 1:1 ratio with G proteins, more recent evidence over the past twenty years has challenged this view (White et al., 1998; Jones et al., 1998; Kunishima et al., 2000). Various studies have shown that many, if not all GPCRs are capable of self-assembling as homomeric complexes. In addition, multiple reports have proposed the existence of heteromeric receptors. At this point, the ability for dimer formation (both homomeric and heteromeric) is generally well accepted. The debates however currently surround the location in the cell that dimer formation is initiated, whether the interaction is stable and constitutive or transient, and universal among all GPCRs, and the role of dimerization in optimal receptor function *in vivo*.

Early evidence for dimerization came from studies using receptor crosslinking, photo-affinity labeling and co-immunoprecipitation to show physical interactions between differently tagged versions of the same wild type receptors, as well as trans-complementation studies co-expressing either chimeric or mutant receptor partners (reviewed in (Bouvier, 2001)). Consistent with these data were studies, for example with the V2 vasopressin receptor as well as the β_2-adrenergic receptor, in which receptor trafficking mutants acted in a dominant negative manner when coexpressed with their cognate wild type receptor (Salahpour et al., 2004; Zhu and Wess, 1998). These latter results also suggested that dimer formation occurs prior to trafficking to the cell surface. Subsequently, numerous studies have reported that GPCR homodimerization likely occurs during biosynthesis, prior to ER export (Issafras et al., 2002; Terrillon et al., 2003; Salahpour et al., 2004; Guan et al., 2009).

Some of the earliest, most convincing evidence for heteromeric complex formation, comes from studies on the two isoforms of the metabotropic $GABA_B$ receptor (GBR1 and GBR2) (Jones et al., 1998; Kaupmann et al., 1998; Kuner et al., 1999; Ng et al., 1999; White et al., 1998). When expressed alone, GBR1 is retained in the ER as immature protein and unable to traffic to the cell surface. On the other hand, when GBR2 is expressed alone, it can traffic to the surface, but is unable to bind GABA and induce intracellular signaling. However, when the two are co-expressed, both isoforms are found at the cell surface as

mature proteins and function is restored. Further studies have revealed that the mechanism for the rescue of trafficking is through a direct interaction between GBR1 and GBR2, which masks an ER retention motif on the C-terminus of GBR1 (Margeta-Mitrovic et al., 2000). Overall, these studies suggest that receptor homodimerization, and at least for the $GABA_B$ receptor, heterodimerization, may be a prerequisite for proper protein folding, trafficking and function for some receptors.

The emergence of Bioluminescence Resonance Energy Transfer (BRET) as a novel technique for measuring receptor assembly provided researchers with a superior method of measuring receptor self-assembly and co-assembly, compared to the more invasive biochemical techniques used in the past. BRET assays were originally developed as an alternative to FRET, for use in detecting interactions between circadian clock proteins (Xu et al., 1999). This new method incorporates the use of a bioluminescent donor molecule, luciferase, as an alternative to the traditional fluorescent donor protein used in FRET, thus eliminating technical issues with photobleaching. Later, BRET was adapted for use in mearuring interactions between 7-transmembrane receptors, and has since become a primary tool in detecting homomeric and heteromeric interactions of GPCRs (Angers, et al., 2000). BRET assays are performed on live, intact cells, measuring protein-protein interactions in the context of a cellular environment (reviewed in Gandia et al., 2008b). BRET, like FRET is capable of detecting an interaction distance within no more than 100Å, making it a more sensitive technique for measuring receptor-receptor interactions. Furthermore, this technique is relatively high throughput, thus enabling researchers to test a wide variety of interaction partners (for more information regarding BRET methodology, see Appendix B). Thus, the establishment of this technique has greatly increased the number of reports of GPCR homo- and hetero-dimerization in heterologous expression systems.

Despite growing evidence that GPCRs exist primarily as dimeric entities at the cell surface, some studies have confirmed that receptor monomers are indeed functional, and capable of coupling to G proteins and producing efficient signal transduction (Ernst et al., 2007; Kuszak et al., 2009; Whorton et al., 2007; Whorton et al., 2008). On the other hand, studies on both the dopamine D2 receptor as well as the leukotriene B4-receptor have shown that the minimal functional unit consists of two protomers and one G protein. Interestingly, in both these cases, only one protomer of the GPCR dimer is activated by its agonist to transmit a signal, resulting in what has been termed, an “asymmetrical activated dimer” (Damian et al.,

2006; Han et al., 2009). Furthermore, studies on the metabotropic glutamate receptor showed that both protomers of a receptor dimer must be activated in order to optimally couple to a G protein complex, providing support for a dimer being the required functional unit.

The most direct evidence for oligomerization of GPCRs *in vivo* comes from a recent study using knock-in mice expressing two different mutant LH receptors; one that can signal but not bind LH, and one that can bind LH but not signal. For either case, the mice displayed highly regressed reproductive tracts, however when the two knock-in strains were crossed, reproductive activity was restored (Rivero-Muller et al., 2010). This study has elegantly shown an example where receptor oligomerization can affect function through transactivation, *in vivo*. However, the question still remains as to whether a monomeric or dimeric/oligomeric form is preferential *in vivo*, and whether or not oligomerization is universal among all GPCRs. From the evidence presented above, it seems that the mechanism is not likely the same for all GPCRs (Gurevich and Gurevich, 2008a).

1.4.4 Dimers or Higher Order Oligomers?

Thus far, when discussing receptor self- and co-assembly, the term dimer is used, which traditionally has been chosen since it is the simplest form of oligomer that can explain the numerous observations to date. However, many studies have also provided evidence for dimerization rather than the formation of higher order oligomers (Goin and Nathanson, 2006; Harikumar et al., 2008; Maurel et al., 2008). For example, one study modeled BRET saturation curves using an equation that predicts the probability of a receptor forming dimeric versus higher order oligomeric complexes (Mercier et al., 2002). They found that homomeric β_2-adrenergic receptors produced a BRET saturation curve that was best described by the formation of dimers. Furthermore, a study using the leukotriene B4 receptor has shown that the stoichiometry of receptor to G protein is likely 2:1 (Baneres and Parello, 2003). However, certain studies have also described a potential for the formation of higher-order oligomeric complexes (Fung et al., 2009; Gandia et al., 2008a; Guo et al., 2008; Maurel et al., 2008; Vidi et al., 2008). Nevertheless, these studies do not discount a potential for dimeric receptor clustering at the plasma membrane, which could resemble and/or behave as a higher order oligomer (Franco et al., 2003). Recent evidence from FRAP and higher resolution FRET studies has however provided convincing results suggesting that the $ß_2$-AR exists as a higher order oligomer (Dorsch et al., 2009; Fung et al., 2009).

1.4.5 The Structure of Rhodopsin as a Model for Other GPCRs

The rhodopsin receptor was the first of only a few GPCRs crystallized to date (Palczewski et al., 2000). As such, it has served as a homology model for structure prediction of other GPCRs. It has proved to be a good model, at least in comparison to the β_1 and β_2 adrenergic and adenosine 2A receptors, which are the only other receptors of known crystal structure (reviewed in Rosenbaum et al., 2009). These four proteins display a similar overall architecture, with the most significant differences present in their helical packing interactions.

The native oligomeric structure of rhodopsin has been determined through atomic force microscopy, revealing a model in which rhodopsin exists as both dimers and higher-order oligomers (Figure 1.3, Fotiadis et al., 2003; Liang et al., 2003). Intradimeric interactions occur between TM4 and TM5, and contacts between TM1 and TM2 and between third intracellular loops connect dimers to form large paracrystalline arrays. Thus, dimers are thought to potentially exist as the building blocks for higher-order oligomeric structures (Fotiadis et al., 2006). The existence of both dimers and oligomers, even at a low density of rhodopsin expression, has been confirmed using luminescence resonance energy transfer and fluorescence resonance energy transfer methods (Mansoor et al., 2006). Despite these results, rhodopsin is in fact functional as a monomer, and interacts with transducin in a 1:1 ratio (Hofmann et al., 2009). Furthermore, rhodopsin oligomers couple less efficiently to G proteins than monomers (Bayburt et al., 2007). However, when rhodopsin was solubilized with various detergents, resulting in different preparations of monomers, dimers and higher order oligomers, the latter group was most effective in activating transducin (Jastrzebska et al., 2006). Thus the existence of both monomers and higher order oligomers in vivo is a possibility, however the exact role of each and the proportion of monomers and oligomers is not clear. Given the structural similarities between rhodopsin and other GPCRs, the general information on the structure and function of rhodopsin can provide insight into oligomerization of other GPCRs (Lau et al., 2007).

1.4.6 Functional Relevance of GPCR Dimerization

Substantial literature has reported that GPCR dimers are not a result of a transient interaction, but form as constitutive complexes early in biogenesis, thus proposing a role for dimer formation in receptor folding, maturation and trafficking to the cell surface (Bulenger

et al., 2005; Terrillon and Bouvier, 2004). This has primarily been shown through the dominant negative effects of trafficking-deficient GPCR mutants, by addition of ER retention sequences to one protomer to induce retention on its putative partner, and more recently through the use of pharmacological chaperones as cell-surface rescue agents of dimerization-impaired receptor mutants (Brothers et al., 2004; Calebiro et al., 2005; Canals et al., 2009; Salahpour et al., 2004).

The relevance of homo- and heteromerization to receptor function has been an area of intense research, some of which has suggested that dimerization provides the most appropriate structural framework for G protein binding, thereby optimizing the efficiency of signal transduction (Fotiadis et al., 2006). As described earlier, the $GABA_B$ receptor clearly requires assembly as a heterodimer as its basic functional unit. Similarly, although agonist binding to only one protomer of the mGluR5 homodimer induces the active state of the receptor, binding to both protomers is required for full activity (Kniazeff et al., 2004). Several reports have proposed functional roles for receptor oligomers in receptor internalization, cross-inhibition, positive and negative cooperativity in ligand binding, as well as modulation of signaling activity (reviewed in (Han et al., 2009; Milligan, 2009; Szidonya et al., 2008)). Convincing evidence for the presence of heteromeric receptors *in vivo* comes from a study showing that the tissue specific analgesic, 6'-guanidinonaltrindole, selectively targets the δ-κ opioid receptor heteromer (Waldhoer et al., 2005). Furthermore, the response elicited by this ligand differs from that observed when either opioid receptor type is expressed alone.

In chapter 3 of this thesis, the ability for the GIP and GLP-1 receptors to form both homomeric and heteromeric receptors will be investigated using BRET and functional rescue experiments.

1.5 Regulation of GPCR Expression and Function by N-Glycosylation

1.5.1 Mechanism of N-Glycosylation

The vast majority of membrane proteins exist as glycoproteins in their mature state, as a result of N-glycosylation, which is a covalent modification that is initiated in the ER during translation. When a nascent polypeptide chain enters the ER lumen through the Sec61 translocon complex, its sequence is scanned by oligosaccharyltransferase (OST). OST recognizes asparagines (N) that are located within a specific consensus motif, NXS/T, where

X cannot be Proline (Shakin-Eshleman et al., 1996). Once the motif is found, OST covalently modifies the asparagines by addition of a pre-assembled core glycan tree, consisting of 2 N-acetylglucosamine, 9 mannose and 3 glucose residues (Figure 1.4). This "core-glycosylated" peptide undergoes sequential cleavage of the outermost 2 glucose residues, which is a prerequisite for subsequent association of the peptide with ER chaperones, including calnexin, calreticulin and other folding substrates. Once proper protein folding is complete, the third glucose residue is removed from the core-glycan, and the protein is released from the ER. The membrane-bound protein is then transported in a vesicle to the Golgi network, where additional modifications may occur, including removal of mannose residues, followed by the addition of more complex oligosaccharides. In contrast to core-glycosylation, which is a homogeneous process, the extent of complex glycosylation that occurs in the Golgi, including sugar composition as well as the number and size of branches in the oligosaccharide tree, varies greatly depending on protein, species, and cell type (Dennis et al., 2009).

The number of NXS/T consensus motifs found on a protein varies depending on the protein itself, as well as the species. The one commonality however, is that all consensus motifs are located on extracellular regions of transmembrane proteins. It is thought that approximately 90% of consensus motifs are in fact glycosylated, however differences in the efficiency of recognition of individual sites by OST allows for the presence of variably glycosylated products at the cell surface (Allen et al., 1995; Gavel and von Heijne, 1990; Petrescu et al., 2004).

Of the many proposed functions of N-glycosylation, one of its roles in the early secretory pathway, aside from enabling newly synthesized glycoproteins to interact with ER chaperones, is to facilitate the folding and assembly of a polypeptide. This likely occurs by increasing the hydrophilicity of a polypeptide, thereby reducing the potential for aggregation, and increasing the solubility of folding intermediates (Helenius, 1994). Other proposed functions of N-glycans include targeting proteins to correct cellular compartments such as the plasma membrane; facilitating oligomerization and other protein-protein interactions; increasing protein stability and solubility; and modifying a protein's charge and isoelectric point, all of which can impact a protein's ability to correctly function at the cell surface (Cohen, 2006; Mitra et al., 2006). Moreover, the impact of N-glycosylation on protein function is highlighted by studies, which reveal severe phenotypes when glycosylation is impaired (Ohtsubo and Marth, 2006).

Despite the proposed role of N-glycosylation in the expression and function of a properly folded protein, it is important to note that not all proteins are equally dependent on this process. Whereas the abolishment of N-glycosylation can result in a complete misfolding of many proteins, rendering them non-functional and targeting them for degradation, some proteins may only suffer a partial loss in secretion efficiency and/or function, while others may be entirely unaffected (Helenius and Aebi, 2004; Trombetta, 2003).

1.5.2 Differential Roles for N-Glycosylation of GPCRs

Of all known post-translational modifications occurring for GPCRs, N-glycosylation is the most common. It has been shown to play a role in both the cell surface expression profiles and function of many GPCRs. However, the exact role of N-glycosylation as well as the extent of modulation is not the same for all GPCRs.

The impact of N-glycosylation on cell surface expression has been studied for a diversity of GPCRs. For some, a certain amount of N-glycosylation is required for minimal cell surface expression. For example, of the four consensus N-glycosylation sites found in the human VPAC1 receptor, three are glycosylated, and mutation of two of these three sites abolishes receptor expression at the cell surface, causing retention in the ER due to misfolding of the mutant receptor (Couvineau et al., 1996; Langer et al., 2008). Similarly, the AT-1a angiotensin II, D5 dopamine and follicle stimulating hormone receptors are all retained in intracellular compartments when N-glycosylation is removed (Davis et al., 1995; Deslauriers et al., 1999; Karpa et al., 1999). In contrast, mutation of all putative N-glycosylation sites in the M2 muscarinic, type 1α metabotropic glutamate, α_1-adrenergic, and H2 histamine receptors produced no visible effects on cell surface expression (Fukushima et al., 1995; Mody et al., 1999; Sawutz et al., 1987; van Koppen and Nathanson, 1990). Many other receptors that have been studied fit somewhere in between these two extremes, where N-glycosylation seems to facilitate, but not be absolutely required for receptor cell surface expression. For example, the β_2-AR displayed a reduction in cell surface expression without any direct impact on receptor function when N-glycosylation was impaired (Rands et al., 1990).

For some (but not all) receptors that are able to at least partly express at the cell surface after removal of N-glycosylation, their function is impaired. Observed changes in ligand binding affinities, ligand potency, G protein coupling efficiency, as well as coupling to

downstream effectors have been linked to removal of N-glycosylation in certain receptors (Benya et al., 2000; Michineau et al., 2004; Mody et al., 1999; Pang et al., 1999; Roy et al., 2010; Zhong et al., 2004). Furthermore, altered membrane receptor stability and turnover rates have been noted for glycosylation-deficient human δ and κ opioid receptors (Li et al., 2007; Markkanen and Petaja-Repo, 2008).

The binding of newly synthesized glycoproteins to chaperones in the ER is thought to promote not only correct folding, but also oligomerization of some proteins. Thus, removal of N-glycosylation may impair normal protein oligomerization since certain chaperones would no longer be able to bind the protein of interest. Indeed, studies examining nicotinic acetylcholine receptors have reported that removal of N-glycosylation impairs subunit assembly and thus formation of functional complexes (Wanamaker and Green, 2005). Similarly, N-glycosylation has been shown to regulate dimerization of the epidermal growth factor receptor, as well as the bradykinin B2 and β_1-adrenergic receptors (Fernandes et al., 2001; He et al., 2002; Michineau et al., 2006). This however is not likely the case for all GPCRs, since many receptors that are known to dimerize are still able to assemble and traffic to the cell surface when glycosylation is impaired. For example, β1-/α2a- adrenergic receptor heterodimerization is enhanced when N-glycosylation of the β1-adrenergic receptor is inhibited (Xu et al., 2003).

1.6 GIP and GLP-1 Receptors

1.6.1 GIP and GLP-1 Receptor Expression and Function

Both the Glucose-dependent Insulinotropic Polypeptide receptor (GIPR) and the Glucagon-Like Peptide-1 receptor (GLP-1R) belong to the family B subgroup of GPCRs. Sequence and structural similarities within this subgroup include the presence of a large extracellular N-terminus preceded by a short signal peptide that is required for insertion into the ER during translation. Family B receptors also possess three highly conserved disulfide bonds located on the N-termini that act to stabilize the secondary structure and are likely important for ligand binding (Figure 1.5) (Bazarsuren et al., 2002; Lisenbee et al., 2005). The human GIP and GLP-1 receptors contain 466 and 463 amino acids, respectively, and share approximately 40% sequence identity. Each receptor binds a specific ligand (GIP binds to the

GIPR and GLP-1 binds to the GLP-1R), which are structurally-similar peptide hormones released from intestinal cells in response to food ingestion.

GIPR was first cloned from a rat cerebral cortex cDNA library and is expressed in pancreatic islets, adipose tissue, stomach, small intestine, heart, bone, lung, adrenal cortex (low levels), pituitary, vascular endothelial cells and throughout the brain (Bollag et al., 2000; Usdin et al., 1993; Yip et al., 1998). Numerous studies have revealed the existence of tissue and species-specific GIPR mRNA splice variants, with the pancreatic form being the only variant studied in depth (McIntosh et al., 2009). GLP-1R was originally cloned from a rat pancreatic islet cDNA library (Thorens, 1992). In humans and rodents, only one structurally identical form of GLP-1R has been identified to date (Wei and Mojsov, 1995). This form is widely expressed in pancreatic islets, lung, stomach, GI tract, heart, kidney and throughout the brain (Bullock et al., 1996; Campos et al., 1994; Dunphy et al., 1998). GLP-1R mRNA has also been detected in canine adipose tissue and muscle, however evidence for expression in these tissues in humans or rodents is weak (Sandhu et al., 1999).

The hormones, GIP and GLP-1 are secreted from intestinal endocrine cells into the blood, in response to nutrient ingestion, and bind GIPR and GLP-1R, respectively. On pancreatic β cells, for example, GIP or GLP-1 ligand binding to their respective receptors initiates a wide array of intracellular events, which ultimately contribute to insulin synthesis and release, glucose metabolism, as well as β-cell proliferation and inhibition of apoptosis (Baggio and Drucker, 2007; Doyle and Egan, 2007; McIntosh et al., 2009). In addition to their actions on the pancreas, these hormones have also been shown to act on other tissues such as the brain, heart, adipose tissue, bone, stomach and liver (Baggio and Drucker, 2007).

Of all targeted cells, the contribution of GIPR and GLP-1R activation to insulin release in pancreatic β cells has been studied in most depth due to 1) their critical involvement in maintaining appropriate blood glucose levels and 2) their potential as drug targets for type-2 diabetes mellitus. Indeed, GLP-1R activation has been used as a clinical therapy for T2DM since 2005. When activated, GIPR and GLP-1R act to enhance glucose-stimulated insulin release and this effect is responsible for approximately 50% of postprandial insulin release (Elrick et al., 1964). The insulinotropic effect of receptor activation in rodents is dependent on a threshold extracellular glucose concentration of approximately 4mM (Jia et al., 1995). The intracellular events that take place in order for this to occur are generally well understood. Both receptors couple to and activate $G\alpha_s$ proteins as a result of ligand binding,

which causes AC stimulation, thereby increasing local cAMP concentration and subsequent activation of PKA and exchange protein directly activated by cAMP (EPAC) among other downstream effectors (Ahrèn, 2009; Baggio and Drucker, 2007). Increases in cAMP as well as PKA activation facilitate membrane depolarization by modulation of ion channels and increasing mitochondrial ATP synthesis and intracellular [Ca^{2+}], as well as directly targeting the exocytotic machinery, altogether contributing to exocytosis of insulin granules (Lu et al., 1993; McIntosh et al., 2009). It should be noted that the GLP-1R can also couple to $G\alpha_q$ and $G\alpha_i$, leading to activation of other effectors, such as phospholipase C (Hallbrink et al., 2001; Montrose-Rafizadeh et al., 1999; Wheeler et al., 1993).

Studies of individual and double GIPR and GLP-1R receptor knockout mice yield further insight into the physiological significance of these receptors in contributing to glucose-dependent insulin release. GIPR-/- mice display glucose intolerance due to impaired glucose-stimulated insulin secretion after oral glucose ingestion, however the observed effects are mild, which has been explained by compensatory mechanisms such as enhanced GLP-1 sensitivity (Miyawaki et al., 1999; Pamir et al., 2003). GLP-1R-/- mice are mildly hyperglycemic in the fasting state and also exhibit impaired glucose-stimulated insulin secretion, but display enhanced GIP secretion and action, again suggesting compensatory β-cell responses to GIP (Pederson et al., 1998; Scrocchi et al., 1996). Double receptor knockout mice exhibit a further impairment in glucose-induced insulin secretion following glucose ingestion with higher glycemic excursion profiles and decreased levels of circulating insulin, compared to single incretin receptor knockouts (Hansotia et al., 2004).

1.6.2 Structural Characteristics of GIPR and GLP-1R

When a ligand binds to its cognate receptor, it induces a conformational change in the receptor, which enables efficient coupling to specific G proteins. The N-termini, as well as specific regions of extracellular loops and transmembrane domains of GIPR and GLP-1R are essential for ligand binding. GIPR-GLP-1R chimeric studies showed that the N-terminus of the GIPR is responsible for ligand binding and the TM1 domain is important for receptor activation (Gelling et al., 1997). Both denaturation of GLP-1R and the production of glucagon-N-terminal chimeras abolished GLP-1R affinity for native GLP-1 (Bazarsuren et al., 2002; Wilmen et al., 1996). The presence of charged residues in EC1, TM2 and TM4 are also important for GLP-1 binding (Al-Sabah and Donnelly, 2003; Xiao et al., 2000).

Resolution of the crystal structures of the N-termini of both GIPR and GLP-1R in complex with their respective ligands showed the C-terminal end of the ligand binds in an alpha-helical conformation to surface grooves within the N-terminus, and the N-terminus of the ligand is free to bind to other regions of the receptor (Parthier et al., 2007; Runge et al., 2008; Underwood et al., 2010). From these and other studies examining ligand binding of similar receptors, a general "two-domain model" of hormone binding has been proposed for family B GPCRs (Hoare, 2005; Parthier et al., 2009). In this model, the C-terminal end of the ligand complexes with the N-terminus of the receptor, thus promoting interaction of the N-terminal portion of the ligand with the extracellular loops and transmembrane domains of the receptor. This latter interaction induces a conformational change that enables the receptor to couple to and activate its G protein complex.

The exact residues involved in G protein and AC coupling to both the GIPR and GLP-1R remain to be elucidated. For many GPCRs, the 3rd intracellular loop (IL3) is a critical region for G protein coupling. Mutation of specific residues in the IC3 of the GLP-1R produces significant decreases in cAMP production while maintaining GLP-1 affinity for the receptor (Mathi et al., 1997; Salapatek et al., 1999; Takhar et al., 1996). Additionally, it is thought that distinct domains within the GLP-1R IC3 directly couple to specific G proteins (Hallbrink et al., 2001; Montrose-Rafizadeh et al., 1999). The majority of the C-terminus of the GIPR is not needed for intracellular signaling since a mutant with the distal 50 amino acids removed was able to produce GIP-induced cAMP increases. However, a minimum receptor length of 405 amino acids was needed for proper membrane insertion and cell surface expression of GIPR (Wheeler et al., 1999).

Upon stimulation, both the GIPR and GLP-1R undergo desensitization and internalization, and specific residues located on their C-termini are involved in regulating these processes. Specific cysteine and serine residues located on the GIPR C-terminus are important for homologous receptor desensitization and internalization (Tseng and Zhang, 1998a; Tseng and Zhang, 2000; Wheeler et al., 1999). Furthermore, RGS2, GRK2 and β-arrestin-1 have all been implicated in GIP-induced receptor desensitization (Tseng and Zhang, 1998b; Tseng and Zhang, 2000). GLP-1R undergoes homologous desensitization and internalization upon phosphorylation of three serine doublets on the C-terminus (Widmann et al., 1997). Heterologous desensitization has been observed by PKA phosphorylation of four key serine doublets on the C-terminus (Widmann et al., 1996b). Moreover, the GLP-1R

internalizes via a clathrin-coated pit-dependent mechanism and the recognition sequence for this is thought to be located in the C-terminus, since C-terminal truncations impair internalization rates (Vazquez et al., 2005; Widmann et al., 1997).

1.6.3 Evidence for Formation of GIPR and GLP-1R Homomers and Heteromers

Although GPCR oligomerization has been most extensively studied for family A receptors, several family B GPCRs have been shown to form homomeric receptors, using either BRET and/or morphological FRET assays. These include the secretin receptor (Harikumar et al., 2007), vasoactive intestinal polypeptide receptors (Harikumar et al., 2006), pituitary adenylate cyclase activating polypeptide receptor (Maurel et al., 2008), calcitonin receptor (Seck et al., 2003) and the parathyroid hormone receptor (Pioszak et al., 2010), as well as the GIP receptor (Vrecl et al., 2006). Furthermore, several of these receptors are also capable of forming heteromers in heterologous expression systems (Harikumar et al., 2008).
Of the family B oligomers, the secretin receptor oligomers have been the most extensively analyzed. They are thought to functionally express as constitutive homodimers, but not higher order oligomers, which likely facilitates G protein binding since agonist potency is severely reduced in a mutant incapable of forming dimers (Harikumar et al., 2007; Harikumar et al., 2008). Lipid exposed residues in the 4^{th} transmembrane domain were found to be critical for dimer formation, whereas neither the N- nor C- termini contribute to dimerization (Harikumar et al., 2007). One study using morphological FRET imaging revealed that secretin receptor dimer formation likely occurs intracellularly, during maturation of nascent polypeptides (Lisenbee et al., 2005).

A group of family B GPCRs, including the GLP-1R was tested for hetero-oligomerization with the secretin receptor, using BRET. All combinations, except for that with the calcitonin receptor produced positive hetero-oligomeric BRET signals, although significantly lower than the secretin homodimer BRET signal (Harikumar et al., 2008). Similarities in structure between two associating receptor partners can be an important determinant of receptor dimerization, thus it is not surprising that many structurally-similar family B receptors are capable of associating with themselves and with each other. Since GIPR and GLP-1R have similar structures and function, and are expressed in the same cells, it is plausible that they are able to form functional receptor heteromers. In chapter three of this thesis, I investigate this possibility using BRET, as well as by testing the effect of co-

expression of a trafficking-defective GIPR glycosylation mutant with wild type GLP-1R. Furthermore, the ability for both GIPR and GLP-1R to form homomeric receptors is examined.

1.6.4 N-glycosylation of GIPR and GLP-1R

Both the GIPR and GLP-1R are expressed as glycoproteins in various cells. The pancreatic GIPR is expressed as a glycoprotein with an apparent molecular weight of 59kDa, as shown by cross-linking studies (Amiranoff et al., 1986; Couvineau et al., 1984). Two different-size GLP-1R forms, 64kDa and 44kDa have been detected in insulinoma cells, COS cells, transfected fibroblasts, and pancreatic islet cells (Moens et al., 1996; Widmann et al., 1995; Widmann et al., 1996a). Peptide: N-Glycosidase F (PNGase F) treatment converts both forms to a single species at 35kDa, suggesting that the GLP-1R is expressed as a glycoprotein. Furthermore, only the 65kDa form is able to bind the GLP-1R in COS cells which suggests that only the high molecular weight species is functionally expressed at the cell surface (Widmann et al., 1995).

The human GIPR and GLP-1R contain 2 and 3 N-glycosylation consensus sequences, respectively, all located on their N-termini, however whether each of these sites is occupied by N-glycans is not known. Furthermore, the exact role of N-glycosylation at individual sites in GIPR and GLP-1R function and cell surface expression is unclear. Inhibition of glycosylation of GLP-1R in RINm5F cells, by treatment with tunicamycin, resulted in a concentration-dependent decrease in the number of GLP-1R binding sites at the cell surface, and a corresponding decrease in cAMP production (Göke et al., 1994). A more recent study has shown using immunocytochemistry, that with tunicamycin treatment, EGFP-tagged GLP-1R was no longer observed on the cell surface, but instead localizes to cytosolic compartments (Huang et al., 2010). Together these results suggest that N-glycosylation is necessary for proper expression of GLP-1R at the cell surface. In chapter three of this thesis, I also examine the extent to which each receptor is N-glycosylated, as well as the effect that glycosylation at certain sites has on receptor function and surface expression.

1.7 Statement of Thesis Objectives and Hypotheses

It is well accepted that HCN channels assemble as stable, constitutive tetramers as a prerequisite for the formation of a functional channel. Furthermore, the existence of heteromeric channels has been proposed for various isoform combinations. HCN2 and HCN4 are co-expressed in various tissues and numerous studies have determined that they physically and/or functionally interact in heterologous expression systems, supporting the hypothesis that *HCN2 and HCN4 co-assemble to form functional heteromers*. In chapter two of this thesis, this hypothesis is tested by 1) determining if HCN2 and HCN4 are capable of co-assembling in CHO cells and 2) examining whether these isoforms show a preference for self-assembly versus co-assembly. Furthermore, I will also provide evidence supporting the formation of heteromeric HCN2-HCN4 channels in native tissue.

Of the GPCRs that are known to dimerize, in contrast to HCN channels, many of them are still able to function as monomers. Thus, the formation of these "elective" dimers or higher-order oligomers may act to optimize receptor expression and function. It is currently not known whether the GIP and GLP-1 receptors exist predominantly as monomeric or dimeric entities. Furthermore, since these receptors are similar in regard to both structure and function, if they do in fact dimerize it is also plausible that they are able to form receptor heteromers. In chapter 3 of this thesis, the hypothesis that *GIP and GLP-1 receptors are able to form receptor homomers and heteromers in CHO cells* will be tested.

The effects of N-glycosylation on receptor trafficking and functional expression are diverse and seem to vary depending on the protein studied. Both GIP and GLP-1 receptors are expressed as glycoproteins in native tissues, thus providing support for the final hypothesis of this thesis, which is that *N-glycosylation is important for the functional expression of GIP and GLP-1 receptors*. In chapter 3, examining the contribution of individual glycosylation sites as well as the role of N-glycosylation in both GIP and GLP-1 receptor surface expression and function, will test this hypothesis.

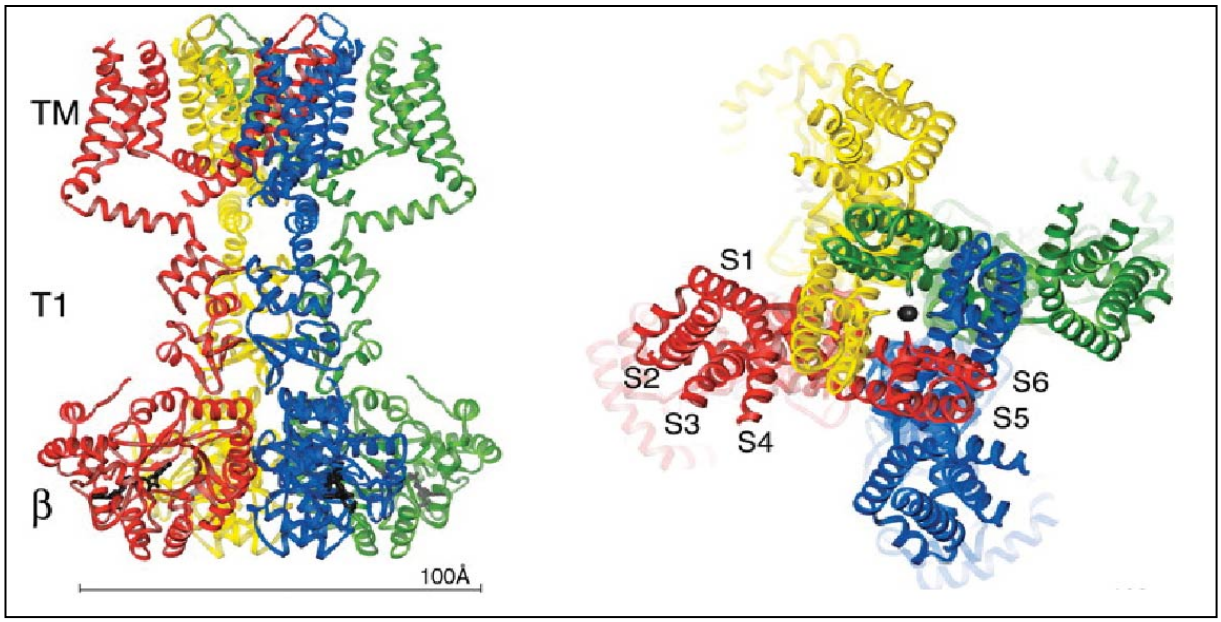

Figure 1.1 Crystal structure of Kv1.2 in complex with its β2 subunit from the side with the extracellular region above (left) or from the extracellular side of the pore (right)

Each subunit of the tetramer is uniquely colored. The T1 domain can be seen from the side view (left) and is located immediately adjacent to the S1 domain in the intracellular region. Adapted from (Long et al., 2005)

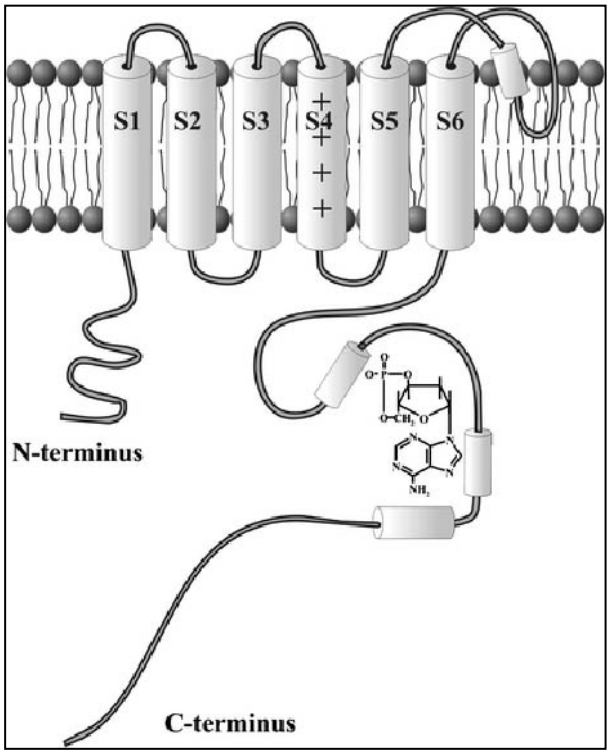

Figure 1.2 Cartoon model of HCN channel topology, depicting one of four subunits

One subunit is composed of six transmembrane segments (S1-S6). S4 is the putative voltage sensor and is characterized by the presence of basic residues within this domain. Within the C-terminus are the domains involved in binding cyclic nucleotides (CNBD), and is depicted here in complex with a cAMP molecule.
Adapted from (Baruscotti et al., 2010)

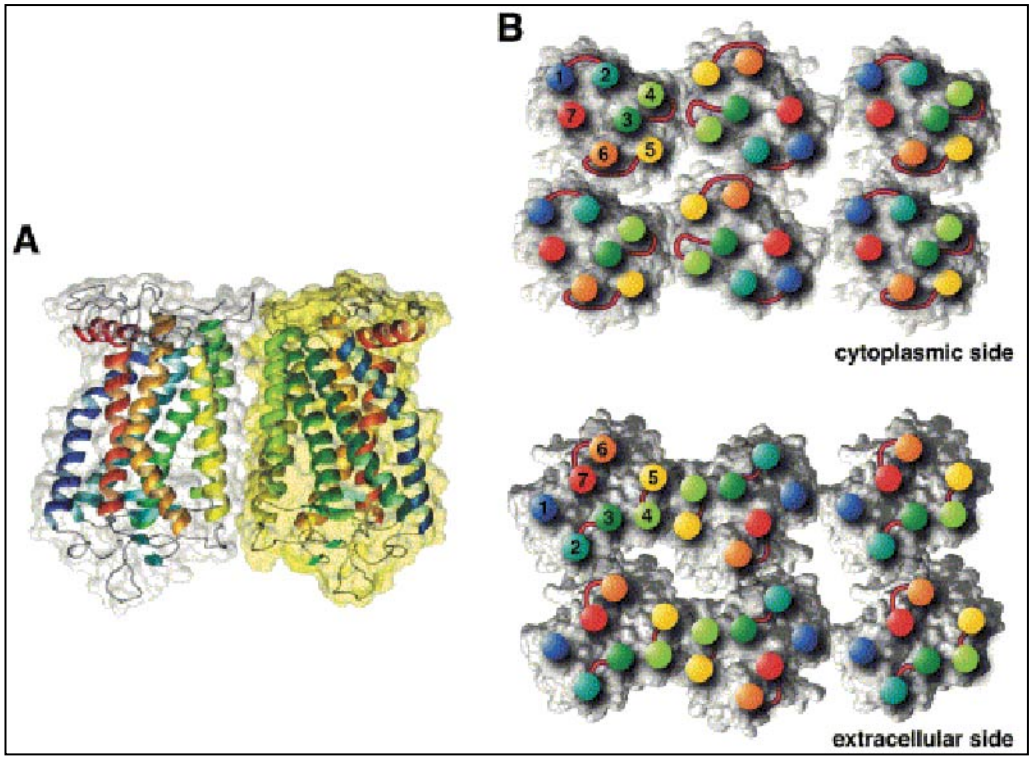

Figure 1.3 Model for packing arrangement of rhodopsin molecules within paracrystalline arrays of native disc membranes

A: Ribbon model of the rhodopsin dimer, viewed from the side. Monomer interactions exist between transmembrane helices IV (yellow-green) and V (green). B: Model for arrangement of rhodopsin oligomers within a paracrystalline array, as seen from the cytoplasmic side (top) and extracellular side (bottom). Positions of helix ends are marked by colored discs and the corresponding helix numbers. Only one half of a second row of oligomers is shown.
From (Fotiadis et al., 2004)

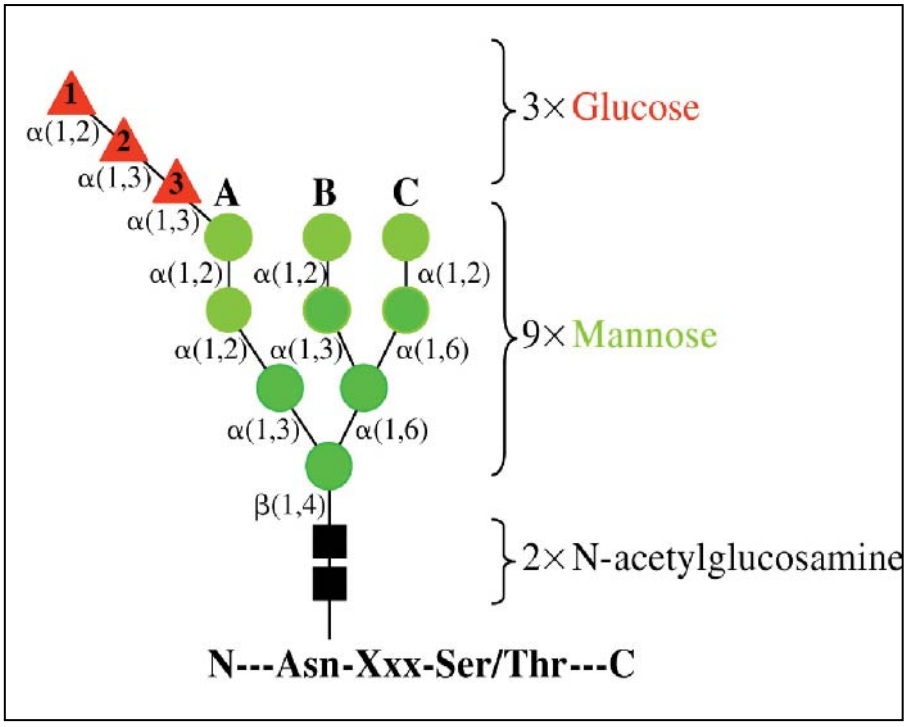

Figure 1.4 Cartoon diagram of the core glycan added to protein nascent chains at their N-glycosylation consensus sequence

The core oligosaccharide is composed of two N-acetylglucosamine residues (black squares), nine mannose residues (green circles), and three glucose residues (red triangles). The three N-glycan branches are labeled A, B and C, and linkages between each residue are shown. Adapted from (Ruddock and Molinari, 2006)

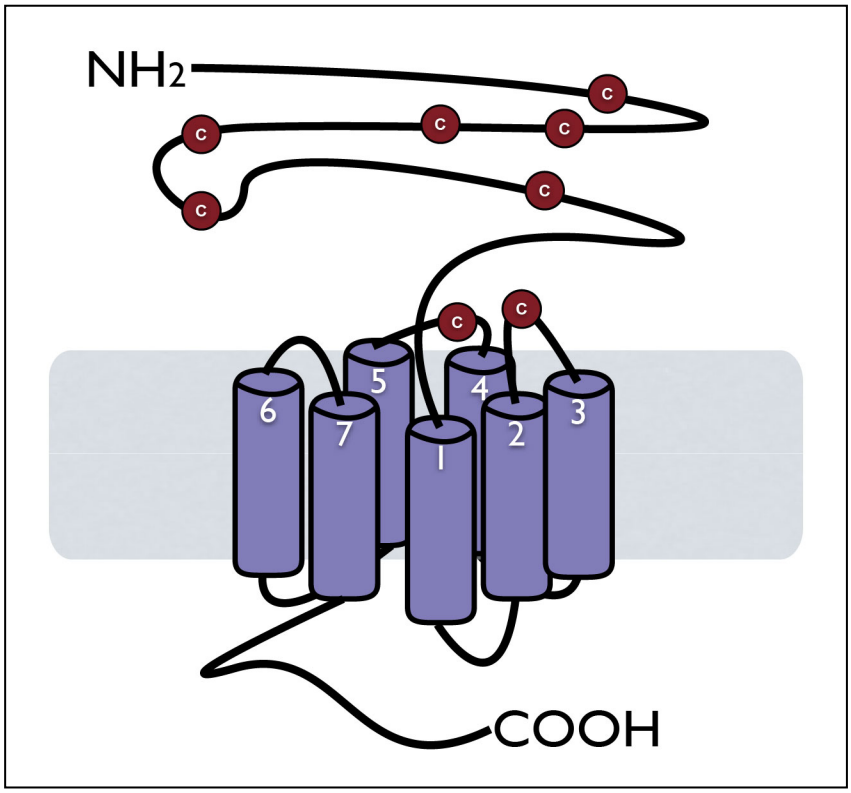

Figure 1.5 Cartoon depiction of a typical family B GPCR topology

Structure includes seven transmembrane domains, an extracellular N-terminus and intracellular C-terminus. Structural features unique to family B GPCRs include a long extracellular N-terminus, and six conserved cysteines located on extracellular domains.

1.8 References

Abbas, S. Y., Ying, S. W. and Goldstein, P. A. (2006). Compartmental distribution of hyperpolarization-activated cyclic-nucleotide-gated channel 2 and hyperpolarization-activated cyclic-nucleotide-gated channel 4 in thalamic reticular and thalamocortical relay neurons. *Neuroscience* **141,** 1811-1825.

Ahrèn, B. (2009). Islet G protein-coupled receptors as potential targets for treatment of type 2 diabetes. *Nat. Rev. Drug Discov.* **8,** 369-385.

Allen, S., Naim, H. Y. and Bulleid, N. J. (1995). Intracellular folding of tissue-type plasminogen activator. effects of disulfide bond formation on N-linked glycosylation and secretion. *J. Biol. Chem.* **270,** 4797-4804.

Al-Sabah, S. and Donnelly, D. (2003). The positive charge at lys-288 of the glucagon-like peptide-1 (GLP-1) receptor is important for binding the N-terminus of peptide agonists. *FEBS Lett.* **553,** 342-346.

Altomare, C., Terragni, B., Brioschi, C., Milanesi, R., Pagliuca, C., Viscomi, C., Moroni, A., Baruscotti, M. and DiFrancesco, D. (2003). Heteromeric HCN1-HCN4 channels: A comparison with native pacemaker channels from the rabbit sinoatrial node. *J. Physiol.* **549,** 347-359.

Amiranoff, B., Couvineau, A., Vauclin-Jacques, N. and Laburthe, M. (1986). Gastric inhibitory polypeptide receptor in hamster pancreatic beta cells. direct cross-linking, solubilization and characterization as a glycoprotein. *Eur. J. Biochem.* **159,** 353-358.

Angers, S., Salahpour, A., Joly, E., Hilairet, S., Chelsky, D., Dennis, M., Bouvier, M. (2000). Detection of beta 2-adrenergic receptor dimerization in living cells using bioluminescence resonance energy transfer (BRET). *Proc. Natl. Acad. Sci. U.S.A.* **28,** 3684-3689.

Arvan, P., Zhao, X., Ramos-Castaneda, J. and Chang, A. (2002). Secretory pathway quality control operating in golgi, plasmalemmal, and endosomal systems. *Traffic* **3,** 771-780.

Baggio, L. L. and Drucker, D. J. (2007). Biology of incretins: GLP-1 and GIP. *Gastroenterology* **132,** 2131-2157.

Banères, J. L. and Parello, J. (2003). Structure-based analysis of GPCR function: Evidence for a novel pentameric assembly between the dimeric leukotriene B4 receptor BLT1 and the G-protein. *J. Mol. Biol.* **329,** 815-829.

Barlowe, C. (2003). Signals for COPII-dependent export from the ER: What's the ticket out? *Trends Cell Biol.* **13,** 295-300.

Barrera, N. P., Henderson, R. M., Murrell-Lagnado, R. D. and Edwardson, J. M. (2007). The stoichiometry of P2X2/6 receptor heteromers depends on relative subunit expression levels. *Biophys. J.* **93,** 505-512.

Baruscotti, M., Bottelli, G., Milanesi, R., Difrancesco, J. C. and Difrancesco, D. (2010). HCN-related channelopathies. *Pflugers Arch.* **460,** 405-415.

Baruscotti, M., Bucchi, A. and Difrancesco, D. (2005). Physiology and pharmacology of the cardiac pacemaker ("funny") current. *Pharmacol. Ther.* **107,** 59-79.

Bayburt, T. H., Leitz, A. J., Xie, G., Oprian, D. D. and Sligar, S. G. (2007). Transducin activation by nanoscale lipid bilayers containing one and two rhodopsins. *J. Biol. Chem.* **282,** 14875-14881.

Bazarsuren, A., Grauschopf, U., Wozny, M., Reusch, D., Hoffmann, E., Schaefer, W., Panzner, S. and Rudolph, R. (2002). In vitro folding, functional characterization, and disulfide pattern of the extracellular domain of human GLP-1 receptor. *Biophys. Chem.* **96,** 305-318.

Benya, R. V., Kusui, T., Katsuno, T., Tsuda, T., Mantey, S. A., Battey, J. F. and Jensen, R. T. (2000). Glycosylation of the gastrin-releasing peptide receptor and its effect on expression, G protein coupling, and receptor modulatory processes. *Mol. Pharmacol.* **58,** 1490-1501.

Biel, M., Wahl-Schott, C., Michalakis, S. and Zong, X. (2009). Hyperpolarization-activated cation channels: From genes to function. *Physiol. Rev.* **89,** 847-885.

Bollag, R. J., Zhong, Q., Phillips, P., Min, L., Zhong, L., Cameron, R., Mulloy, A. L., Rasmussen, H., Qin, F., Ding, K. H. et al. (2000). Osteoblast-derived cells express functional glucose-dependent insulinotropic peptide receptors. *Endocrinology* **141,** 1228-1235.

Bouvier, M. (2001). Oligomerization of G-protein-coupled transmitter receptors. *Nat. Rev. Neurosci.* **2,** 274-286.

Brewster, A. L., Bernard, J. A., Gall, C. M. and Baram, T. Z. (2005). Formation of heteromeric hyperpolarization-activated cyclic nucleotide-gated (HCN) channels in the hippocampus is regulated by developmental seizures. *Neurobiol. Dis.* **19,** 200-207.

Brothers, S. P., Cornea, A., Janovick, J. A. and Conn, P. M. (2004). Human loss-of-function gonadotropin-releasing hormone receptor mutants retain wild-type receptors in the endoplasmic reticulum: Molecular basis of the dominant-negative effect. *Mol. Endocrinol.* **18,** 1787-1797.

Brown, H. F., DiFrancesco, D. and Noble, S. J. (1979). How does adrenaline accelerate the heart? *Nature* **280,** 235-236.

Brown, H. F., DiFrancesco, D. (1980) Voltage-clamp investigations of membrane currents underlying pace-maker activity in rabbit sino-atrial node. *J. Physiol.* **308,** 331-351.

Brown, H. F., Giles, W. and Noble, S. J. (1977). Membrane currents underlying activity in frog sinus venosus. *J. Physiol.* **271,** 783-816.

Bulenger, S., Marullo, S. and Bouvier, M. (2005). Emerging role of homo- and heterodimerization in G-protein-coupled receptor biosynthesis and maturation. *Trends Pharmacol. Sci.* **26,** 131-137.

Bullock, B. P., Heller, R. S. and Habener, J. F. (1996). Tissue distribution of messenger ribonucleic acid encoding the rat glucagon-like peptide-1 receptor. *Endocrinology* **137,** 2968-2978.

Calebiro, D., de Filippis, T., Lucchi, S., Covino, C., Panigone, S., Beck-Peccoz, P., Dunlap, D. and Persani, L. (2005). Intracellular entrapment of wild-type TSH receptor by oligomerization with mutants linked to dominant TSH resistance. *Hum. Mol. Genet.* **14,** 2991-3002.

Campos, R. V., Lee, Y. C. and Drucker, D. J. (1994). Divergent tissue-specific and developmental expression of receptors for glucagon and glucagon-like peptide-1 in the mouse. *Endocrinology* **134,** 2156-2164.

Canals, M., Lopez-Gimenez, J. F. and Milligan, G. (2009). Cell surface delivery and structural re-organization by pharmacological chaperones of an oligomerization-defective alpha(1b)-adrenoceptor mutant demonstrates membrane targeting of GPCR oligomers. *Biochem. J.* **417,** 161-172.

Chan, C. S., Shigemoto, R., Mercer, J. N. and Surmeier, D. J. (2004). HCN2 and HCN1 channels govern the regularity of autonomous pacemaking and synaptic resetting in globus pallidus neurons. *J. Neurosci.* **24,** 9921-9932.

Chen, S., Wang, J. and Siegelbaum, S. A. (2001). Properties of hyperpolarization-activated pacemaker current defined by coassembly of HCN1 and HCN2 subunits and basal modulation by cyclic nucleotide. *J. Gen. Physiol.* **117,** 491-504.

Christie, M. J., North, R. A., Osborne, P. B., Douglass, J. and Adelman, J. P. (1990). Heteropolymeric potassium channels expressed in xenopus oocytes from cloned subunits. *Neuron* **4,** 405-411.

Cohen, D. M. (2006). Regulation of TRP channels by N-linked glycosylation. *Semin. Cell Dev. Biol.* **17,** 630-637.

Couvineau, A., Amiranoff, B., Vauclin-Jacques, N. and Laburthe, M. (1984). The GIP receptor on pancreatic beta cell tumor: Molecular identification by covalent cross-linking. *Biochem. Biophys. Res. Commun.* **122,** 283-288.

Couvineau, A., Fabre, C., Gaudin, P., Maoret, J. J. and Laburthe, M. (1996). Mutagenesis of N-glycosylation sites in the human vasoactive intestinal peptide 1 receptor. evidence that asparagine 58 or 69 is crucial for correct delivery of the receptor to plasma membrane. *Biochemistry* **35,** 1745-1752.

Covarrubias, M., Wei, A. A. and Salkoff, L. (1991). Shaker, shal, shab, and shaw express independent K+ current systems. *Neuron* **7,** 763-773.

Damian, M., Martin, A., Mesnier, D., Pin, J. P. and Baneres, J. L. (2006). Asymmetric conformational changes in a GPCR dimer controlled by G-proteins. *EMBO J.* **25,** 5693-5702.

David, M., Richer, M., Mamarbachi, A. M., Villeneuve, L. R., Dupre, D. J. and Hebert, T. E. (2006). Interactions between GABA-B1 receptors and kir 3 inwardly rectifying potassium channels. *Cell. Signal.* **18,** 2172-2181.

Davis, D., Liu, X. and Segaloff, D.L. (1995). Identification of the sites of N-linked glycosylation on the follicle-stimulating hormone (FSH) receptor and assessment of their role in FSH receptor function. *Mol. Endocrinol.* **9,** 159-170

Deal, K. K., Lovinger, D. M. and Tamkun, M. M. (1994). The brain Kv1.1 potassium channel: In vitro and in vivo studies on subunit assembly and posttranslational processing. *J. Neurosci.* **14,** 1666-1676.

Dennis, J. W., Lau, K. S., Demetriou, M. and Nabi, I. R. (2009). Adaptive regulation at the cell surface by N-glycosylation. *Traffic* **10,** 1569-1578.

Deslauriers, B., Ponce, C., Lombard, C., Larguier, R., Bonnafous, J. C. and Marie, J. (1999). N-glycosylation requirements for the AT1a angiotensin II receptor delivery to the plasma membrane. *Biochem. J.* **339 (Pt 2),** 397-405.

Deutsch, C. (2002). Potassium channel ontogeny. *Annu. Rev. Physiol.* **64,** 19-46.

Deutsch, C. (2003). The birth of a channel. *Neuron* **40,** 265-276.

DiFrancesco, D. (1991). The contribution of the 'pacemaker' current (if) to generation of spontaneous activity in rabbit sino-atrial node myocytes. *J. Physiol.* **434,** 23-40.

DiFrancesco, D., and Tortora, P. (1991). Direct activation of cardiac pacemaker channels by intracellular cyclic AMP. *Nature* **351,** 145-147.

Doan, T. N., Stephans, K., Ramirez, A. N., Glazebrook, P. A., Andresen, M. C. and Kunze, D. L. (2004). Differential distribution and function of hyperpolarization-activated channels in sensory neurons and mechanosensitive fibers. *J. Neurosci.* **24,** 3335-3343.

Dorsch, S., Klotz, K. N., Engelhardt, S., Lohse, M. J. and Bunemann, M. (2009). Analysis of receptor oligomerization by FRAP microscopy. *Nat. Methods* **6,** 225-230.

Doyle, M. E. and Egan, J. M. (2007). Mechanisms of action of glucagon-like peptide 1 in the pancreas. *Pharmacol. Ther.* **113,** 546-593.

Dunphy, J. L., Taylor, R. G. and Fuller, P. J. (1998). Tissue distribution of rat glucagon receptor and GLP-1 receptor gene expression. *Mol. Cell. Endocrinol.* **141,** 179-186.

Ellgaard, L. and Helenius, A. (2003). Quality control in the endoplasmic reticulum. *Nat. Rev. Mol. Cell Biol.* **4,** 181-191.

Elrick, H., Stimmler, L., Hlad, C. J.,Jr and Arai, Y. (1964). Plasma insulin response to oral and intravenous glucose administration. *J. Clin. Endocrinol. Metab.* **24,** 1076-1082.

Er, F., Larbig, R., Ludwig, A., Biel, M., Hofmann, F., Beuckelmann, D. J. and Hoppe, U. C. (2003). Dominant-negative suppression of HCN channels markedly reduces the native pacemaker current I(f) and undermines spontaneous beating of neonatal cardiomyocytes. *Circulation* **107,** 485-489.

Ernst, O. P., Gramse, V., Kolbe, M., Hofmann, K. P. and Heck, M. (2007). Monomeric G protein-coupled receptor rhodopsin in solution activates its G protein transducin at the diffusion limit. *Proc. Natl. Acad. Sci. U. S. A.* **104,** 10859-10864.

Fernandes, H., Cohen, S. and Bishayee, S. (2001). Glycosylation-induced conformational modification positively regulates receptor-receptor association: A study with an aberrant epidermal growth factor receptor (EGFRvIII/DeltaEGFR) expressed in cancer cells. *J. Biol. Chem.* **276,** 5375-5383.

Fotiadis, D., Jastrzebska, B., Philippsen, A., Muller, D. J., Palczewski, K. and Engel, A. (2006). Structure of the rhodopsin dimer: A working model for G-protein-coupled receptors. *Curr. Opin. Struct. Biol.* **16,** 252-259.

Fotiadis, D., Liang, Y., Filipek, S., Saperstein, D. A., Engel, A. and Palczewski, K. (2003). Atomic-force microscopy: Rhodopsin dimers in native disc membranes. *Nature* **421,** 127-128.

Fotiadis, D., Liang, Y., Filipek, S., Saperstein, D. A., Engel, A. and Palczewski, K. (2004). The G protein-coupled receptor rhodopsin in the native membrane. *FEBS Lett.* **564,** 281-288.

Franco, R., Canals, M., Marcellino, D., Ferre, S., Agnati, L., Mallol, J., Casado, V., Ciruela, F., Fuxe, K., Lluis, C. et al. (2003). Regulation of heptaspanning-membrane-receptor function by dimerization and clustering. *Trends Biochem. Sci.* **28,** 238-243.

Fredriksson, R., Lagerstrom, M. C., Lundin, L. G. and Schioth, H. B. (2003). The G-protein-coupled receptors in the human genome form five main families. phylogenetic analysis, paralogon groups, and fingerprints. *Mol. Pharmacol.* **63,** 1256-1272.

Fukushima, Y., Oka, Y., Saitoh, T., Katagiri, H., Asano, T., Matsuhashi, N., Takata, K., van Breda, E., Yazaki, Y. and Sugano, K. (1995). Structural and functional analysis of the

canine histamine H2 receptor by site-directed mutagenesis: N-glycosylation is not vital for its action. *Biochem. J.* **310 (Pt 2),** 553-558.

Fung, J. J., Deupi, X., Pardo, L., Yao, X. J., Velez-Ruiz, G. A., Devree, B. T., Sunahara, R. K. and Kobilka, B. K. (2009). Ligand-regulated oligomerization of beta(2)-adrenoceptors in a model lipid bilayer. *EMBO J.* **28,** 3315-3328.

Gandia, J., Galino, J., Amaral, O. B., Soriano, A., Lluis, C., Franco, R. and Ciruela, F. (2008a). Detection of higher-order G protein-coupled receptor oligomers by a combined BRET-BiFC technique. *FEBS Lett.* **582,** 2979-2984.

Gandia, J., Lluis, C., Ferre, S., Franco, R. and Ciruela, F. (2008b). Light resonance energy transfer-based methods in the study of G protein-coupled receptor oligomerization. *Bioessays* **30,** 82-89.

Gavel, Y. and von Heijne, G. (1990). Sequence differences between glycosylated and non-glycosylated asn-X-Thr/Ser acceptor sites: Implications for protein engineering. *Protein Eng.* **3,** 433-442.

Gelling, R. W., Wheeler, M. B., Xue, J., Gyomorey, S., Nian, C., Pederson, R. A. and McIntosh, C. H. (1997). Localization of the domains involved in ligand binding and activation of the glucose-dependent insulinotropic polypeptide receptor. *Endocrinology* **138,** 2640-2643.

Goin, J. C. and Nathanson, N. M. (2006). Quantitative analysis of muscarinic acetylcholine receptor homo- and heterodimerization in live cells: Regulation of receptor down-regulation by heterodimerization. *J. Biol. Chem.* **281,** 5416-5425.

Göke, R., Just, R., Lankat-Buttgereit, B. and Göke, B. (1994). Glycosylation of the GLP-1 receptor is a prerequisite for regular receptor function. *Peptides* **15,** 675-681.

Guan, R., Feng, X., Wu, X., Zhang, M., Hébert, T.E. and Segaloff, D.L. (2009). Bioluminescence resonance energy transfer studies reveal constitutive dimerization of the human lutropin receptor and a lack of correlation between receptor activation and the propensity for dimerization. *J. Biol. Chem.* **284,** 7483-7494

Guo, W., Urizar, E., Kralikova, M., Mobarec, J. C., Shi, L., Filizola, M. and Javitch, J. A. (2008). Dopamine D2 receptors form higher order oligomers at physiological expression levels. *EMBO J.* **27,** 2293-2304.

Gurevich, V. V. and Gurevich, E. V. (2008a). GPCR monomers and oligomers: It takes all kinds. *Trends Neurosci.* **31,** 74-81.

Gurevich, V. V. and Gurevich, E. V. (2008b). How and why do GPCRs dimerize? *Trends Pharmacol. Sci.* **29,** 234-240.

Hallbrink, M., Holmqvist, T., Olsson, M., Ostenson, C. G., Efendic, S. and Langel, U. (2001). Different domains in the third intracellular loop of the GLP-1 receptor are responsible for galpha(s) and galpha(i)/Galpha(o) activation. *Biochim. Biophys. Acta* **1546,** 79-86.

Halliwell, J. V., Adams, P. R. (1982). Voltage-clamp analysis of muscarinic excitation in hippocampal neurons. *Brain Res.* **250,** 71-92.

Han, Y., Moreira, I. S., Urizar, E., Weinstein, H. and Javitch, J. A. (2009). Allosteric communication between protomers of dopamine class A GPCR dimers modulates activation. *Nat. Chem. Biol.* **5,** 688-695.

Hansotia, T., Baggio, L. L., Delmeire, D., Hinke, S. A., Yamada, Y., Tsukiyama, K., Seino, Y., Holst, J. J., Schuit, F. and Drucker, D. J. (2004). Double incretin receptor knockout (DIRKO) mice reveal an essential role for the enteroinsular axis in transducing the glucoregulatory actions of DPP-IV inhibitors. *Diabetes* **53,** 1326-1335.

Harikumar, K. G., Happs, R. M. and Miller, L. J. (2008). Dimerization in the absence of higher-order oligomerization of the G protein-coupled secretin receptor. *Biochim. Biophys. Acta* **1778,** 2555-2563.

Harikumar, K. G., Morfis, M. M., Lisenbee, C. S., Sexton, P. M. and Miller, L. J. (2006). Constitutive formation of oligomeric complexes between family B G protein-coupled vasoactive intestinal polypeptide and secretin receptors. *Mol. Pharmacol.* **69,** 363-373.

Harikumar, K. G., Morfis, M. M., Sexton, P. M. and Miller, L. J. (2008). Pattern of intra-family hetero-oligomerization involving the G-protein-coupled secretin receptor. *J. Mol. Neurosci.* **36,** 279-285.

Harikumar, K. G., Pinon, D. I. and Miller, L. J. (2007). Transmembrane segment IV contributes a functionally important interface for oligomerization of the class II G protein-coupled secretin receptor. *J. Biol. Chem.* **282,** 30363-30372.

He, J., Xu, J., Castleberry, A. M., Lau, A. G. and Hall, R. A. (2002). Glycosylation of beta(1)-adrenergic receptors regulates receptor surface expression and dimerization. *Biochem. Biophys. Res. Commun.* **297,** 565-572.

Hebert, D. N. and Molinari, M. (2007). In and out of the ER: Protein folding, quality control, degradation, and related human diseases. *Physiol. Rev.* **87,** 1377-1408.

Helenius, A. (1994). How N-linked oligosaccharides affect glycoprotein folding in the endoplasmic reticulum. *Mol. Biol. Cell* **5,** 253-265.

Helenius, A. and Aebi, M. (2004). Roles of N-linked glycans in the endoplasmic reticulum. *Annu. Rev. Biochem.* **73,** 1019-1049.

Hille, B. (2001). Ionic channels of excitable membranes, pp427-429. In *Ionic Channels of Excitable Membranes*, pp. 427-429. Sunderland, MA: Sinauer Associates.

Hoare, S. R. (2005). Mechanisms of peptide and nonpeptide ligand binding to class B G-protein-coupled receptors. *Drug Discov. Today* **10,** 417-427.

Hofmann, K. P., Scheerer, P., Hildebrand, P. W., Choe, H. W., Park, J. H., Heck, M. and Ernst, O. P. (2009). A G protein-coupled receptor at work: The rhodopsin model. *Trends Biochem. Sci.* **34,** 540-552.

Huang, Y., Wilkinson, G. F. and Willars, G. B. (2010). Role of the signal peptide in the synthesis and processing of the glucagon-like peptide-1 receptor. *Br. J. Pharmacol.* **159,** 237-251.

Isacoff, E. Y., Jan, Y. N. and Jan, L. Y. (1990). Evidence for the formation of heteromultimeric potassium channels in xenopus oocytes. *Nature* **345,** 530-534.

Issafras, H., Angers, S., Bulenger, S., Blanpain, C., Parmentier, M., Labbé-Jullié, C., Bouvier, M. and Marullo, S. (2002). Constitutive agonist-independent CCR5 oligomerization and antibody-mediated clustering occurring at physiological levels of receptors. *J. Biol. Chem.* **277,** 34666-34673.

Jaakola, V. P., Griffith, M. T., Hanson, M. A., Cherezov, V., Chien, E. Y., Lane, J. R., Ijzerman, A. P. and Stevens, R. C. (2008). The 2.6 angstrom crystal structure of a human A2A adenosine receptor bound to an antagonist. *Science* **322,** 1211-1217.

Jastrzebska, B., Fotiadis, D., Jang, G. F., Stenkamp, R. E., Engel, A. and Palczewski, K. (2006). Functional and structural characterization of rhodopsin oligomers. *J. Biol. Chem.* **281,** 11917-11922.

Jia, X., Brown, J. C., Ma, P., Pederson, R. A. and McIntosh, C. H. (1995). Effects of glucose-dependent insulinotropic polypeptide and glucagon-like peptide-I-(7-36) on insulin secretion. *Am. J. Physiol.* **268,** E645-51.

Jiang, Y., Lee, A., Chen, J., Ruta, V., Cadene, M., Chait, B. T. and MacKinnon, R. (2003). X-ray structure of a voltage-dependent K+ channel. *Nature* **423,** 33-41.

Johnson, A. E. and van Waes, M. A. (1999). The translocon: A dynamic gateway at the ER membrane. *Annu. Rev. Cell Dev. Biol.* **15,** 799-842.

Jones, K. A., Borowsky, B., Tamm, J. A., Craig, D. A., Durkin, M. M., Dai, M., Yao, W. J., Johnson, M., Gunwaldsen, C., Huang, L. Y. et al. (1998). GABA(B) receptors function as a heteromeric assembly of the subunits GABA(B)R1 and GABA(B)R2. *Nature* **396,** 674-679.

Karpa, K. D., Lidow, M. S., Pickering, M. T., Levenson, R. and Bergson, C. (1999). N-linked glycosylation is required for plasma membrane localization of D5, but not D1, dopamine receptors in transfected mammalian cells. *Mol. Pharmacol.* **56,** 1071-1078.

Kaupmann, K., Malitschek, B., Schuler, V., Heid, J., Froestl, W., Beck, P., Mosbacher, J., Bischoff, S., Kulik, A., Shigemoto, R. et al. (1998). GABA(B)-receptor subtypes assemble into functional heteromeric complexes. *Nature* **396,** 683-687.

Kerschensteiner, D., Soto, F. and Stocker, M. (2005). Fluorescence measurements reveal stoichiometry of K+ channels formed by modulatory and delayed rectifier alpha-subunits. *Proc. Natl. Acad. Sci. U. S. A.* **102,** 6160-6165.

Kniazeff, J., Bessis, A. S., Maurel, D., Ansanay, H., Prezeau, L. and Pin, J. P. (2004). Closed state of both binding domains of homodimeric mGlu receptors is required for full activity. *Nat. Struct. Mol. Biol.* **11,** 706-713.

Kobori, T., Smith, G. D., Sandford, R. and Edwardson, J. M. (2009). The transient receptor potential channels TRPP2 and TRPC1 form a heterotetramer with a 2:2 stoichiometry and an alternating subunit arrangement. *J. Biol. Chem.* **284,** 35507-35513.

Kosolapov, A. and Deutsch, C. (2003). Folding of the voltage-gated K+ channel T1 recognition domain. *J. Biol. Chem.* **278,** 4305-4313.

Krebs, A., Villa, C., Edwards, P. C. and Schertler, G. F. (1998). Characterisation of an improved two-dimensional p22121 crystal from bovine rhodopsin. *J. Mol. Biol.* **282,** 991-1003.

Kreusch, A., Pfaffinger, P. J., Stevens, C. F. and Choe, S. (1998). Crystal structure of the tetramerization domain of the shaker potassium channel. *Nature* **392,** 945-948.

Kuner, R., Kohr, G., Grunewald, S., Eisenhardt, G., Bach, A. and Kornau, H. C. (1999). Role of heteromer formation in GABAB receptor function. *Science* **283,** 74-77.

Kunishima, N., Shimada, Y., Tsuji, Y., Sato, T., Yamamoto, M., Kumasaka, T., Nakanishi, S., Jingami, H. and Morikawa, K. (2000). Structural basis of glutamate recognition by a dimeric metabotropic glutamate receptor. *Nature* **407,** 971-977.

Kuszak, A. J., Pitchiaya, S., Anand, J. P., Mosberg, H. I., Walter, N. G. and Sunahara, R. K. (2009). Purification and functional reconstitution of monomeric mu-opioid receptors: Allosteric modulation of agonist binding by Gi2. *J. Biol. Chem.* **284,** 26732-26741.

Lagerstrom, M. C. and Schioth, H. B. (2008). Structural diversity of G protein-coupled receptors and significance for drug discovery. *Nat. Rev. Drug Discov.* **7,** 339-357.

Langer, I., Leroy, K., Gaspard, N., Brion, J. P. and Robberecht, P. (2008). Cell surface targeting of VPAC1 receptors: Evidence for implication of a quality control system and the proteasome. *Biochim. Biophys. Acta* **1783,** 1663-1672.

Lau, K. S., Partridge, E. A., Grigorian, A., Silvescu, C. I., Reinhold, V. N., Demetriou, M. and Dennis, J. W. (2007). Complex N-glycan number and degree of branching cooperate to regulate cell proliferation and differentiation. *Cell* **129,** 123-134.

Li, J. G., Chen, C. and Liu-Chen, L. Y. (2007). N-glycosylation of the human kappa opioid receptor enhances its stability but slows its trafficking along the biosynthesis pathway. *Biochemistry* **46,** 10960-10970.

Li, M., Jan, Y. N. and Jan, L. Y. (1992). Specification of subunit assembly by the hydrophilic amino-terminal domain of the shaker potassium channel. *Science* **257,** 1225-1230.

Liang, Y., Fotiadis, D., Filipek, S., Saperstein, D. A., Palczewski, K. and Engel, A. (2003). Organization of the G protein-coupled receptors rhodopsin and opsin in native membranes. *J. Biol. Chem.* **278,** 21655-21662.

Lisenbee, C. S., Dong, M. and Miller, L. J. (2005). Paired cysteine mutagenesis to establish the pattern of disulfide bonds in the functional intact secretin receptor. *J. Biol. Chem.* **280,** 12330-12338.

Liu, H. L., Chen, C. W. and Lin, J. C. (2005). Homology models of the tetramerization domain of six eukaryotic voltage-gated potassium channels Kv1.1-Kv1.6. *J. Biomol. Struct. Dyn.* **22,** 387-398.

Long, S. B., Campbell, E. B. and Mackinnon, R. (2005). Crystal structure of a mammalian voltage-dependent shaker family K+ channel. *Science* **309,** 897-903.

Lu, J., Robinson, J. M., Edwards, D. and Deutsch, C. (2001). T1-T1 interactions occur in ER membranes while nascent kv peptides are still attached to ribosomes. *Biochemistry* **40,** 10934-10946.

Lu, M., Wheeler, M. B., Leng, X. H. and Boyd, A. E.,3rd. (1993). The role of the free cytosolic calcium level in beta-cell signal transduction by gastric inhibitory polypeptide and glucagon-like peptide I(7-37). *Endocrinology* **132,** 94-100.

Ludwig, A., Zong, X., Jeglitsch, M., Hofmann, F. and Biel, M. (1998). A family of hyperpolarization-activated mammalian cation channels. *Nature* **393,** 587-591.

Ludwig, A., Zong, X., Stieber, J., Hullin, R., Hofmann, F. and Biel, M. (1999). Two pacemaker channels from human heart with profoundly different activation kinetics. *EMBO J.* **18,** 2323-2329.

Ma, D., Zerangue, N., Lin, Y. F., Collins, A., Yu, M., Jan, Y. N. and Jan, L. Y. (2001). Role of ER export signals in controlling surface potassium channel numbers. *Science* **291,** 316-319.

Maccaferri, G., Mangoni, M., Lazzari, A., DiFrancesco, D. (1993). Properties of the hyperpolarization-activated current in rat hippocampal CA1 pyramidal cells. *J. Neurophysiol.* **69,** 2129-2136

MacKinnon, R. (1991). Determination of the subunit stoichiometry of a voltage-activated potassium channel. *Nature* **350,** 232-235.

Magee, J. C. (1998). Dendritic hyperpolarization-activated currents modify the integrative properties of hippocampal CA1 pyramidal neurons. *J. Neurosci.* **18,** 7613-7624.

Magee, J. C. (1999). Dendritic Ih normalizes temporal summation in hippocampal CA1 neurons. *Nat. Neurosci.* **2,** 848.

Mansoor, S. E., Palczewski, K. and Farrens, D. L. (2006). Rhodopsin self-associates in asolectin liposomes. *Proc. Natl. Acad. Sci. U. S. A.* **103,** 3060-3065.

Margeta-Mitrovic, M., Jan, Y. N. and Jan, L. Y. (2000). A trafficking checkpoint controls GABA(B) receptor heterodimerization. *Neuron* **27,** 97-106.

Marionneau, C., Couette, B., Liu, J., Li, H., Mangoni, M. E., Nargeot, J., Lei, M., Escande, D. and Demolombe, S. (2005). Specific pattern of ionic channel gene expression associated with pacemaker activity in the mouse heart. *J. Physiol.* **562,** 223-234.

Markkanen, P. M. and Petaja-Repo, U. E. (2008). N-glycan-mediated quality control in the endoplasmic reticulum is required for the expression of correctly folded delta-opioid receptors at the cell surface. *J. Biol. Chem.* **283,** 29086-29098.

Mathi, S. K., Chan, Y., Li, X. and Wheeler, M. B. (1997). Scanning of the glucagon-like peptide-1 receptor localizes G protein-activating determinants primarily to the N-terminus of the third intracellular loop. *Mol. Endocrinol.* **11,** 424-432.

Maurel, D., Comps-Agrar, L., Brock, C., Rives, M. L., Bourrier, E., Ayoub, M. A., Bazin, H., Tinel, N., Durroux, T., Prezeau, L. et al. (2008). Cell-surface protein-protein interaction analysis with time-resolved FRET and snap-tag technologies: Application to GPCR oligomerization. *Nat. Methods* **5,** 561-567.

McCormick, P. J., Miao, Y., Shao, Y., Lin, J. and Johnson, A. E. (2003). Cotranslational protein integration into the ER membrane is mediated by the binding of nascent chains to translocon proteins. *Mol. Cell* **12,** 329-341.

McIntosh, C. H., Widenmaier, S. and Kim, S. J. (2009). Glucose-dependent insulinotropic polypeptide (gastric inhibitory polypeptide; GIP). *Vitam. Horm.* **80,** 409-471.

Mercier, J. F., Salahpour, A., Angers, S., Breit, A. and Bouvier, M. (2002). Quantitative assessment of beta 1- and beta 2-adrenergic receptor homo- and heterodimerization by bioluminescence resonance energy transfer. *J. Biol. Chem.* **277,** 44925-44931.

Meyer, B.H., Segura, J.M., Martinez, K.L., Hovius, R., George, N., Johnsson, K. and Vogel, H. (2006). FRET imaging reveals that functional neurokinin-1 receptors are monomeric and reside in membrane microdomains of live cells. *Proc. Natl. Acad. Sci. U. S. A.* **103,** 2138-2143.

Michels, G., Er, F., Khan, I., Sudkamp, M., Herzig, S. and Hoppe, U. C. (2005). Single-channel properties support a potential contribution of hyperpolarization-activated cyclic nucleotide-gated channels and if to cardiac arrhythmias. *Circulation* **111,** 399-404.

Michineau, S., Alhenc-Gelas, F. and Rajerison, R. M. (2006). Human bradykinin B2 receptor sialylation and N-glycosylation participate with disulfide bonding in surface receptor dimerization. *Biochemistry* **45,** 2699-2707.

Michineau, S., Muller, L., Pizard, A., Alhenc-Gelas, F. and Rajerison, R. M. (2004). N-linked glycosylation of the human bradykinin B2 receptor is required for optimal cell-surface expression and coupling. *Biol. Chem.* **385,** 49-57.

Milligan, G. (2007). G protein-coupled receptor dimerisation: Molecular basis and relevance to function. *Biochim. Biophys. Acta* **1768,** 825-835.

Milligan, G. (2009). G protein-coupled receptor hetero-dimerization: Contribution to pharmacology and function. *Br. J. Pharmacol.* **158,** 5-14.

Milligan, G. and Bouvier, M. (2005). Methods to monitor the quaternary structure of G protein-coupled receptors. *FEBS J.* **272,** 2914-2925.

Mitra, N., Sinha, S., Ramya, T. N. and Surolia, A. (2006). N-linked oligosaccharides as outfitters for glycoprotein folding, form and function. *Trends Biochem. Sci.* **31,** 156-163.

Miyawaki, K., Yamada, Y., Yano, H., Niwa, H., Ban, N., Ihara, Y., Kubota, A., Fujimoto, S., Kajikawa, M., Kuroe, A. et al. (1999). Glucose intolerance caused by a defect in the entero-insular axis: A study in gastric inhibitory polypeptide receptor knockout mice. *Proc. Natl. Acad. Sci. U. S. A.* **96,** 14843-14847.

Mody, N., Hermans, E., Nahorski, S. R. and Challiss, R. A. (1999). Inhibition of N-linked glycosylation of the human type 1alpha metabotropic glutamate receptor by tunicamycin: Effects on cell-surface receptor expression and function. *Neuropharmacology* **38,** 1485-1492.

Moens, K., Heimberg, H., Flamez, D., Huypens, P., Quartier, E., Ling, Z., Pipeleers, D., Gremlich, S., Thorens, B. and Schuit, F. (1996). Expression and functional activity of glucagon, glucagon-like peptide I, and glucose-dependent insulinotropic peptide receptors in rat pancreatic islet cells. *Diabetes* **45,** 257-261.

Montrose-Rafizadeh, C., Avdonin, P., Garant, M. J., Rodgers, B. D., Kole, S., Yang, H., Levine, M. A., Schwindinger, W. and Bernier, M. (1999). Pancreatic glucagon-like peptide-1 receptor couples to multiple G proteins and activates mitogen-activated protein kinase pathways in chinese hamster ovary cells. *Endocrinology* **140,** 1132-1140.

Moosmang, S., Biel, M., Hofmann, F. and Ludwig, A. (1999). Differential distribution of four hyperpolarization-activated cation channels in mouse brain. *Biol. Chem.* **380,** 975-980.

Moosmang, S., Stieber, J., Zong, X., Biel, M., Hofmann, F. and Ludwig, A. (2001). Cellular expression and functional characterization of four hyperpolarization-activated pacemaker channels in cardiac and neuronal tissues. *Eur. J. Biochem.* **268,** 1646-1652.

Much, B., Wahl-Schott, C., Zong, X., Schneider, A., Baumann, L., Moosmang, S., Ludwig, A. and Biel, M. (2003). Role of subunit heteromerization and N-linked glycosylation in the formation of functional hyperpolarization-activated cyclic nucleotide-gated channels. *J. Biol. Chem.* **278,** 43781-43786.

Muller, D. J., Wu, N. and Palczewski, K. (2008). Vertebrate membrane proteins: Structure, function, and insights from biophysical approaches. *Pharmacol. Rev.* **60,** 43-78.

Murray, A. R., Fliesler, S. J. and Al-Ubaidi, M. R. (2009). Rhodopsin: The functional significance of asn-linked glycosylation and other post-translational modifications. *Ophthalmic Genet.* **30,** 109-120.

Nagaya, N. and Papazian, D. M. (1997). Potassium channel alpha and beta subunits assemble in the endoplasmic reticulum. *J. Biol. Chem.* **272,** 3022-3027.

Ng, G. Y., Clark, J., Coulombe, N., Ethier, N., Hebert, T. E., Sullivan, R., Kargman, S., Chateauneuf, A., Tsukamoto, N., McDonald, T. et al. (1999). Identification of a GABAB receptor subunit, gb2, required for functional GABAB receptor activity. *J. Biol. Chem.* **274,** 7607-7610.

Notomi, T. and Shigemoto, R. (2004). Immunohistochemical localization of ih channel subunits, HCN1-4, in the rat brain. *J. Comp. Neurol.* **471,** 241-276.

Ohtsubo, K. and Marth, J. D. (2006). Glycosylation in cellular mechanisms of health and disease. *Cell* **126,** 855-867.

Ottschytsch, N., Raes, A., Van Hoorick, D. and Snyders, D. J. (2002). Obligatory heterotetramerization of three previously uncharacterized kv channel alpha-subunits identified in the human genome. *Proc. Natl. Acad. Sci. U. S. A.* **99,** 7986-7991.

Palczewski, K., Kumasaka, T., Hori, T., Behnke, C. A., Motoshima, H., Fox, B. A., Le Trong, I., Teller, D. C., Okada, T., Stenkamp, R. E. et al. (2000). Crystal structure of rhodopsin: A G protein-coupled receptor. *Science* **289,** 739-745.

Pamir, N., Lynn, F. C., Buchan, A. M., Ehses, J., Hinke, S. A., Pospisilik, J. A., Miyawaki, K., Yamada, Y., Seino, Y., McIntosh, C. H. et al. (2003). Glucose-dependent insulinotropic polypeptide receptor null mice exhibit compensatory changes in the enteroinsular axis. *Am. J. Physiol. Endocrinol. Metab.* **284,** E931-9.

Pang, R. T., Ng, S. S., Cheng, C. H., Holtmann, M. H., Miller, L. J. and Chow, B. K. (1999). Role of N-linked glycosylation on the function and expression of the human secretin receptor. *Endocrinology* **140,** 5102-5111.

Panyi, G. and Deutsch, C. (1996). Assembly and suppression of endogenous Kv1.3 channels in human T cells. *J. Gen. Physiol.* **107,** 409-420.

Parthier, C., Kleinschmidt, M., Neumann, P., Rudolph, R., Manhart, S., Schlenzig, D., Fanghanel, J., Rahfeld, J. U., Demuth, H. U. and Stubbs, M. T. (2007). Crystal structure of the incretin-bound extracellular domain of a G protein-coupled receptor. *Proc. Natl. Acad. Sci. U. S. A.* **104,** 13942-13947.

Parthier, C., Reedtz-Runge, S., Rudolph, R. and Stubbs, M. T. (2009). Passing the baton in class B GPCRs: Peptide hormone activation via helix induction? *Trends Biochem. Sci.* **34,** 303-310.

Pederson, R. A., Satkunarajah, M., McIntosh, C. H., Scrocchi, L. A., Flamez, D., Schuit, F., Drucker, D. J. and Wheeler, M. B. (1998). Enhanced glucose-dependent insulinotropic polypeptide secretion and insulinotropic action in glucagon-like peptide 1 receptor -/- mice. *Diabetes* **47,** 1046-1052.

Petrescu, A. J., Milac, A. L., Petrescu, S. M., Dwek, R. A. and Wormald, M. R. (2004). Statistical analysis of the protein environment of N-glycosylation sites: Implications for occupancy, structure, and folding. *Glycobiology* **14,** 103-114.

Phartiyal, P., Jones, E. M. and Robertson, G. A. (2007). Heteromeric assembly of human ether-a-go-go-related gene (hERG) 1a/1b channels occurs cotranslationally via N-terminal interactions. *J. Biol. Chem.* **282,** 9874-9882.

Phartiyal, P., Sale, H., Jones, E. M. and Robertson, G. A. (2008). Endoplasmic reticulum retention and rescue by heteromeric assembly regulate human ERG 1a/1b surface channel composition. *J. Biol. Chem.* **283,** 3702-3707.

Pin, J. P., Neubig, R., Bouvier, M., Devi, L., Filizola, M., Javitch, J. A., Lohse, M. J., Milligan, G., Palczewski, K., Parmentier, M. et al. (2007). International union of basic and clinical pharmacology. LXVII. recommendations for the recognition and nomenclature of G protein-coupled receptor heteromultimers. *Pharmacol. Rev.* **59,** 5-13.

Pioszak, A. A., Harikumar, K. G., Parker, N. R., Miller, L. J. and Xu, H. E. (2010). Dimeric arrangement of the parathyroid hormone receptor and a structural mechanism for ligand-induced dissociation. *J. Biol. Chem.* **285,** 12435-12444.

Pongs, O. (2009). Ins and outs of cardiac voltage-gated potassium channels. *Curr. Opin. Pharmacol.* **9,** 311-315.

Proenza, C., Tran, N., Angoli, D., Zahynacz, K., Balcar, P. and Accili, E. A. (2002). Different roles for the cyclic nucleotide binding domain and amino terminus in assembly and expression of hyperpolarization-activated, cyclic nucleotide-gated channels. *J. Biol. Chem.* **277,** 29634-29642.

Qu, Y., Whitaker, G. M., Hove-Madsen, L., Tibbits, G. F. and Accili, E. A. (2008). Hyperpolarization-activated cyclic nucleotide-modulated 'HCN' channels confer regular and faster rhythmicity to beating mouse embryonic stem cells. *J. Physiol.* **586,** 701-716.

Rands, E., Candelore, M. R., Cheung, A. H., Hill, W. S., Strader, C. D. and Dixon, R. A. (1990). Mutational analysis of beta-adrenergic receptor glycosylation. *J. Biol. Chem.* **265,** 10759-10764.

Rasmussen, S. G., Choi, H. J., Rosenbaum, D. M., Kobilka, T. S., Thian, F. S., Edwards, P. C., Burghammer, M., Ratnala, V. R., Sanishvili, R., Fischetti, R. F. et al. (2007). Crystal structure of the human beta2 adrenergic G-protein-coupled receptor. *Nature* **450,** 383-387.

Reddy, P. S. and Corley, R. B. (1998). Assembly, sorting, and exit of oligomeric proteins from the endoplasmic reticulum. *Bioessays* **20,** 546-554.

Rivero-Muller, A., Chou, Y. Y., Ji, I., Lajic, S., Hanyaloglu, A. C., Jonas, K., Rahman, N., Ji, T. H. and Huhtaniemi, I. (2010). Rescue of defective G protein-coupled receptor function in vivo by intermolecular cooperation. *Proc. Natl. Acad. Sci. U. S. A.* **107,** 2319-2324.

Rosenbaum, D. M., Rasmussen, S. G. and Kobilka, B. K. (2009). The structure and function of G-protein-coupled receptors. *Nature* **459,** 356-363.

Roy, S., Perron, B. and Gallo-Payet, N. (2010). Role of asparagine-linked glycosylation in cell surface expression and function of the human adrenocorticotropin receptor (melanocortin 2 receptor) in 293/FRT cells. *Endocrinology* **151,** 660-670.

Ruddock, L. W. and Molinari, M. (2006). N-glycan processing in ER quality control. *J. Cell. Sci.* **119,** 4373-4380.

Runge, S., Thogersen, H., Madsen, K., Lau, J. and Rudolph, R. (2008). Crystal structure of the ligand-bound glucagon-like peptide-1 receptor extracellular domain. *J. Biol. Chem.* **283,** 11340-11347.

Ruppersberg, J. P., Schroter, K. H., Sakmann, B., Stocker, M., Sewing, S. and Pongs, O. (1990). Heteromultimeric channels formed by rat brain potassium-channel proteins. *Nature* **345,** 535-537.

Salahpour, A., Angers, S., Mercier, J. F., Lagace, M., Marullo, S. and Bouvier, M. (2004). Homodimerization of the beta2-adrenergic receptor as a prerequisite for cell surface targeting. *J. Biol. Chem.* **279,** 33390-33397.

Salapatek, A. M., MacDonald, P. E., Gaisano, H. Y. and Wheeler, M. B. (1999). Mutations to the third cytoplasmic domain of the glucagon-like peptide 1 (GLP-1) receptor can functionally uncouple GLP-1-stimulated insulin secretion in HIT-T15 cells. *Mol. Endocrinol.* **13,** 1305-1317.

Salkoff, L., Baker, K., Butler, A., Covarrubias, M., Pak, M. D. and Wei, A. (1992). An essential 'set' of K+ channels conserved in flies, mice and humans. *Trends Neurosci.* **15,** 161-166.

Sandhu, H., Wiesenthal, S. R., MacDonald, P. E., McCall, R. H., Tchipashvili, V., Rashid, S., Satkunarajah, M., Irwin, D. M., Shi, Z. Q., Brubaker, P. L. et al. (1999). Glucagon-like peptide 1 increases insulin sensitivity in depancreatized dogs. *Diabetes* **48,** 1045-1053.

Santoro, B. and Baram, T. Z. (2003). The multiple personalities of h-channels. *Trends Neurosci.* **26,** 550-554.

Santoro, B., Chen, S., Luthi, A., Pavlidis, P., Shumyatsky, G. P., Tibbs, G. R. and Siegelbaum, S. A. (2000). Molecular and functional heterogeneity of hyperpolarization-activated pacemaker channels in the mouse CNS. *J. Neurosci.* **20,** 5264-5275.

Santoro, B., Liu, D. T., Yao, H., Bartsch, D., Kandel, E. R., Siegelbaum, S. A. and Tibbs, G. R. (1998). Identification of a gene encoding a hyperpolarization-activated pacemaker channel of brain. *Cell* **93,** 717-729.

Santoro, B. and Tibbs, G. R. (1999). The HCN gene family: Molecular basis of the hyperpolarization-activated pacemaker channels. *Ann. N. Y. Acad. Sci.* **868,** 741-764.

Sawutz, D. G., Lanier, S. M., Warren, C. D. and Graham, R. M. (1987). Glycosylation of the mammalian alpha 1-adrenergic receptor by complex type N-linked oligosaccharides. *Mol. Pharmacol.* **32,** 565-571.

Schertler, G. F., Villa, C. and Henderson, R. (1993). Projection structure of rhodopsin. *Nature* **362,** 770-772.

Schulteis, C. T., Nagaya, N. and Papazian, D. M. (1998). Subunit folding and assembly steps are interspersed during shaker potassium channel biogenesis. *J. Biol. Chem.* **273,** 26210-26217.

Scrocchi, L. A., Brown, T. J., MaClusky, N., Brubaker, P. L., Auerbach, A. B., Joyner, A. L. and Drucker, D. J. (1996). Glucose intolerance but normal satiety in mice with a null mutation in the glucagon-like peptide 1 receptor gene. *Nat. Med.* **2,** 1254-1258.

Seck, T., Baron, R. and Horne, W. C. (2003). The alternatively spliced deltae13 transcript of the rabbit calcitonin receptor dimerizes with the C1a isoform and inhibits its surface expression. *J. Biol. Chem.* **278,** 23085-23093.

Seifert, R., Scholten, A., Gauss, R., Mincheva, A., Lichter, P. and Kaupp, U. B. (1999). Molecular characterization of a slowly gating human hyperpolarization-activated channel predominantly expressed in thalamus, heart, and testis. *Proc. Natl. Acad. Sci. U. S. A.* **96,** 9391-9396.

Shakin-Eshleman, S. H., Spitalnik, S. L. and Kasturi, L. (1996). The amino acid at the X position of an asn-X-ser sequon is an important determinant of N-linked core-glycosylation efficiency. *J. Biol. Chem.* **271,** 6363-6366.

Shen, N. V., Chen, X., Boyer, M. M. and Pfaffinger, P. J. (1993). Deletion analysis of K+ channel assembly. *Neuron* **11,** 67-76.

Shen, N. V. and Pfaffinger, P. J. (1995). Molecular recognition and assembly sequences involved in the subfamily-specific assembly of voltage-gated K+ channel subunit proteins. *Neuron* **14,** 625-633.

Shi, W., Wymore, R., Yu, H., Wu, J., Wymore, R. T., Pan, Z., Robinson, R. B., Dixon, J. E., McKinnon, D. and Cohen, I. S. (1999). Distribution and prevalence of hyperpolarization-activated cation channel (HCN) mRNA expression in cardiac tissues. *Circ. Res.* **85,** e1-6.

Stieber, J., Stockl, G., Herrmann, S., Hassfurth, B. and Hofmann, F. (2005). Functional expression of the human HCN3 channel. *J. Biol. Chem.* **280,** 34635-34643.

Stillitano, F., Lonardo, G., Zicha, S., Varro, A., Cerbai, E., Mugelli, A. and Nattel, S. (2008). Molecular basis of funny current (if) in normal and failing human heart. *J. Mol. Cell. Cardiol.* **45,** 289-299.

Szidonya, L., Cserzo, M. and Hunyady, L. (2008). Dimerization and oligomerization of G-protein-coupled receptors: Debated structures with established and emerging functions. *J. Endocrinol.* **196,** 435-453.

Takhar, S., Gyomorey, S., Su, R. C., Mathi, S. K., Li, X. and Wheeler, M. B. (1996). The third cytoplasmic domain of the GLP-1[7-36 amide] receptor is required for coupling to the adenylyl cyclase system. *Endocrinology* **137,** 2175-2178.

Tan, C. M., Brady, A. E., Nickols, H. H., Wang, Q. and Limbird, L. E. (2004). Membrane trafficking of G protein-coupled receptors. *Annu. Rev. Pharmacol. Toxicol.* **44,** 559-609.

Terrillon, S. and Bouvier, M. (2004). Roles of G-protein-coupled receptor dimerization. *EMBO Rep.* **5,** 30-34.

Terrillon, S., Durroux, T., Mouillac, B., Breit, A., Ayoub, M.A., Taulan, M., Jockers, R., Barberis, C. and Bouvier, M. (2003). Oxytocin and vasopressin V1a and V2 receptors form constitutive homo- and heterodimers during biosynthesis. *Mol. Endocrinol.* **17,** 677-691.

Thorens, B. (1992). Expression cloning of the pancreatic beta cell receptor for the gluco-incretin hormone glucagon-like peptide 1. *Proc. Natl. Acad. Sci. U. S. A.* **89,** 8641-8645.

Tran, N., Proenza, C., Macri, V., Petigara, F., Sloan, E., Samler, S. and Accili, E. A. (2002). A conserved domain in the NH2 terminus important for assembly and functional expression of pacemaker channels. *J. Biol. Chem.* **277,** 43588-43592.

Trombetta, E. S. (2003). The contribution of N-glycans and their processing in the endoplasmic reticulum to glycoprotein biosynthesis. *Glycobiology* **13,** 77R-91R.

Tseng, C. C. and Zhang, X. Y. (1998a). The cysteine of the cytoplasmic tail of glucose-dependent insulinotropic peptide receptor mediates its chronic desensitization and down-regulation. *Mol. Cell. Endocrinol.* **139,** 179-186.

Tseng, C. C. and Zhang, X. Y. (1998b). Role of regulator of G protein signaling in desensitization of the glucose-dependent insulinotropic peptide receptor. *Endocrinology* **139,** 4470-4475.

Tseng, C. C. and Zhang, X. Y. (2000). Role of G protein-coupled receptor kinases in glucose-dependent insulinotropic polypeptide receptor signaling. *Endocrinology* **141,** 947-952.

Tu, L., Santarelli, V., Sheng, Z., Skach, W., Pain, D. and Deutsch, C. (1996). Voltage-gated K+ channels contain multiple intersubunit association sites. *J. Biol. Chem.* **271,** 18904-18911.

Ulens, C. and Tytgat, J. (2001). Functional heteromerization of HCN1 and HCN2 pacemaker channels. *J. Biol. Chem.* **276,** 6069-6072.

Underwood, C. R., Garibay, P., Knudsen, L. B., Hastrup, S., Peters, G. H., Rudolph, R. and Reedtz-Runge, S. (2010). Crystal structure of glucagon-like peptide-1 in complex with the extracellular domain of the glucagon-like peptide-1 receptor. *J. Biol. Chem.* **285,** 723-730.

Usdin, T. B., Mezey, E., Button, D. C., Brownstein, M. J. and Bonner, T. I. (1993). Gastric inhibitory polypeptide receptor, a member of the secretin-vasoactive intestinal peptide receptor family, is widely distributed in peripheral organs and the brain. *Endocrinology* **133,** 2861-2870.

van Koppen, C. J. and Nathanson, N. M. (1990). Site-directed mutagenesis of the m2 muscarinic acetylcholine receptor. analysis of the role of N-glycosylation in receptor expression and function. *J. Biol. Chem.* **265,** 20887-20892.

Vazquez, P., Roncero, I., Blazquez, E. and Alvarez, E. (2005). Substitution of the cysteine 438 residue in the cytoplasmic tail of the glucagon-like peptide-1 receptor alters signal transduction activity. *J. Endocrinol.* **185,** 35-44.

Vidi, P. A., Chen, J., Irudayaraj, J. M. and Watts, V. J. (2008). Adenosine A(2A) receptors assemble into higher-order oligomers at the plasma membrane. *FEBS Lett.* **582,** 3985-3990.

Vrecl, M., Drinovec, L., Elling, C. and Heding, A. (2006). Opsin oligomerization in a heterologous cell system. *J. Recept. Signal Transduct. Res.* **26,** 505-526.

Wahl-Schott, C. and Biel, M. (2009). HCN channels: Structure, cellular regulation and physiological function. *Cell Mol. Life Sci.* **66,** 470-494.

Wainger, B. J., DeGennaro, M., Santoro, B., Siegelbaum, S. A. and Tibbs, G. R. (2001). Molecular mechanism of cAMP modulation of HCN pacemaker channels. *Nature* **411,** 805-810.

Waldhoer, M., Fong, J., Jones, R. M., Lunzer, M. M., Sharma, S. K., Kostenis, E., Portoghese, P. S. and Whistler, J. L. (2005). A heterodimer-selective agonist shows in vivo relevance of G protein-coupled receptor dimers. *Proc. Natl. Acad. Sci. U. S. A.* **102,** 9050-9055.

Wanamaker, C. P. and Green, W. N. (2005). N-linked glycosylation is required for nicotinic receptor assembly but not for subunit associations with calnexin. *J. Biol. Chem.* **280,** 33800-33810.

Wang, M., Ramos, B. P., Paspalas, C. D., Shu, Y., Simen, A., Duque, A., Vijayraghavan, S., Brennan, A., Dudley, A., Nou, E., Mazer, J. A., McCormick, D. A., Arnsten, A. F. (2007). Alpha2A-adrenoceptors strengthen working memory networks by inhibiting cAMP-HCN channel signaling in prefrontal cortex. *Cell* **129,** 397-410.

Warne, T., Serrano-Vega, M. J., Baker, J. G., Moukhametzianov, R., Edwards, P. C., Henderson, R., Leslie, A. G., Tate, C. G. and Schertler, G. F. (2008). Structure of a beta1-adrenergic G-protein-coupled receptor. *Nature* **454,** 486-491.

Wei, Y. and Mojsov, S. (1995). Tissue-specific expression of the human receptor for glucagon-like peptide-I: Brain, heart and pancreatic forms have the same deduced amino acid sequences. *FEBS Lett.* **358,** 219-224.

Weitz, D., Ficek, N., Kremmer, E., Bauer, P. J. and Kaupp, U. B. (2002). Subunit stoichiometry of the CNG channel of rod photoreceptors. *Neuron* **36,** 881-889.

Wheeler, M. B., Gelling, R. W., Hinke, S. A., Tu, B., Pederson, R. A., Lynn, F., Ehses, J. and McIntosh, C. H. (1999). Characterization of the carboxyl-terminal domain of the rat glucose-dependent insulinotropic polypeptide (GIP) receptor. A role for serines 426 and 427 in regulating the rate of internalization. *J. Biol. Chem.* **274,** 24593-24601.

Wheeler, M. B., Lu, M., Dillon, J. S., Leng, X. H., Chen, C. and Boyd, A. E.,3rd. (1993). Functional expression of the rat glucagon-like peptide-I receptor, evidence for coupling to both adenylyl cyclase and phospholipase-C. *Endocrinology* **133,** 57-62.

White, J. H., Wise, A., Main, M. J., Green, A., Fraser, N. J., Disney, G. H., Barnes, A. A., Emson, P., Foord, S. M. and Marshall, F. H. (1998). Heterodimerization is required for the formation of a functional GABA(B) receptor. *Nature* **396,** 679-682.

Whorton, M. R., Bokoch, M. P., Rasmussen, S. G., Huang, B., Zare, R. N., Kobilka, B. and Sunahara, R. K. (2007). A monomeric G protein-coupled receptor isolated in a high-density lipoprotein particle efficiently activates its G protein. *Proc. Natl. Acad. Sci. U. S. A.* **104,** 7682-7687.

Whorton, M. R., Jastrzebska, B., Park, P. S., Fotiadis, D., Engel, A., Palczewski, K. and Sunahara, R. K. (2008). Efficient coupling of transducin to monomeric rhodopsin in a phospholipid bilayer. *J. Biol. Chem.* **283,** 4387-4394.

Widmann, C., Dolci, W. and Thorens, B. (1995). Agonist-induced internalization and recycling of the glucagon-like peptide-1 receptor in transfected fibroblasts and in insulinomas. *Biochem. J.* **310 (Pt 1),** 203-214.

Widmann, C., Dolci, W. and Thorens, B. (1996a). Desensitization and phosphorylation of the glucagon-like peptide-1 (GLP-1) receptor by GLP-1 and 4-phorbol 12-myristate 13-acetate. *Mol. Endocrinol.* **10,** 62-75.

Widmann, C., Dolci, W. and Thorens, B. (1996b). Heterologous desensitization of the glucagon-like peptide-1 receptor by phorbol esters requires phosphorylation of the cytoplasmic tail at four different sites. *J. Biol. Chem.* **271,** 19957-19963.

Widmann, C., Dolci, W. and Thorens, B. (1997). Internalization and homologous desensitization of the GLP-1 receptor depend on phosphorylation of the receptor carboxyl tail at the same three sites. *Mol. Endocrinol.* **11,** 1094-1102.

Wilmen, A., Göke, B. and Göke, R. (1996). The isolated N-terminal extracellular domain of the glucagon-like peptide-1 (GLP)-1 receptor has intrinsic binding activity. *FEBS Lett.* **398,** 43-47.

Winklmeier, A., Weyand, M., Schreier, C., Kalbitzer, H. R. and Kremer, W. (2009). Crystallization and preliminary X-ray diffraction studies of the tetramerization domain derived from the human potassium channel Kv1.3. *Acta Crystallogr. Sect. F. Struct. Biol. Cryst. Commun.* **65,** 688-691.

Xiao, Q., Jeng, W. and Wheeler, M. B. (2000). Characterization of glucagon-like peptide-1 receptor-binding determinants. *J. Mol. Endocrinol.* **25,** 321-335.

Xu, J., He, J., Castleberry, A. M., Balasubramanian, S., Lau, A. G. and Hall, R. A. (2003). Heterodimerization of alpha 2A- and beta 1-adrenergic receptors. *J. Biol. Chem.* **278,** 10770-10777.

Xu, J., Yu, W., Jan, Y. N., Jan, L. Y. and Li, M. (1995). Assembly of voltage-gated potassium channels. conserved hydrophilic motifs determine subfamily-specific interactions between the alpha-subunits. *J. Biol. Chem.* **270,** 24761-24768.

Xu, Y., Piston, D. W., Johnson, C. H. (1999). A bioluminescence resonance energy transfer (BRET) system: application to interacting circadian clock proteins. *Proc. Natl. Acad. Sci. U.S.A.* **96,** 151-156.

Xue, T., Marban, E. and Li, R. A. (2002). Dominant-negative suppression of HCN1- and HCN2-encoded pacemaker currents by an engineered HCN1 construct: Insights into structure-function relationships and multimerization. *Circ. Res.* **90,** 1267-1273.

Yanagihara, K. and Irisawa, H. (1980). Inward current activated during hyperpolarization in the rabbit sinoatrial node cell. *Pflugers Arch.* **385,** 11-19.

Ye, B. and Nerbonne, J. M. (2009). Proteolytic processing of HCN2 and co-assembly with HCN4 in the generation of cardiac pacemaker channels. *J. Biol. Chem.* **284,** 25553-25559.
Yip, R. G., Boylan, M. O., Kieffer, T. J. and Wolfe, M. M. (1998). Functional GIP receptors are present on adipocytes. *Endocrinology* **139,** 4004-4007.

Yu, F. H., Yarov-Yarovoy, V., Gutman, G. A. and Catterall, W. A. (2005). Overview of molecular relationships in the voltage-gated ion channel superfamily. *Pharmacol. Rev.* **57,** 387-395.

Zerangue, N., Schwappach, B., Jan, Y. N. and Jan, L. Y. (1999). A new ER trafficking signal regulates the subunit stoichiometry of plasma membrane K(ATP) channels. *Neuron* **22,** 537-548.

Zha, Q., Brewster, A. L., Richichi, C., Bender, R. A. and Baram, T. Z. (2008). Activity-dependent heteromerization of the hyperpolarization-activated, cyclic-nucleotide gated (HCN) channels: Role of N-linked glycosylation. *J. Neurochem.* **105,** 68-77.

Zhong, H., Lai, J. and Yau, K. W. (2003). Selective heteromeric assembly of cyclic nucleotide-gated channels. *Proc. Natl. Acad. Sci. U. S. A.* **100,** 5509-5513.

Zhong, H., Molday, L. L., Molday, R. S. and Yau, K. W. (2002). The heteromeric cyclic nucleotide-gated channel adopts a 3A:1B stoichiometry. *Nature* **420,** 193-198.

Zhong, X., Kriz, R., Seehra, J. and Kumar, R. (2004). N-linked glycosylation of platelet P2Y12 ADP receptor is essential for signal transduction but not for ligand binding or cell surface expression. *FEBS Lett.* **562,** 111-117.

Zhu, X. and Wess, J. (1998). Truncated V2 vasopressin receptors as negative regulators of wild-type V2 receptor function. *Biochemistry* **37,** 15773-15784.

2 HCN2 AND HCN4 ISOFORMS SELF-ASSEMBLE AND CO-ASSEMBLE WITH EQUAL PREFERENCE TO FORM FUNCTIONAL PACEMAKER CHANNELS[1]

2.1 Introduction

Hyperpolarization-activated Cyclic Nucleotide-modulated (HCN) channels, which underlie hyperpolarization-activated or funny currents (Ih or If) in excitable cells, are made up of subunits which assemble as tetramers to form functional channels (Robinson and Siegelbaum, 2003). Four mammalian HCN isoforms, (HCN1-4) (Gauss et al., 1998; Ishii et al., 1999; Ludwig et al., 1998; Santoro et al., 1997; Santoro et al., 1998), possess various overlapping patterns of expression in the heart and throughout the central nervous system suggesting they could form heteromeric channels in these tissues (Accili et al., 2002; Kaupp and Seifert, 2001; Robinson and Siegelbaum, 2003). Previous studies suggested that the following combinations of HCN isoforms are able to co-assemble and form functional channels in heterologous expression systems: HCN1 with HCN2 (Altomare et al., 2003; Chen et al., 2001; Proenza et al., 2002; Ulens and Tytgat, 2001), and HCN1 with HCN4 (Altomare et al., 2003). On the other hand, whether HCN2 and HCN4 isoforms co-assemble and form functional channels has been suggested but not directly shown, and therefore is an important objective of the present experiments.

The best evidence for coassembly of HCN2 and HCN4 in native tissue comes from studies in the embryonic heart and adult thalamus. In the embryonic mouse heart, mRNA for HCN2, and both mRNA and protein for HCN4, have been found (Garcia-Frigola et al., 2003; Mommersteeg et al., 2007; Stieber et al., 2003; Yasui et al., 2001). Knockout of HCN4 reduced, but did not abolish, I_f and increased rates of I_f activation in myocytes of the embryonic heart consistent with the presence of other HCN isoforms in these cells (Stieber et al., 2003). Immunohistochemical approaches have demonstrated HCN2 and HCN4 protein in thalamocortical relay nuclei (Notomi and Shigemoto, 2004; Santoro et al., 2000), and colocalization in cells of the ventrobasal complex and reticular nucleus of the thalamus (Abbas et al., 2006). Finally, knockout of HCN2 reduced, but again did not abolish, I_f in

[1] A version of this chapter has been published. Whitaker GM, Angoli D, Nazzari H, Shigemoto R, Accili EA. (2007). HCN2 and HCN4 isoforms self-assemble and co-assemble with equal preference to form functional pacemaker channels. *Journal of Biological Chemistry* 282, 22900-22909

thalamocortical neurons, consistent with the presence of other HCN isoforms in these cells (Ludwig et al., 2003).

Co-assembly of HCN2 and HCN4 is supported by evidence of interaction of the two isoforms in heterologous expression systems. When co-expressed in human embryonic kidney cells, HCN2 and HCN4 were found to both colocalize and co-immunoprecipitate, and cell surface fluorescence of an HCN2 trafficking mutant channel was rescued when co-expressed with HCN4 (Much et al., 2003). Reduction in HCN4 current density following co-expression with a non-functional HCN2 pore mutant in Chinese Hamster Ovary (CHO) cells (Er et al., 2003) also suggests that HCN2 and HCN4 interact in a physical and/or functional way. Although these data could be explained by co-assembly of HCN2 and HCN4, they can also be readily explained by indirect interactions other than co-assembly. For example, functional and physical associations between ion channel subunits have been reported for voltage-gated potassium channels, which are distantly related in primary structure and do not co-assemble. One example is between the human-ether-a-go-go related gene (HERG) and KCNQ1 which exist as separate groups of homomeric channels within macromolecular complexes both in native tissue and when overexpressed in mammalian cells (Ehrlich et al., 2004). Therefore, these data suggest, but do not confirm the formation of functional heteromeric HCN2-HCN4 channels.

Evidence in favor of functional co-assembly of HCN2 and HCN4 in live cells comes from single I_f channel recordings in co-transfected CHO cells. These single channels possessed intermediate activation kinetics, in theory reflecting contributions from both subunits (Michels et al., 2005). However, whether the measured channels in that study truly represent HCN channels remains controversial (Dekker and Yellen, 2006; DiFrancesco, 1986; Johnson and Zagotta, 2005).

Among the HCN isoforms that do coassemble, whether HCN isoforms have a preference for self-assembly over co-assembly with other isoforms is not known. Because the primary amino acid sequences of the four mammalian HCN isoforms are very similar, it is possible that their abilities to self- or to co-assemble may also be similar. After exclusion of the non-conserved regions of the cytoplasmic N- and C-termini, the amino acid homology among the four mammalian isoforms is very high (≥ 94% conserved), and HCN2 and HCN4 isoforms bear the strongest conservation of primary sequence among the four isoforms (≥ 96% conserved) (Jackson et al., 2007). However, the differences between HCN2 and HCN4, both

those within the conserved region as well as those within the cytoplasmic N and C-termini, could modify the extent to which these isoforms co-assemble under different conditions.

In this study, we demonstrate that co-assembly of HCN2 and HCN4 in live CHO cells occurs with equal preference compared to self-assembly, using multiple approaches including Bioluminescence Resonance Energy Transfer (BRET), a novel approach to analyze tetramerization of ion channel subunits. BRET measurements, together with results from electrophysiological and imaging experiments, demonstrate that HCN2 and HCN4 subunits co-assemble, and that they do so with equal preference to self-assembly when expressed in CHO cells. Finally, we provide evidence in support of the co-assembly of HCN2 and HCN4 in the rat thalamus and embryonic mouse heart.

2.2 Experimental Procedures

2.2.1 Molecular Biology

The construction of an HCN2 C-terminal deletion (lacking the cyclic nucleotide binding domain and the remainder of the C-terminus distal to it, HCN2ΔCNBD) was described previously (Proenza et al., 2002; Tran et al., 2002). An extracellular HA epitope was inserted between the S3 and S4 transmembrane domain of HCN2ΔCNBD (Figure 2.4A). This construct was made by digesting HCN2-HA (kind gift from Dr MC Sanguinetti) at common HCN2 restriction sites such that the HA tag was removed and placed in HCN2ΔCNBD. For BRET constructs, *Renilla*-luciferase (Rluc) or Green Fluorescent Protein (GFP) tags were added to the N-terminal end of HCN2, HCN2ΔN lacking residues 2-189 as described previously (Proenza et al., 2002), HCN4 or Kv1.5 cDNA. BRET vectors (pRlucC and pGFPC, Perkin Elmer Inc. MA, USA) were digested at restriction sites complementary to those present on 5' and 3' ends of HCN2, HCN4 or Kv1.5, such that the tags were expressed in frame with the channel cDNA when ligated. Resulting sequences were confirmed by automated DNA sequencing (DNA sequencing core facility, Vancouver, British Columbia). All tagged constructs were tested by patch clamp electrophysiology and produced currents characteristic of their wild type counterparts (data not shown).

2.2.2 Cell Culture and Expression

CHO-K1 cells (American Type Culture Collection, VA, USA) were maintained in Hams F-12 medium (Invitrogen, Ontario, Canada) supplemented with 50μg/ml penicillin / streptomycin (Invitrogen) and 10% fetal bovine serum (Invitrogen), and incubated at 37°C with 5% CO_2. For electrophysiology and immunocytochemistry, cells were plated onto glass coverslips in 35 mm dishes. After 48h, CHO cells were transiently transfected with mammalian expression vectors encoding wild type and/or mutant channels (2 μg per dish) using FuGene6 transfection reagent (Roche Diagnostics, Quebec, Canada). For electrophysiology, cells were also co-transfected with the GFP reporter plasmid for identification using fluorescent microscopy (0.5-0.7 μg per dish).

2.2.3 Whole Cell Patch Clamp Electrophysiology and Analysis

One to two days following transfection, a shard of coverslip plated with cells was transferred to a recording chamber (~ 200 μl volume) and continually perfused (0.5 - 1.0 ml/min) with a low K^+ extracellular solution (5.4 mM KCl, 135 mM NaCl, 0.5 mM $MgCl_2$, 1.8 mM $CaCl_2$, 5 mM HEPES, pH to 7.4 with NaOH). Following rupture of the patch membrane, the solution was changed to a high K^+ recording solution (135 mM KCl, 5.4 mM NaCl, 0.5 mM $MgCl_2$, 1.8 mM $CaCl_2$, 5 mM HEPES, pH to 7.4 with KOH) to maximize current amplitude. Patch pipettes were filled with a solution containing 130 mM K-aspartate, 10 mM NaCl, 0.5 mM $MgCl_2$, 5 mM HEPES, and 1 mM EGTA and adjusted to pH of 7.4 with KOH. In some experiments, this solution was supplemented with 2 mM cAMP (as noted). Whole-cell hyperpolarization-activated currents (I_f) were measured using borosilicate glass electrodes (Sutter Instrument Co, CA, USA), which had a resistance of 2.0-4.0 MΩ when filled with the intracellular solution. Currents were recorded using an Axopatch 200B amplifier and Clampex software (Axon Instruments Inc.). Data were filtered at 2 kHz and were analyzed using Clampfit (Molecular devises, CA, USA) and Origin (Microcal, CA, USA) software. All experiments were conducted at room temperature (20-22 °C). Currents were not leak-subtracted. The voltage-dependence of activation was determined from tail currents at -65 mV following 2s test pulses ranging from -50 mV to –150 mV, in 20 mV steps.

Normalized tail current amplitudes were plotted as a function of test potential and values were fit with a Boltzmann function

$$f(V) = I_{max}/(1 + e^{(V_{1/2}-V)/k})$$

to determine the midpoint of activation ($V_{1/2}$) and slope factor (k). Each test pulse was followed by a 200-500 ms pulse to +5 mV to ensure complete channel deactivation, and the resting current was allowed to return to its baseline value before subsequent voltage pulses. Time constants to assess rates of I_f activation were generated using a single exponential fitting procedure. An initial delay during I_f activation was not well described by a single exponential function therefore was not used in our fits (Altomare et al., 2001;Santoro et al., 2000).

2.2.4 Immunocytochemistry, Fluorescence Microscopy with Structured Illumination and Determination of Pearson Correlation Coefficients

Forty-eight hours after transfection, cells on coverslips were washed briefly with PBS and fixed with 2% paraformaldehyde in PBS for 5min. Fixed cells were washed twice with PBS, some were permeabilized for 10min using 0.2% Triton X-100, and all were blocked with 10% normal goat serum (NGS) and 10% BSA for 10 minutes. After one wash with PBS containing 1% NGS, cells were incubated with primary antibodies for 1 hour at room temperature. Anti-HA (Sigma-Aldrich, Ontaria, Canada) or anti-Rluc (Chemicon International Inc., CA, USA) mouse monoclonal antibodies were used as needed at a dilution of 1:500 in 1%NGS/PBS. Cells were subsequently washed with PBS three times, and incubated with Alexa-555 tagged goat anti-mouse secondary antibodies (Molecular Probes, Ontario, Canada) at a dilution of 1:1500 in PBS with 1% NGS+BSA for one hour at room temperature in the dark. After washing 3 times in PBS, coverslips were rinsed in ddH_2O and mounted on slides using Gel Mount (Sigma-Aldrich Inc.). Cells were visualized using a Zeiss Axiovert 200 fluorescence microscope with Apotome structured illumination module, with a 63X oil immersion objective lens. Results reported represent a minimum of four transfections for each set of the imaging experiments described. To correlate intensities of fluorescence for each pair of proteins, Pearson correlation coefficients were calculated from individual cells co-transfected with different combinations of Kv1.5 and/or HCN isoforms, tagged with GFP or

Rluc. Calculation of the Pearson correlation coefficient from captured images of individual cells was determined by the following equation:

$$\frac{\Sigma [(GVC1 - MVCI) \times (GVC2 - MVC2)]}{\sqrt{[\Sigma(GVC1 - MVC1)^2 \times \Sigma(GVC2 - MVC2)^2]}}$$

(GV: Gray value; MV: Mean value; C: Channel.)

This allows channel 1 and channel 2 to be related by a linear equation [GVC2=a*(GVC1) + b)]. The values range from -1 to +1 representing an increasing correlation of the voxel intensities of channel 1 and 2. Therefore, the Pearson correlation coefficient describes the relationship of varying intensities of fluorescence between two proteins of interest throughout a cell.

2.2.5 Bioluminescence Resonance Energy Transfer (BRET) Analysis

BRET experimental methods were based on a study examining the dimerization of G protein-coupled receptors (Mercier et al., 2002). CHO cells were transiently transfected with a constant amount (0.5µg) of Rluc-tagged and varying amounts of GFP-tagged constructs (0.5µg-2.0µg) in order to measure optimal expression ratios for BRET experiments. Forty-eight hours after transfection, cells were washed twice with D-PBS (Invitrogen), detached with 0.05% Trypsin-EDTA (Invitrogen) and resuspended in D-PBS supplemented with 2µg/ml aprotinin. Approximately 100,000 cells were then distributed into individual wells of 96-well Optiplates (Perkin Elmer). Using a Victor 3V plate reader (Perkin Elmer), expression of GFP-tagged constructs was assessed by directly exciting GFP with a 400-410nm excitation filter. Expression of Rluc-tagged constructs was assessed using luminescence values obtained in the BRET assay. Fold over background of emission was determined for both Rluc- and GFP-tagged constructs by comparing luminescence and fluorescence values to background values in untransfected cells. Although we varied the amount of cDNA of the GFP-tagged constructs, the resulting expression levels did not vary greatly and therefore all samples were used in subsequent BRET experiments. For BRET measurements, DeepBlueC substrate (Perkin Elmer) was added to cells (final concentration of 5µM) and Rluc emission was measured through a 370-450 nm filter. Resulting GFP emission was in turn measured through a 500-530nm filter. BRET ratios were calculated by the ratio of GFP emission to Rluc emission.

Ratios were corrected for background by subtracting emission ratios from untransfected cells after addition of DeepBlueC substrate. BRET values are expressed as the mean ± SD for 6 independent experiments for each set of constructs performed in duplicate and using different Rluc-tagged: GFP-tagged transfection ratios in each experiment (n=24). Graphical presentation and statistical analysis were performed using Prism 4 software (GraphPad Software, CA, USA).

2.2.6 Immunoprecipitation and Western Blotting of Rat Thalamus

Rat thalami were obtained as previously described (Ghavanini et al., 2005). Tissue was processed in RIPA lysis buffer (50mM Tris at pH 8.0, 1% NP-40, 150mM NaCl, 1mM EDTA, 1mM PMSF, 2mM each of Na_3VO_4 and NaF, and 10ug/mL each of aprotinin, pepstatin and leupeptin) by multiple passes through 16G, then 23G syringes, and incubated on ice for 30min, followed by centrifugation to remove cell debris. Lysates were precleared with normal rabbit IgG and protein-A beads (Sigma-aldrich) for 2h at 4°C and then incubated with primary antibodies (rabbit anti-HCN2 or rabbit anti-HCN4, Alomone Labs, Israel) and protein A beads overnight at 4°C. For negative controls, primary antibodies were preincubated with supplied antigens for 1 hour prior to incubation with precleared lysates. Beads were collected by centrifugation and washed 3 times in ice cold PBS then boiled in sample buffer with 2-mercaptoethanol for 10min, then loaded into 8% SDS-PAGE gels. Gels were transferred to PVDF membranes, blots were washed 2 times in TBS-T, then blocked with 5% non-fat dry milk in TBS-T for 1 hour. Blots were incubated with primary antibody overnight at 4°C (guinea pig anti-HCN4 – 1:500, or rabbit anti-HCN2 – 1:400) in 5% non-fat milk with 3% BSA. After 3 washes with TBS-T, blots were incubated with horseradish peroxidase-conjugated secondary antibodies at a dilution of 1:3000 in 5% non-fat milk for 1 hour at room temperature. After 3 washes with TBS-T, signals were obtained with ECL detection reagents (GE Healthcare, NJ, USA). All IP experiments were carried out in triplicate (n=3 rats).

2.2.7 Immunohistochemistry

Mouse day 18 embryos were obtained from CD1 mice. Isolated tissue was cryosectioned into 10µm sections, mounted on poly-L lysine treated slides (Wax-it histology services, UBC) and stored at -80°C. Sections were fixed in 4% paraformaldehyde for 10min, then washed twice with PBS. Sections were then permeabilized with 0.2% Triton X-100 for

15min, washed 3 times in PBS, then blocked with 10% normal donkey serum in PBS for 1 hour at room temperature. Sections were then incubated with primary antibody overnight at 4°C. Primary antibody dilutions were as follows: guinea pig anti-HCN2 and anti-HCN4 (Notomi and Shigemoto, 2004) 1:500, goat anti-HCN4 (Santa Cruz Biotechnology Inc., CA, USA) 1:50, and rabbit anti-HCN2 (Alomone Labs) 1:200. For negative controls, tissue sections were incubated with either goat or guinea pig IgG, or with rabbit anti-HCN2 preincubated with its supplied antigen (3:1 antigen to antibody ratio). Tissue sections were washed 3 times in PBS, followed by incubation with Alexa 488 or 555 - tagged secondary antibodies raised in donkey (1:1000, Molecular Probes). After 3 washes in PBS, DAPI (Molecular Probes, 1:50000) was added to tissue for 5min, followed by 2 washes in PBS. Coverslips were mounted on tissue using GelMount (Sigma-Aldrich) and heart tissue was visualized as described for transfected cells. These experiments were carried out on sections of heart tissue from two embryonic mice. In each field of view, four areas were analyzed. Correlation coefficients were determined in each area and averaged to yield one value per field of view. Values for Pearson Correlation Coefficients were presented as means ± s.e.m. in *N* number of fields of view.

2.3 Results

2.3.1 Tetrameric Assembly of HCN2 and HCN4 Isoforms

Because of their similarity to voltage-gated potassium channels, HCN channels are likely tetrameric and their co-assembly can be described by a binomial distribution. This distribution is determined from the proportion of subunits present to the n^{th} power (p^n), where 'n' is equal to the number of different subunit isoforms in a given channel (Hille, 2001). When co-expressed, two isoforms with equal preference for homomeric and heteromeric assembly will co-assemble according to a binomial distribution, while any preference toward homomeric or heteromeric assembly would alter this distribution pattern.

Here, we sought to determine whether HCN2 and HCN4 subunits co-assemble to form heteromeric channels and whether they exhibit a preference for homomeric versus heteromeric assembly. This was accomplished using two approaches in which HCN2 and HCN4 were tagged to Rluc or GFP epitopes. Co-transfection allowed us to obtain measurements from channels made up of a mixture of subunits possessing each tag (Figure 2.1, bracketed section).

Thus, both self-assembly and co-assembly could be determined independently and compared. These assays cannot measure channels made up of subunits containing the same tag, or differentiate among channels that exhibit different stoichiometries, but they can report on the sum of all channels possessing both subunits.

We utilized the voltage-gated channel subunit Kv1.5 as a negative control. Kv1.5 is found in the same superfamily as the HCN channel family and has a similar overall structure, but is not expected to co-assemble with HCN subunits. However, when co-expressed in CHO cells, Kv1.5 is highly colocalized with both HCN2 and HCN4, as determined by measuring colocalization coefficients in the present imaging studies (see below). Thus, Kv1.5 provides a critical negative control for potential interactions among subunits that did not involve co-assembly. These types of interactions include both specific interactions, for example between adjacent but separate tetrameric channels, and non-specific interactions possibly due to overexpression of protein in intracellular compartments. Co-transfection of differentially tagged HCN2 and HCN4 with themselves provide positive controls for co-assembly.

2.3.2 Homomeric and Heteromeric Combinations of HCN2 and HCN4 Produce Equally High Pearson Correlation Coefficients in CHO Cells

We first acquired immunofluorescent images of CHO cells co-expressing constructs tagged with GFP or Rluc (Figure 2.2A), and determined the extents to which the intensities of their fluorescence correlated. To quantify this, we utilized a Pearson correlation (see Methods). For two subunits that co-assemble to form a tetrameric ion channel, their varying levels of expression throughout a cell would be expected to be interdependent. Therefore, the variation of their intensities of fluorescence would correlate to a greater extent than for two subunits that associate in another way (e.g. two subunits that form separate channels which are localized to a similar region) or that do not associate at all, and yield a positive Pearson Correlation Coefficient.

We co-transfected CHO cells with HCN2-GFP or HCN4-GFP with HCN2-Rluc, HCN4-Rluc or Kv1.5-Rluc and correlated the intensities of fluorescence for each combination of two isoforms. A strength of this approach is that the same molecules, GFP and Rluc, were measured for all correlations, thus there is no variability in our measurements due to the use of different antibodies. We hypothesized that HCN2 or HCN4, when co-transfected with

themselves or with each other, would yield Pearson correlation coefficients that were significantly higher than those produced by co-transfection of either HCN2 or HCN4 with Kv1.5, if they formed homomeric or heteromeric channels.

We found that Pearson Correlation Coefficients were significantly larger in cells co-transfected with HCN2-GFP and HCN2-Rluc, HCN2-GFP and HCN4-Rluc, HCN4-GFP and HCN4-Rluc, or HCN4-GFP and HCN2-Rluc, than those determined from cells that were co-transfected with either HCN2-GFP or HCN4-GFP, and Kv1.5-Rluc (Figure 2.2B,C). Since HCN isoforms do not co-assemble with Kv1.5, the larger Pearson correlation coefficients determined for the different combinations of HCN subunits suggest co-assembly among them. This conclusion is strengthened by our finding that Pearson correlation coefficients determined from cells co-transfected with HCN2-GFP and HCN2-Rluc, or HCN4-GFP and HCN4-Rluc (which are expected to self-assemble), were not significantly different from those determined from cells co-transfected with HCN2-GFP and HCN4-Rluc, or HCN4-GFP and HCN2-Rluc, respectively. These similarities also suggest that HCN2 and HCN4 isoforms form homomeric channels and heteromeric channels with equal preference under these conditions.

It should be noted that Pearson correlation coefficients (which correlate the intensities of fluorescence of the two proteins in a given region), give more information about the nature of interaction between two proteins than simply quantifying the extent of co-localization. For example, although the Pearson correlations were significantly lower for combinations of Kv1.5 and HCN isoforms, the colocalization coefficient (which measure whether or not there is pixel overlap between two channels) was high ($r > 0.85$) for all combinations including those with Kv1.5 and HCN isoforms. This suggests that although Kv1.5 does not co-assemble with HCN2 or HCN4 isoforms, they do colocalize to similar regions within the cell. This is not unexpected because separate homomeric channels may share similar pathways of biogenesis and trafficking, and thus they may be localized to similar areas of cells, especially when overexpressed.

2.3.3 Homomeric and Heteromeric Combinations of HCN2 and HCN4 Produce Equally High BRET Ratios in CHO Cells

In order to study co-assembly of HCN2 and HCN4 channels in live cells, we utilized BRET technology. This approach, which has been widely used to examine and demonstrate receptor-protein interactions and receptor dimerization (Hébert et al., 2006), offers several advantages for the analysis of protein interactions. BRET measures two proteins which are located within 10 nm of each other. Like its methodological cousin, Fluorescence Energy Transfer or FRET, BRET allows for measurements in live cells and avoids a number of issues associated with more invasive approaches. Unlike FRET, BRET does not require an initial light source and thus avoids photobleaching. An added and powerful advantage is that BRET measurements are taken from a large population of live cells, rather than from individual cells (Milligan and Bouvier, 2005). Thus, BRET seems well suited for the determination of tetrameric ion channel assembly.

Once both Rluc- and GFP-tagged constructs are expressed in CHO cells, DeepBlueC is added to live cells, resulting in oxidation and emission at 380 nm. Emission at this wavelength excites GFP if the two proteins are within 10 nm of each other (Figure 2.3A,B). To test the ability of our system to detect BRET, we carried out experiments using CHO cells co-transfected with β_1-adrenergic receptors tagged with GFP or Rluc. We were able to reproduce previously published results showing high BRET ratios with β_1-adrenergic receptors (data not shown), which supports the formation of homodimers (Mercier et al., 2002). For these experiments, we hypothesized that HCN2 or HCN4, when co-transfected with themselves or with each other, would yield BRET values that were significantly higher than those produced by co-transfection of either HCN2 or HCN4 with Kv1.5.

We compared BRET ratios from cells co-transfected with the same combinations of tagged constructs used in the imaging experiments (above). In addition, we used CHO cells transfected with Kv1.5-Rluc to determine background levels of emission at 510 nm. We found that BRET ratios determined from cells co-transfected with HCN2-GFP and HCN2-Rluc, HCN2-GFP and HCN4-Rluc, HCN4-GFP and HCN4-Rluc, or HCN4-GFP and HCN2-Rluc were significantly larger that those obtained from cells co-transfected with either HCN2-GFP or HCN4-GFP, and Kv1.5-Rluc (Figure 2.3C,D). Furthermore, we found that the BRET ratios determined from cells co-transfected with HCN2-GFP or HCN4-GFP and Kv1.5-Rluc were

not significantly different from those determined from cells transfected with only Kv1.5-Rluc, indicating that our negative control produced near-background levels of BRET. These data strongly suggest that HCN2 and HCN4 co-assemble to form functional channels in live CHO cells. In addition, the levels of BRET determined from cells co-transfected with HCN2-GFP and HCN4-Rluc, or HCN4-GFP and HCN2-Rluc, were not significantly different from homomeric combinations of Rluc- and GFP-tagged constructs. These data further support an equal preference for homomeric and heteromeric channel assembly in live CHO cells.

Importantly, BRET values were similar between cells co-transfected with HCN4-GFP and HCN4-Rluc, and HCN2-GFP and HCN2-Rluc (between cells containing homomeric HCN2 channels or HCN4 channels), suggesting that the distances between GFP and Rluc tags in both homomeric channels were similar. Levels of emission among GFP-tagged constructs, and among Rluc-tagged constructs, were similar, also suggesting that the overall levels of expression among constructs were similar (for both BRET and imaging experiments).

As an additional negative control, we co-transfected CHO cells with wild type HCN2 or HCN4 and an N-terminally truncated HCN2 channel (HCN2ΔN). We have shown previously that the N-terminus is required for assembly and expression of functional HCN2 channels (Proenza et al., 2002; Tran et al., 2002). The BRET ratios for cells co-transfected with HCN2ΔN-Rluc and HCN2-GFP or HCN2ΔN-Rluc and HCN4-GFP were significantly lower than wild type but not significantly different from each other or from the Kv1.5-Rluc negative control (Figure 2.3E). These data support the coassembly of HCN2 and HCN4 isoforms.

2.3.4 Functional Evidence for Co-Assembly of HCN2 and HCN4 in CHO Cells

To obtain direct evidence for functional co-assembly of HCN2 and HCN4 channels in CHO cells, we used immunofluorescent imaging and the whole cell patch clamp approach to examine cell surface expression and functional rescue respectively, of a mutant HCN2 by wild type HCN4. This mutant HCN2 channel lacks the cyclic nucleotide binding domain and the distal C-terminus (HCN2ΔCNBD) and, when expressed alone, does not produce functional channels in CHO cells (Proenza et al., 2002) or HEK 293 cells (Stieber et al., 2003). This has been attributed to increased intracellular retention. We hypothesized that HCN4 would rescue mutant channel function and that cell surface expression of mutant HCN2 protein would be increased in cells transfected with both constructs.

In order to determine whether HCN2ΔCNBD protein could be rescued to the cell surface by HCN4, we utilized wild type and mutant HCN2 constructs that possessed an HA epitope on the extracellular S3-S4 linker. We examined the fluorescence intensity on the surface of non-permeabilized CHO cells transfected with HCN2-HA or HCN2ΔCNBD-HA alone or non-permeabilized cells co-transfected with HCN2ΔCNBD-HA and HCN4-GFP. At an exposure time of 50ms, HCN2ΔCNBD-HA fluorescence was only visible at the cell surface in cells that also expressed HCN4-GFP (Figure 2.4A). At this exposure time, intracellular fluorescence was observed at similar intensities in permeabilized cells transfected with HCN2-HA or HCN2ΔCNBD-HA, or co-transfected with HCN2ΔCNBD-HA and HCN4 (Proenza et al., 2002). This strongly suggests that the mutant channel was rescued to the cell surface when co-expressed with HCN4.

To support functional heteromerization between these isoforms, we next compared I_f in CHO cells transfected with HCN2 and HCN4, or with HCN2ΔCNBD and HCN4. Because wild type HCN2 homomeric channels display faster activation kinetics, and open at more positive potentials than homomeric HCN4 channels (Figure 2.4D), we hypothesized that in cells transfected with HCN4, co-transfection with HCN2ΔCNBD would confer faster rates of I_f activation and shift channel activation to more positive potentials.

The rates of I_f activation were considerably faster in cells co-transfected with both HCN4 and HCN2ΔCNBD compared to I_f in cells transfected with wild type HCN4 alone (Figure 2.4B,C) and were nearly as fast as for the wild type HCN2 channel. This could be explained in at least three ways. First, it could mean that the mutant HCN2 subunit dominated the rate at which the mixed channels open. This is consistent with previous findings from HCN1 and HCN2 co-expression where the faster HCN1 isoform largely dictated heteromeric channel activation kinetics (Ulens and Tytgat, 2001). Second, it could be explained by the presence of a large proportion of channels containing predominantly the mutant HCN2 subunit. This seems less likely given the fact that I_f density increased dramatically (see below), suggesting that the channels also contained a large proportion of HCN4 subunits. Third, this could reflect an intrinsic ability of the mutant subunit to activate more quickly than even the wild type HCN2. Although HCN2ΔCNBD does not produce functional channels in mammalian cells, it does form functional channels in *Xenopus* oocytes, which activate more rapidly than wild type HCN2 channels (Wainger et al., 2001). Thus, when HCN2ΔCNBD is co-transfected with HCN4 in our experiments, the resulting channels might be expected to

activate more quickly than otherwise, even in channels that contain equal numbers of both subunits.

We found that I_f activation curves were significantly shifted to more positive potentials (Figure 2.4D). These data support the co-assembly of HCN2ΔCNBD and HCN4 to form functional channels. Additionally, the slope of the I_f activation curve was unchanged in all cases. This is consistent with a predominantly heteromeric population of channels, since two independent populations of homomeric channels with different $V_{½}$ values would be expected to produce a single and more shallow activation curve (Chen et al., 2001).

Cyclic AMP binding to the CNBD allows HCN2 and HCN4 channels to open more easily in response to hyperpolarization (DiFrancesco and Tortora, 1991) and maximum facilitation of opening by cAMP requires binding by all four subunits (Ulens and Siegelbaum, 2003). Because the mutant HCN2 subunits lack the binding site for cAMP, heteromeric channels made up of HCN2ΔCNBD and HCN4 isoforms would be expected to respond less strongly to cAMP. To determine the ability of the channels to respond to cAMP, we compared I_f activation curves in the presence or absence of cAMP (2 mM cAMP in the pipette solution) from cells transfected with HCN4, or co-transfected with HCN4 and HCN2ΔCNBD. As expected, with cAMP present, the $V_{1/2}$ of activation significantly shifted (t-test, $p<0.02$) to more positive potentials in cells expressing only HCN4 alone by ~10 mV (without cAMP: $V_{1/2}$=-118.6 ± 1.8mV, n=26 cells; with cAMP: $V_{1/2}$ = -109.1 ± 3.4mV, n=7 cells). However, when HCN4 was co-expressed with HCN2ΔCNBD, there was no significant difference (t-test, $p>0.05$) in $V_{1/2}$ in the presence or absence of cAMP (without cAMP: $V_{1/2}$= -109.8± 3.1mV, n=12 cells; with cAMP: $V_{1/2}$=-115.2± 2.4 mV, n=5 cells). The lack of cAMP effect is consistent with a predominantly heteromeric population of channels in cells expressing HCN4 and HCN2ΔCNBD. Also, the position of the I_f activation curve in cells expressing HCN4, in the presence of cAMP, and in cells expressing HCN4 and HCN2ΔCNBD, were similar (~-109 mV). This similarity is expected because cAMP binding removes the inhibitory effect of the CNBD on the transmembrane regions, as would deletion of the CNBD, such that the channels can open at more positive voltages (Wainger et al., 2001).

Finally, we found that current density was significantly greater (more than doubled) in cells expressing both HCN4 and HCN2ΔCNBD compared to cells expressing either HCN2 or HCN4 alone (Figure 2.4E). Again, this is consistent with rescue of a significant amount of

HCN2ΔCNBD subunits to the cell surface by co-assembly with HCN4 and the formation of heteromeric channels.

2.3.5 Evidence Supporting Co-Assembly of HCN2 and HCN4 in Native Tissue

Colocalization of HCN2 and HCN4 has been documented in both the mouse and rat thalamus (Abbas et al., 2006; Notomi and Shigemoto, 2004). In addition, knockout of HCN2 reduced, but did not eliminate, I_f in thalamic neurons suggesting these cells possess other HCN isoforms (Ludwig et al., 2003). To determine if HCN2 and HCN4 physically interacted in the rat thalamus, we used immunoprecipitation. We found that when HCN4 was immunoprecipitated from thalamic tissue protein lysates, HCN2 was also detected in these complexes with HCN4 (Figure 2.5A). Similarly we were also able to immunoprecipitate HCN2 from tissue lysates, resulting in co-precipitation of HCN4 (Figure 2.5B).

There is evidence that HCN2 and HCN4 mRNA, as well as HCN4 protein, are detected in mouse embryonic cardiomyocytes (Garcia-Frigola et al., 2003;Mommersteeg et al., 2007;Stieber et al., 2003;Yasui et al., 2001). However, the presence and cellular distribution of HCN2 protein, and whether HCN2 and HCN4 colocalize, is unknown. Therefore, we analyzed the expression patterns of HCN2 and HCN4 in hearts from embryonic (E18) mice, using specific antibodies and immunohistochemistry. In sections of the atrium and ventricle, we found some areas where HCN2 and HCN4 colocalized (Figure 2.6). Other areas were also identified that showed expression of either HCN2 or HCN4, or that did not express either isoform. Next, we measured the Pearson correlation coefficient in regions of HCN2 and HCN4 co-expression. As described above, this is a measure of the extent to which the intensities of each isoform correlate and a positive correlation would be expected from two subunits that co-assemble to form a tetrameric channel. To do this, we measured four regions of co-expression from a number (n) of different fields of view. We found positive correlations of ~0.5 in these regions of co-expression (Figure 2.6C). This interdependent variation of intensity is consistent with co-assembly of HCN2 and HCN4 within these regions of colocalization.

To determine whether HCN2 and HCN4 physically interact in the embryonic heart, we used again used immunoprecipitation. We found that these isoforms could not be co-immunoprecipitated from this tissue. This negative result may be due to the distribution of HCN2 and HCN4 in regions where they do not colocalize. Because our functional data demonstrates a predominantly heteromeric population of channels in CHO cells transfected

with HCN2 and HCN4, their co-assembly in cardiomyocytes containing both isoforms seems possible.

2.4 Discussion

Our results demonstrate that HCN2 and HCN4 isoforms co-assemble to form functional heteromeric channels in live CHO cells. Furthermore, they delineate, for the first time, equal preference for co-assembly versus self-assembly between HCN isoforms. When co-transfected in CHO cells, HCN2 and HCN4 appear to form homomeric and heteromeric channels in equal amounts and, thus, do not preferentially self-assemble under these conditions. These experiments complement and expand upon existing studies that demonstrate interactions, but not functional co-assembly, between HCN2 and HCN4 isoforms when expressed in mammalian cells (Er et al., 2003; Much et al., 2003).

Our results are the first to suggest co-assembly of ion channel subunits of the voltage-gated cation channel family based on BRET. This approach offers a number of advantages over previous studies, which include the determination of interactions in live populations of cells without resorting to more invasive approaches. It is possible that the higher BRET values produced by co-transfected combinations of HCN2 and HCN4 are due to homomeric channels which are located within 10 nm of each other. The similarity of BRET values between cells expressing either HCN2 or HCN4 (positive controls), and cells expressing both HCN2 and HCN4, suggests that adjacent and intersubunit interactions contribute equally to the measured values. Nevertheless, a high affinity of HCN2 and HCN4 homomeric channels for each other, compared to other channels such as Kv1.5, and physical interactions between them could explain the unusual clustering and gating cooperativity of I_f channels seen in single channel studies of sinoatrial myocytes and HEK cells expressing HCN2 (Dekker and Yellen, 2006; DiFrancesco and Tortora, 1991).

In this study, we found for the first time that HCN2 and HCN4 co-immunoprecipitate from the rat thalamus, which is consistent with their co-assembly in this tissue. We also found that HCN2 and HCN4 colocalize, and their intensities correlate positively, in isolated regions of the embryonic mouse heart. Despite our inability to demonstrate co-immunoprecipitation of HCN2 and HCN4 from embryonic heart tissue, our functional data demonstrating a predominantly heteromeric population channels in CHO cells transfected with HCN2 and HCN4 suggests that they coassemble in cardiomyocytes expressing both isoforms.

In summary, our results demonstrate that HCN2 and HCN4 heteromerize and homomerize with equal preference when co-expressed in CHO cells. Our data also support the co-assembly of HCN2 and HCN4 in the rat thalamus, and mouse embryonic heart. Our data also suggest that other mechanisms may be actively invoked, that prevent co-assembly between HCN2 and HCN4. The extent of co-assembly in specific cells within these tissues may depend upon cell- or species-specific factors such as interactions of HCN isoforms with other proteins, varying affinities of isoforms for each other, the total and relative amounts of each isoform that are synthesized and the location of sites of synthesis within the cell. Individual cells may regulate each of these factors in their own way to control the localization and stoichiometry of homomeric and heteromeric channel formation. The ability to monitor self-assembly, co-assembly and stoichiometry of HCN channels in native tissue remains an important future goal, but adaptation of the approaches described in this paper for native tissue may be a useful starting point.

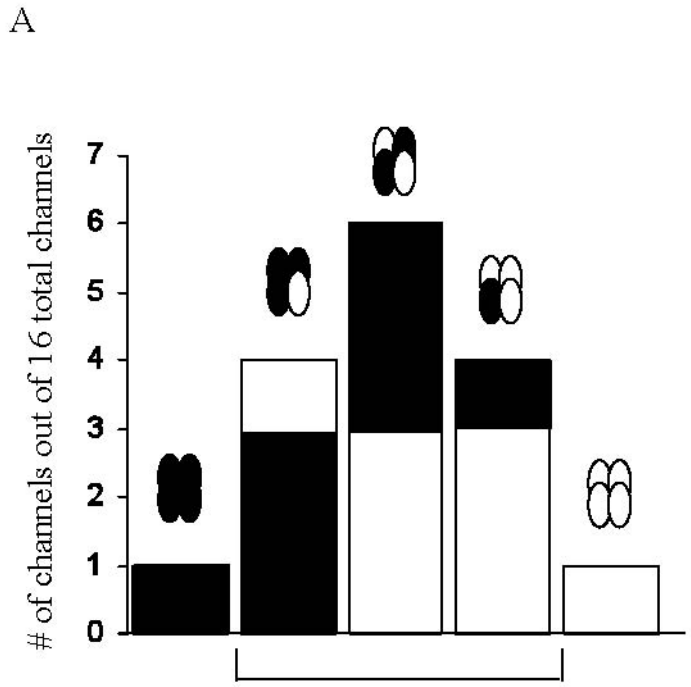

Figure 2.1 Tetrameric assembly of Rluc- and GFP-tagged subunits

Subunits tagged with Rluc and GFP could form tetrameric channels according to a binomial distribution. Depicted are 2^4, or 16 total channels from 4 possible combinations of subunit assembly (shown above each bar), in which Rluc- and GFP-tagged subunits assemble without preference. The number of channels per combination, out of 16 total channels, is plotted on the y-axis. In this diagram, Rluc-tagged subunits are white whereas GFP-tagged subunits are black. The bracket denotes the group of possible stoichiometric Rluc-GFP combinations that can be detected by the imaging and BRET approaches used in this study.

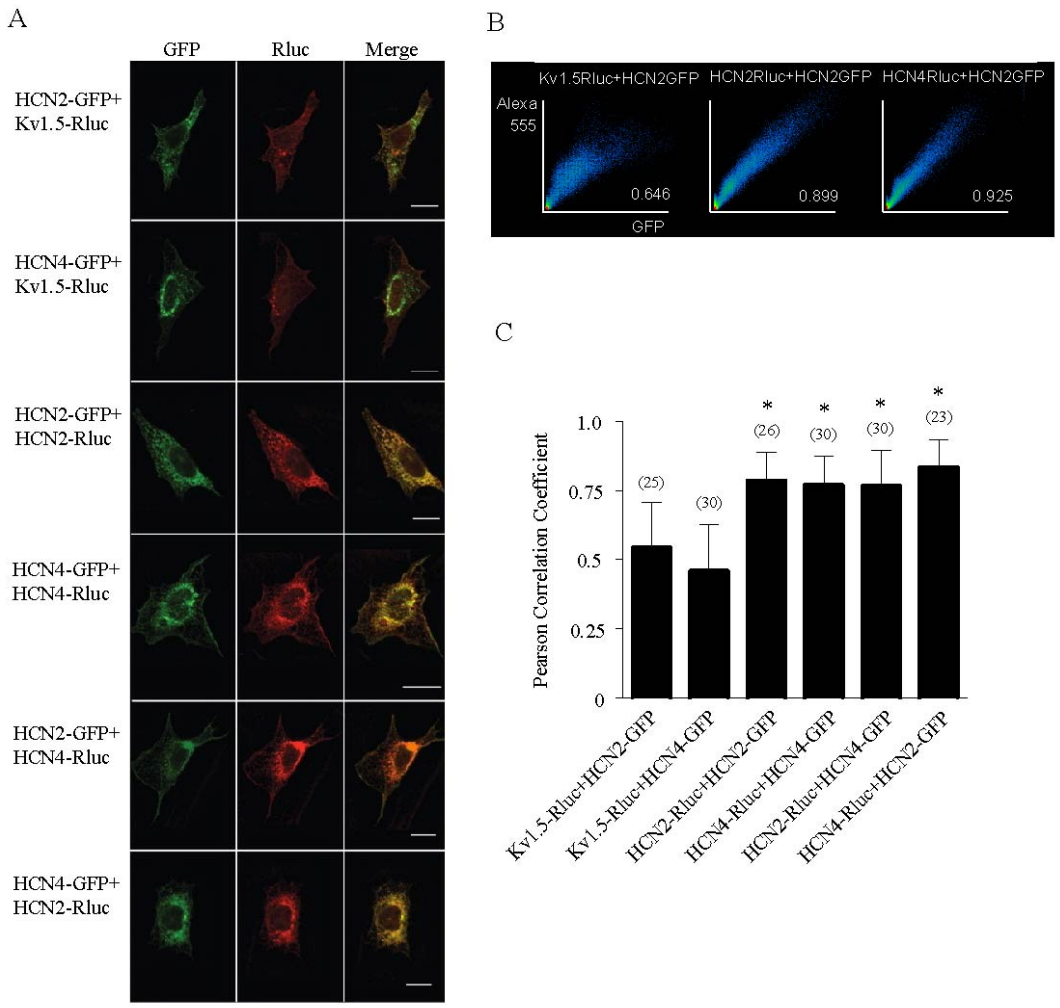

Figure 2.2 Correlation of fluorescent intensities in co-transfected CHO cells support similar levels of self-assembly and co-assembly of HCN2 and HCN4

A. Images of CHO cells co-transfected with combinations of HCN2, HCN4 and Kv1.5 constructs. Rluc-tagged constructs are shown in red and GFP-tagged constructs are shown in green with areas of colocalization depicted in yellow. Scale bars represent 10μm. B. Colocalization scatterplots of representative images in 'A' of cells co-transfected with HCN2-GFP and Kv1.5-Rluc, HCN2-Rluc or HCN4-Rluc. Intensity of GFP fluorescence is represented on the 'x' axis and intensity of Alexa555 (or Rluc) fluorescence on the 'y' axis. The frequency of pixel overlap at a given relative fluorescence intensity is plotted with greater frequency of overlap in red (toward origin of axes) and lower in blue. Pearson correlation coefficients determined from the values of intensities in each graph are shown. C. Bar graph of Pearson correlation coefficients determined from cells co-transfected with different construct combinations. Values represent means ± SD for each set of constructs and 'n' values depict number of cells used to determine mean Pearson correlation coefficients. Statistical comparisons were carried out using a one-way ANOVA analysis followed by Bonferroni's multiple comparison post-test comparing all pairs. All combinations of HCN construct co-expression show Pearson correlation coefficients that are not significantly different from each other ($p>0.05$) but are significantly greater than those determined from combinations of Kv1.5RLuc with the HCN constructs ($p<0.001$, asterisks).

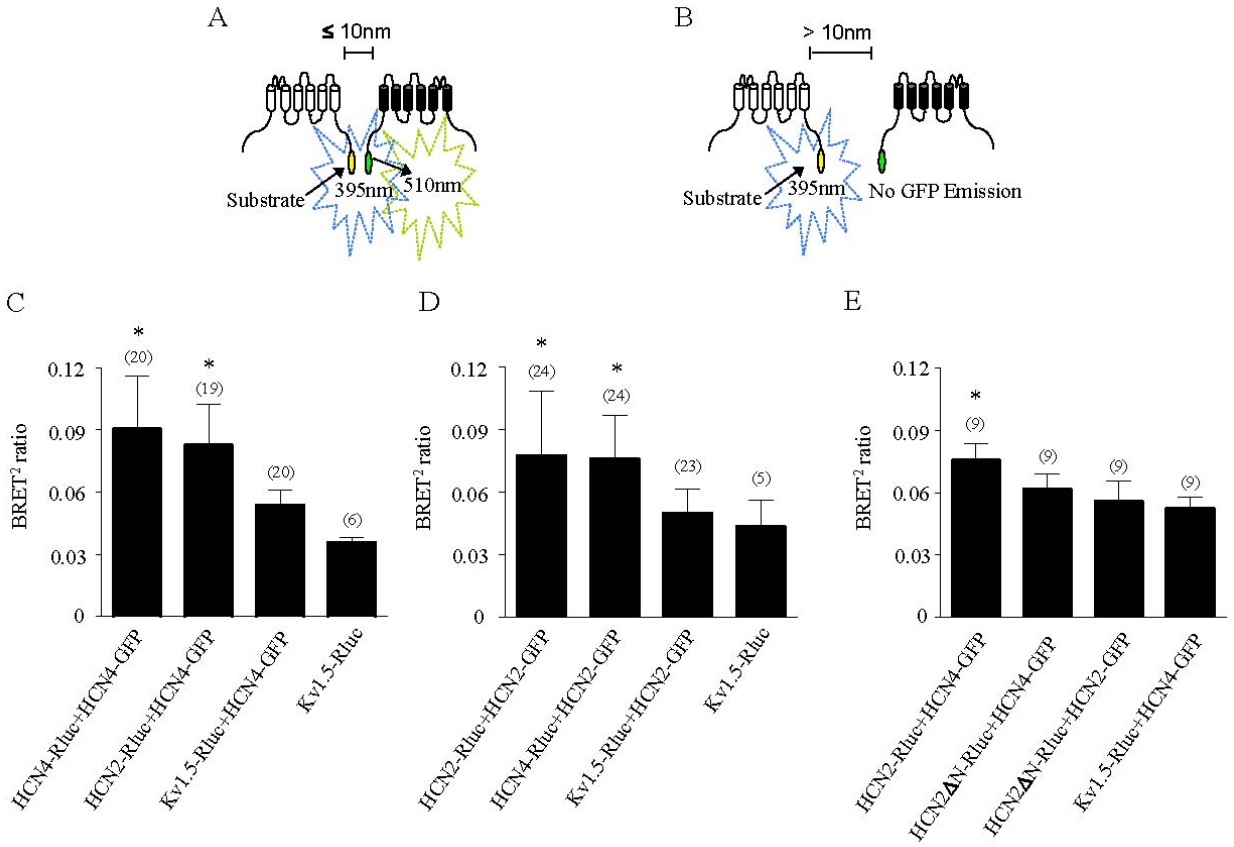

Figure 2.3 BRET ratios support similar levels of self-assembly and co-assembly of HCN2 and HCN4 isoforms in live CHO cells

A. Upon degradation of its substrate (DeepBlueC coelenterazine), *Renilla*-luciferase (Rluc, yellow) emits light at 395nm. Emission at this wavelength will excite GFP (green) if it is located within 10nm of the Rluc protein. The GFP will then emit light at 510nm. The intensity of GFP emission depends on the proximity of GFP to Rluc. B. If Rluc and GFP are greater than 10nm from each other, the emission from Rluc will not excite GFP and the calculated BRET ratio will be low. BRET ratios are calculated by dividing the recorded GFP emission (relative fluorescent units) by Rluc emission (relative luminescent units). C, D, E. Bar graphs of BRET values determined from cells co-transfected with different channel construct combinations. Values represent means ± SD for each set of constructs and 'n' values depict number of cell populations used to determine mean values over 3-6 independent transfections. Experiments were performed in duplicate at four different Rluc:GFP cDNA ratios. Statistical comparisons were carried out using a one-way ANOVA analysis followed by Bonferroni's multiple comparison post-test comparing all pairs. The asterisks (C and D) indicate significant differences from the BRET ratios produced by co-transfection of Kv1.5-Rluc and HCN2-GFP or HCN4-GFP, or Kv1.5-Rluc transfected alone. All combinations of HCN isoforms (homomeric and heteromeric) are significantly greater than negative controls ($p < 0.01$) but are not different from each other ($p > 0.05$). Kv1.5-Rluc + HCN2-GFP and Kv1.5-Rluc + HCN4-GFP BRET ratios are not significantly greater than the Kv1.5-RLuc background BRET ratio ($p > 0.05$). The asterisk (E) indicates a significant difference in BRET ratios between HCN2-Rluc + HCN4-GFP and all other pairs ($p < 0.01$). BRET ratios for all other pairs were not significantly different from each other ($p > 0.05$).

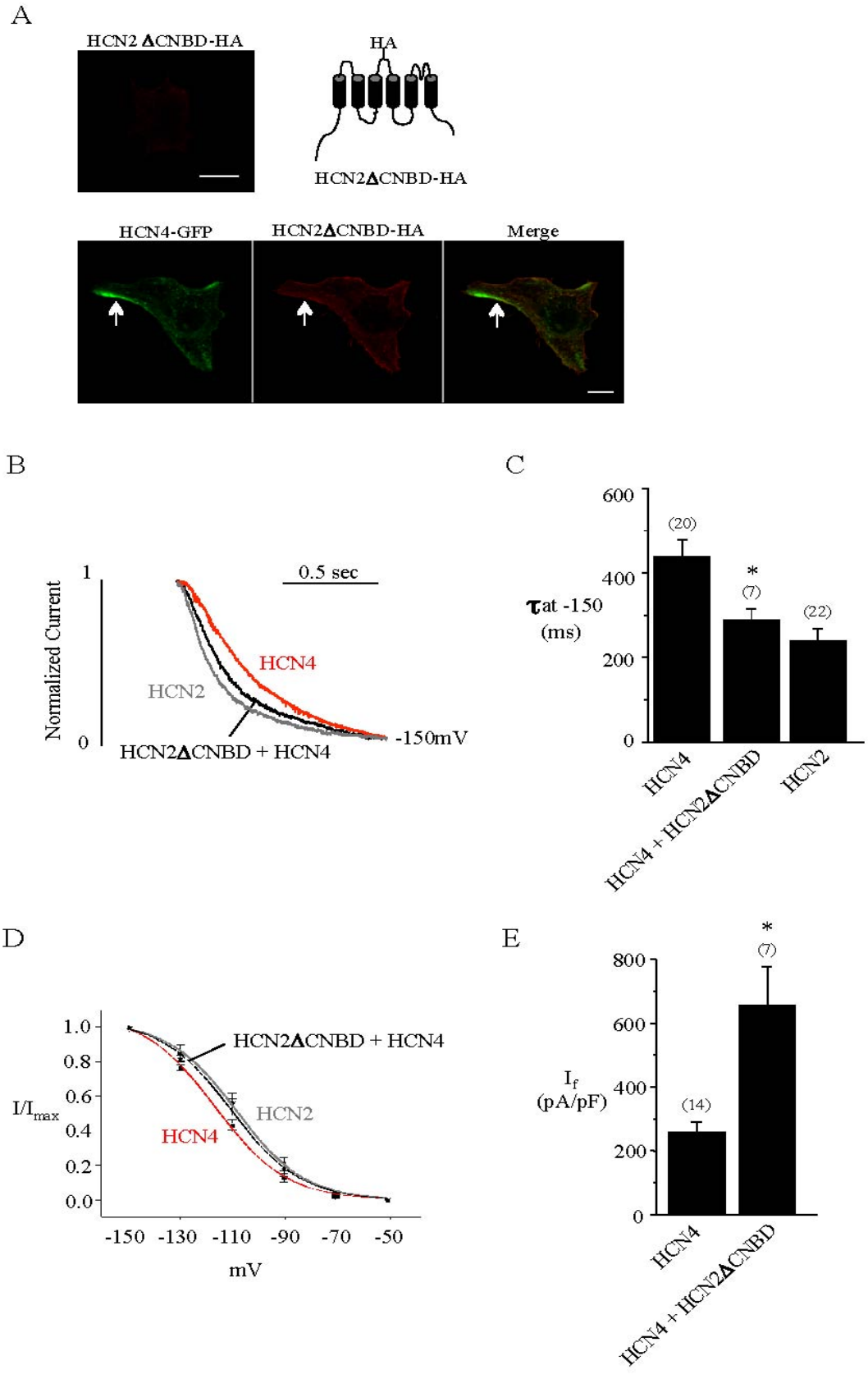

Figure 2.4 HCN4 rescues an HCN2 trafficking mutant to the cell surface and forms functional heteromeric channels

Figure 2.4 HCN4 rescues an HCN2 trafficking mutant to the cell surface and forms functional heteromeric channels

A. Images of non-permeabilized CHO cells transfected with HCN2ΔCNBD, containing a hemagluttanin (HA) tag, (above) or co-transfected with HCN4-GFP (below). Note increased fluorescence on surface of the cell transfected with both proteins (as shown by arrows). This increase in cell surface fluorescence indicates the rescue of the HCN2 trafficking mutant by HCN4 to the cell surface. Scale bars represent 10um. Images are representative of typical cells visualized from at least 5 transfections. Top right: Schematic depicting the location of the HA epitope within the S3-S4 extracellular loop of HCN2ΔCNBD. B. Representative current traces, normalized to a maximum value of one, recorded from cells expressing HCN4, HCN2ΔCNBD with HCN4, or HCN2 in response to a test voltage step to –150 mV from a holding potential of -35 mV. C. Time constants of I_f activation (τ_{act}) versus test voltage determined from current traces recorded from CHO cells expressing HCN4 (443.7 ± 38.7 ms), HCN2ΔCNBD with HCN4 (293.7 ± 24.2 ms), or HCN2 (244.0 ± 27.3 ms) (right). Asterisks indicate significant differences from HCN4 (one-tailed t-test, $p < 0.05$). D. Activation curves from cells expressing HCN4, HCN2ΔCNBD with HCN4, or HCN2. V½ and k values of –119.6 ± 1.5 mV and 13.8 ± 2.1, -110.7 ± 2.0 mV and 13.9 ± 1.2, and –107.7 ± 2.7 mV and 13.4 ± 1.2, respectively (n = 7 cells). E. Bar graph depicting whole-cell current densities (normalized to cell capacitance) of HCN4 (259.8 ± 31.9 pA/pF), or HCN2ΔCNBD with HCN4 (658.8 ± 118.9 pA/pF). Asterisks indicate a significant difference between HCN2ΔCNBD co-transfected with HCN4, and HCN4 (one-tailed t-test, $p < 0.05$). For each bar graph, the number of cells in each group is shown in brackets above each bar. Values represent means ± s.e.m.

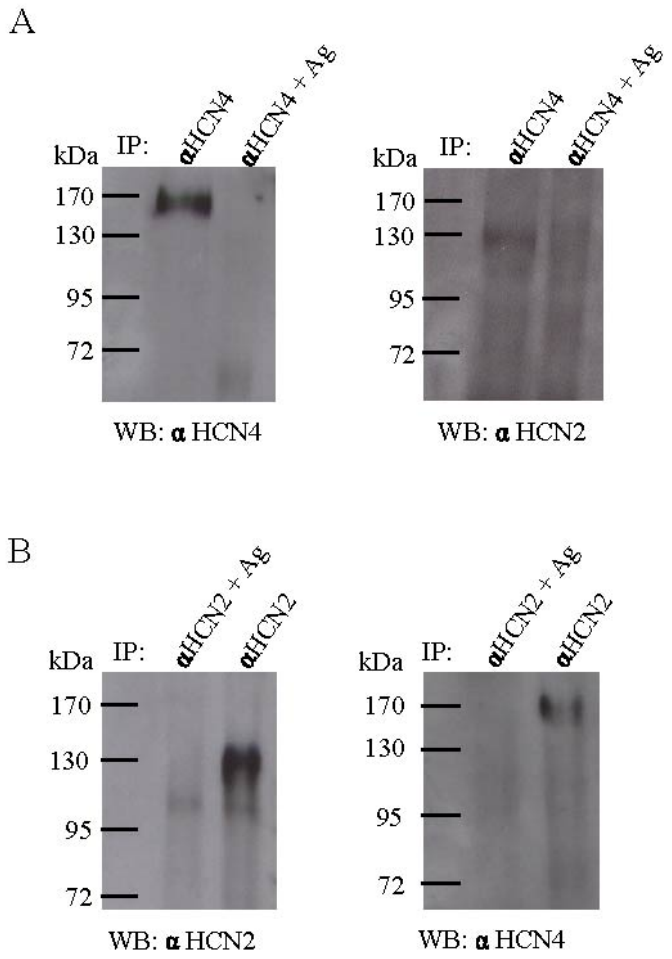

Figure 2.5 HCN2 and HCN4 co-immunoprecipitate from the rat thalamus

A. Western blots showing HCN4 immunoprecipitation (IP) using a guinea pig anti-HCN4 antibody, with or without pre-incubation of with its antigen. Left: Western blot (WB) is probed with a guinea pig anti-HCN4 antibody to show efficiency of HCN4 pull down (left lane), as well as lack of HCN4 when the antibody is pre-incubated with its antigen (right lane). A single HCN4 band is visible in the left lane at approximately 170kDa. Right: The same western blot, but stripped and reprobed with a rabbit anti-HCN2 antibody. Left lane shows that HCN2 is pulled down with HCN4 IP. A single HCN2 band is visible at approximately 130kDa. Right lane shows lack of HCN2 co-immunoprecipitation when the anti-HCN4 immunoprecipitating antibody is pre-incubated with its antigen. B. Western blots showing HCN2 immunoprecipitation (IP) using a rabbit anti-HCN2 antibody, with or without pre-incubation with its antigen. Left: Western blot (WB) is probed with a rabbit anti-HCN2 antibody to show lack of a band when HCN2 is pre-incubated with its antigen (left lane), and shows efficiency of HCN2 pull down in the right lane. A single HCN2 band is visible in the right lane at approximately 130kDa. Right: The same western blot, but stripped and reprobed with a guinea pig anti-HCN4 antibody. Left lane shows lack of HCN4 co-immunoprecipitation when the anti-HCN2 immunoprecipitating antibody is pre-incubated with its antigen. Right lane shows that HCN4 is pulled down with HCN2 IP. A single HCN4 band is visible at approximately 170kDa.

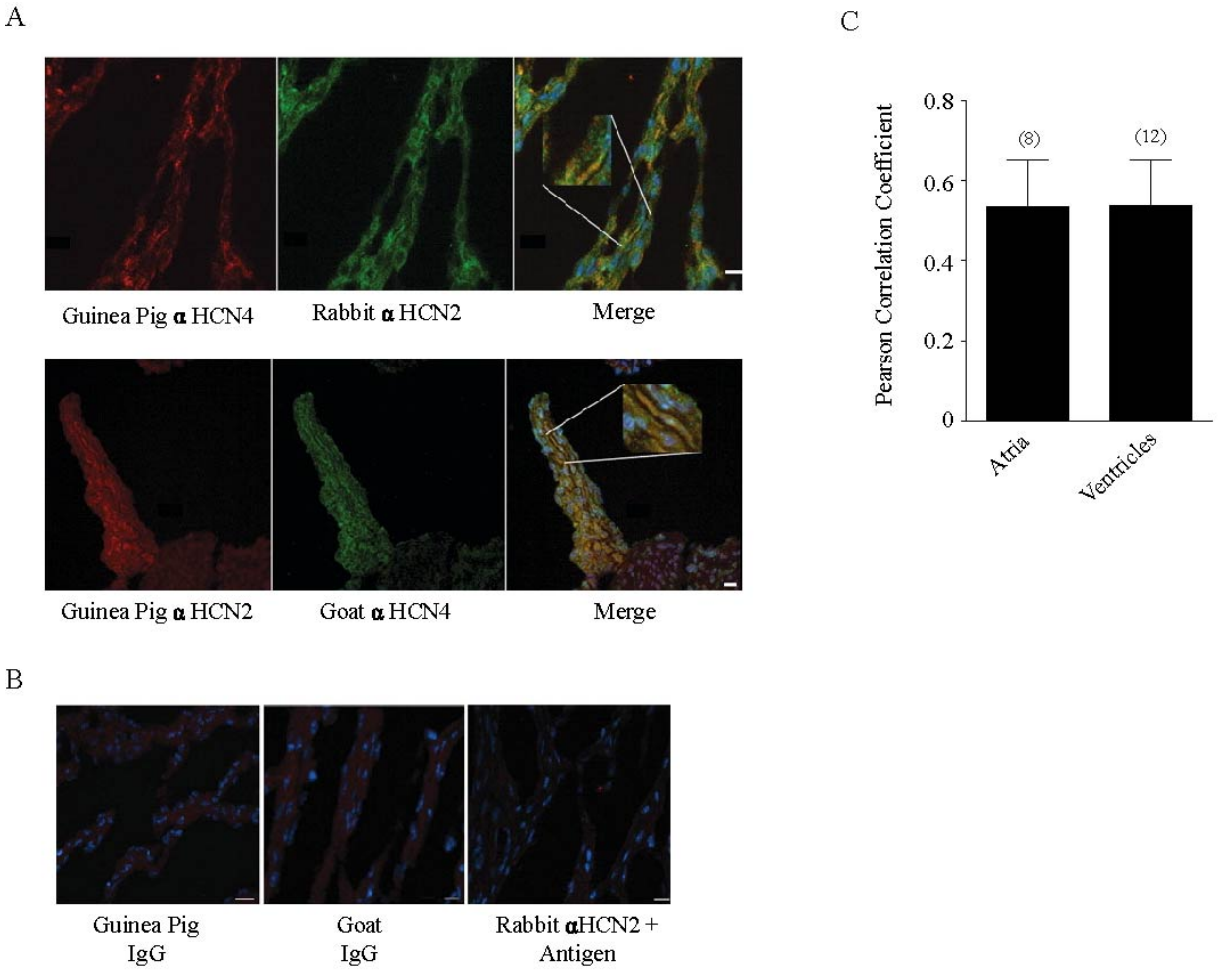

Figure 2.6 HCN2 and HCN4 colocalize within certain regions of the embryonic mouse heart

A. Images of heart tissue sections taken from E18 embryonic mice, and co-stained with two different sets of primary antibodies against HCN2 and HCN4. Top: Guinea Pig anti-HCN4 (red) co-stained with rabbit anti-HCN2 (green). Bottom: Guinea Pig anti-HCN2 (red) co-stained with goat anti-HCN4 (green). Merged images are on the right and regions of colocalization are seen in yellow with one region highlighted in the inset. Merged images also show DAPI nuclear staining in blue. Scale bars represent 10µm. B. Images of heart tissue sections taken from E18 embryonic mice and stained with negative control IgG (for guinea pig and goat), or with rabbit anti-HCN2 pre-incubated with its antigen. Nuclear staining is shown in blue to highlight location of cells but lack of background staining. Scale bars represent 10µm. C. Pearson correlation coefficients from regions of HCN2 and HCN4 colocalization within the atria and ventricles of E18 embryonic mice. Four areas of colocalization were chosen from each field of view and the means from each field of view were used in the calculation of Pearson correlation coefficients. The total fields of view for each tissue are shown in brackets above each bar. Error bars represent standard deviations from the mean.

2.5 References

Abbas, S. Y., Ying, S. W. and Goldstein, P. A. (2006). Compartmental distribution of hyperpolarization-activated cyclic-nucleotide-gated channel 2 and hyperpolarization-activated cyclic-nucleotide-gated channel 4 in thalamic reticular and thalamocortical relay neurons. *Neuroscience* **141,** 1811-1825.

Accili, E. A., Proenza, C., Baruscotti, M. and DiFrancesco, D. (2002). From funny current to HCN channels: 20 years of excitation. *News Physiol. Sci.* **17,** 32-37.

Altomare, C., Bucchi, A., Camatini, E., Baruscotti, M., Viscomi, C., Moroni, A. and DiFrancesco, D. (2001). Integrated allosteric model of voltage gating of HCN channels. *J. Gen. Physiol.* **117,** 519-532.

Altomare, C., Terragni, B., Brioschi, C., Milanesi, R., Pagliuca, C., Viscomi, C., Moroni, A., Baruscotti, M. and DiFrancesco, D. (2003). Heteromeric HCN1-HCN4 channels: A comparison with native pacemaker channels from the rabbit sinoatrial node. *J. Physiol.* **549,** 347-359.

Chen, S., Wang, J. and Siegelbaum, S. A. (2001). Properties of hyperpolarization-activated pacemaker current defined by coassembly of HCN1 and HCN2 subunits and basal modulation by cyclic nucleotide. *J. Gen. Physiol.* **117,** 491-504.

Dekker, J. P. and Yellen, G. (2006). Cooperative gating between single HCN pacemaker channels. *J. Gen. Physiol.* **128,** 561-567.

DiFrancesco, D. (1986). Characterization of single pacemaker channels in cardiac sino-atrial node cells. *Nature* **324,** 470-473.

DiFrancesco, D. and Tortora, P. (1991). Direct activation of cardiac pacemaker channels by intracellular cyclic AMP. *Nature* **351,** 145-147.

Ehrlich, J. R., Pourrier, M., Weerapura, M., Ethier, N., Marmabachi, A. M., Hebert, T. E. and Nattel, S. (2004). KvLQT1 modulates the distribution and biophysical properties of HERG. A novel alpha-subunit interaction between delayed rectifier currents. *J. Biol. Chem.* **279,** 1233-1241.

Er, F., Larbig, R., Ludwig, A., Biel, M., Hofmann, F., Beuckelmann, D. J. and Hoppe, U. C. (2003). Dominant-negative suppression of HCN channels markedly reduces the native pacemaker current I(f) and undermines spontaneous beating of neonatal cardiomyocytes. *Circulation* **107,** 485-489.

Garcia-Frigola, C., Shi, Y. and Evans, S. M. (2003). Expression of the hyperpolarization-activated cyclic nucleotide-gated cation channel HCN4 during mouse heart development. *Gene Expr. Patterns* **3,** 777-783.

Gauss, R., Seifert, R. and Kaupp, U. B. (1998). Molecular identification of a hyperpolarization-activated channel in sea urchin sperm. *Nature* **393,** 583-587.

Ghavanini, A. A., Mathers, D. A. and Puil, E. (2005). Glycinergic inhibition in thalamus revealed by synaptic receptor blockade. *Neuropharmacology* **49,** 338-349.

Hébert, T. E., Gales, C. and Rebois, R. V. (2006). Detecting and imaging protein-protein interactions during G protein-mediated signal transduction in vivo and in situ by using fluorescence-based techniques. *Cell Biochem. Biophys.* **45,** 85-109.

Hille, B. (2001). Ionic channels of excitable membranes. In *Ionic Channels of Excitable Membranes*, pp. 427-429. Sunderland, MA: Sinauer Associates.

Ishii, T. M., Takano, M., Xie, L. H., Noma, A. and Ohmori, H. (1999). Molecular characterization of the hyperpolarization-activated cation channel in rabbit heart sinoatrial node. *J. Biol. Chem.* **274,** 12835-12839.

Jackson, H. A., Marshall, C. R. and Accili, E. A. (2007). Evolution and structural diversification of hyperpolarization-activated cyclic nucleotide-gated channel genes. *Physiol. Genomics* **29,** 231-245.

Johnson, J. P.,Jr and Zagotta, W. N. (2005). The carboxyl-terminal region of cyclic nucleotide-modulated channels is a gating ring, not a permeation path. *Proc. Natl. Acad. Sci. U. S. A.* **102,** 2742-2747.

Kaupp, U. B. and Seifert, R. (2001). Molecular diversity of pacemaker ion channels. *Annu. Rev. Physiol.* **63,** 235-257.

Ludwig, A., Budde, T., Stieber, J., Moosmang, S., Wahl, C., Holthoff, K., Langebartels, A., Wotjak, C., Munsch, T., Zong, X. et al. (2003). Absence epilepsy and sinus dysrhythmia in mice lacking the pacemaker channel HCN2. *EMBO J.* **22,** 216-224.

Ludwig, A., Zong, X., Jeglitsch, M., Hofmann, F. and Biel, M. (1998). A family of hyperpolarization-activated mammalian cation channels. *Nature* **393,** 587-591.

Mercier, J. F., Salahpour, A., Angers, S., Breit, A. and Bouvier, M. (2002). Quantitative assessment of beta 1- and beta 2-adrenergic receptor homo- and heterodimerization by bioluminescence resonance energy transfer. *J. Biol. Chem.* **277,** 44925-44931.

Michels, G., Er, F., Khan, I., Sudkamp, M., Herzig, S. and Hoppe, U. C. (2005). Single-channel properties support a potential contribution of hyperpolarization-activated cyclic nucleotide-gated channels and if to cardiac arrhythmias. *Circulation* **111,** 399-404.

Milligan, G. and Bouvier, M. (2005). Methods to monitor the quaternary structure of G protein-coupled receptors. *FEBS J.* **272,** 2914-2925.

Mommersteeg, M. T., Hoogaars, W. M., Prall, O. W., de Gier-de Vries, C., Wiese, C., Clout, D. E., Papaioannou, V. E., Brown, N. A., Harvey, R. P., Moorman, A. F. et al. (2007). Molecular pathway for the localized formation of the sinoatrial node. *Circ. Res.* **100,** 354-362.

Much, B., Wahl-Schott, C., Zong, X., Schneider, A., Baumann, L., Moosmang, S., Ludwig, A. and Biel, M. (2003). Role of subunit heteromerization and N-linked glycosylation in the formation of functional hyperpolarization-activated cyclic nucleotide-gated channels. *J. Biol. Chem.* **278,** 43781-43786.

Notomi, T. and Shigemoto, R. (2004). Immunohistochemical localization of ih channel subunits, HCN1-4, in the rat brain. *J. Comp. Neurol.* **471,** 241-276.

Proenza, C., Tran, N., Angoli, D., Zahynacz, K., Balcar, P. and Accili, E. A. (2002). Different roles for the cyclic nucleotide binding domain and amino terminus in assembly and expression of hyperpolarization-activated, cyclic nucleotide-gated channels. *J. Biol. Chem.* **277,** 29634-29642.

Robinson, R. B. and Siegelbaum, S. A. (2003). Hyperpolarization-activated cation currents: From molecules to physiological function. *Annu. Rev. Physiol.* **65,** 453-480.

Santoro, B., Chen, S., Luthi, A., Pavlidis, P., Shumyatsky, G. P., Tibbs, G. R. and Siegelbaum, S. A. (2000). Molecular and functional heterogeneity of hyperpolarization-activated pacemaker channels in the mouse CNS. *J. Neurosci.* **20,** 5264-5275.

Santoro, B., Grant, S. G., Bartsch, D. and Kandel, E. R. (1997). Interactive cloning with the SH3 domain of N-src identifies a new brain specific ion channel protein, with homology to eag and cyclic nucleotide-gated channels. *Proc. Natl. Acad. Sci. U. S. A.* **94,** 14815-14820.

Santoro, B., Liu, D. T., Yao, H., Bartsch, D., Kandel, E. R., Siegelbaum, S. A. and Tibbs, G. R. (1998). Identification of a gene encoding a hyperpolarization-activated pacemaker channel of brain. *Cell* **93,** 717-729.

Stieber, J., Herrmann, S., Feil, S., Loster, J., Feil, R., Biel, M., Hofmann, F. and Ludwig, A. (2003). The hyperpolarization-activated channel HCN4 is required for the generation of pacemaker action potentials in the embryonic heart. *Proc. Natl. Acad. Sci. U. S. A.* **100,** 15235-15240.

Tran, N., Proenza, C., Macri, V., Petigara, F., Sloan, E., Samler, S. and Accili, E. A. (2002). A conserved domain in the NH2 terminus important for assembly and functional expression of pacemaker channels. *J. Biol. Chem.* **277,** 43588-43592.

Ulens, C. and Siegelbaum, S. A. (2003). Regulation of hyperpolarization-activated HCN channels by cAMP through a gating switch in binding domain symmetry. *Neuron* **40,** 959-970.

Ulens, C. and Tytgat, J. (2001). Functional heteromerization of HCN1 and HCN2 pacemaker channels. *J. Biol. Chem.* **276,** 6069-6072.

Wainger, B. J., DeGennaro, M., Santoro, B., Siegelbaum, S. A. and Tibbs, G. R. (2001). Molecular mechanism of cAMP modulation of HCN pacemaker channels. *Nature* **411,** 805-810.

Yasui, K., Liu, W., Opthof, T., Kada, K., Lee, J. K., Kamiya, K. and Kodama, I. (2001). I(f) current and spontaneous activity in mouse embryonic ventricular myocytes. *Circ. Res.* **88,** 536-542.

3 REGULATION OF GIP AND GLP-1 RECEPTOR CELL SURFACE EXPRESSION BY N-LINKED GLYCOSYLATION AND RECEPTOR HETEROMERIZATION[2]

3.1 Introduction

The hormones Glucose-dependent Insulinotropic Polypeptide (GIP) and Glucagon-like Peptide-1 (GLP-1) are released from gut endocrine cells into the circulation, in response to food ingestion. These peptide hormones act on specific G protein-coupled receptors (GPCRs), located in multiple tissues (Baggio and Drucker, 2007; McIntosh et al., 2009), including the pancreatic β cell where both GIP and GLP-1 augment glucose-induced insulin secretion.

As for other intrinsic membrane proteins and GPCRs (Dong et al., 2007; Gurevich and Gurevich, 2008a), the GIP and GLP-1 receptors (GIPR, GLP-1R) are likely synthesized in the rough endoplasmic reticulum (ER) and pass through various steps of post-translational modifications and quality control to ensure delivery of a correctly folded form to the cell surface. N-glycosylation and receptor oligomerization are two key processes that regulate the exit of many GPCRs from the ER and delivery to the plasma membrane (Bulenger et al., 2005; Dong et al., 2007; Gurevich and Gurevich, 2008b). However, the influence of these processes on GIPR and GLP-1R expression and function has not been comprehensively studied.

Both GIPR and GLP-1R are expressed as glycoproteins in native tissues implying that N-glycosylation plays a role in their function and/or cell surface expression (Amiranoff et al., 1986; Moens et al., 1996; Widmann et al., 1996). Indeed, treatment with tunicamycin, a fungicide that inhibits N-glycosylation, reduced the number of GLP-1 binding sites and GLP-1-induced cAMP production in the RINm5F cell line in a concentration-dependent manner, suggesting that N-glycosylation is important for functional surface expression (Göke et al., 1994). The impact of N-glycosylation on GIPR surface expression or on GIP and GLP-1 potentiation of glucose-induced insulin secretion remains largely unexplored. Like all family B GPCRs, both GIPR and GLP-1R possess a large leucine-rich extracellular N-terminus with several potential sites for N-glycosylation (Mayo et al., 2003; Usdin et al., 1993), but the

[2] A version of this chapter has been submitted for publication Whitaker GM, Lynn FC, Fulton C, McIntosh CHS, Accili EA. (2010) Regulation of GIP and GLP-1 receptor cell surface expression by N-linked glycosylation and receptor heteromerization.

extent to which each site is used and their individual impact on receptor function is not known.

Although able to function as monomers (Chabre and le Maire, 2005; Meyer et al., 2006; Whorton et al., 2007), GPCRs have been suggested to exist as homo- or hetero-oligomeric structures that influence cell surface expression and function (White et al., 1998; Baneres and Parello, 2003; Salahpour et al., 2004; Kniazeff et al., 2004; Milligan, 2009). However, whether oligomerization occurs among all GPCRs is unclear and has been intensely debated (Bulenger et al., 2005; Chabre et al., 2009; Gurevich and Gurevich, 2008b). Studies using Bioluminescence Resonance Energy Transfer (BRET) support homomeric association of the GIPR (Vrecl et al., 2006) as well as heteromerization of the GLP-1 and secretin receptors (Harikumar et al., 2008). However, self-association of the GLP-1R or close associations between the structurally-related GIPR and GLP-1R have not been demonstrated; this is potentially critical given the overlap of GIPR and GLP-1R expression and function in tissues such as the endocrine pancreas.

In this chapter, N-glycosylation and oligomerization of the incretin receptors, GIPR and GLP-1R is examined. To establish the extent to which each of the putative sites are N-glycosylated and their impact on function, we have carried out a mutational analysis of the N-terminus of the human GIPR and GLP-1R and examined cell signaling and surface expression using various approaches. Our data support a critical and, in the case of the GIPR, essential role for N-glycosylation in functional cell surface expression. Furthermore, we show that N-glycosylation is required for efficient GIP potentiation of glucose-induced insulin secretion from the pancreatic β-cell line, INS-1. Finally, we demonstrate that close associations of co-expressed GIPR and GLP-1R occur, which act to restore functional expression of the GIPR that is otherwise abolished by the lack of N-glycosylation, suggesting the formation of receptor heteromers.

3.2 Experimental Procedures

3.2.1 Molecular Biology

Human GLP-1R cDNA was purchased from GeneCopoeia (OmicsLink Expression Clone EX-A0510-M02). Overlapping PCR mutagenesis was used to remove the stop codon and add common restriction sites in order to insert GLP-1R cDNA into pcDNA3.1-V5

(Invitrogen Corp) such that the V5 epitope was expressed on the C-terminal end of the receptor (GLP-1R-V5). The human GIPR was purchased from Addgene (plasmid 14942, kindly donated by B Thorens, Gremlich et al., 1995). Overlapping PCR mutagenesis was used to remove the short form of the receptor and its stop codon from this plasmid as well as insert common restriction sites such that the cDNA could be inserted into pcDNA3.1-V5 with the V5 epitope expressed on the C-terminus of the receptor (GIPR-V5). For N-terminally HA-tagged constructs, overlapping PCR mutagenesis was used to insert the HA epitope (YPYDVPDYA) directly downstream of the GIPR and GLP-1R putative signal peptide sequences on their N-termini. Quickchange PCR mutagenesis (Stratagene) was used to make all glycosylation point mutations in both V5-tagged and HA-tagged GIPR and GLP-1R constructs. For BRET constructs, pGFP-N and pRLuc-N vectors (PerkinElmer), along with GIPR-V5 and GLP-1R-V5 were digested using common restriction sites such that either GFP or *Renilla* Luciferase (RLuc) fusion proteins were expressed in frame on the C-termini of both receptors. All tagged constructs were tested for functionality using cAMP assays (data not shown). The ion channel HCN2-GFP was utilized as a control, having been tested functionally in a previous study (Whitaker et al., 2007).

3.2.2 Cell Culture and Expression

CHO-KI cells (American Type Culture Collection) were maintained in Ham's F-12 medium (Invitrogen Corp) supplemented with 50µg/ml penicillin/streptomycin (Invitrogen Corp) and 10% fetal bovine serum (Sigma-Aldrich) and incubated at 37°C with 5% CO_2. After 24h, once cells were approximately 80% confluent, they were transiently transfected with mammalian expression vectors encoding tagged wild type or mutant receptors using FuGene6 transfection reagent (Roche Diagnostics).

3.2.3 Tunicamycin Treatment

Three µg of cDNA were used for transfection in 50mm dishes. Six hours after transfection, tunicamycin (5µg/ml, Santa Cruz Biotechnology Inc) or DMSO was added to cells, which were then incubated overnight. Cells were then lysed for 30 minutes on ice with radioimmunoprecipitation assay buffer (RIPA buffer: 50mM Tris at pH 8.0, 1% Nonidet P-40, 150mM NaCl, 1mM EDTA, 1mM PMSF, 2mM each Na_3VO_4 and NaF, and 10µg/ml each aprotinin, pepstatin, and leupeptin). 20µg of protein were loaded in 10% SDS-PAGE gels.

3.2.4 Cell Surface Biotinylation

Three µg of cDNA were used for transfections in 50mm dishes. 24 hours after transfection, cells were washed twice with 1x PBS (pH 8.0), then 1ml Versene (Invitrogen Corp) was added to detach cells. Cells were collected and washed twice with 1x PBS. 300µl of 5mM Sulfo-NHS-SS-Biotin (Thermo Scientific) were added to cells for 45minutes at room temperature. Cells were washed with 1xPBS supplemented with 100mM glycine to quench biotin reaction. Cells were then resuspended in RIPA buffer and lysed on ice for 30 minutes followed by centrifugation to collect supernatant. 100µg of biotinylated lysate were added to 100 µl of 50% streptavidin-conjugated agarose beads (Sigma-Aldrich), and the bead-lysate mix was incubated overnight at 4°C with rotation. Beads were washed with 1x PBS supplemented with 0.1% NP-40, and incubated with Laemmli sample buffer supplemented with 1mM DTT for 1 hour at room temperature, then loaded in 10% SDS-PAGE gels.

3.2.5 Western Blotting

Proteins separated on SDS-PAGE gels were transferred onto PVDF membranes using the i-Blot transfer device (Invitrogen Corp). Membranes were then blocked with 5% non-fat milk in TBST overnight at 4°C. Mouse-anti V5 (1:1000, Invitrogen Corp) was added to the membrane and incubated for 2.5 hours at room temperature. Blots were washed three times in TBST, followed by addition of 1:3000 anti-mouse secondary antibody conjugated to horseradish peroxidase (Santa Cruz Biotechnology Inc) for 1 hour at room temperature. Blots were washed in TBST, followed by chemiluminescence detection.

3.2.6 ELISA Assays

Three µg of cDNA were used for transfections in 50mm dishes. 24 hours after transfection, cells were seeded into 96-well assay plates (Corning Inc) at a density of approximately 100,000 cells per well. After 24 hours, cells were fixed with 4% paraformaldehyde and antigen detected with mouse-anti HA primary antibody (1:1000, Sigma-Aldrich), followed by anti-mouse-HRP conjugated secondary antibody (1:1000 Santa Cruz Biotechnology Inc) and SuperSignal ELISA Femto Maximum Sensitivity Substrate (Thermo Scientific). Signals were detected using the Victor 3V plate reader (PerkinElmer). Each condition was carried out in triplicate, and data were collected from a minimum of 5

independent transfections. Mutants and wild type receptor data were compared using one-way ANOVA followed by Dunnett's multiple comparison tests (Graph Pad Prism).

3.2.7 TR-FRET cAMP Assays

For transfections in 50 mm dishes, 0.5µg of cDNA was used. 24 hours after transfection, cells were rinsed with 1x HBSS (Invitrogen Corp), detached with 1mL Versene (Invitrogen Corp), then resuspended at a density of 6000 cells per 5µl in stimulation buffer, pH 7.4 (1x HBSS supplemented with 5mM HEPES buffer, 0.1% BSA and 0.5mM IBMX). Both GLP-1 7-36 amide and GIP peptides (Sigma-Aldrich) were diluted in stimulation buffer. Assay was then performed according to LANCE TR-FRET cAMP assay kit protocol (PerkinElmer), in 96-well white optiplates (PerkinElmer). Peptide stimulation of cells was carried out for 30 minutes and detection for 1 hour at room temperature, followed by fluorescence detection on a Victor 3V plate reader (PerkinElmer), according to LANCE protocol parameters. RFU values generated at each dose were subtracted from values obtained using untransfected cells. Data for cAMP curves were fitted to the sigmoidal dose-response equation (Graph Pad Prism) and EC_{50} values for individual experiments were calculated. Each curve was generated from at least 5 independent transfections and EC_{50} values were compared to wild type using one-way ANOVA, followed by Dunnett's multiple comparison tests.

3.2.8 BRET Assays

Here, 0.5µg of RLuc-tagged construct and 0.5-3µg of GFP-tagged construct cDNA were used for transfections in 50mm dishes. BRET experimental methods were carried out according to our previously published protocol, and based on the original study examining β_1-adrenergic receptor dimerization (Whitaker and Accili, 2008; Mercier et al., 2002). 24 hours after transfection, cells were rinsed with DPBS (Invitrogen Corp) and treated with 1mL of 0.5% trypsin-EDTA (Invitrogen Corp). 3ml of HAM's F12 media containing FBS were added; cells were centrifuged at 800xg and resuspended in BRET Buffer (DPBS supplemented with 2µg/ml Aprotinin). Approximately 100,000 cells were distributed into 96-well white optiplates (PerkinElmer). Using a Victor 3V plate reader (PerkinElmer), expression of GFP-tagged constructs was assessed by directly exciting GFP with a 400-410nm excitation filter. Expression of Rluc-tagged constructs was assessed using luminescence values obtained in the BRET assay. For BRET measurements, DeepBlueC

substrate (PerkinElmer) was added to the cells at a final concentration of 5μM, and Rluc emission was measured through a 370-450 nm filter. Resulting GFP emission was in turn measured with a 500-530 nm filter. All raw data were corrected by subtracting the BRET ratio and GFP/Rluc values determined from cells transfected with only RLuc-tagged construct (plotted at 0,0). Data were fitted to a single binding site equation by non-linear regression (GraphPad Prism).

3.2.9 Culture of INS-1 Cells

INS-1 (clone 831/12) cells were obtained from Dr. C.B. Newgard (Duke University) (Hohmeier et al., 2000). Cell lines were maintained at 37°C with 5% CO_2. Cells were grown in RPMI-1640 medium containing 11mM glucose, supplemented with 10% fetal bovine serum (Cansera, Rexdale ON), and penicillin/streptomycin, supplemented with 10mM HEPES (pH 7.4), 1 mM sodium pyruvate, 2mM glutamine and 50 uM β-mercaptoethanol.

3.2.10 Saturation Binding Analysis in INS-1 Cells

INS-1 cells were plated in 24 well plates at a density of 5 x 10^5 cells/well and allowed to grow for 24 hours, then treated with 1 μg/ml tunicamycin for 24 hours. Saturation binding experiments were carried out as previously described (Lynn et al., 2003). Data were analyzed using a one site model for GIP binding and then fitted to a curve with the equation: $Y=B_{max}*X/(Kd+X)$, where B_{max} is the binding obtained when cells are saturated with ^{125}I-GIP, and Kd is the concentration of ^{125}I-GIP required to reach half-maximal binding. The number of receptors on each cell was determined using the specific activity of the radiolabel and Avogadro's number.

3.2.11 Insulin Release from INS-1 Cells

Cells were plated into 24 well plates (5 x 10^5 cells/well) and grown for 24 hours. Cells were treated with 1 μg/ml tunicamycin for 24 hours, followed by incubation with either 5.5 mM or 11 mM glucose with or without 50 nM GIP for 30 minutes at 37 °C, then assayed for insulin content using RIA. The means were compared using two-tailed ANOVA followed by Dunnett's multiple comparison tests.

3.3 Results

3.3.1 Multiple N-Glycosylation Consensus Sites are Present and Utilized on the N-Termini of the Human GIPR and GLP-1R

The human GIPR and GLP-1R possess large N-terminal domains containing 2 and 3 putative N-glycosylation sites, respectively, as predicted by the NXS/T consensus sequences for N-glycosylation where X≠Proline. The locations of the two putative sites in the GIPR correspond closely to those of the GLP-1R (Figure 3.1A), suggesting some evolutionary conservation of N-glycosylation between them. The human GLP-1R has an additional N-glycosylation site (N115), the closest to the first transmembrane domain, which appears as an insertion when aligned with the GIPR sequence. As for the human GLP-1R, mouse and rat GIPR have three putative N-glycosylation sites on their N-termini (Figure 3.1B). However, the location of the third site in the rodent GIPR does not correspond to that in the GLP-1R, but is instead found between the two conserved sites (N62 and N77). Here, we focus on N-glycosylation of sites within the N-termini of the human GIPR and GLP-1R.

To determine whether each of the putative N-glycosylation sites is utilized, we individually and progressively mutated all sites in the human GIPR and GLP-1R from *Asn* to *Gln* and performed western blotting to determine whether corresponding shifts in molecular weight were produced. Both wild type receptors migrated at higher molecular weights than when treated with tunicamycin, an antibiotic that selectively inhibits oligosaccharyltransferase, thereby blocking N-acetylglucosamine addition onto dolicho-phosphate (Figure 3.2A,B). Furthermore, mutation of all putative N-glycosylation sites yielded single bands that migrated at lower weights, unaltered by tunicamycin. The molecular weights of receptors with single site mutations were reduced compared to wild type GIPR and GLP-1R, but were still greater than those following treatment with tunicamycin. Together, these data suggest that all putative sites in both receptors can be glycosylated when expressed in CHO cells. A second band of higher molecular weight is present in tunicamycin-treated GIPRs, and is also present in N62,77Q-GIPR lanes on blots with longer exposure times (data not shown), suggesting the presence of a second unglycosylated form. Two bands migrating at different weights can be seen in the absence of tunicamycin for most constructs, likely representing the presence of both core and complex glycosylated species. Treatment of cell

lysates with PNGase, which cleaves sugar moieties from *Asn* residues, produced band patterns identical to those using tunicamycin (data not shown), as expected.

3.3.2 N-Glycosylation Faciliates Cell Surface Expression of the GIPR more than the GLP-1R

To examine the influence of N-glycosylation on cell surface expression, GIPR and GLP-1R levels were quantified at the plasma membrane by ELISA, using externally HA-tagged receptor constructs. When individual sites were mutated, a significant decrease in GIPR but not in GLP-1R cell surface expression was observed when compared to wild type receptors (Figure 3.3A). With all N-glycosylation sites ablated, surface expression of GLP-1R was still detected, whereas GIPR cell surface expression was virtually abolished. This trend was maintained when cell surface levels were calculated as a fraction of whole cell levels (Figure 3.3C). Thus, the relative reduction in mutant surface protein localization was not predominantly a result of decreases in intracellular receptor levels (Figure 3.3B).

To complement our findings from cell surface ELISA experiments, we examined receptor surface protein using biotinylation assays. Not surprisingly, the intensities of the bands in western blots for both receptors at the cell surface and total lysates showed patterns that reflected those obtained by cell surface ELISA (Figure 3.4). For both GIPR and GLP-1R lacking N-glycosylation sites, the total protein (Figure 3.4, lower protein lysates) was somewhat reduced whereas the cell surface protein (Figure 3.4, upper biotinylated protein) was more strongly decreased (N63,82,115Q-GLP-1RV5) or absent (N62,77Q-GIPRV5). Interestingly, there was a more pronounced reduction in amount of cell surface protein for N77Q-GIPR when compared to the N62Q-GIPR, again consistent with the findings from the ELISA experiments (Figure 3.3A).

The blots of biotinylated protein also reveal multiple forms of wild type incretin receptors at the cell surface, likely representing variably N-glycosylated forms. Single and double mutations of the GLP-1R, as well as the N62Q-GIPR, were also found at the cell surface in multiple forms. In contrast, only a single immature form was observed for the N77Q-GIPR and for GLP-1R lacking all N-glycosylation sites.

3.3.3 Potency and Efficacy of the cAMP Response of the GIPR and GLP-1R to Their Natural Ligands are Augmented by N-Glycosylation at a Single Site

To investigate the role of N-glycosylation in receptor function, cAMP production was measured in CHO cells expressing GIPR or GLP-1R using a FRET-based assay. For both wild type receptors, increases in cAMP levels were observed in response to increasing concentrations of their respective ligands (GIP or GLP-1; Figure 3.5). Elimination of all N-glycosylation sites abolished cAMP production by GIP but not by GLP-1. This is not surprising given the observed absence of GIPR but not GLP-1R at the cell surface.

In all instances, with the exception of N77Q-GIPR, removal of a single glycosylation site on either receptor resulted in concentration-response curves similar to those of corresponding wild type receptors (Figure 3.5A and B, upper). Furthermore, N63,82Q-GLP-1R displayed concentration-response curves that did not differ from wild type GLP-1R (Figure 3.5B, lower). In contrast, the EC_{50} values for N63,82,115Q-GLP-1R and N77Q-GIPR were significantly right-shifted relative to those determined for the wild type receptors (Table 3.1). The amplitude of the cAMP response was also reduced for N63,82,115Q-GLP-1R. The rightward shift of the concentration-response curves imply that optimal receptor function, and/or its coupling to adenylyl cyclase, was impaired by mutation of N77 of GIPR, and of all three N-glycosylation sites of GLP-1R. These two mutant receptors also displayed the lowest abundance on the cell surface (see Figure 3.3), suggesting a connection between the quantity of receptors expressed at the surface and the sensitivity of the cAMP response.

The right-shift of the N77Q-GIPR, but not the N62Q-GIPR, concentration-response curve suggests that the role of N-glycosylation at individual sites is not necessary the same. Interestingly, cell surface ELISA data also suggest that site N77 plays a stronger role in regulating cell surface expression (see Figure 3.3). Non-uniformity among multiple sites in other intrinsic membrane proteins of the plasma membrane has been noted in other studies (Chang et al., 2008; Hebert et al., 1997; Mialet-Perez et al., 2004).

3.3.4 Function and Cell Surface Expression of a GIPR Mutant Lacking N-Glycosylation is Rescued by Close Association with the Wild Type GLP-1R

It has been suggested that many GPCRs exist as homo- or heterodimers and/or higher order oligomers at the cell surface and, in some cases, this interaction may be initiated early in the biosynthetic pathway (Issafras et al., 2002; Terrillon et al., 2003; Salahpour et al., 2004; Guan et al., 2009). Because the GIPR and GLP-1R have a relatively high level of sequence identity (Figure 3.1) and have similar expression profiles and physiological function, we reasoned that the GLP-1R might form functional complexes with the GIPR. To test this, we first examined whether cell surface expression and function of the GIPR mutant lacking N-glycosylation could be rescued by co-expression with wild type GLP-1R. Cyclic AMP levels were again measured in CHO cells expressing each receptor construct. In cells expressing N62,77Q-GIPR only, the amount of cAMP was unchanged from baseline in response to GIP. In contrast, the levels of cAMP increased in a concentration-dependent manner by GIP in cells co-expressing N62,77Q-GIPR along with the wild type GLP-1R, although the EC_{50} value was right shifted compared to wild type GIPR (Figure 3.6A, Table 3.2). These results show that functional expression of N62,77Q-GIPR was rescued by co-expressed wild type GLP-1R.

In an attempt to quantify the extent of N62,77Q-GIPR cell surface rescue by wild type GLP-1R, cell surface ELISA was again used. When the HA-tagged mutant GIPR was co-expressed with wild type GLP-1R, the measured cell surface luminescence was very low and not significantly altered as compared to co-expression with the untagged version of itself (Figure 3.6B, upper). Since the amplitude of cAMP responses to GIP were identical for both wild type GIPR, and mutant GIPR in the presence of GLP-1R, it appears that rescue of a very small amount of the N62,77Q-GIPR, below the level of detection by cell surface ELISA, suffices to fully restore activation of adenylyl cyclase in the CHO cell system. The could be reflective of a high number of spare wild type receptors localized to the cell surface, at least in our overexpression system.

The rescue of only a small fraction of N62,77Q-GIPR to the cell surface could be explained by a corresponding retention of wild type GLP-1R by the GIPR mutant. However, this was not the case since the amount of HA-tagged GLP-1R at the cell surface was unchanged by co-expression with N62,77Q-GIPR (Figure 3.6B, upper). Moreover, when co-

expressed, the total level of mutant GIPR and wild type GLP-1R were no different than when each was co-expressed with non-HA tagged versions (Figure 3.6B, lower). Therefore, it seems more likely that functional rescue of the mutant GIPR is due to a low level of association with the wild type GLP-1R, which is below the detection sensitivity of the ELISA assay.

The low level of association between N62,77Q-GIPR and wild type GLP-1R could be due to the small differences in their primary sequences, thus potentially limiting interaction between key regions. To test this, we co-expressed N62,77Q-GIPR with wild type GIPR and measured cell surface and total protein expression of both receptor constructs by ELISA. Co-expression of wild type GIPR did not rescue cell surface expression of its mutant counterpart, nor was its own level at the cell surface altered (Figure 3.7, left). Thus, the extent of receptor homology is not likely a factor for limiting the amount of cell surface rescue of the mutant GIPR.

The functional rescue of the N62,77Q-GIPR by the wild type GLP-1R nevertheless suggests some form of physical association. To test for this, we utilized BRET to measure the effects of co-expressing GFP-labeled forms of GLP-1R with R*Luc*-tagged GIPR (Figure 3.8A). For a negative control, we used GFP-tagged hyperpolarization-activated channel (HCN2-GFP), a structurally similar membrane protein that has been shown to localize to the cell surface and function normally when expressed in CHO cells (Whitaker et al., 2007), but which would not be expected to assemble with either receptor. We also tested the effects of co-expressing GFP- and R*Luc*- labeled GLP-1R (Figure 3.8B), as well as GFP- and R*Luc*-labeled GIPR (Figure 3.8C). For all three receptor combinations, the BRET saturation curves reached higher maximal values than their respective negative controls. The high values of BRET obtained, coupled with the rescue of N62,77Q-GIPR function by the wild type GLP-1R, support heteromeric and homomeric associations of the GIPR and GLP-1R.

3.3.5 N-Glycosylation Maintains Cell Surface GIP Receptor Number and GIP-Potentiated Insulin Secretion in INS-1 Cells

The roles of GIPR N-glycosylation in regulating ligand binding, surface receptor number and insulin secretion were studied in separate experiments, performed by Francis Lynn. The INS-1 β-cell line demonstrates similar physiological responses to those of native β-

cells, including GIP-induced potentiation of insulin secretion in the presence of glucose (Hohmeier et al., 2000). INS-1 cells were treated with tunicamycin and specific binding of GIP was measured using a radioligand binding assay. Tunicamycin lowered cell surface ^{125}I-GIP binding, which, at saturating levels, corresponded to a 70% decrease in cell surface GIPR number (Figure 3.9A). The dissociation constants (Kd) of GIP from the surface of these cells did not significantly differ between the control (455 ± 50 pM) and tunicamycin (345 ± 100 pM) treated cells, suggesting that ligand binding affinity was not impaired by removal of N-glycosylation.

To investigate the impact of N-glycosylation on GIPR function, GIP-stimulated insulin secretion was measured in tunicamycin-treated and untreated INS-1 cells. In the absence of tunicamycin, GIP (50 nM) significantly and strongly potentiated insulin secretion, when increasing glucose was increased from 5.5 mM to 11 mM (Figure 3.9B). Tunicamycin treatment, however, blunted the incretin effect of GIP. Tunicamycin did not modify insulin secretion in response to glucose alone, suggesting that GIP potentiation was eliminated specifically by the inhibition of N-glycosylation. These results are consistent with a reduction in GIP receptor number, but do not discount a potential impairment in GIPR signal transduction by the deficiency in N-glycosylation.

3.4 Discussion

Upon translation of the GIPR or GLP-1R nascent chains in the endoplasmic reticulum, they become subject to glycosylation at *Asn* residues located in the extracellular N-terminus. We have shown that each of the *Asn* residues is glycosylated when either the human GIPR or GLP-1R is expressed in CHO cells. For both receptors, cell surface expression and/or function were impaired by removal of N-glycosylation, although the GIPR was more strongly affected and possessed a single site (N77) in which N-glycosylation more strongly affected cell surface localization and function. Our results from ELISA experiments suggest that the decrease in cell surface receptor expression can be attributed to factors independent of variations in total expression.

Importantly, we found that N-glycosylation regulates GIPR cell surface expression and the potentiation of glucose-induced insulin secretion by nanomolar levels of GIP in INS-1 cells. These data are similar to those obtained with the GLP-1R in RINm5F cells, where cell surface receptor number and GLP-1-induced cAMP production are reduced by tunicamycin

treatment (Göke et al., 1994). Thus, N-glycosylation maintains a level of GIPR and GLP-1R surface expression that is critical for appropriate downstream signaling and regulation of insulin secretion. Notably, we also found that 30% of the normal total number of GIP receptors were detected after tunicamycin treatment despite an absence of GIP-potentiation of glucose induced insulin secretion. This implies that a threshold number of GIP receptors exist, which must be surpassed in order to potentiate insulin secretion to a level that could be measured by our assay.

When cAMP production was assayed in response to increasing concentrations of ligand, cells containing glycosylation-deficient GLP-1R or N77Q-GIPR exhibited a right-shifted concentration-response curves. This could have reflected a direct defect in GIP or GLP-1 binding to their respective receptors, or to a coupling problem with the signal transduction machinery. However, our data of GIP-binding to INS-1 cells, and previous data on GLP-1 binding to RINm5F cells (Göke et al., 1994), showed that binding affinity was unaffected by tunicamycin treatment, whereas the total surface receptor number was significantly decreased along with potentiation of insulin secretion. These data are consistent with those in other studies of bradykinin B2, P_2Y_{12} purinergic, and the type 1α metabotropic glutamate receptors, which also found that ligand-binding affinity was unaltered by inhibition of N-glycosylation (Michineau et al., 2004; Mody et al., 1999; Zhong et al., 2004). Thus, the reduction in incretin sensitivity that we observed is probably due to impaired coupling of binding to downstream signaling machinery. Since cell surface expression and, in the case of the glycosylation-deficient GLP-1R, the maximum cAMP response were also reduced in concert with sensitivity, it is possible that the efficiency of coupling to downstream effector molecules such as adenylyl cyclase depends on cell surface receptor number. Such a relationship between EC_{50} and cell surface number has been reported for the β_2-adrenergic receptor, but the mechanism underlying this association remains unknown (Ostrom et al., 2001; Patel et al., 2008). In these studies, the β_2-adrenergic receptor was localized to caveolae to a lesser extent when cell surface number was reduced; this suggests that efficient signal transduction requires localization of receptors to these structures, which contain the necessary machinery for cAMP production.

The rescue of mutant GIPR function by the wild type GLP-1R, and the close association between the two receptors as measured by BRET, suggests that they are able to associate in a receptor complex. According to a recent definition, receptor heteromers are

"composed of at least two functional receptor units with biochemical properties that are demonstrably different from those of its individual components" (Ferre et al., 2009). Functional co-assembly is also supported by the fact that signaling by the rescued GIPR was less sensitive to stimulation by GIP when compared to the wild type receptor, as seen by the right shift in EC_{50}. However, this right shift could also be explained by a corresponding reduction in number of mutant receptors at the cell surface, compared to wild type. Therefore, it remains uncertain as to whether oligomerization of GIPR and GLP-1R produces a receptor complex with unique properties. We also found that oligomerization may have been limited between glycosylation-deficient GIPR and the wild type GLP-1R, based on the lack of cell surface rescue. Indeed, various studies have shown that when N-glycosylation is removed, regular receptor dimer formation and stability is impaired, thereby impacting the receptor heteromer's ability to express at the cell surface and/or correctly function (Fernandes et al., 2001; He et al., 2002; Langer et al., 2008; Michineau et al., 2006; Wanamaker and Green, 2005).

Regulation of GIPR and GLP-1R by N-glycosylation may have important implications for type 2 diabetes (T2DM). There is a reduced incretin effect in human T2DM patients (Nauck et al., 1986), which has been attributed to reduced β-cell responsiveness to GIP (Nauck et al., 1993) and, to a lesser extent, GLP-1 (Hojberg et al., 2009). Moreover, reduced incretin receptor expression has been observed in animal models of T2DM (McIntosh et al., 2009). It will be important to determine if N-glycosylation is impaired in Type II diabetes, and whether this results in a reduction in cell surface GIPR and GLP-1R number along with the decreased incretin response of the β-cell. The finding that heteromerization between GIPR and GLP-1R can occur suggests that the much milder reduction in GLP-1 responsiveness could be a direct consequence of the more profound and fundamental observed decrease in GIPR expression. This possibility could explain the restoration of responses to both incretins in diabetic patients in whom glucose was almost normalized by insulin treatment (Hojberg et al., 2009). Evidence for heteromerization of GIPR and GLP-1R in tissues such as the pancreas would be an essential next step in determining the potential physiological consequences, as well as the therapeutic implications of such an interaction.

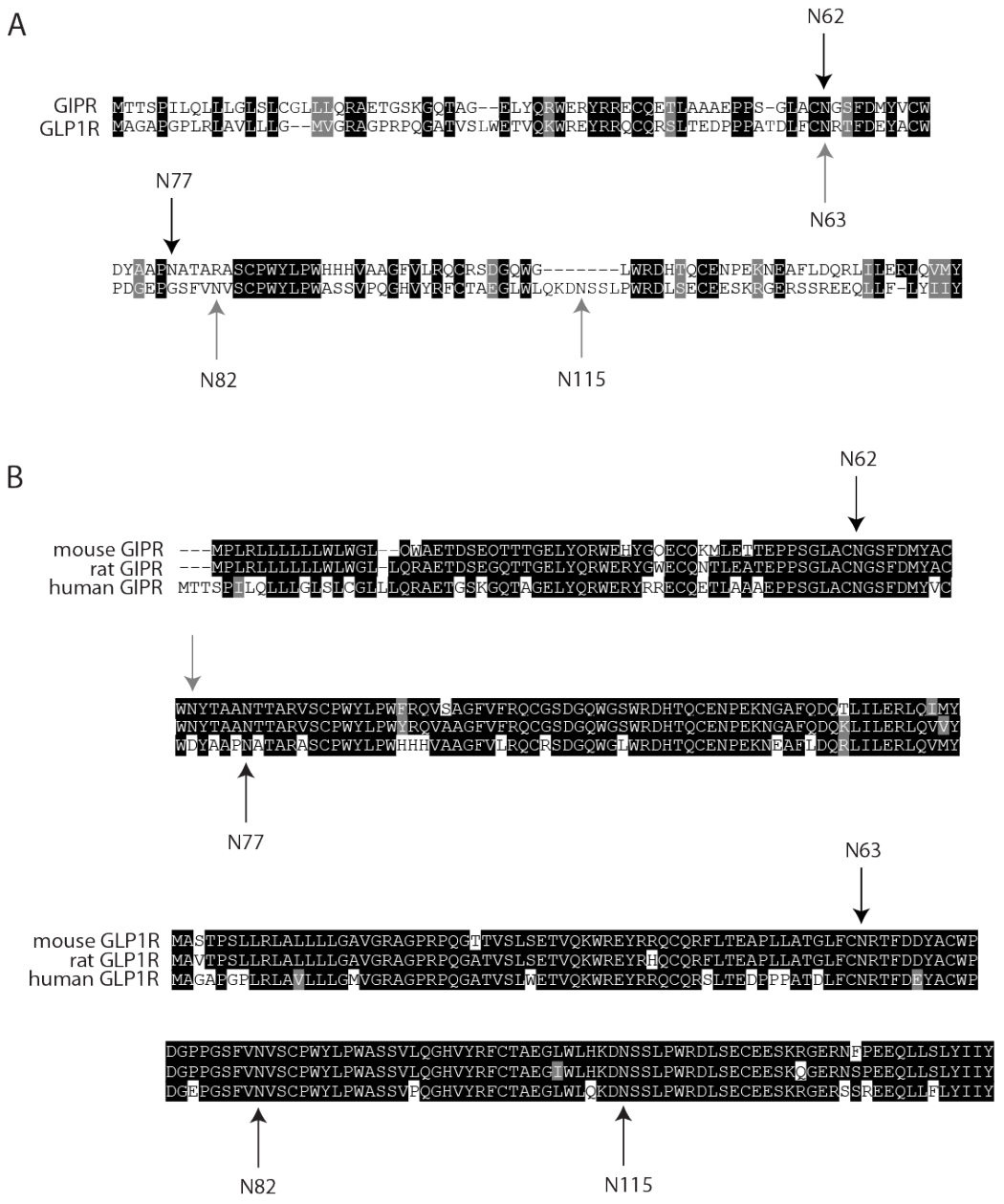

Figure 3.1 Consensus sites for N-glycosylation are found in the N-termini of the closely related human GIPR and GLP-1R

The amino acid sequences for human GIPR and GLP-1R (A) and three mammalian species for each receptor (B) were aligned by *ClustalW*. *Shading* was carried out using *Boxshade* on the Swiss EMBnet node web site (www.ch.embnet.org/software/BOX_form.html). Amino acids highlighted in *black* represent complete identities, whereas those highlighted in *gray* represent conserved identities. Arrows are placed above or below putative N-glycosylation sites and the numbers correspond to their location in the human sequences. In "A", the black and gray arrows correspond to the *Asn* (N) residues in the human GIPR and GLP-1R, respectively. In "B", the gray arrow corresponds to an *Asn* site found in the rodent sequences but not the human sequence.

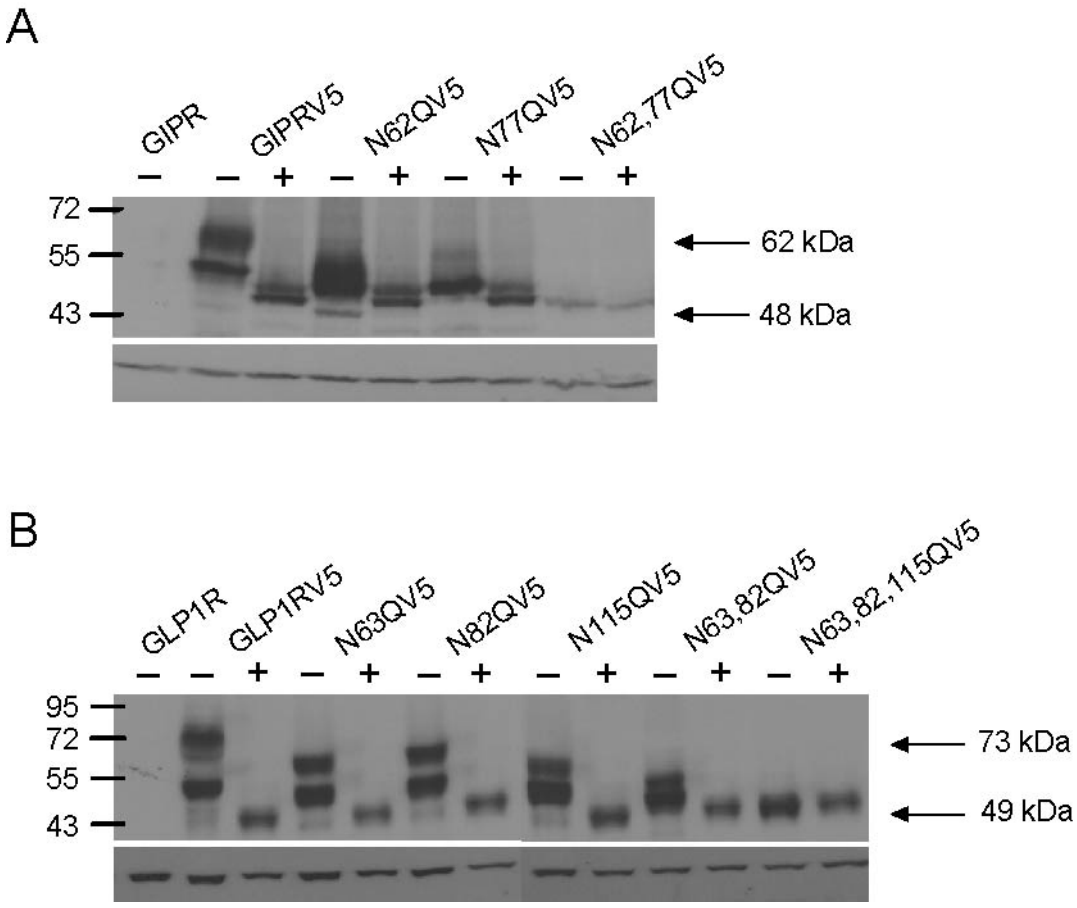

Figure 3.2 All putative N- glycosylation sites found on the N-termini of human GIPR and GLP-1R are used

Western Blots of C-terminally V5-tagged GIPR (above) and GLP-1R (below) and respective tagged mutant receptors in which Asn residues in putative N-glycosylation sites were substituted by Gln, as indicated. Upper blots were probed with mouse monoclonal antibody against the V5 epitope. For both receptors, the lowest blot was probed with a rabbit polyclonal antibody for actin to control for loading. Lanes marked with "+" were treated with tunicamycin, and "–" with DMSO control. Untagged GIPR and GLP-1R are used as negative controls for non-specific antibody binding. Upper and lower arrows indicate the molecular weights for the heaviest bands and lightest bands. The predicted molecular weight for the immature form of GIPRV5 is 57.7kDa and of GLP-1RV5 is 57.4kDa.

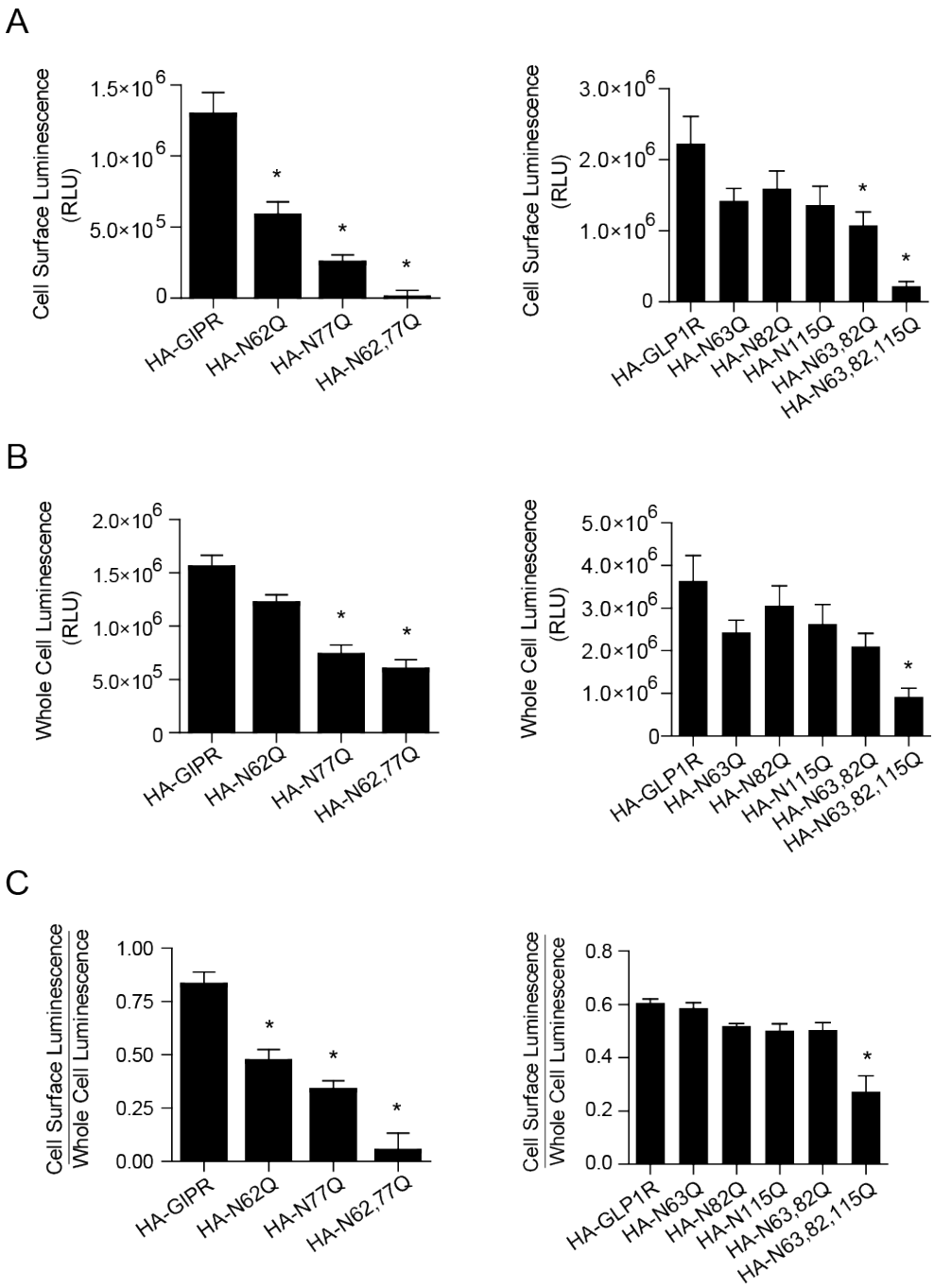

Figure 3.3 N-glycosylation more strongly impacts cell surface expression of the GIPR than the GLP-1R

Plots of cell surface luminescence (A), whole cell luminescence (B) and their ratio (C) from cells expressing N-terminally HA-tagged GIPR (left) and GLP-1R (right) as measuring using ELISA. All constructs were assayed in triplicate from 4-5 separate transfections. Each group of triplicates was corrected for background luminescence from untransfected cells and from cells treated with only secondary HRP-conjugated antibody for each transfected condition. Asterisks represent significance ($p<0.05$) as determined using a one-way ANOVA, followed by Dunnett's multiple comparison tests, comparing mutant constructs to tagged wild type receptors.

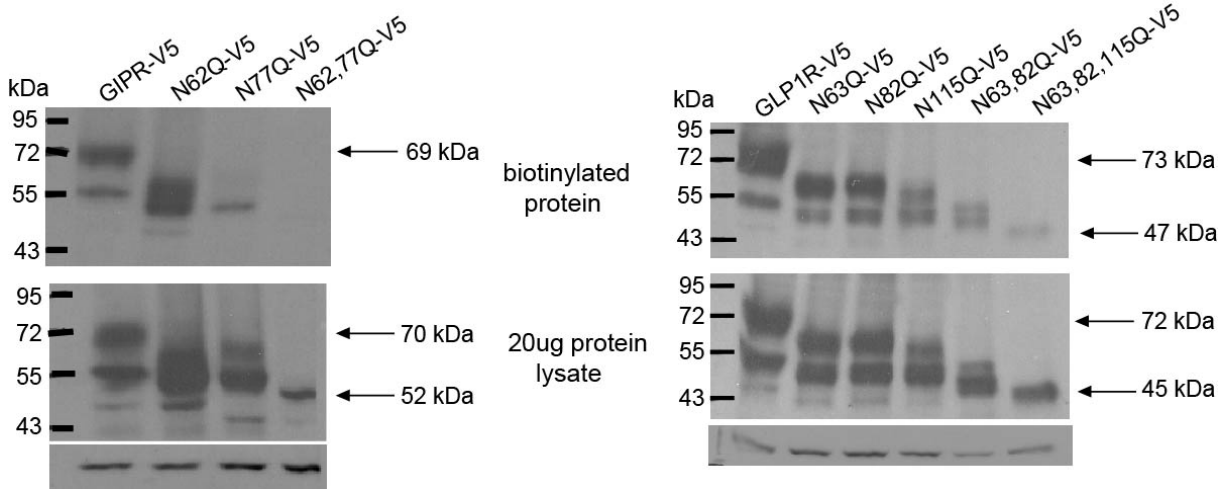

Figure 3.4 N-glycosylation increases levels of cell surface isoforms of GIPR and GLP-1R protein

Western blots of biotinylated cell surface protein (upper) and total protein lysate (lower) for V5-tagged GIPR (left) and GLP-1R (right). Upper and middle blots were probed with a mouse monoclonal antibody to the V5 epitope while the lower blots were probed with a rabbit polyclonal antibody to actin as a loading control. Note the absence of biotinylated protein in the lane containing N62,77Q-GIPR but not in the lane containing N63,82,115Q-GLP-1R.

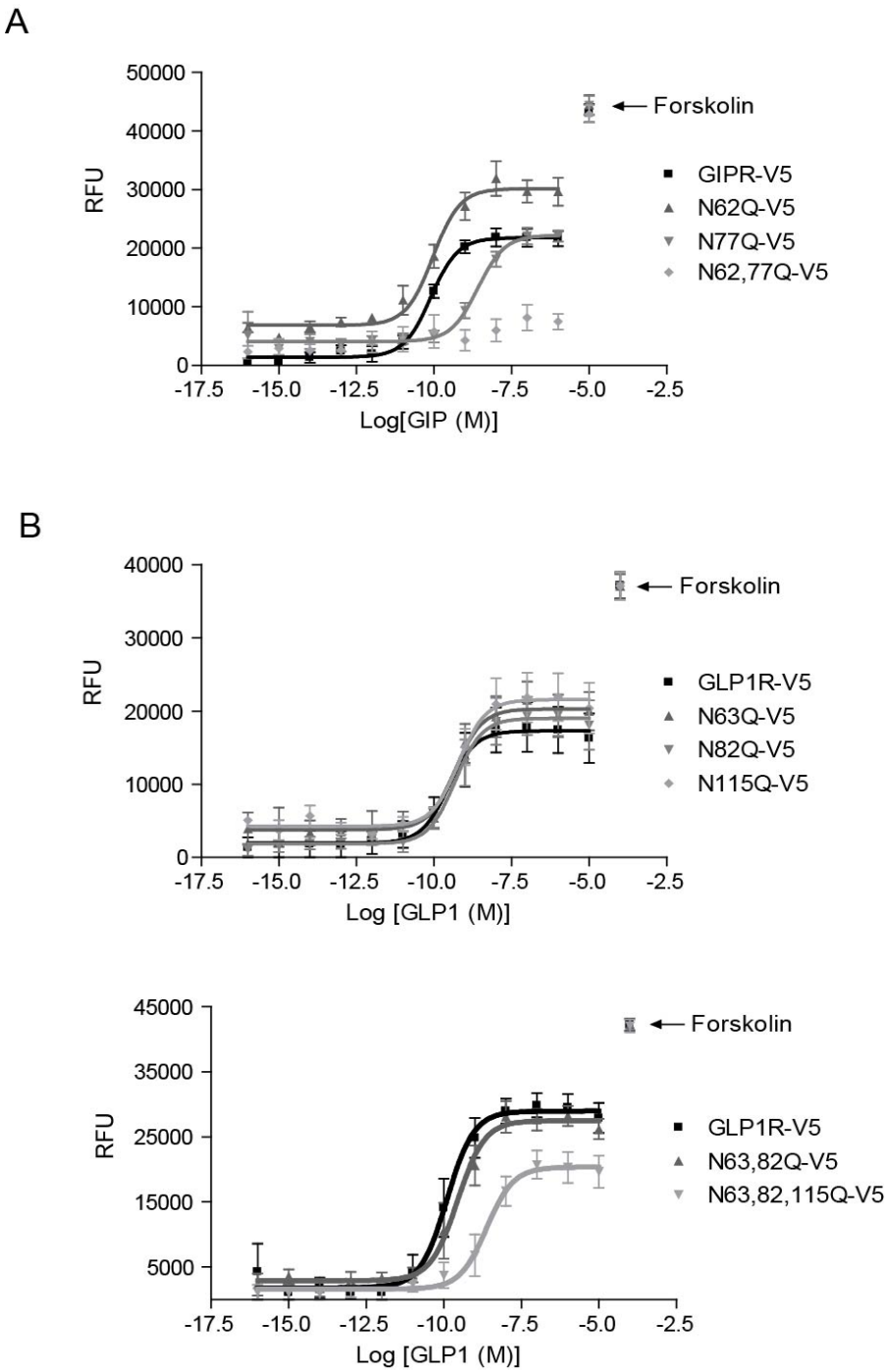

Figure 3.5 Potency and efficacy of GIP and GLP-1 effects on cAMP production in CHO cells are enhanced by N-glycosylation of their receptors

Plots of Relative Fluorescence Units (RFU) versus log of concentration of GIP (A) or GLP-1 (B). RFU values were determined by FRET assay which was carried out using CHO cells expressing GIPR or GLP-1R constructs as indicated. Forskolin was used to control for variations in total cell number. Mean data ± SE (performed in duplicate for an n=5 separate transfections) at each ligand concentration were plotted, converted to a logarithmic scale, and fitted using a sigmoidal dose-response curve.

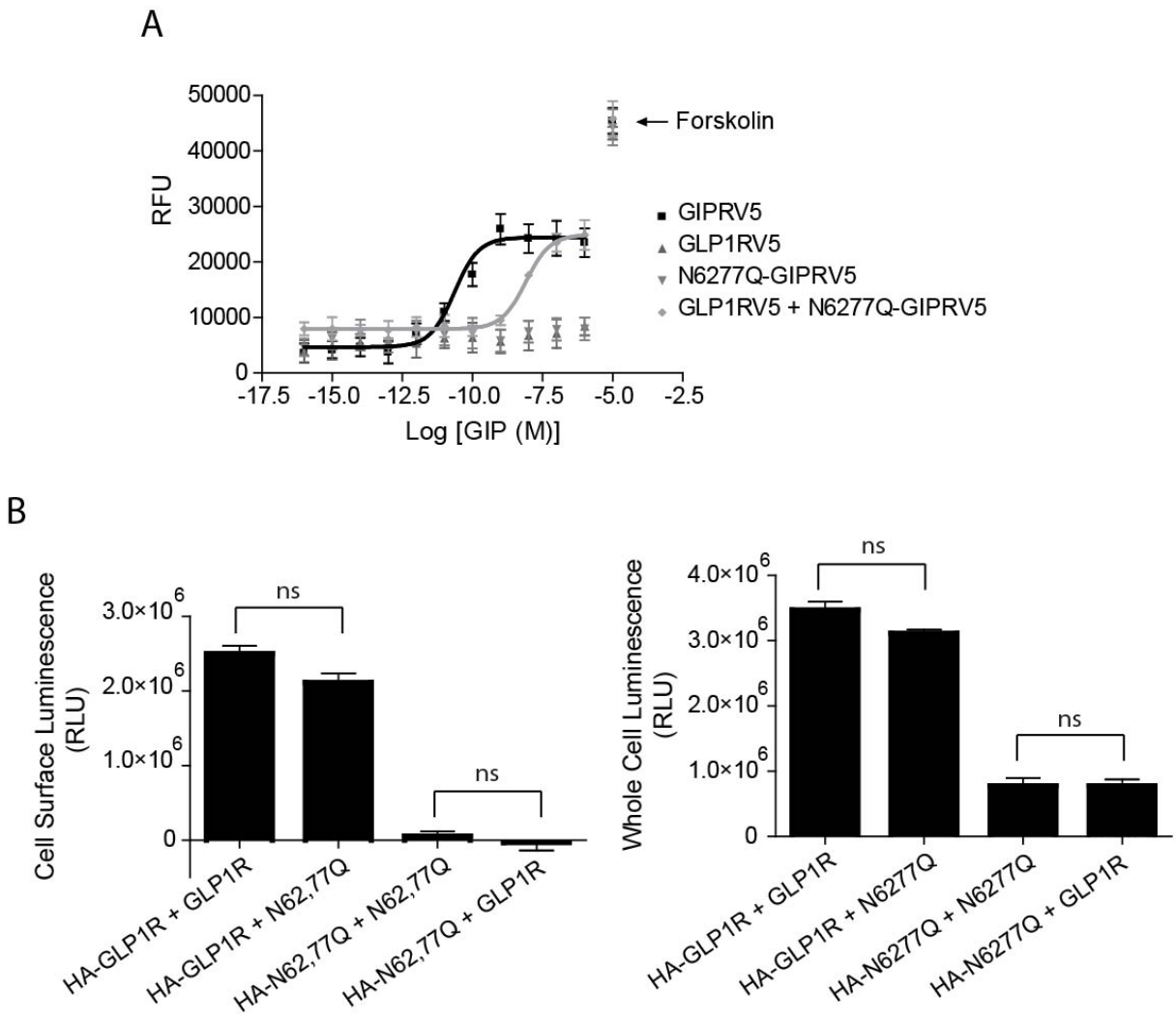

Figure 3.6 Function but not cell surface expression of N62,77Q-GIPR is rescued by co-expression of wild type GLP-1R

A**.** Plots of Relative Fluorescence Units (RFU, indicative of cAMP production) versus log of concentration of GIP. RFU values were determined by FRET assay, which was carried out using cells expressing GIPR and GLP-1R as indicated. Forskolin was used to control for variations in total cell number. Mean data ± SE (n=5 transfections) at each ligand concentration were fit using a sigmoidal dose-response curve. B. Plots of cell surface (left) and whole cell (right) luminescence from cells co-expressing N-terminally HA-tagged GIPR and/or GLP-1R, as indicated. All constructs were assayed in triplicate from 4-5 separate transfections. Each group of triplicates was corrected for background luminescence from untransfected cells and from cells treated with only secondary HRP-conjugated antibody for each transfected condition. Pairs of receptors (grouped in brackets), consisting of one HA-tagged construct and a second untagged construct, were statistically compared by a two-tailed unpaired t-test ($p>0.05$ for each comparison made).

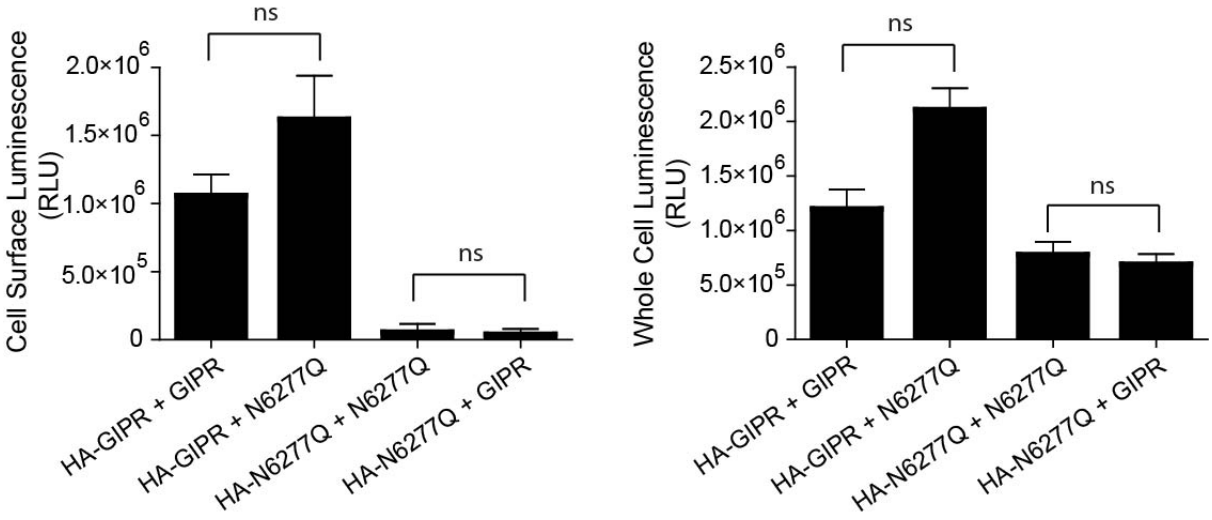

Figure 3.7 Cell surface expression of N62,77Q-GIPR is not rescued by co-expression with the wild type GIPR

Plots of cell surface (left) and whole cell (right) luminescence from cells co-expressing HA-tagged GIPR as indicated. All constructs were assayed in triplicate from 4-5 separate transfections. Each group of triplicates was corrected for background luminescence from untransfected cells and from cells treated with only secondary HRP-conjugated antibody for each transfected condition. Pairs of receptors (grouped in brackets), consisting of one HA-tagged construct and a second untagged construct, were statistically compared by a two-tailed unpaired t-test ($p>0.05$ for each comparison made).

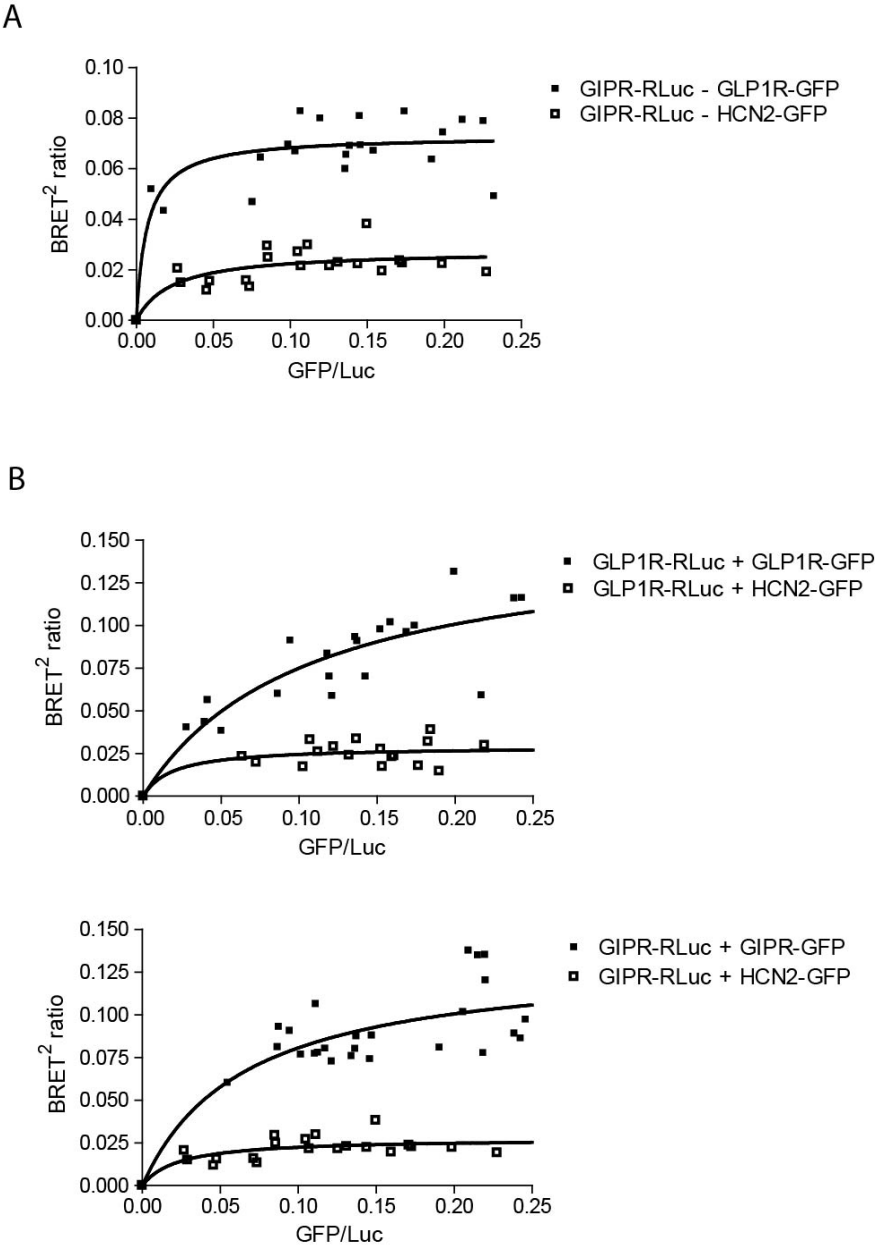

Figure 3.8 BRET values for cells expressing GIPR and GLP-1R suggest heteromeric and homomeric associations

Plots of BRET ratio versus the ratio of GFP/Luc from cells co-expressing RLuc- and GFP-tagged combinations of GIPR, GLP-1R and HCN2 channels, as indicated in the legends. Data were collected from at least separate 5 transfections and fit with a non-linear regression equation assuming a single binding site (GraphPad Prism). A, Curves from GIPR+GLP-1R (BRETmax = 0.073±0.003) compared to GIPR+HCN2 negative control (BRETmax = 0.028±0.004). B, Curves from GLP-1R+GLP-1R (BRETmax=0.15±0.03), compared to GLP-1R+HCN2 negative control (BRETmax=0.029±0.006). C, Curves from GIPR+GIPR (BRETmax=0.13±0.02), compared to GIPR+HCN2 negative control (BRETmax=0.028±0.004). Data in A, B and C were statistically analyzed using a two-tailed unpaired t test and for all conditions, Bmax was significantly greater than negative controls, $p<0.001$.

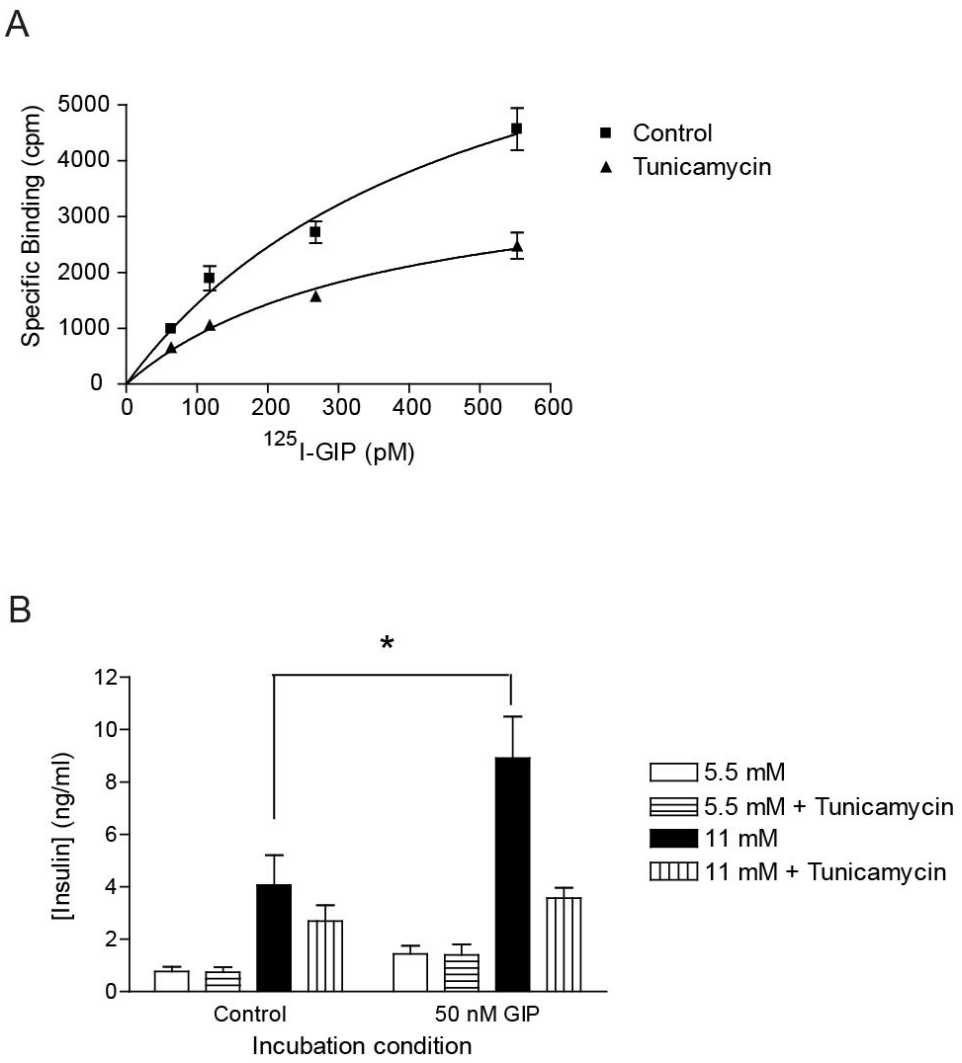

Figure 3.9 N-glycosylation regulates GIP receptor number and GIP-potentiated insulin secretion in INS-1 cells

A. Plot of specific binding versus concentration of ^{125}I-GIP saturation carried out in INS-1 cells with or without 1μg/ml tunicamycin. Data were fit with a non-linear regression equation assuming a single binding site (GraphPad Prism). Control cells expressed an average of 2443±400 GIP receptors on the cell surface (Kd 455 ± 50pM), whereas tunicamycin-treated cells expressed 760±70 GIP receptors on the cell surface (Kd 345 ± 100pM). B. Plot of insulin release in response to glucose and/or GIP, from INS-1 cells with or without 1μg/ml tunicamycin. Data are expressed as mean ± SEM, n=4 separate experiments. Asterisk indicates a significant increase in insulin release compared to basal conditions without addition of 50nM GIP ($P<0.05$), as determined using two-way ANOVA followed by Bonferroni post-tests (this figure was adapted with permission from the PhD thesis of Dr Francis C. Lynn, 2003).

A

	EC_{50} (M)			Amplitude (RFU)		
	Mean	SE	P Value	Mean	SE	P Value
GIPR-V5	8.2×10^{-11}	1.7×10^{-11}	–	2.2×10^{4}	1.3×10^{3}	–
N62Q-V5	1.0×10^{-10}	1.5×10^{-11}	P > 0.05	2.7×10^{4}	3.3×10^{3}	P > 0.05
N77Q-V5	3.1×10^{-9}	1.1×10^{-9}	P < 0.01	2.2×10^{4}	6.5×10^{2}	P > 0.05
N62,77Q-V5	–	–	–	8.0×10^{3}	1.4×10^{3}	P < 0.01

B

	EC_{50} (M)			Amplitude (RFU)		
	Mean	SE	P value	Mean	SE	P value
GLP1R-V5	4.1×10^{-10}	1.2×10^{-10}	–	1.7×10^{4}	3.7×10^{3}	–
N63Q-V5	6.3×10^{-10}	1.4×10^{-10}	P > 0.05	1.9×10^{4}	3.9×10^{3}	P > 0.05
N82Q-V5	7.1×10^{-10}	2.6×10^{-10}	P > 0.05	1.9×10^{4}	2.6×10^{3}	P > 0.05
N115Q-V5	7.2×10^{-10}	1.1×10^{-10}	P > 0.05	2.0×10^{4}	4.2×10^{3}	P > 0.05

	EC_{50} (M)			Amplitude (RFU)		
	Mean	SE	P value	Mean	SE	P value
GLP1R-V5	2.2×10^{-10}	1.1×10^{-10}	–	2.9×10^{4}	9.0×10^{2}	–
N63,82Q-V5	5.8×10^{-10}	2.9×10^{-10}	P > 0.05	2.8×10^{4}	1.9×10^{3}	P > 0.05
N63,82,115QV5	2.7×10^{-9}	6.8×10^{-10}	P < 0.01	2.0×10^{4}	2.0×10^{3}	P < 0.01

Table 3.1 Mean EC_{50} values and amplitude of responses for cAMP concentration-response curves in figure 3.5

EC_{50} values were determined for each individual experiment, using a sigmoidal dose-response equation. Compared to wild-type receptors, the EC_{50} values for N77Q-GIPR and N63,82,115Q-GLP-1R were significantly right shifted, as shown by a one-way ANOVA analysis followed by Dunnett's multiple comparison test. The changes in RFU values for the N62,77Q-GIPR were small and could not be accurately fitted. The amplitude of response was calculated by subtracting the lowest RFU values from the highest for each individual experiment.

	EC_{50} (M)			Amplitude (RFU)		
	Mean	SE	P Value	Mean	SE	P Value
GIPR-V5	3.4×10^{-11}	1.1×10^{-11}	–	2.3×10^{4}	2.8×10^{3}	–
N62,77Q-V5	–	–	–	5.0×10^{3}	7.1×10^{2}	$P < 0.01$
GLP1R-V5	–	–	–	6.3×10^{3}	2.0×10^{3}	$P < 0.01$
GLP1R-V5 + N62,77Q-V5	1.1×10^{-8}	5.2×10^{-9}	$P < 0.0001$	1.9×10^{4}	2.3×10^{3}	$P > 0.05$

Table 3.2 Mean EC_{50} values and amplitude of response for cAMP concentration-response curves in figure 3.6A

EC_{50} values were determined for each individual experiment, using a sigmoidal concentration-response equation. Compared to wild type GIPR, the EC_{50} values for N62,77Q-GIPR when co-expressed with the wild type GLP-1R was significantly right shifted, as shown by a one-way ANOVA analysis followed by Dunnett's multiple comparison test. The changes in RFU values for N62,77Q-GIPR or the GLP-1R were small and could not be accurately fit. The amplitude of response was calculated by subtracting the lowest RFU values from the highest for each individual experiment.

3.5 References

Amiranoff, B., Couvineau, A., Vauclin-Jacques, N. and Laburthe, M. (1986). Gastric inhibitory polypeptide receptor in hamster pancreatic beta cells. direct cross-linking, solubilization and characterization as a glycoprotein. *Eur. J. Biochem.* **159,** 353-358.

Baggio, L. L. and Drucker, D. J. (2007). Biology of incretins: GLP-1 and GIP. *Gastroenterology* **132,** 2131-2157.

Banères, J. L. and Parello, J. (2003). Structure-based analysis of GPCR function: Evidence for a novel pentameric assembly between the dimeric leukotriene B4 receptor BLT1 and the G-protein. *J. Mol. Biol.* **329,** 815-829.

Bulenger, S., Marullo, S. and Bouvier, M. (2005). Emerging role of homo- and heterodimerization in G-protein-coupled receptor biosynthesis and maturation. *Trends Pharmacol. Sci.* **26,** 131-137.

Chabre, M., Deterre, P. and Antonny, B. (2009). The apparent cooperativity of some GPCRs does not necessarily imply dimerization. *Trends Pharmacol. Sci.* **30,** 182-187.

Chabre, M. and le Maire, M. (2005). Monomeric G-protein-coupled receptor as a functional unit. *Biochemistry* **44,** 9395-9403.

Chang, X. B., Mengos, A., Hou, Y. X., Cui, L., Jensen, T. J., Aleksandrov, A., Riordan, J. R. and Gentzsch, M. (2008). Role of N-linked oligosaccharides in the biosynthetic processing of the cystic fibrosis membrane conductance regulator. *J. Cell. Sci.* **121,** 2814-2823.

Dong, C., Filipeanu, C. M., Duvernay, M. T. and Wu, G. (2007). Regulation of G protein-coupled receptor export trafficking. *Biochim. Biophys. Acta* **1768,** 853-870.

Fernandes, H., Cohen, S. and Bishayee, S. (2001). Glycosylation-induced conformational modification positively regulates receptor-receptor association: A study with an aberrant epidermal growth factor receptor (EGFRvIII/DeltaEGFR) expressed in cancer cells. *J. Biol. Chem.* **276,** 5375-5383.

Ferre, S., Baler, R., Bouvier, M., Caron, M. G., Devi, L. A., Durroux, T., Fuxe, K., George, S. R., Javitch, J. A., Lohse, M. J. et al. (2009). Building a new conceptual framework for receptor heteromers. *Nat. Chem. Biol.* **5,** 131-134.

Göke, R., Just, R., Lankat-Buttgereit, B. and Göke, B. (1994). Glycosylation of the GLP-1 receptor is a prerequisite for regular receptor function. *Peptides* **15,** 675-681.

Gremlich, S., Porret, A., Hani, E. H., Cherif, D., Vionnet, N., Froguel, P. and Thorens, B. (1995). Cloning, functional expression, and chromosomal localization of the human pancreatic islet glucose-dependent insulinotropic polypeptide receptor. *Diabetes* **44,** 1202-1208.

Guan, R., Feng, X., Wu, X., Zhang, M., Hébert, T.E. and Segaloff, D.L. (2009). Bioluminescence resonance energy transfer studies reveal constitutive dimerization of the human lutropin receptor and a lack of correlation between receptor activation and the propensity for dimerization. *J. Biol. Chem.* **284,** 7483-7494

Gurevich, V. V. and Gurevich, E. V. (2008a). GPCR monomers and oligomers: It takes all kinds. *Trends Neurosci.* **31,** 74-81.

Gurevich, V. V. and Gurevich, E. V. (2008b). How and why do GPCRs dimerize? *Trends Pharmacol. Sci.* **29,** 234-240.

Harikumar, K. G., Morfis, M. M., Sexton, P. M. and Miller, L. J. (2008). Pattern of intra-family hetero-oligomerization involving the G-protein-coupled secretin receptor. *J. Mol. Neurosci.* **36,** 279-285.

He, J., Xu, J., Castleberry, A. M., Lau, A. G. and Hall, R. A. (2002). Glycosylation of beta(1)-adrenergic receptors regulates receptor surface expression and dimerization. *Biochem. Biophys. Res. Commun.* **297,** 565-572.

Hebert, D. N., Zhang, J. X., Chen, W., Foellmer, B. and Helenius, A. (1997). The number and location of glycans on influenza hemagglutinin determine folding and association with calnexin and calreticulin. *J. Cell Biol.* **139,** 613-623.

Hohmeier, H. E., Mulder, H., Chen, G., Henkel-Rieger, R., Prentki, M. and Newgard, C. B. (2000). Isolation of INS-1-derived cell lines with robust ATP-sensitive K+ channel-dependent and -independent glucose-stimulated insulin secretion. *Diabetes* **49,** 424-430.

Hojberg, P. V., Vilsboll, T., Zander, M., Knop, F. K., Krarup, T., Volund, A., Holst, J. J. and Madsbad, S. (2008). Four weeks of near-normalization of blood glucose has no effect on postprandial GLP-1 and GIP secretion, but augments pancreatic B-cell responsiveness to a meal in patients with type 2 diabetes. *Diabet. Med.* **25,** 1268-1275.

Issafras, H., Angers, S., Bulenger, S., Blanpain, C., Parmentier, M., Labbé-Jullié, C., Bouvier, M. and Marullo, S. (2002). Constitutive agonist-independent CCR5 oligomerization and antibody-mediated clustering occurring at physiological levels of receptors. *J. Biol. Chem.* **277,** 34666-34673.

Kniazeff, J., Bessis, A. S., Maurel, D., Ansanay, H., Prezeau, L. and Pin, J. P. (2004). Closed state of both binding domains of homodimeric mGlu receptors is required for full activity. *Nat. Struct. Mol. Biol.* **11,** 706-713.

Langer, I., Leroy, K., Gaspard, N., Brion, J. P. and Robberecht, P. (2008). Cell surface targeting of VPAC1 receptors: Evidence for implication of a quality control system and the proteasome. *Biochim. Biophys. Acta* **1783,** 1663-1672.

Lynn, F. C., Thompson, S. A., Pospisilik, J. A., Ehses, J. A., Hinke, S. A., Pamir, N., McIntosh, C. H. and Pederson, R. A. (2003). A novel pathway for regulation of glucose-dependent insulinotropic polypeptide (GIP) receptor expression in beta cells. *FASEB J.* **17,** 91-93.

Mayo, K. E., Miller, L. J., Bataille, D., Dalle, S., Göke, B., Thorens, B. and Drucker, D. J. (2003). International union of pharmacology. XXXV. the glucagon receptor family. *Pharmacol. Rev.* **55,** 167-194.

McIntosh, C. H., Widenmaier, S. and Kim, S. J. (2009). Glucose-dependent insulinotropic polypeptide (gastric inhibitory polypeptide; GIP). *Vitam. Horm.* **80,** 409-471.

Mercier, J. F., Salahpour, A., Angers, S., Breit, A. and Bouvier, M. (2002). Quantitative assessment of beta 1- and beta 2-adrenergic receptor homo- and heterodimerization by bioluminescence resonance energy transfer. *J. Biol. Chem.* **277,** 44925-44931.

Meyer, B. H., Segura, J. M., Martinez, K. L., Hovius, R., George, N., Johnsson, K. and Vogel, H. (2006). FRET imaging reveals that functional neurokinin-1 receptors are monomeric and reside in membrane microdomains of live cells. *Proc. Natl. Acad. Sci. U. S. A.* **103,** 2138-2143.

Mialet-Perez, J., Green, S. A., Miller, W. E. and Liggett, S. B. (2004). A primate-dominant third glycosylation site of the beta2-adrenergic receptor routes receptors to degradation during agonist regulation. *J. Biol. Chem.* **279,** 38603-38607.

Michineau, S., Alhenc-Gelas, F. and Rajerison, R. M. (2006). Human bradykinin B2 receptor sialylation and N-glycosylation participate with disulfide bonding in surface receptor dimerization. *Biochemistry* **45,** 2699-2707.

Michineau, S., Muller, L., Pizard, A., Alhenc-Gelas, F. and Rajerison, R. M. (2004). N-linked glycosylation of the human bradykinin B2 receptor is required for optimal cell-surface expression and coupling. *Biol. Chem.* **385,** 49-57.

Milligan, G. (2007). G protein-coupled receptor dimerisation: Molecular basis and relevance to function. *Biochim. Biophys. Acta* **1768,** 825-835.

Milligan, G. (2009). G protein-coupled receptor hetero-dimerization: Contribution to pharmacology and function. *Br. J. Pharmacol.* **158,** 5-14.

Mody, N., Hermans, E., Nahorski, S. R. and Challiss, R. A. (1999). Inhibition of N-linked glycosylation of the human type 1alpha metabotropic glutamate receptor by tunicamycin: Effects on cell-surface receptor expression and function. *Neuropharmacology* **38,** 1485-1492.

Moens, K., Heimberg, H., Flamez, D., Huypens, P., Quartier, E., Ling, Z., Pipeleers, D., Gremlich, S., Thorens, B. and Schuit, F. (1996). Expression and functional activity of glucagon, glucagon-like peptide I, and glucose-dependent insulinotropic peptide receptors in rat pancreatic islet cells. *Diabetes* **45,** 257-261.

Nauck, M., Stockmann, F., Ebert, R. and Creutzfeldt, W. (1986). Reduced incretin effect in type 2 (non-insulin-dependent) diabetes. *Diabetologia* **29,** 46-52.

Nauck, M. A., Heimesaat, M. M., Orskov, C., Holst, J. J., Ebert, R. and Creutzfeldt, W. (1993). Preserved incretin activity of glucagon-like peptide 1 [7-36 amide] but not of synthetic human gastric inhibitory polypeptide in patients with type-2 diabetes mellitus. *J. Clin. Invest.* **91,** 301-307.

Ostrom, R. S., Gregorian, C., Drenan, R. M., Xiang, Y., Regan, J. W. and Insel, P. A. (2001). Receptor number and caveolar co-localization determine receptor coupling efficiency to adenylyl cyclase. *J. Biol. Chem.* **276,** 42063-42069.

Patel, H. H., Murray, F. and Insel, P. A. (2008). Caveolae as organizers of pharmacologically relevant signal transduction molecules. *Annu. Rev. Pharmacol. Toxicol.* **48,** 359-391.

Salahpour, A., Angers, S., Mercier, J. F., Lagace, M., Marullo, S. and Bouvier, M. (2004). Homodimerization of the beta2-adrenergic receptor as a prerequisite for cell surface targeting. *J. Biol. Chem.* **279,** 33390-33397.

Terrillon, S., Durroux, T., Mouillac, B., Breit, A., Ayoub, M.A., Taulan, M., Jockers, R., Barberis, C. and Bouvier, M. (2003). Oxytocin and vasopressin V1a and V2 receptors form constitutive homo- and heterodimers during biosynthesis. *Mol. Endocrinol.* **17,** 677-691.

Usdin, T. B., Mezey, E., Button, D. C., Brownstein, M. J. and Bonner, T. I. (1993). Gastric inhibitory polypeptide receptor, a member of the secretin-vasoactive intestinal peptide receptor family, is widely distributed in peripheral organs and the brain. *Endocrinology* **133,** 2861-2870.

Vrecl, M., Drinovec, L., Elling, C. and Heding, A. (2006). Opsin oligomerization in a heterologous cell system. *J. Recept. Signal Transduct. Res.* **26,** 505-526.

Wanamaker, C. P. and Green, W. N. (2005). N-linked glycosylation is required for nicotinic receptor assembly but not for subunit associations with calnexin. *J. Biol. Chem.* **280,** 33800-33810.

Whitaker, G. M. and Accili, E. A. (2008). Using bioluminescence resonance energy transfer to measure ion channel assembly. *Methods Mol. Biol.* **491,** 189-197.

Whitaker, G. M., Angoli, D., Nazzari, H., Shigemoto, R. and Accili, E. A. (2007). HCN2 and HCN4 isoforms self-assemble and co-assemble with equal preference to form functional pacemaker channels. *J. Biol. Chem.* **282,** 22900-22909.

White, J. H., Wise, A., Main, M. J., Green, A., Fraser, N. J., Disney, G. H., Barnes, A. A., Emson, P., Foord, S. M. and Marshall, F. H. (1998). Heterodimerization is required for the formation of a functional GABA(B) receptor. *Nature* **396,** 679-682.

Whorton, M. R., Bokoch, M. P., Rasmussen, S. G., Huang, B., Zare, R. N., Kobilka, B. and Sunahara, R. K. (2007). A monomeric G protein-coupled receptor isolated in a high-density lipoprotein particle efficiently activates its G protein. *Proc. Natl. Acad. Sci. U. S. A.* **104,** 7682-7687.

Widmann, C., Dolci, W. and Thorens, B. (1996). Heterologous desensitization of the glucagon-like peptide-1 receptor by phorbol esters requires phosphorylation of the cytoplasmic tail at four different sites. *J. Biol. Chem.* **271,** 19957-19963.

Zhong, X., Kriz, R., Seehra, J. and Kumar, R. (2004). N-linked glycosylation of platelet P2Y12 ADP receptor is essential for signal transduction but not for ligand binding or cell surface expression. *FEBS Lett.* **562,** 111-117.

4 CONCLUDING CHAPTER

4.1 Overview

Upon translation of a nascent membrane-bound polypeptide chain, it becomes subject to various modifications, including the addition of N-glycans to specific sites, as well as oligomerization with closely related or identical partners. For many proteins, either or both of these processes play an important or even essential role in proper trafficking and functional cell surface expression. The overall objective of this thesis was to investigate the role of both of these processes in the regulation of functional cell surface expression of membrane proteins. Specifically, in chapter 2, the homomeric and heteromeric assembly of HCN2 and HCN4 channels was examined in CHO cells and in native tissue. In chapter 3, the role of N-glycosylation on regular GIPR and GLP-1R function and expression, as well as the potential for these two receptors to form homomers and heteromers in CHO cells was established.

4.2 Variable Stabilities of Membrane Protein Oligomeric Complexes

The occurrence, stability and functional consequences of membrane protein oligomerization can vary greatly, depending on the protein studied. Many ion channels exist as stable or obligatory oligomers, assembling as a complex in the ER thus forming the required unit for trafficking and functional expression. HCN channels fall into this category, expressing as stable tetramers in order to traffic to the cell surface and conduct current. Their stable tetrameric structure is hypothesized to be due to strong intersubunit interactions between N-termini, similar to the T1 domain of Kv channels (Deutsch, 2002; Tran et al., 2002). Whereas tetrameric assembly of HCN channels is an absolute prerequisite for functional expression, the oligomeric state of GPCRs can vary widely. For example, class C GPCRs exist exclusively as stable, obligatory dimers and their mechanism of intersubunit interaction is well understood (Pin et al., 2003). Conversely, despite numerous studies that show the propensity for class A GPCRs to exist as dimers or higher order oligomers, the stability of these interactions and existence *in vivo* is less clear. Moreover, many class A GPCRs are also functional as monomers, and the structure required for optimal function seems to depend on the receptor studied. For example, when both rhodopsin and NT1 receptors exist in the oligomeric form, they couple less efficiently to G proteins compared to when they are present in monomeric form (Bayburt et al., 2007; White et al., 2007). Another

more recent study reported a shift in β_2-AR equilibrium from tetramers to lower-order oligomers upon coupling to G proteins (Fung et al., 2009). Thus, GPCR oligomerization, at least for some class A receptors, seems to be more dynamic in nature, a consequence of less stable and potentially less specific interactions, between two protomers. More direct evidence for this comes from a study using single molecule imaging, which revealed how the state of muscarinic M1 receptor dimer interactions changed over a time course. It was found that the existence of dimers was primarily a result of dynamic associations over short periods of time, and only 30% of cell surface receptors existed as dimers at any given time (Hern et al., 2010). Other studies where one receptor protomer is immobilized in the membrane and dimer interaction is measured over time, have shown that at least a fraction of β_1-AR and D2R expressed at the cell surface exist as oligomers only transiently (Dorsch et al., 2009; Fonseca and Lambert, 2009). However, similar experiments also reported that unlike the β1-AR, the β_2-AR exists exclusively as a stable dimer at the cell surface (Dorsch et al., 2009). Much less is known about the existence and stability of class B GPCR oligomers, which include the GIPR and GLP-1R. The more widely studied secretin receptor is able to form receptor homomers and heteromers with other GPCRs within the same family. Interestingly, dimerization is initiated during biogenesis and is required for optimal function of the secretin receptor (Harikumar et al., 2007; Harikumar et al., 2008; Lisenbee and Miller, 2006).

Despite the debate over the extent of dimer formation and its actual implications for receptor function, the fact that many GPCRs are able to form oligomeric complexes suggests a potential physiological role, whether the interaction is dynamic or stable. The reported functional consequences of oligomeric GPCR formation are diverse and provide further support for the existence of dimers or higher-order oligomers in native tissue. GPCR oligomerization has been shown to be important for proper receptor maturation and trafficking, ligand binding, and signal transfer between monomers. Some positively or negatively influence cooperativity of ligand binding, form optimal platforms for G protein activation, and modulate co-internalization of heteromeric protomers. Thus the transient nature of interactions recently measured among various class A GPCRs does not discount the potential functional impact of receptor oligomerization. Perhaps, unlike ion channels, which exclusively express as stable tetramers at the cell surface, less stable oligomeric GPCRs may exist in some sort of dynamic equilibrium with monomers, thus providing another means of regulation of signal transduction within the cell (Figure 4.1).

4.3 Tetrameric Assembly of HCN2 and HCN4 Channels in CHO Cells

In this thesis, the potential for heteromeric channel assembly of HCN2 and HCN4 was examined, as well as the propensity for homomeric versus heteromeric assembly, in CHO cells. Using BRET and imaging techniques combined with Pearson Correlation analysis, as well as electrophysiological experiments showing functional rescue of a trafficking-deficient HCN2 by HCN4, we determined that these two isoforms are indeed able to co-assemble, as well as self-assemble, and without preference for one type of assembly versus the other. Furthermore, we showed a physical association of HCN2 and HCN4 in the rat thalamus and overlapping regions of isoform expression in the mouse embryonic heart, thus providing support for co-assembly of these two isoforms *in vivo*. A recent study has shown that HCN2 and HCN4 co-immunoprecipitate from the adult mouse heart, and that the HCN2 isoform is post-translationally cleaved such that the mature protein lacks a C-terminus (Ye and Nerbonne, 2009). Co-expression of the C-terminally-truncated form of HCN2 with HCN4 in heterologous cells produces current that closely resembles cardiac I_f channels. Together, these results provide strong evidence supporting co-assembly of HCN2 and HCN4 in native tissue.

Our novel use of BRET as a method to measure ion channel assembly provides many advantages to other invasive biochemical techniques. First, the assay is performed on live, intact cells thus enabling proteins of interest to remain in their membrane environment. This is important for membrane proteins such as HCN channels since their hydrophobic core regions could cause unwanted aggregation and false positives. One other advantage of this technique is that it provides a higher sensitivity of detection, measuring interaction distances within 100Å or less, of donor and acceptor molecules. Although this is superior to many alternative methods of measurement, close associations between two neighboring channels composed of different isoforms could be incorporated and thus measured within this distance, especially in the context of overexpression systems. However, with the addition of proper positive and negative controls, this issue can be minimized.

The efficiency of BRET signal within this 100Å radius is inversely proportional to the distance between donor and acceptor molecules to the power of 6, according to the equation measuring the Förster resonance energy transfer,

$$E = 1/[1 + (r/Ro)^6]$$

where E is the BRET efficiency, Ro is the Förster distance between donor and acceptor pair, and r is the donor-to-acceptor separation distance. Thus very small variations in distance between donor and acceptor theoretically result in large changes in the BRET signal. Because of this, we were able to compare our positive control, which in this case were donor and acceptor-tagged HCN2 or HCN4 homomeric complexes, with heteromeric HCN2-HCN4 combinations. We found that the BRET ratios for all combinations were equal, suggesting that HCN2 and HCN4 co-assemble and self-assemble without preference. To support these results, we imaged the same tagged-channel combinations as those in BRET assays, using antibodies specific to GFP- and RLuc- tags, which enabled us to keep the antibodies used constant when comparing different isoform combinations. From the imaged co-expressing cells, we compared Pearson Correlation values, which describes the relationship between the intensities of fluorescence of two expressing proteins throughout a cell. This is a superior method to simply comparing overlap coefficients, which measures the degree of overlap, and can be inherently high for all co-expressing membrane protein combinations in an overexpression system. Our rationale for comparing Pearson Correlation Coefficients in order to examine assembly was that two isoforms that co-assemble would be interdependently expressed, at least to some extent, throughout the cell, and thus should theoretically be correlated in terms of their variability of expression throughout a cell. Once again, the use of proper positive and negative controls was crucial for this assay and provided further evidence for HCN2-4 co-assembly and without preference for self-assembly. In both BRET and imaging assays described here, measured isoform interactions did not discriminate between those present within intracellular compartments and at the cell surface. Reproduction of imaging and Pearson Correlation analysis using externally tagged HCN isoform constructs, such that only subunit assembly at the cell surface is measured, would be an interesting next step in examining the relative amount of homomers and heteromers that are functionally expressed at the cell surface, compared to those expressed within a cell. A recent report has described a method using a combination of time-resolved FRET with snap-tag labeling in order to specifically measure cell surface protein-protein interactions (Maurel et al., 2008).

This technique could be adapted and used in our system to detect and quantify the proportion of homomeric and heteromeric HCN channel complexes at the cell surface.

The observed results that HCN2 and HCN4 co-assemble and self-assemble with equal preference suggest that the two isoforms interact to produce a random binomial distribution of heteromeric and homomeric channels within a cell. These results, however do not give information about individual channel stoichiometry. Although they suggest that the interaction is random, thus producing a mixture of all potential stoichiometries, the results could also be explained by a strict 2HCN2:2HCN4 heteromeric assembly or a 3:1 association, with either isoform randomly contributing 3 subunits to the tetramer. However if there truly is no preference for assembly, then the results most likely reflect a binomial mix of all possible stoichiometries between two isoforms within a given cell. Further investigation into the regions of intersubunit interaction could give insight into isoform stoichiometry. The conserved region of the N-terminus, adjacent to the first transmembrane domain is a known site of interaction between HCN1 and HCN2 (Tran et al., 2002). This region may provide a similar framework for channel assembly as the T1 domain does for Kv channels. Thus, careful sequence comparisons within this region, and other areas of the protein could help determine the exact region(s) of interaction, and whether or not it is the same for all mammalian isoforms. HCN3 is the only isoform that is unable to co-immunoprecipitate with HCN2, thus the construction of chimeras where various portions of the conserved N-terminus of HCN3 are inserted into other isoforms could potentially give insight into the exact region of interaction for co-assembly. Once this region is delineated, direct affinities of interaction between isoforms at this location can be analyzed and compared.

4.4 Homomeric and Heteromeric Assembly of HCN2 and HCN4 *In Vivo*

In our experiments examining homomeric versus heteromeric assembly of HCN2 and HCN4, we controlled for expression levels by transfecting constant amounts of DNA for each isoform. In native tissue, isoform expression patterns vary depending on species, cell and tissue type, as well as throughout development and in various pathological states. Thus, our results are not necessarily a clear representation of what is in fact taking place *in vivo*. We have shown that HCN2 and HCN4 co-assemble and self-assemble with equal preference, provided they are co-expressed in similar amounts and in the same time and space, which is not necessarily reflective of native tissue. When examining Pearson correlations of HCN2 and

HCN4 expression in different regions of the embryonic mouse heart, despite areas of fluorescence overlap, the recorded Pearson Correlations were lower. Thus, variable isoform expression levels may affect the degree of co-assembly. Indeed, studies that quantified the amount of Kv1.5 self-assembly versus co-assembly with Kv1.4 found that the levels of homomeric and heteromeric channels varied depending on the relative amounts of each isoform expressed within a cell, thus assuming that a random assembly of subunits was taking place by the law of mass action (Levitan and Takimoto, 1998). A potential next step could be to measure BRET ratios and Pearson Correlations between HCN2 and HCN4 under variable expression levels of each isoform, and further determining if there is a direct correlation between relative expression and assembly preference.

In native tissue, developmental, physiological, pharmacological and pathophysiological stimuli may regulate HCN channel gene expression, which in turn could dynamically alter channel composition. For example, HCN2 to HCN4 mRNA transcript ratios change from 5:1 in the neonatal to 13:1 in the adult heart, along with a negative shift in the voltage-dependence of I_f activation (Shi et al., 1999). A recent study quantifying HCN2 and HCN4 transcript levels in adult rat ventricular myocytes found an associated increase in HCN2 mRNA when HCN4 was overexpressed, along with a depolarizing shift in I_f activation and faster activation kinetics (Zhang et al., 2009). Similarly, knockdown of HCN2 mRNA resulted in a corresponding decrease in HCN4. These results suggest that HCN2 and HCN4 expression is interdependent, and that the ratios of expressing isoforms modulate heteromeric channel formation, and I_f. Thus, relative levels of isoform expression may be a main regulator of homomeric versus heteromeric channel formation in native cells. This gives further support for our results, which suggest that, keeping expression levels constant, there is no preference for either type of assembly, and thus interaction affinities between HCN2 and HCN4 homomers and heteromers are likely equal in native cells. Analysis of the relationship between Overlap Coefficients and Pearson Correlations, as well as relative isoform fluorescence intensities and Pearson Correlations in isolated cardiomyocytes would help determine a direct link between expression levels and channel composition *in vivo*.

The idea that levels of HCN2 and HCN4 expression are interdependent, with changes in expression resulting in variable channel phenotype, has important implications in disease. Various mutations in HCN4 have been associated with inheritable forms of sinus arrhythmia (Baruscotti et al., 2010). Furthermore, HCN4 mRNA expression is upregulated in

hypertrophic cardiomyopathy (Wei-Qing et al., 2010). The question remains as to how other isoforms, as well as the proportion of homomeric to heteromeric channels expressed, are affected by the observed changes in HCN4 expression. Future experiments examining the associated changes in HCN2 (or other isoform) expression in HCN4-affected pathologies, as well as the resulting extent of heteromeric channel assembly, could provide insight into the mechanism of the disease phenotype, and shed light on further treatment options. HCN1 and HCN2 expression are differentially regulated by seizure activity along with associated increases in HCN1/2 heteromerization in the developing rat hippocampus (Brewster et al., 2002; Brewster et al., 2005; Brewster et al., 2007; Zha et al., 2008). Therefore, resulting phenotypes in the diseased state could be at least partially explained by alterations in the ratio of homomeric and heteromeric channels expressed.

Despite the ability for two co-expressing HCN isoforms to heteromerize, differences in isoform distribution patterns throughout a cell would suggest that other mechanisms could also be in place to modulate assembly. For example, despite similar expression levels and regions of colocalization of HCN1 and HCN2 in transfected hippocampal neurons, the distribution of HCN1 was found to be more punctate, whereas HCN2 was more diffuse (Noam et al., 2010). Furthermore, dendritic trafficking profiles were found to be different for these two isoforms, with HCN1 appearing much more mobile than HCN2. Differential trafficking and distribution of individual isoforms could be due to specific interactions with other proteins. Association of ion channels with ancillary subunits or accessory proteins is known to affect channel assembly, trafficking and function (Pongs and Schwarz, 2010). Certain HCN channel isoforms interact with such proteins, for example MiRP1, KCR1 as well as various scaffolding proteins, resulting in modulation of channel trafficking and function (Biel et al., 2009). Thus, this type of interaction cannot be ruled out as a potential regulator of functional HCN2/4 channel heteromerization. Colocalization and quantitative analysis of HCN2 and HCN4 expression and assembly in cells stably expressing individual accessory proteins listed above could provide insight into their potential role in modulating the relative amount of homomeric versus heteromeric channels at the cell surface.

4.5 Functional Relevance of Potential GIPR and GLP-1R Oligomerization

The incretin hormone receptors, GIPR and GLP-1R are known for their ability to augment glucose-stimulated insulin release from beta cells, in response to a meal. As such, research has examined the suitability of either receptor as drug targets for T2DM. To date, drug therapies which act to either increase circulating GLP-1 or directly bind the GLP-1R have been developed. However, classical drug-binding data are fit using equations based on monomeric receptor models and therapeutic strategies have not taken into account the potential existence of receptor oligomers (Casado et al., 2009). Furthermore, the known existence of receptor heteromers could broaden a receptor's therapeutic potential, possibly through the development of heteromer-selective drugs or the identification of heteromer-specific pharmacological profiles. Knowledge as to the oligomeric capabilities of both GIPR and GLP-1R is thus instrumental in further elucidating their therapeutic potential for T2DM. In chapter 3 of this thesis, we report that all combinations of differentially tagged GIPR and GLP-1R produced BRET saturation curves that reflect close interactions, likely in the form of receptor homomers and heteromers. Moreover, we show that a trafficking-deficient GIPR was functionally rescued by co-expression with wild type GLP-1R. Together the results suggest that these receptors are capable of associating as functional receptor complexes, such as dimers or higher-order oligomers.

Although our experiments suggest that the GIPR and GLP-1R are able to form receptor oligomers, they do not describe where in the cell this interaction is initiated, the stability of interaction or the functional consequence of oligomer formation. To determine if oligomerization is initiated in the ER, future experiments could include constructing receptor trafficking mutants by the addition of ER retention sequences to both GIPR and GLP-1R. The potential dominant negative effect that these mutants have on wild type receptor trafficking out of the ER and to the cell surface, as well as whether or not oligomerization remains intact, can then be probed using BRET and imaging techniques, as well as cAMP assays. Another interesting experiment would be to conduct BRET assays from subcellular-fractionated cell lysates, in order to probe for the existence of oligomers within the ER, as well as the extent of oligomerization within the cell and at the surface. This technique has recently been used to show that the lutropin receptor forms a constitutive dimer in the ER and stably remains in this form when expressed at the cell surface (Guan et al., 2009). The stability of GLP-1-GIP

receptor dimers could be examined by cross linking and immobilization of one of the two co-expressing receptor protomers within the membrane, similarly to what has already been done to determine β-AR and D2R dimer stability (Dorsch et al., 2009; Fonseca and Lambert, 2009). Analysis of BRET ratios at different time points or after ligand incubation, would then help determine if the dimeric state is affected by these variables.

The idea that GIPR and GLP-1R could exist, at least partially as receptor heteromers in native tissue could help explain observed receptor phenotypes in T2DM. For example, one of the reasons for the decreased incretin effect in T2DM is an impaired beta cell responsiveness to GIP, despite elevated circulating levels of GIP (McIntosh et al., 2009). This could be due to a decrease in GIP binding efficiency, impaired downstream signaling, GIPR desensitization and/or lower GIPR cell surface expression. Whatever the case, the GLP-1 response is also diminished, however to a much lower extent, which could be a direct consequence of GIPR dysfunction, due to potential heteromeric coupling of GIPR and GLP-1R protomers.

4.6 Regulation of GIPR and GLP-1R Cell Surface Expression by N-Glycosylation

Although both GIPR and GLP-1R are expressed as glycoproteins in native cells, the site and extent of N-glycosylation on each receptor as well as its role in functional receptor expression was previously unclear. N-glycosylation can be important for receptor folding and maturation, dimerization and other interactions with chaperones and accessory proteins, trafficking, ligand binding, receptor stability and residence times at the cell surface (Mitra et al., 2006). In chapter 3 of this thesis, mutational analysis of N-glycosylation consensus sites revealed that all sites bind N-glycans in CHO cells. Complete removal of N-glycosylation severely impaired and completely abolished functional surface expression of GLP-1R and GIPR, respectively. Furthermore, tunicamycin treatment decreased GIPR cell surface number and impaired GIP-potentiated glucose-induced insulin release in INS-1 cells. From these experiments, we concluded that N-glycosylation is important in regulating the amount of GIPR and GLP-1R that is expressed at the cell surface. We also found shifts in EC_{50} from ligand concentration-response curves for some GIPR and GLP-1R N-glycosylation mutants. This suggests a problem with receptor function since ligand potency is decreased. Our experiments as well as earlier reports have ruled out any effect on ligand-binding affinity (Göke et al., 1994). Thus, the shift could be explained by impairment in receptor coupling to

downstream signaling machinery. However, the observed shift was only seen in instances where there was also a substantial decrease in cell surface receptor expression, thus suggesting that the decrease in ligand potency could be a direct result of lower total levels of cell surface protein. A link between ligand potency and cell surface receptor number has been observed for other receptor glycosylation mutants such as the β_1-AR, and was hypothesized to be a result of a lower functional receptor reserve at the cell surface according to the receptor occupancy theory, as well as a decrease in the amount of receptor colocalized to caveolae (He et al., 2002; Ostrom et al., 2001). Moreover, receptor dimerization and clustering are known to enhance function at the cell surface, but both processes can be impaired due to lower levels of receptor surface expression (Franco et al., 2003). Nevertheless, future experiments would need to be conducted to further elucidate a connection between ligand potency and GIPR or GLP-1R cell surface number. One study on M2 muscarinic receptor glycosylation mutants reported differences in IC_{50} upon mutation of asparagine to glutamine, but the shift was abolished when the site was mutated to aspartate (van Koppen and Nathanson, 1990). It would thus be useful to reproduce our experiments, mutating asparagines to other amino acids rather than glutamine to rule out amino acid-specific effects on the observed shift in EC_{50}.

Although our results demonstrate that the addition of N-glycans is important for GIPR and GLP-1R cell surface expression, the question remains as to the mechanism for the observed decrease. Is it a result of misfolding and subsequent degradation of immature protein, thus preventing forward trafficking out of the ER, or are the lower levels of cell surface expression due to decreased stability of the unglycosylated protein thus lowering its time of residence at the cell surface? The former mechanism seems more plausible since N-glycosylation is known to play an important role in protein folding and trafficking out of the ER, and due to the fact that we were unable to detect any protein at the cell surface in the case of GIPRN62,77Q. However this is not the case for all GPCRs, with some showing no impairment in cell surface expression upon removal of N-glycosylation. At the cell surface, N-glycans crosslink with galectin to form an interaction lattice, which helps to limit receptor internalization (Lau et al., 2007). Removal of N-glycans could therefore impact the stability of receptors that are still able to traffic to the cell surface. Immunocytochemistry and imaging microscopy of glycosylation-deficient receptors along with an ER marker can help determine the proportion of ER-retained mutants compared to the amount reaching the cell surface. To examine the stability of various glycosylation-deficient mutants, transfected cells could be

treated with cycloheximide (a chemical that halts protein biosynthesis), followed by immunodetection and band analysis over various time points, in order to compare the lifespan of wild type receptors to glycosylation mutants. One way to specifically measure receptor stability at the cell surface would be to compare ligand-induced internalization rates, or the changes in the amount of observed cell surface-biotinylated protein over time after addition of cycloheximide.

In our experiments, despite an observed rescue of function, we were unable to quantify any amount of cell surface rescue of the non-glycosylated GIPR, when co-expressed with either wild type GLP-1R or GIPR. Moreover, we did not observe any dominant negative retention of GIPR or GLP-1R by this trafficking-defective mutant. These results suggest that oligomer formation may be impaired by lack of N-glycosylation. Thus, a third explanation for the observed decrease in receptor cell surface number could be that inhibition of N-glycosylation impairs GIPR's ability to oligomerize, which could in turn affect ER export if complex formation is indeed required for optimal forward trafficking. BRET assays from cells co-expressing the glycosylation-deficient GIPR with either wild type GIPR or GLP-1R can help determine the importance of N-glycosylation in receptor oligomerization.

Regulation of GIPR and GLP-1R cell surface expression by N-glycosylation may have important implications in T2DM disease and treatment. The extent of N-glycan branching at a given glycosylation site depends on the availability and kinetics of branching enzymes, as well as metabolic flux through the hexosamine pathway (Lau et al., 2007). The increased hexosamine flux observed in T2DM models could modify the glycosylation state of important glycoproteins involved in glucose regulation, including the GIPR and GLP-1R, in turn contributing to altered functional expression of these receptors. It would thus be interesting to quantify and compare the extent of GIPR and GLP-1R glycosylation, in normal and diabetic mouse models, or when hexosamine flux is manipulated in an incretin receptor-expressing beta cell line, such as INS-1 cells.

4.7 Summary

In this thesis, the role of both membrane protein oligomerization and N-glycosylation in the regulation of functional cell surface expression was investigated using HCN channel isoforms, as well as the incretin receptors, GIPR and GLP-1R. To examine protein oligomerization and assembly, BRET assays and immunofluorescence imaging analysis were

used, which provided us with novel and more sensitive methods of quantifying the extent of homomeric versus heteromeric assembly of HCN channels. To determine the role of N-glycosylation on GIPR and GLP-1R surface expression and function, we analyzed various N-glycosylation-deficient mutants for function by ligand-induced cAMP response assays, and their extent of cell surface expression using both cell surface biotinylation and ELISA assays.

All experiments described above were performed using transiently transfected CHO cells. This enabled us to control for expression levels of proteins, easily compare numerous mutants, as well as express various epitope-tagged constructs in order to specifically examine cell surface expression, as well as perform BRET assays. The use of a heterologous overexpression system however is not necessarily reflective of the physiological setting. Thus, an essential next step would be to replicate the results in native tissue, or a native cell line, in order to confirm the physiological relevance of the conclusions drawn. A major roadblock to performing these assays *in vivo* thus far has been the limited availability of well-established, specific antibodies for these membrane proteins. HCN channel antibody use in native tissue is better established, and thus the preference for homomeric versus heteromeric assembly of various isoforms in different tissues and at various stages of development could be examined by carefully comparing Pearson Correlation coefficients in isolated cells, provided proper negative and positive controls are used in conjunction. Furthermore, co-infection of native cell lines with BRET-tagged HCN2 and HCN4 constructs may provide a means of measuring BRET ratios in a more physiological setting, again ensuring that proper negative controls are used. In order to determine whether GIPR and GLP-1R form dimers in a more physiological setting, GIPR or GLP-1R knockout cell lines could be used. Comparing receptor cAMP responses in the presence of GIPR or GLP-1R agonists or antagonists, in wild type versus individual knockout cell lines would give insight into the whether or not these receptors form dimers with altered functional characteristics in native cells. If GIPR and GLP-1R do indeed form receptor dimers in vivo, as suggested by the results from this thesis, the receptor protomers may co-internalize upon ligand addition. Thus, using isolated pancreatic β-cells, internalization of one receptor protomer could be measured in the presence of ligand specific to the other protomer, and vice versa.

Nevertheless, the results from this thesis provide strong support for the modulation of functional surface expression by oligomerization and N-glycosylation. Specifically, we have shown that, when co-expressed in equal amounts, HCN2 and HCN4 do not discriminate

between homomeric versus heteromeric assembly. We have also provided evidence that GIPR and GLP-1R physically interact, likely by complexing as receptor homomers and heteromers. Finally, the exact sites of GIPR and GLP-1R N-glycosylation have been elucidated, along with the role that individual sites play on functional receptor expression. Together, the results from this thesis provide an appropriate framework and rationale for the next step of examining the role of these co-translational modifications *in vivo*.

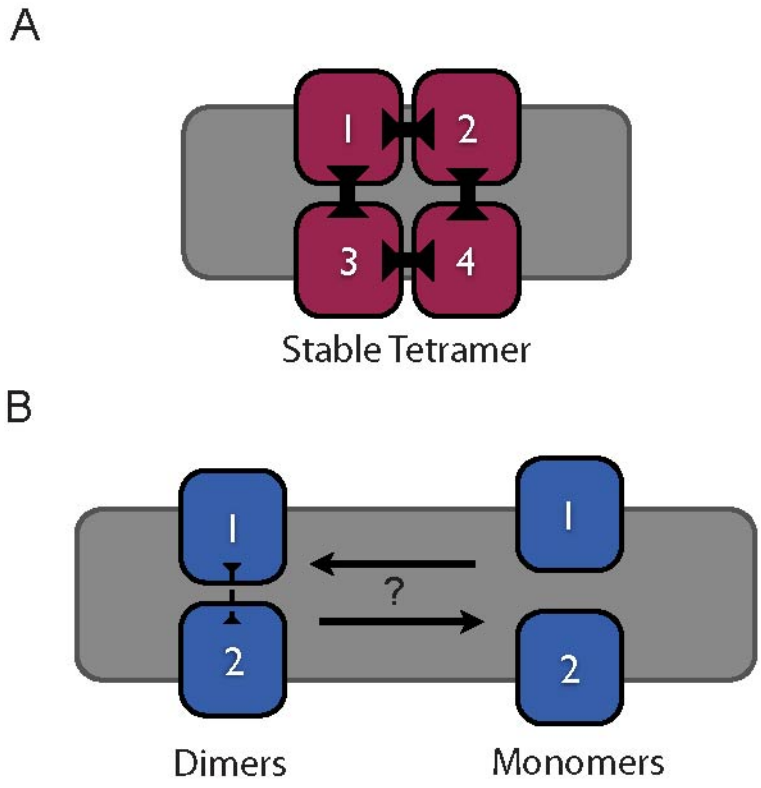

Figure 4.1 Variable stabilities of different membrane complexes

A: Ion channels such as HCN channels form stable tetrameric structures due to strong intersubunit interactions. This type of assembly is required for function. B: Some GPCRs may exist and function as either dimers (or higher order oligomers) or monomers within the cell surface membrane, likely due to less stable, transient interactions between each interacting protomer.

4.8 References

Baruscotti, M., Bottelli, G., Milanesi, R., Difrancesco, J. C. and Difrancesco, D. (2010). HCN-related channelopathies. *Pflugers Arch.*

Bayburt, T. H., Leitz, A. J., Xie, G., Oprian, D. D. and Sligar, S. G. (2007). Transducin activation by nanoscale lipid bilayers containing one and two rhodopsins. *J. Biol. Chem.* **282,** 14875-14881.

Biel, M., Wahl-Schott, C., Michalakis, S. and Zong, X. (2009). Hyperpolarization-activated cation channels: From genes to function. *Physiol. Rev.* **89,** 847-885.

Brewster, A., Bender, R. A., Chen, Y., Dube, C., Eghbal-Ahmadi, M. and Baram, T. Z. (2002). Developmental febrile seizures modulate hippocampal gene expression of hyperpolarization-activated channels in an isoform- and cell-specific manner. *J. Neurosci.* **22,** 4591-4599.

Brewster, A. L., Bernard, J. A., Gall, C. M. and Baram, T. Z. (2005). Formation of heteromeric hyperpolarization-activated cyclic nucleotide-gated (HCN) channels in the hippocampus is regulated by developmental seizures. *Neurobiol. Dis.* **19,** 200-207.

Brewster, A. L., Chen, Y., Bender, R. A., Yeh, A., Shigemoto, R. and Baram, T. Z. (2007). Quantitative analysis and subcellular distribution of mRNA and protein expression of the hyperpolarization-activated cyclic nucleotide-gated channels throughout development in rat hippocampus. *Cereb. Cortex* **17,** 702-712.

Casado, V., Cortes, A., Mallol, J., Perez-Capote, K., Ferre, S., Lluis, C., Franco, R. and Canela, E. I. (2009). GPCR homomers and heteromers: A better choice as targets for drug development than GPCR monomers? *Pharmacol. Ther.* **124,** 248-257.

Deutsch, C. (2002). Potassium channel ontogeny. *Annu. Rev. Physiol.* **64,** 19-46.

Dorsch, S., Klotz, K. N., Engelhardt, S., Lohse, M. J. and Bunemann, M. (2009). Analysis of receptor oligomerization by FRAP microscopy. *Nat. Methods* **6,** 225-230.

Fonseca, J. M. and Lambert, N. A. (2009). Instability of a class a G protein-coupled receptor oligomer interface. *Mol. Pharmacol.* **75,** 1296-1299.

Franco, R., Canals, M., Marcellino, D., Ferre, S., Agnati, L., Mallol, J., Casado, V., Ciruela, F., Fuxe, K., Lluis, C. et al. (2003). Regulation of heptaspanning-membrane-receptor function by dimerization and clustering. *Trends Biochem. Sci.* **28,** 238-243.

Fung, J. J., Deupi, X., Pardo, L., Yao, X. J., Velez-Ruiz, G. A., Devree, B. T., Sunahara, R. K. and Kobilka, B. K. (2009). Ligand-regulated oligomerization of beta(2)-adrenoceptors in a model lipid bilayer. *EMBO J.* **28,** 3315-3328.

Göke, R., Just, R., Lankat-Buttgereit, B. and Göke, B. (1994). Glycosylation of the GLP-1 receptor is a prerequisite for regular receptor function. *Peptides* **15,** 675-681.

Guan, R., Feng, X., Wu, X., Zhang, M., Zhang, X., Hebert, T. E. and Segaloff, D. L. (2009). Bioluminescence resonance energy transfer studies reveal constitutive dimerization of the human lutropin receptor and a lack of correlation between receptor activation and the propensity for dimerization. *J. Biol. Chem.* **284,** 7483-7494.

Harikumar, K. G., Morfis, M. M., Sexton, P. M. and Miller, L. J. (2008). Pattern of intra-family hetero-oligomerization involving the G-protein-coupled secretin receptor. *J. Mol. Neurosci.* **36,** 279-285.

Harikumar, K. G., Pinon, D. I. and Miller, L. J. (2007). Transmembrane segment IV contributes a functionally important interface for oligomerization of the class II G protein-coupled secretin receptor. *J. Biol. Chem.* **282,** 30363-30372.

He, J., Xu, J., Castleberry, A. M., Lau, A. G. and Hall, R. A. (2002). Glycosylation of beta(1)-adrenergic receptors regulates receptor surface expression and dimerization. *Biochem. Biophys. Res. Commun.* **297,** 565-572.

Hern, J. A., Baig, A. H., Mashanov, G. I., Birdsall, B., Corrie, J. E., Lazareno, S., Molloy, J. E. and Birdsall, N. J. (2010). Formation and dissociation of M1 muscarinic receptor dimers seen by total internal reflection fluorescence imaging of single molecules. *Proc. Natl. Acad. Sci. U. S. A.* **107,** 2693-2698.

Lau, K. S., Partridge, E. A., Grigorian, A., Silvescu, C. I., Reinhold, V. N., Demetriou, M. and Dennis, J. W. (2007). Complex N-glycan number and degree of branching cooperate to regulate cell proliferation and differentiation. *Cell* **129,** 123-134.

Levitan, E. S. and Takimoto, K. (1998). Dynamic regulation of K+ channel gene expression in differentiated cells. *J. Neurobiol.* **37,** 60-68.

Lisenbee, C. S. and Miller, L. J. (2006). Secretin receptor oligomers form intracellularly during maturation through receptor core domains. *Biochemistry* **45,** 8216-8226.

Maurel, D., Comps-Agrar, L., Brock, C., Rives, M. L., Bourrier, E., Ayoub, M. A., Bazin, H., Tinel, N., Durroux, T., Prezeau, L. et al. (2008). Cell-surface protein-protein interaction analysis with time-resolved FRET and snap-tag technologies: Application to GPCR oligomerization. *Nat. Methods* **5,** 561-567.

McIntosh, C. H., Widenmaier, S. and Kim, S. J. (2009). Glucose-dependent insulinotropic polypeptide (gastric inhibitory polypeptide; GIP). *Vitam. Horm.* **80,** 409-471.

Mitra, N., Sinha, S., Ramya, T. N. and Surolia, A. (2006). N-linked oligosaccharides as outfitters for glycoprotein folding, form and function. *Trends Biochem. Sci.* **31,** 156-163.

Noam, Y., Zha, Q., Phan, L., Wu, R. L., Chetkovich, D. M., Wadman, W. J. and Baram, T. Z. (2010). Trafficking and surface expression of hyperpolarization-activated cyclic nucleotide-gated (HCN) channels in hippocampal neurons. *J. Biol. Chem.* **285,** 14724-14736

Ostrom, R. S., Gregorian, C., Drenan, R. M., Xiang, Y., Regan, J. W. and Insel, P. A. (2001). Receptor number and caveolar co-localization determine receptor coupling efficiency to adenylyl cyclase. *J. Biol. Chem.* **276,** 42063-42069.

Pin, J. P., Galvez, T. and Prezeau, L. (2003). Evolution, structure, and activation mechanism of family 3/C G-protein-coupled receptors. *Pharmacol. Ther.* **98,** 325-354.

Pongs, O. and Schwarz, J. R. (2010). Ancillary subunits associated with voltage-dependent K+ channels. *Physiol. Rev.* **90,** 755-796.

Shi, W., Wymore, R., Yu, H., Wu, J., Wymore, R. T., Pan, Z., Robinson, R. B., Dixon, J. E., McKinnon, D. and Cohen, I. S. (1999). Distribution and prevalence of hyperpolarization-activated cation channel (HCN) mRNA expression in cardiac tissues. *Circ. Res.* **85,** e1-6.

Tran, N., Proenza, C., Macri, V., Petigara, F., Sloan, E., Samler, S. and Accili, E. A. (2002). A conserved domain in the NH2 terminus important for assembly and functional expression of pacemaker channels. *J. Biol. Chem.* **277,** 43588-43592.

van Koppen, C. J. and Nathanson, N. M. (1990). Site-directed mutagenesis of the m2 muscarinic acetylcholine receptor. analysis of the role of N-glycosylation in receptor expression and function. *J. Biol. Chem.* **265,** 20887-20892.

Wei-Qing, H., Qing-Nuan, K., Lin, X., Cheng-Hao, G. and Qi-Yi, Z. (2010). Expression of hyperpolarization-activated cyclic nucleotide-gated cation channel (HCN4) is increased in hypertrophic cardiomyopathy. *Cardiovasc. Pathol.*

White, J. F., Grodnitzky, J., Louis, J. M., Trinh, L. B., Shiloach, J., Gutierrez, J., Northup, J. K. and Grisshammer, R. (2007). Dimerization of the class A G protein-coupled neurotensin receptor NTS1 alters G protein interaction. *Proc. Natl. Acad. Sci. U. S. A.* **104,** 12199-12204.

Ye, B. and Nerbonne, J. M. (2009). Proteolytic processing of HCN2 and co-assembly with HCN4 in the generation of cardiac pacemaker channels. *J. Biol. Chem.* **284,** 25553-25559.

Zha, Q., Brewster, A. L., Richichi, C., Bender, R. A. and Baram, T. Z. (2008). Activity-dependent heteromerization of the hyperpolarization-activated, cyclic-nucleotide gated (HCN) channels: Role of N-linked glycosylation. *J. Neurochem.* **105,** 68-77.

Zhang, Q., Huang, A., Lin, Y. C. and Yu, H. G. (2009). Associated changes in HCN2 and HCN4 transcripts and I(f) pacemaker current in myocytes. *Biochim. Biophys. Acta* **1788,** 1138-1147.

APPENDIX A: HYPERPOLARIZATION-ACTIVATED CYCLIC NUCLEOTIDE-MODULATED 'HCN' CHANNELS CONFER REGULAR AND FASTER RHYTHMICITY TO BEATING MOUSE EMBRYONIC STEM CELLS [3]

[3] This paper has been published. Yang Q, Whitaker GM, Hove-Madsen L, Tibbits GF, Accili EA. (2008) Hyperpolarization-activated cyclic nucleotide-modulated 'HCN' channels confer regular and faster rhythmicity to beating mouse embryonic stem cells. *Journal of Physiology* 586(3), 701-716

Hyperpolarization-activated cyclic nucleotide-modulated 'HCN' channels confer regular and faster rhythmicity to beating mouse embryonic stem cells

Yang Qu[1,2], Gina M. Whitaker[3], Leif Hove-Madsen[4], Glen F. Tibbits[1,2] and Eric A. Accili[3]

[1]*Cardiac Membrane Research Laboratory, Simon Fraser University, Burnaby, BC, Canada*
[2]*Cardiovascular Sciences, Child and Family Research Institute, Vancouver, BC, Canada*
[3]*Department of Cellular and Physiological Sciences, University of British Columbia, Vancouver, BC, Canada*
[4]*Laboratorio de Fisiologia Celular, Servei de Cardiologia, Hospital de Sant Pau, 08025 Barcelona, Spain*

The hyperpolarization-activated cation current (I_f), and the hyperpolarization-activated cyclic nucleotide-modulated 'HCN' subunits that underlie it, are important components of spontaneous activity in the embryonic mouse heart, but whether they contribute to this activity in mouse embryonic stem cell-derived cardiomyocytes has not been investigated. We address this issue in spontaneously beating cells derived from mouse embryonic stem cells (mESCs) over the course of development in culture. I_f and action potentials were recorded from single beating cells at early, intermediate and late development stages using perforated whole-cell voltage- and current-clamp techniques. Our data show that the proportion of cells expressing I_f, and the density of I_f in these cells, increased during development and correlated with action potential frequency and the rate of diastolic depolarization. The I_f blocker ZD7288 (0.3 μM) reduced I_f and the beating rate of embryoid bodies. Taken together, the activation kinetics of I_f and results from Western blots are consistent with the presence of the HCN2 and HCN3 isoforms. At all stages of development, isoproterenol (isoprenaline) and acetylcholine shifted the voltage dependence of I_f to more positive and negative voltages, respectively, and they also increased and decreased the beating rate of embryonic cell bodies, respectively. Together, the data suggest that current through HCN2 and HCN3 channels confers regular and faster rhythmicity to mESCs, which mirrors the developing embryonic mouse heart, and contributes to modulation of rhythmicity by autonomic stimulation.

(Resubmitted 3 September 2007; accepted after revision 16 November 2007; first published online 22 November 2007)
Corresponding author E. A. Accili: Department of Cellular and Physiological Sciences, University of British Columbia, 2350 Health Sciences Mall, Vancouver, BC, Canada V6R 1Z3. Email: eaccili@interchange.ubc.ca

The timely appearance of spontaneous and repetitive activity is a critical feature of the embryonic heart. Hyperpolarization-activated cyclic nucleotide-gated channels (HCN), which underlie the hyperpolarization-activated or 'funny' current I_h/I_f, contribute to spontaneous beating in the adult sinoatrial node (DiFrancesco *et al.* 1986; DiFrancesco, 1993; Accili *et al.* 2002; Robinson & Siegelbaum, 2003) as well as in the embryonic heart (Stieber *et al.* 2003). During development of the mouse heart, expression of I_f was detectable as early as embryonic day 8.5, approximately a day after contractions of the heart begin, and both I_f density and beating rate peak at embryonic day 9.5–10 (Porter & Rivkees, 2001; Stieber *et al.* 2003). Cardiomyocytes from embryonic mice lacking HCN4 have significantly lower levels of I_f and lower beating frequencies (Stieber *et al.* 2003). Because the morphology of their hearts was normal, it was suggested that these HCN4-lacking mice die at embryonic day 9.5–11.5 because of inadequate perfusion.

Because of the dependence of the murine embryo upon blood flow, it can be difficult to investigate the molecular basis of cardiac pacemaker activity during development in the mouse. To overcome this problem, embryonic stem (ES) cell-derived cardiomyocytes have been utilized because they recapitulate features of embryonic cardiac development (Maltsev *et al.* 1994; Zhang *et al.* 2002). Upon differentiation, mESCs exhibit cardiac specific genes and ionic currents and action potentials typical of different parts of the heart, and they beat spontaneously (Robbins *et al.* 1990; Maltsev *et al.* 1993, 1994; Klug *et al.* 1996;

L. Hove-Madsen, G. F. Tibbits and E. A. Accili are joint senior authors.

DOI: 10.1113/jphysiol.2007.144329

White & Claycomb, 2005). I_f and HCN channel RNA are expressed in a heterogeneous proportion of mESCs at both early and late stages (Maltsev *et al.* 1994; Abi-Gerges *et al.* 2000; Kolossov *et al.* 2005; Wang *et al.* 2005; White & Claycomb, 2005), and I_f density increases during mESC development (Abi-Gerges *et al.* 2000). However, the contribution of HCN channels to spontaneous beating in mESCs at each of these stages has yet to be assessed directly.

In this study, we examined the properties of I_f and investigated its contribution to spontaneous activity in mESCs at different stages of development using the perforated current and voltage patch clamp approaches, as well as Western blotting. We found that beating rates of mESCs increase during development as does I_f density. This confers more regular and faster rhythmicity, and parallels the increase in beating rate observed in the embryonic mouse heart. Taken together, the activation kinetics of I_f channel and results from Western blots are consistent with the presence of the HCN2 and HCN3 isoforms. Our data also suggest that the modulation of I_f contributes to autonomic stimulation of beating rate over the course of the development. Together with previous studies, our findings support the use of mESCs as a model for the developing mouse heart.

Methods

Culture of mESCs cells and differentiation into cardiomyocytes

Mouse embryonic stem cell line R1 (ATCC, USA) was used in the study (Nagy *et al.* 1993). To maintain the ES cells at an undifferentiated state, cells were cultured on 0.1% gelatin-coated culture dishes in ES-DMEM, consisting of DMEM (Invitrogen), supplemented with 15% fetal bovine serum (Wiscent), 2.0 mM L-alanyl-L-glutamine (ATCC), 0.1 mM non-essential amino acids (ATCC), 100 U ml^{-1} penicillin (Invitrogen), 100 μg ml^{-1} streptomycin (Invitrogen), 0.1 mM 2-mercaptoethanol (Sigma) and 1000 U ml^{-1} mouse leukaemia inhibitory factor (LIF) (Chemicon). The hanging drop method was used for differentiation of cardiomyocytes (Wobus *et al.* 1991; Maltsev *et al.* 1993). On day 1 of differentiation, ES cells were plated on a 100 mm Petri dish cover in 50–60 single drops. Each drop contained 400–800 cells in 20 μl of differentiation medium (ES-DMEM without LIF). The cover was gently inverted and put on top of the Petri dish containing PBS. The hanging drops were cultured for 2 days. On day 3, cell clusters (embryoid bodies, EBs) formed in hanging drops were flushed with the differentiation medium and grown further for 4 days. On day 7, EBs were plated out onto 0.1% gelatin-coated 24-well culture plates (Falcon) at 1–2 Ebs per well in 1 ml of medium. Spontaneous beating was observed ~1–2 days after plating (day 7 + 1–2).

Cell isolation

Single beating cells were isolated from embryoid bodies as previously described (Maltsev *et al.* 1994). Beating areas of ~10–20 EBs at each development stages were dissected at room temperature using two 23G1 needles. The whole process altogether took no more than 30 min. Tissue fragments were then incubated in low-Ca^{2+} medium with 1 mg ml^{-1} collagenase (Yakult, Japan, 500 U mg^{-1}; (mM): NaCl 120, KCl 5.4, $MgSO_4$-$7H_2O$ 5, $CaCl_2$ 0.03, sodium pyruvate 5, glucose 20, taurine 20, Hepes 10; pH 6.9 adjusted with NaOH) for 30 min at 37°C, while being titrated gently every 10 min. The dissociation process was continued in high-K^+ solution (mM): KCl 85, K_2HPO_4 30, $MgSO_4$ 5, EDTA 1, Na_2ATP 2, pyruvic acid 5, creatine 5, taurine 20, glucose 20, pH 7.4) for another 1 h with the gentle shaking at room temperature. Isolated cells were plated on poly D-lysine-coated glass bottom culture dishes (No.1.5, MatTek Corporation) and cultured overnight in differentiation medium. Single spontaneous beating cells and beating clusters could be observed the next day.

Electrophysiology studies

Perforated whole-cell patch-clamp technique (using amphotericin) was performed on single spontaneous beating cells using a MultiClamp 700A computer-controlled patch amplifier (Axon Instruments, Union City, CA, USA). The glass bottom culture dishes were mounted on the stage of microscope (Eclipse TE300 Nikon) and cells were viewed using a ×60 oil immersion objective. The dish was perfused by gravity at a rate of 0.2 ml min^{-1} with extracellular solution. The patch pipettes (1–2 MΩ) were pulled from thin-walled glass capillaries (World Precision Instruments) using a vertical puller (Narishige PP-830, Japan). Seals with a resistance of 1–2 GΩ were formed under the voltage-clamp configuration. The access resistance dropped to less than 30 MΩ within 10–20 min of seal formation. Junction potential was not corrected. Only recordings in which voltage error was less than 10% of the command voltage were accepted. Ninety per cent of the currents measured were less than 0.5 nA at −150 mV. The clamping mode was switched between current clamp and voltage clamp for the measurement of action potentials or currents. The data were digitized (Digidata, 1322A) at 20 kHz and filtered at 1 kHz acquired using Clampex (version 8.2, Axon Instruments). All experiments were done at 22°C.

The standard external solution contained (mM): NaCl 140, KCl 5.4, $CaCl_2$ 1.8, $MgCl_2$ 1, Hepes 10 and glucose 10, and adjusted to pH 7.4 with NaOH. For the measurement of I_f, the standard solution was modified by adding $BaCl_2$ (2 mM) and $MnCl_2$ (2 mM) to suppress potassium and calcium currents, as previously described (DiFrancesco *et al.* 1986; Accili *et al.* 1997). The internal pipette solution

contained (mM): NaCl 10, KCl 50, KOH 80, aspartic acid 80, $MgCl_2$ 1, Hepes 10 and MgATP 3, pH 7.2 adjusted with KOH. The final concentration of amphotericin B (Sigma; solubilized in dimethyl sulfoxide) was 250 μg ml^{-1} in the patch pipette. ZD7288 was purchased from Tocris (Ellisville, USA).

Western blot analysis

Beating areas from mouse embryonic stem cells were isolated from embryoid bodies as previously described (Maltsev *et al.* 1994). Undifferentiated stem cells and Chinese hamster ovary (CHO) cells were detached from culture plates with a rubber policeman. Cells were washed with PBS and processed in RIPA lysis buffer (50 mM Tris at pH 8.0, 1% NP-40, 150 mM NaCl, 1 mM EDTA, 1 mM PMSF, 2 mM each of Na_3VO_4 and NaF, and 10 μg ml^{-1} each of aprotinin, pepstatin and leupeptin) by multiple passes through a 23G syringe, and incubated on ice for 30 min, followed by centrifugation to remove cell debris. All experiments using embryonic mouse tissue were carried out at the University of British Columbia. In accordance with guidelines from the Canadian Council for Animal Care and the University of British Columbia Committee on Animal Care, female CD1 mice ($n = 3$) were deeply anaesthetized using CO_2 and killed by cervical dislocation. Day 18 embryos were removed (18–20 per mouse), and whole hearts were isolated and processed in RIPA lysis buffer as described above. Cell lysates were loaded into 8% SDS–polyacrilamide gels. Gels were transferred to polyvinylidene difluoride membranes, and blots were washed twice in TBS-T and then blocked with 5% non-fat dry milk in TBS-T for 1 h. Blots were incubated with primary antibody overnight at 4°C in 5% non-fat milk. After three washes with TBS-T, blots were incubated with horseradish peroxidase-conjugated secondary antibodies at a dilution of 1 : 3000 in 5% non-fat milk for 1 h at room temperature. After three washes with TBS-T, signals were obtained with ECL detection reagents (GE Healthcare). The following primary antibodies were used: Rb polyclonal HCN1, HCN2, HCN3 and HCN4 (Alomone Laboratories), goat polyclonal HCN1, HCN4 (Santa Cruz Biotechnology Inc.), Rb polyclonal HCN3 (kind gift from R. Shigemoto), mouse monoclonal HCN4 (Affinity Bioreagents), and guinea pig polyclonal HCN2 (kind gift from R. Shigemoto), as well as goat polyclonal GAPDH (SantaCruz Biotechnology Inc.). HCN antibodies were chosen because they identified appropriate bands in CHO cells transfected with the corresponding isoform. For a positive identification of isoforms, bands on each blot were required to be at or near both the predicted molecular weight as well as the weight detected from CHO cell lysates expressing individual isoforms, and recognized by at least two different antibodies. Western blotting experiments were carried out on three or more preparations of mESCs, and five times using mouse embryonic tissue.

Data analysis

I_f was measured as the difference between the instantaneous currents and the steady-state currents, at the beginning and end of test voltage pulses. Currents were normalized to membrane capacitance. Rates of I_f activation were determined using the following function (Clampfit 8.2, Axon Instruments),

$$f(t) = \sum A_i e^{-t/\tau i} + C,$$

where $i = 1$ or 2 (a single or double exponential fit), A is the amplitude of the fitting component(s), τ is the time constant, and C is the shift of the fitted trace from zero. A delay in I_f activation was noted in each current trace. As this delay is not well fitted by simple exponential functions, this portion of the trace was not utilized in our fits (Santoro *et al.* 2000; Altomare *et al.* 2001; Macri *et al.* 2002).

To obtain steady-state I_f activation curves, the relations between normalized tail currents and test voltage were fitted with the following Boltzmann equation:

$$I = 1/(1 + \exp[V - V_{1/2}]/k),$$

where V is the test voltage, $V_{1/2}$ is the mid-activation voltage and k is the slope factor (Origin 6.0, MicroCal Software Inc., Northampton, MA, USA). Activation thresholds were determined by fitting these relations from individual cells with the Boltzmann equation, and empirically determining the point at which these relations are continuously larger than zero.

Action potential frequency was measured as the total number of spikes within a 1 min recording. The average rates of diastolic depolarization (DDR) were determined by averaging the measurements from 10 consecutive action potentials.

Unless otherwise stated, data are presented as means ± S.E.M. Statistical significance of the results was tested using a one-way or two-way ANOVA, Tukey test for multiple comparisons or Student's t test for paired samples as indicated. A P value of < 0.05 was considered significant.

Results

Properties of I_f in mouse embryonic stem cells (mESCs)

The properties of I_f were studied in early (day 7 + 2–4), intermediate (day 7 + 5–8) and late stage (day 7 + 9–15) cells. Hyperpolarizing pulses elicited slowly activating inward currents, characteristic of I_f, in early, intermediate and late stage myocytes. I_f was present in these cells as early as day 7 + 2, the earliest time tested. I_f density was significantly larger in late stage cells compared to the early stage cells (Fig. 1*A*).

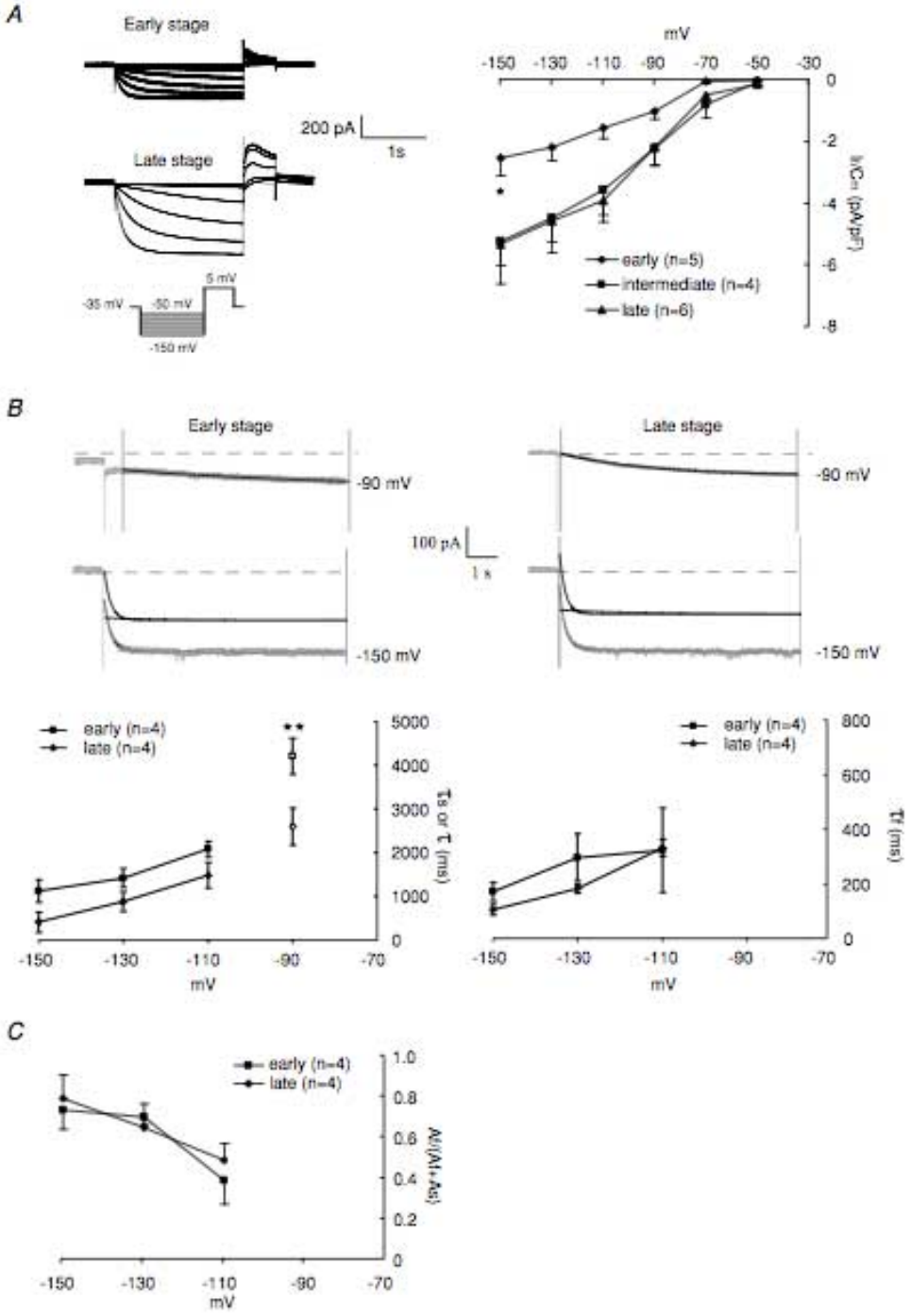

Figure 1. The density and kinetics of I_f change during development
A, left, representative I_f traces recorded in the presence of 2 mM Ba^{2+} and 2 mM Mn^{2+} from both early and late stage cells. Cells were held at −35 mV and stepped to hyperpolarizing test pulses from −50 to −150 mV for

To study the activation kinetics of I_f, cells were stepped to test voltages for a relatively long duration (8 s) to achieve full activation and allow for better fitting (Fig. 1*B*). At −150 mV, −130 mV and −110 mV, I_f at both early and late stages was fitted better with a standard double exponential function rather than a single exponential function. At these voltages, the fast time constants determined by fitting did not differ significantly between early and late stages. However, the slow time constants were consistently and significantly larger at these voltages in the early stage cells ($P < 0.0005$). At −90 mV, I_f recorded from both early and late stage cells activated more slowly and the current traces were fitted better with a single exponential function. At this voltage, the time constant of activation in cells at early stage was significantly larger, indicative of a slower rate of I_f activation in these cells. These rates of activation are slower, and faster, than those obtained for I_f in mammalian cells transfected with HCN2 and HCN3, respectively.

We also determined the amplitudes of each exponential component at −110 mV, −130 mV and −150 mV, and the relative amount of the fast component as a fraction of the total amplitude. Previous studies have shown that the relative amount of the fast component increases at more negative potentials in oocytes expressing HCN2 but not HCN1. Here, we found that the amplitude of the slow exponential component was relatively constant at each test voltage, while the amplitude of the fast exponential component increased when the holding potentials became more hyperpolarized. Thus, the relative amount of the fast component was larger at more negative voltages, consistent with previous studies of HCN2, but not HCN1. This is plotted in Fig. 1*C*, which also shows that this relationship was similar between the early and late stages.

Since repetitive long pulses were not tolerated by the cells, a 2 s prepulse was applied at each test potential to measure the steady-state activation of I_f. As shown in Fig. 2*A*, the voltage dependence of I_f activation at the early and late stages was similar. The half-activation voltages ($V_{1/2}$) and the slopes of activation (k) for the early stage cells were -90.29 ± 3.35 mV and 10.22 ± 0.94 ($n = 7$), respectively; for the late stage cells they were -88.02 ± 0.75 mV and 11.45 ± 0.67 ($n = 4$, $P > 0.05$), respectively. The activation thresholds, determined from Boltzmann curves from individual cells, were also similar and were -47.72 ± 1.88 mV at early stage and -46.06 ± 1.92 mV at late stage ($P > 0.05$).

Instantaneous I_f–V relations were generated as described in our previous studies of I_f/HCN channels (e.g. Proenza *et al.* 2002; Macri & Accili, 2004). Values for slope conductance (G_f) and reversal potential (E_f) were determined by fitting current amplitudes negative to −30 mV with a straight line, for each individual cell (Fig. 2*B*). Values for G_f were 20.71 ± 4.46 pS pF^{-1} at early stage and 54.42 ± 16.59 pS pF^{-1} at late stage ($P < 0.01$), confirming the increase in I_f density. The values for E_f were -28.17 ± 4.99 mV for the early stage cells and -22.14 ± 7.12 mV for the late stage cells ($P > 0.05$) (Fig. 2*B*). These values for E_f in physiological intracellular and extracellular solutions are consistent with the mixed permeability of I_f channels (DiFrancesco, 1981).

HCN2 and HCN3 isoforms are found in mESCs and in the embryonic mouse heart

In order to determine which HCN isoforms underlie I_f in mESCs, we carried out Western blotting using antibodies specific for the four mammalian isoforms. For a positive identification of isoforms, bands on each blot were required to be at or near both the predicted molecular weight as well as the weight detected from CHO cell lysates expressing individual isoforms. Additionally, isoforms had to be clearly recognized by at least two antibodies. Based on these criteria, HCN2 and HCN3 isoforms were identified in both the early and late stage mESCs, as well as in undifferentiated mESCs. We also found both HCN2 and HCN3 in day 18 embryonic mouse hearts (Fig. 3*B* and *C*). Lastly, we found that HCN3 isoform expression in mESCs decreased over the time course of their development in culture (Fig. 3*C*). We were not able to identify HCN1 or HCN4 protein in mESCs, before or after differentiation (Fig. 3*A* and *D*).

2 s in 20 mV intervals. The voltage protocol is shown below the current traces. i_f was measured as the difference between the instantaneous currents and the steady-state currents, at the beginning and end of test voltage pulses. The currents were normalized by membrane capacitance to reduce variability in amplitude due to variations in cell surface area. Right, i_f as a function of voltage is plotted at each stage (*$P < 0.05$). *B*, upper, representative current traces from both early (left) and late stage cells (right) at −90 mV, fitted with a single exponential function; and at −150 mV, fitted with a double exponential function (see Methods). The fast and slow components for the double exponential fit are shown in black. Lower, slow time constants (τ_s, lower left) and fast time constants (τ_f, lower right) at each stage are plotted against the test voltages. τ values at −90 mV at each stage are plotted individually in the lower left panel (open symbols) Differences between early and late stage values of τ_s were significantly different ($P = 0.0003$, two-way ANOVA analysis). **Significant difference in τ value between early and late stage at −90 mV (*t* test, $P < 0.05$). *C*, the amplitude of slow and fast exponential components (A_s and A_f) were determined from double exponential fits (see Methods). The relative amplitude of A_f was calculated as $A_f/(A_f + A_s)$ and plotted against voltage.

I_f density correlates with action potential frequency and rate of diastolic depolarization of mESCs during development

We next examined the action potential, the ability of the cells to beat, and the contribution of I_f to beating frequency over the course of development. The beating cells from ES cells were classified into the same three stages used for the examination of I_f. At the early stage, spontaneous action potentials were irregular and intermingled with small fluctuations in membrane potential. This type of action potential feature was accompanied by an irregular beating pattern. Cells at the intermediate and late stages beat more regularly, faster and more vigorously (Fig. 4*A*). The frequency of action potentials (Fig. 4*B*, top) and DDR (Fig. 4*B*, middle) were both increased in the intermediate and late stage cells. The maximal diastolic potential (MDP) and the threshold of action potentials did not change significantly over this period of time (Fig. 4*B*, bottom). Thus, this increase in beating frequency was due primarily to the shortening of the time required to reach the threshold. The MDP recorded from spontaneously active cells at early and late stage were -43.75 ± 1.74 mV and -47.71 ± 1.82 mV, respectively, which were close to the values for I_f activation threshold.

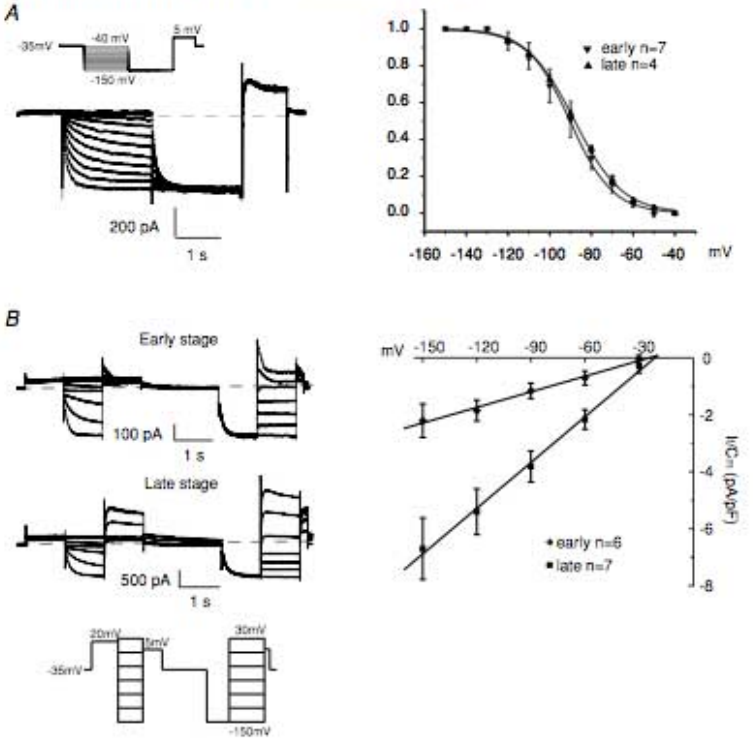

Figure 2. The steady-state activation and reversal potentials of I_f do not change during development
A, left, representative current traces from a late stage cell. The voltage protocol is shown above the current traces. I_f tails were elicited in response to a pulse to −150 mV, following test voltages, to minimize contamination by other conductances at less negative and positive pulses. Right, steady-state I_f activation curves of the early and late stage cells. Tail currents were determined from the difference between the peak current and the steady-state current, normalized and plotted against test voltage. The relations were fitted with the Boltzmann equation (see Methods). *B*, left, representative current traces to determine the instantaneous I_f from both early and late stage cells. The voltage protocol is shown below the current traces. Right, instantaneous I_f was plotted against voltages negative to −30 mV. The voltage-independent/leakage currents were subtracted from the total instantaneous currents at each test voltage to yield instantaneous I_f. To determine the actual reversal potential, a straight line fit was performed for each cell and an average value was obtained.

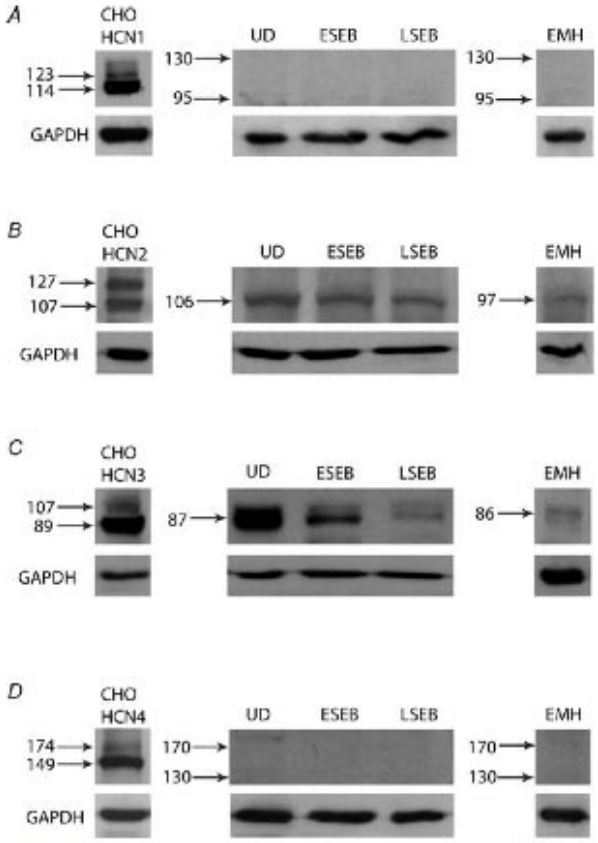

Figure 3. HCN2 and HCN3 are the predominant isoforms in differentiated and undifferentiated mESCs
A, Western blot probed with antibodies raised in rabbit (Alomone) and specific for HCN1 (upper), or raised in goat and specific for GAPDH (lower). Left, HCN1 expressed in CHO cells gives two bands at 123 and 114 kDa, as shown by the arrows. Centre, HCN1 was not detected in undifferentiated (UD), early stage EBs (ESEB) and late stage EBs (LSEB). Right, HCN1 was not detected in day 18 embryonic mouse. Arrows point to 95 and 130 kDa which encompass the area that HCN1 would be expected to migrate to if present. *B*, Western blot probed with antibodies raised in rabbit (Alomone) and specific for HCN2 (upper), or raised in goat and specific for GAPDH (lower). Left, HCN2 expressed in CHO cells gives two bands at 127 and 107 kDa, as shown by the arrows. Centre, HCN2 in undifferentiated (UD), early stage EBs (ESEB) and late stage EBs (LSEB). The arrow identifies the band at 106 kDa. Right, HCN2 expressed in day 18 embryonic mouse at a molecular weight of approximately 97 kDa as identified by the arrow. *C*, Western blot probed with antibodies raised in rabbit (Shigemoto) and specific for HCN3 (upper), or raised in goat and specific for GAPDH (lower). Left, HCN3 expressed in CHO cells shows two bands at 107 and 89 kDa, as shown by the arrows. Centre, HCN3 in undifferentiated (UD), early stage mESCs (ESEB) and late stage mESCs. The arrow identifies the band at 87 kDa. Right, HCN3 expressed in day 18 embryonic mouse at a molecular weight of approximately 86 kDa as identified by the arrow. *D*, Western blot probed with antibodies raised in rabbit (Alomone) and specific for HCN4 (upper), or raised in goat and specific for GAPDH (lower). Left, HCN4 expressed in CHO cells gives two bands at 174 and 149 kDa, as shown by the arrows. Centre, HCN4 was not detected in undifferentiated (UD), early stage EBs (ESEB) and late stage EBs (LSEB). Right, HCN4 was not detected in day 18 embryonic mouse. Arrows point to 130 and 170 kDa which encompass the area that HCN4 would be expected to migrate to if present. The predicted molecular weights for the unmodified proteins are: HCN1 ~100 kDa, HCN2 ~95 kDa, HCN3 ~86 kDa, HCN4 ~132 kDa. GAPDH was used as a loading control for total amount of protein. Data shown are representative of three independent experiments, from three separate preparations of mESCs.

To determine whether the increase in beating frequency and rate of diastolic depolarization were related to increases in I_f, action potentials and I_f were recorded from the same cells by switching from current to voltage clamp. I_f was activated by stepping the cells to −150 mV for 2 s, from a holding potential of −35 mV. Of the cells that beat, 47% displayed I_f at the early stage whereas 84% of beating cells possessed I_f at the late stage (Fig. 5*A*, upper panel; $P < 0.001$). It is possible that this difference is due to our inability to detect I_f, which could underestimate the proportion of cells expressing I_f to a greater extent at the early stage. However, the currents would have to be very small in order for them to go undetected, less than ~5 pA in our system. This is much smaller than the average current amplitudes measured, which were ~80 pA for early stage cells and ~320 pA for late stage cells at −150 mV.

I_f density was also significantly larger in the intermediate and late stage cells (Fig. 5*A*, lower panel), which was consistent with the increase in DDR and action potential frequency. This increase occurred despite the concomitant

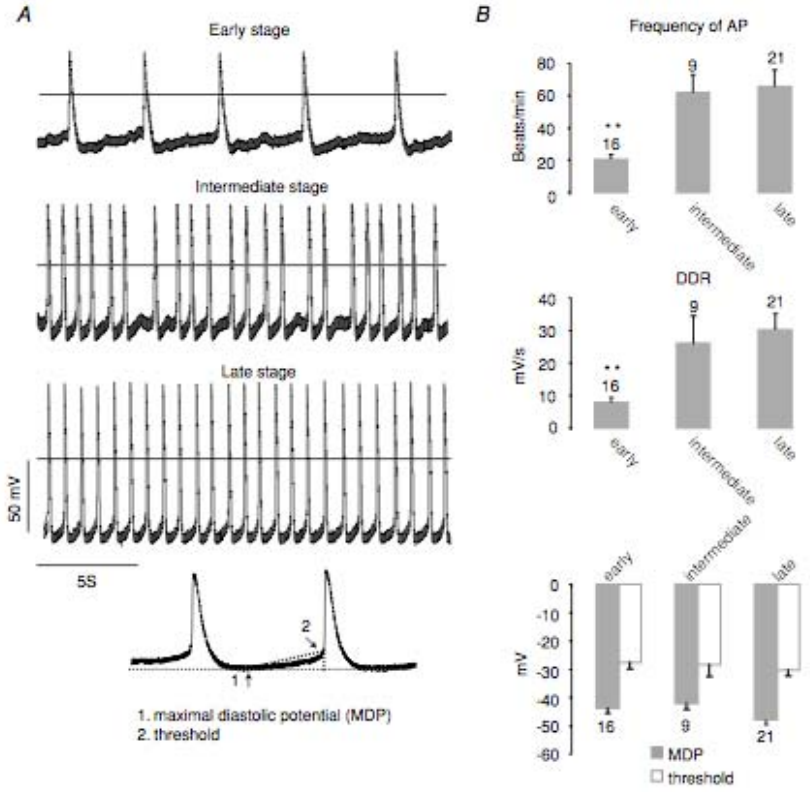

Figure 4. The frequency of action potential firing and the rate of the diastolic depolarization (DDR) increase over the course of mESC development in culture

A, representative action potential recordings from single beating cells at early, intermediate and late stages. Membrane currents were held at 0 pA and the lines indicate a membrane potential of 0 mV. *B*, top, frequency of spontaneous action potential firing at each stage (**compared to the late stage cells, $P < 0.01$). Middle, the rate of diastolic depolarization (DDR) at each stage (**compared to the late stage cells, $P < 0.01$). Bottom, the maximal diastolic potential (MDP) and action potential threshold at each stage. The parameters are illustrated in the inset, on the left. DDR was determined by the slope from the MDP to the threshold for AP firing. The threshold was considered as the base of the fast uprising phase. The number of cells for each group is shown above or below each bar. There were no significant differences in these parameters among action potentials recorded at the different stages of development.

increase in the cell capacitance (Fig. 5*A*, middle panel). The difference in I_f density between the early and late stage cells may be underestimated for two reasons. First, the inability to detect very small currents would preferentially overestimate I_f density in small cells. Second, the voltage error would preferentially underestimate I_f density in large cells. However, in both cases, the errors induced are limited and do not affect our conclusions regarding a difference in I_f density.

The faster beating rates of EBs at the late stage may be related to both an increase in the I_f density and the number of cells that possess I_f. We examined this more closely by correlating I_f density with DDR and action potential frequency. I_f density was positively correlated with DDR and action potential frequency (Fig. 5*B* and *C*). Together, the data are consistent with a contribution of I_f to maintain higher and more regular beating rates in mESCs.

Inhibition of I_f reduces beating frequency

We examined the effect of I_f inhibition on beating frequency with the selective inhibitor ZD7288. To reduce the possibility of non-specific actions, we utilized a relatively low concentration of ZD7288, 0.3 μM, on the

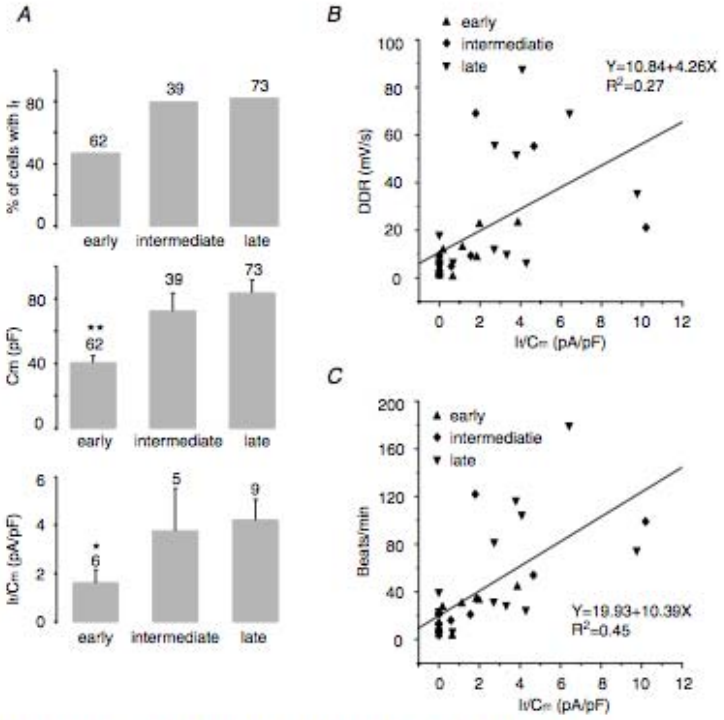

Figure 5. I_f density correlate with beating rate and diastolic depolarization rate in mESCs
A, upper, the percentage of beating cells that express I_f at each stage ($P < 0.001$, Chi-square contingency analysis, the P value was drawn from the table of critical values of the t distribution). The number of cells in each group is shown above the bars. These measurements were carried out in a complete set of cells, including recordings with and without Ba^{2+} and Mn^{2+}. Middle, cell membrane capacitance at each stage (**compared to the late stage cells, $P < 0.01$). Lower, I_f density measured at −150 mV at each stage (*compared to the late stage cells, $P < 0.05$). These measurements were recorded specifically from beating cells in the absence of Ba^{2+} and Mn^{2+}. Successful recordings of I_f and action potentials were obtained from a subset of these cells (see *B* and *C*). Only cells expressing I_f were included in the calculation. *B*, rates of diastolic depolarization (DDR) correlate with I_f density at −150 mV ($n = 32$, $P < 0.01$). *C*, action potential frequency correlates with I_f density at −150 mV ($n = 32$, $P < 0.01$). For *B* and *C*, points represent values from individual cells from which recordings of both I_f and action potentials were obtained, and were fitted by linear regression.

single beating EBs. The action of this drug is slow but its perfusion for ~30 min strongly and significantly slowed beating rates down to ~20 beats min^{-1} in the early and intermediate stage, and to ~35 beats min^{-1} in the late stage. The observed effect of ZD7288 was not due to time-dependent rundown of I_f as the beating rate of EBs in the absence of the drug was unchanged over the same period of time (Fig. 6*A*).

The inhibitory effect of ZD7288 on I_f in mESCs was also tested. I_f was slowly reduced in the presence of 0.3 μM ZD7288 at voltage steps ranging from −70 mV to −150 mV. After 30 min perfusion with ZD7288 a significant decrease in I_f by approximately 15% was seen at −150 mV at both stages (Fig. 6*B*). The data in Fig. 6 suggest that the amount of block of I_f was similar over the range of potentials examined. The time course of the effect of ZD7288 on I_f is consistent with its effect on beating EBs. The similarity in the amount of inhibition of I_f in early and late stage cells is also consistent with its actions on beating EBs at the two stages. Taken together, these data strongly support a contribution of I_f to maintenance of faster beating in mESCs at all stages of development.

Autonomic regulation of I_f contributes to the regulation of heart rate at early and late stages of development in mESCs

Autonomic regulation has not been reported in the R1 stem cell line. To determine whether β-adrenergic and/or muscarinic modulation of I_f is associated with modulation of rhythmicity and/or frequency of spontaneous beating, in the R1 cell line, the actions of the β-adrenergic agonist isoproterenol (Iso) and the muscarinic agonist acetylcholine (ACh) were examined on the beating frequency of EBs. As shown in Fig. 7*A*, perfusion of Iso (1 μM) significantly increased beating rate in EBs, to a similar extent in both early and late stage cells ($P > 0.05$).

To test if the observed effects of Iso could be attributed to an effect on I_f, two protocols were utilized. First, cells were pulsed to −90 mV, from −35 mV, and I_f was

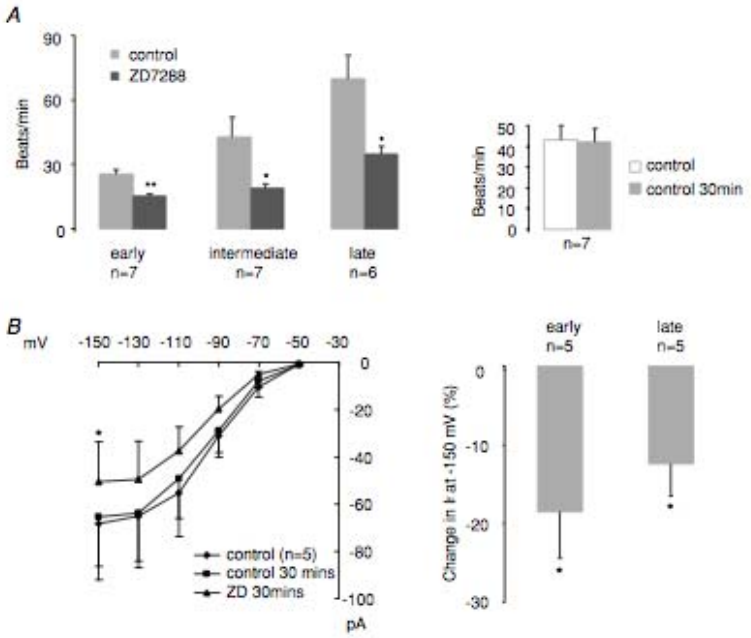

Figure 6. Inhibition of I_f reduces the beating frequency of embryoid bodies (EBs)
A, the beating frequency of single EBs is significantly reduced after 30 min perfusion with 0.3 μM ZD7288 (*$P < 0.05$; **$P < 0.01$). The inset (on the right) shows control group data, measured before and after 30 min without the drug ($P > 0.05$). *B*, left, I_f was reduced after 30 min perfusion with 0.3 μM ZD7288. Right, the change in I_f at −150 mV at both stages was calibrated from the change in the control group and normalized to the currents recorded 30 min after the seal opening ($P < 0.05$, one sample *t* test).

measured every 10 s before and during the application of Iso. Perfusion with Iso (1 μM) for 1 min increased I_f at −90 mV, as shown in Fig. 7*B* (upper traces, compare black and grey traces). The increase was approximately 18% at both early and late stages (Fig. 7*B*, bar graph). To test for a shift in the voltage dependence of I_f activation in mESCs, a two-pulse protocol was used. The cells were pulsed first to −90 mV for 5 s, and then to −130 mV for 3 s. After 1 min,

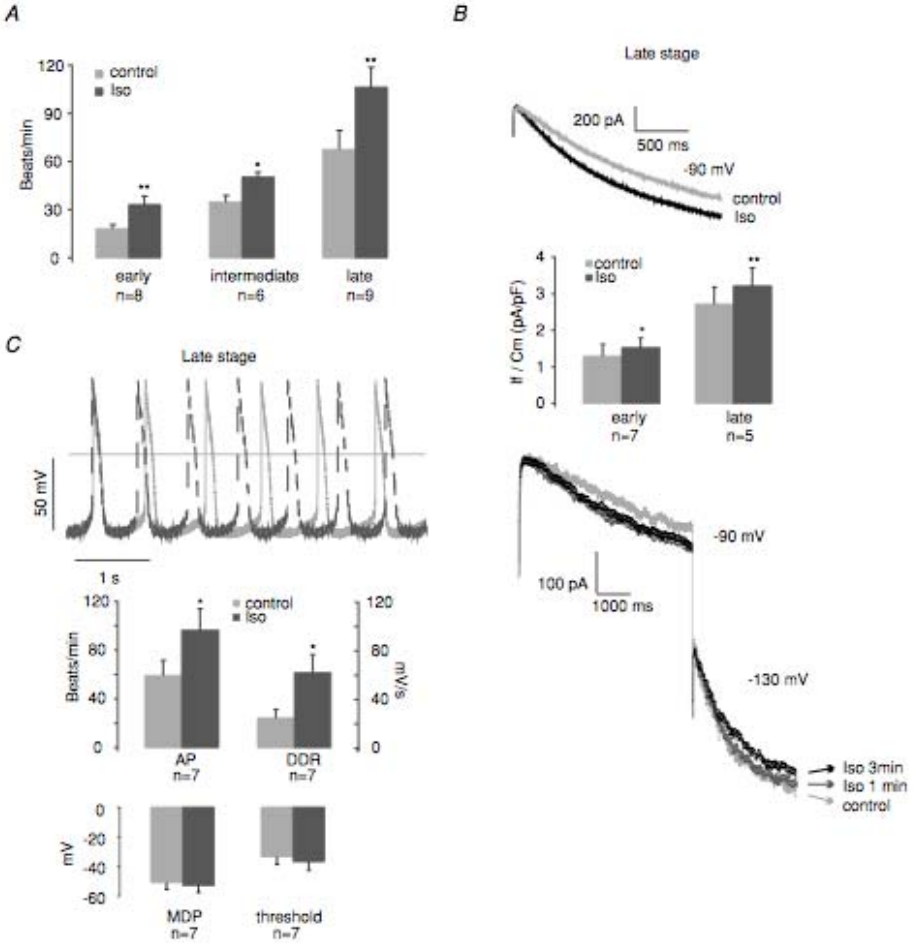

Figure 7. Isoproterenol (Iso) shifts the I_f activation curve to more positive potentials and increases beating rate, in both early and late stage cells

A, a bar graph of the beating rate of single EBs before and during perfusion with 1 μM Iso at each stage (*$P < 0.05$; **$P < 0.01$). *B*, upper, I_f traces elicited at −90 mV for 2 s in a late stage cell before (grey) and during (black) perfusion of Iso. Middle, bar graph of the change of I_f at −90 mV in response to Iso at early and late stages (*$P < 0.05$; **$P < 0.01$). Lower, I_f traces from a late stage cell before applying Iso (grey), during perfusion of Iso after 1 min (dark grey) and after 3 min (black). Cells were held at −90 mV for 5 s then stepped to −130 mV for 3 s. Note the increase in I_f amplitude at −90 mV in response to Iso but the lack of any change at −130 mV after 1 min. *C*, upper, action potentials recorded from a late stage cell before (continuous) and during perfusion of Iso (dashed). Middle, bar graphs of action potential frequency and DDR before and during perfusion of Iso (*$P < 0.05$). Below, bar graph of MDP and activation threshold before and during perfusion of Iso ($P > 0.05$).

Iso increased I_f at −90 mV but did not alter the maximum amount of current (Fig. 7*B*, lower traces, compare light and dark grey traces). The increase of I_f in the mid-activation range and the lack of any increase in the fully activated range indicates that Iso shifted the voltage dependence of I_f activation to more positive voltages. Rundown of I_f was not apparent after 1 min perfusion, but it was apparent after 3 min in Iso (compare black and dark grey traces), which was noticeable especially at −130 mV. At −90 mV, the rundown after 3 min in Iso was slight; the current was still larger than the control current. Thus, the effect of Iso on I_f was still notable in the face of current rundown.

To determine the effects of autonomic stimulation on the action potential, spontaneous electrical activity was recorded in the absence and presence of Iso (1 μM). Reliable recordings of action potentials from early stage cells, before and during perfusion of Iso, were difficult to obtain because they often stopped beating or the beating became very irregular during the recordings. Therefore, these experiments were carried out only at the late stage. In these cells, Iso increased both DDR and action potential frequency without the change of MDP and action potential activation threshold (Fig. 7*C*).

The effects of ACh were the opposite to those of Iso. Perfusion of ACh (1 μM) significantly decreased beating rate in EBs. The effects were similar between early and late stages (Fig. 8*A*), but smaller in the intermediate stage EBs ($P < 0.01$), compared to the late stage EBs. The same protocols used for Iso were utilized to determine the effects of ACh on I_f. Perfusion with ACh (1 μM) for 1 min decreased I_f at −90 mV, as shown in Fig. 8*B* (upper traces, compare light grey and dark grey traces). Upon washout of ACh, I_f returned to control values (black trace), indicating the reduction was not due to current rundown. The decrease was about 15% at both the early and later stages (Fig. 8*B*, bar graph). To test for a shift in the voltage dependence of I_f activation in mESCs, the same two-pulse protocol was used as above. After perfusion of ACh for ~1 min, ACh decreased I_f at −90 mV but did not affect the current at −130 mV (Fig. 8*B*, lower traces, compare light and dark grey traces). The decrease in I_f in the mid-activation range and the lack of any decrease in the fully activated range indicates that ACh shifted the voltage dependence of I_f activation to more negative voltages. After 3 min in ACh, a small decrease in current was apparent at −90 mV and a larger decrease in current was apparent at −130 mV (compare black and dark grey traces). As, after 3 min in ACh, the decrease of I_f at −130 mV was similar to that as observed in Iso, it was also probably due to the current rundown.

Opposite to Iso, ACh decreased both DDR and action potential frequency, without a change in MDP and activation threshold (Fig. 8*C*). In either ACh or Iso, both DDR and action potential frequency were modified in parallel, which suggests that changes in beating frequency were due in large measure to changes in the time required to reach threshold. Furthermore, the changes in DDR are consistent with a contribution of I_f to the changes in beating rate induced by autonomic stimulation. Taken together, the data suggest that modulation of I_f contributes to alterations in beating frequency elicited by autonomic stimulation.

Discussion

HCN channels and I_f confer faster and more regular rhythmicity to beating mouse embryonic stem cells

In this paper, we show that HCN channels and I_f confer more regular and faster rhythmicity to beating mESCs. This conclusion is based on the following evidence. I_f density was correlated with action potential frequency and the rate of diastolic depolarization. A subset of mESCs without detectable I_f beat significantly more slowly and more irregularly than cells with I_f. The threshold for I_f activation and maximal diastolic potentials recorded from spontaneously active cells were similar and potentially overlap. The beating rate of single EBs and I_f were reduced by relatively low concentrations of the I_f blocker ZD7288. A developmental change of I_f is also associated to the increased beating rate during mESC development. I_f density, the proportion of cells expressing I_f, and the I_f activation rate all increased in the late stage mESCs, which may synergistically contribute to the faster rates of beating following the development.

As is the case for other spontaneously active cells, such as cardiomyocytes of the sinoatrial node, mechanisms not involving I_f contribute to the generation and modulation of spontaneous activity in mESCs. In mESCs, a contribution to beating and the diastolic depolarization from the T-type calcium channel has recently been suggested (Zhang *et al.* 2003). Other potential contributors include inward currents from the L-type calcium and sodium channels, instantaneous currents such as the Na^+-sensitive background current ($I_{Na,b}$), and release of intracellular calcium from ryanodine-sensitive stores, all of which have been suggested to contribute to spontaneous activity in the neonatal and adult sinoatrial node (Hagiwara *et al.* 1992; Noble *et al.* 1992; Irisawa *et al.* 1993; Baruscotti *et al.* 1996; Bogdanov *et al.* 2001). Further studies will be required to determine which mechanisms contribute in mESCs, and to what extent each is involved under different conditions.

In our studies, we found a subset of beating mESCs that did not possess detectable I_f. These cells beat more slowly than those with detectable levels of I_f, consistent with a contribution from HCN channels to beating. In addition to the above mentioned mechanisms, a slower, rhythmic, release of intracellular calcium through IP_3-sensitive stores may contribute to beating in mESCs that do not possess I_f (Viatchenko-Karpinski *et al.* 1999; Mery *et al.* 2005; Maltsev *et al.* 2006).

HCN isoforms and electrophysiological characteristics of I_f in mESC

In this study, Western blot analyses suggest that HCN2 and HCN3 isoforms are present in both early and late stage mESCs, as well as in the undifferentiated cells. The amount of HCN3 decreased over the course of development in culture. This profile is consistent with the electrophysiological data. The rate of I_f activation in mESCs is slower and faster than rates of I_f activation

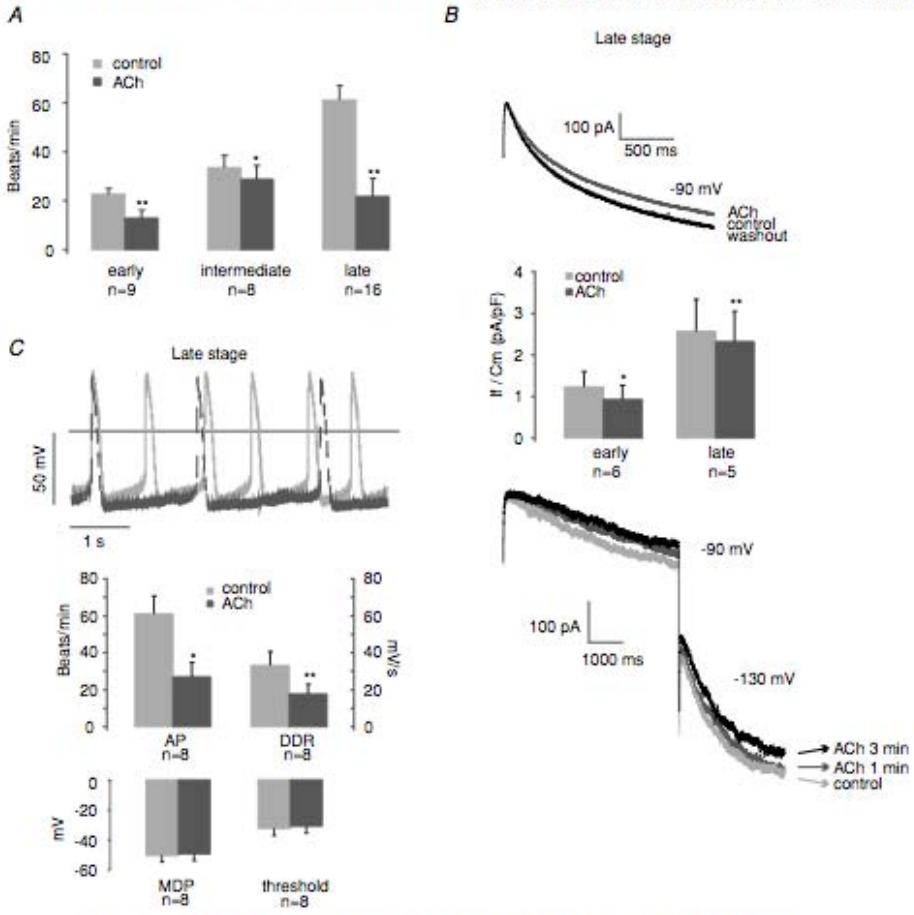

Figure 8. Acetylcholine (ACh) shifts the I_f activation curve to more negative potentials and decreases beating rate, in early and late stage cells

A, bar graph of the beating rate of single EBs before and during perfusion with 1 μM ACh at each stage (*$P < 0.05$; **$P < 0.01$). *B*, upper, I_f traces elicited at −90 mV for 2 s in a late stage cell before (grey) and during (black) perfusion of ACh. Note the return of the current to control values after 1 min. Middle, bar graph of the change of I_f at −90 mV in response to ACh at early and late stages (*$P < 0.05$; **$P < 0.01$). Lower, I_f traces from a late stage cell before applying ACh (light grey), during perfusion of ACh after 1 min (dark grey) and after 3 min (black). Cells were held at −90 mV for 5 s then stepped to −130 mV for 3 s. Note the decrease in I_f amplitude at −90 mV in response to ACh but the lack of any change at −130 mV, after 1 min. *C*, above, action potentials recorded from a late stage cell before (continuous) and during perfusion of ACh (dashed). Note the decrease in the MDP of cells during perfusion of ACh. Middle, bar graph of action potential frequency and DDR before and during perfusion of ACh (*$P < 0.05$). Below, bar graph of MDP and activation threshold before and during perfusion of ACh (**$P > 0.05$).

recorded from mammalian cells expressing HCN2 and HCN3, respectively. The decrease in the amount of more slowly activating HCN3 channels could also explain the increase in the rate of I_f activation from early to late stage. These findings are consistent with those of the embryonic mouse heart, which has been shown to possess large amounts of HCN2, and lesser amounts of HCN3 (Yasui *et al.* 2001; Kuwahara *et al.* 2003; Stieber *et al.* 2003; Whitaker *et al.* 2007). We were not able to detect HCN1 or HCN4 protein in our preparations. This may have been due to low amounts in, or their absence from, these cells, or because the antibodies we used were not able to detect them.

We also found both HCN2 and HCN3, but not HCN1 or HCN4, in undifferentiated mESCs. This is consistent with findings from another study which, using the same R1 cell line, were able to measure I_f and identified transcripts for HCN2 and HCN3, but not for HCN1 or HCN4, in undifferentiated mESCs (Wang *et al.* 2005).

The activation kinetics of I_f, and the position of the I_f activation curve, determined from mouse embryonic cardiomyocytes (Yasui *et al.* 2001; Stieber *et al.* 2003; Herrmann *et al.* 2007) are similar to those we determined in mESCs. The quickening of I_f activation rate found in our experiments may contribute to the increase in beating frequency observed over the course of development in culture. In contrast, the beating rates of human embryonic stem cells (hESCs) decrease along with the rate of I_f activation (Sartiani *et al.* 2007). Consistent with the developmental change in beating frequencies of stem cells, embryonic heart rates increase in mouse and decrease in human, but it is not known whether the rates of I_f activation change. In human embryonic stem cells, the decrease in rate of I_f activation is correlated with a decrease in the expression of HCN1 and HCN4, whereas levels of HCN2 remain constant over the course of development. Interestingly, these authors suggest that the change in isoform expression may be more consistent with a ventricular, rather than pacemaker, phenotype. More detailed experiments will be required to identify stem cells programmed to become specific cardiac cell types with certainty.

Beating rate and I_f are modulated by autonomic agonists

In this study, both the beating rate and I_f were reduced and increased by ACh and Iso, respectively, to a similar extent in early and late stage mESCs. These results suggest that the mechanisms responsible for autonomic modulation are already developed at the early stage in mESCs. Our findings in the R1 cell line are not completely consistent with the previous studies using the D3 mouse stem cell line. One study suggested muscarinic stimulation via I_f only occurs at the early stage, while β-adrenergic stimulation was observed only at the late stage (Abi-Gerges *et al.* 2000). Another study (Banach *et al.* 2003) found that the muscarinic response on beating EBs could be observed only at later stages of development in culture (after D7 + 5). Differences may be due to the heterogeneity of the mESC phenotype. Also, both of those studies used carbachol to examine muscarinic responsiveness, whose actions sometimes differ from those of ACh, which we used in our study.

As mouse HCN3 does not respond to cAMP, unlike mouse HCN2 (Mistrik *et al.* 2005), we might have expected that the extent of I_f modulation by ACh and Iso would have differed between the early and late cells, especially if they form two separate sets of homomeric channels. However, it is not clear as to whether HCN2 and HCN3 co-assemble to form heteromeric channels, and how these mixed channels would respond to changes in cAMP. The similarity in the effects of autonomic stimulation of I_f between the early and late stage cells suggests that HCN2 and HCN3 channels may form heteromeric channels in early stage mESCs that respond in a way that is not different from the response of channels made up of predominantly HCN2 subunits in late stage mESCs.

Summary and perspectives

In summary, we show that HCN channel expression is developmentally regulated, and that it confers more regular and faster rhythmicity to mESCs over the course of development in culture. Both I_f density and beating frequency increase over the course of development which, together with previous studies, suggest that the R1 cell line mirrors the developmental pattern observed in embryonic mouse hearts. The use of mESCs as a model for the development of the embryonic mouse heart is also supported by our data showing that HCN2 and HCN3 are found in both mESCs and the embryonic mouse heart. Further studies are needed to uncover the pattern of HCN isoform expression in the mouse embryonic heart which is presently not clear. An understanding of the mechanisms that regulate HCN expression during embryonic development, and how this expression is related to the emergence of a pacemaker cell phenotype, are important issues that also need to be addressed. The ease with which they can be manipulated genetically, and studied by electrophysiological and other approaches, make mESCs a useful and important model system for studying these issues.

References

Abi-Gerges N, Ji GJ, Lu ZJ, Fischmeister R, Hescheler J & Fleischmann BK (2000). Functional expression and regulation of the hyperpolarization activated non-selective cation current in embryonic stem cell-derived cardiomyocytes. *J Physiol* **523**, 377–389.

Accili EA, Proenza C, Baruscotti M & DiFrancesco D (2002). From funny current to HCN channels: 20 years of excitation. *News Physiol Sci* **17**, 32–37.

Accili EA, Redaelli G & DiFrancesco D (1997). Differential control of the hyperpolarization-activated current (i_f) by cAMP gating and phosphatase inhibition in rabbit sino-atrial node myocytes. *J Physiol* **500**, 643–651.

Altomare C, Bucchi A, Camatini E, Baruscotti M, Viscomi C, Moroni A & DiFrancesco D (2001). Integrated allosteric model of voltage gating of HCN channels. *J Gen Physiol* **117**, 519–532.

Banach K, Halbach MD, Hu P, Hescheler J & Egert U (2003). Development of electrical activity in cardiac myocyte aggregates derived from mouse embryonic stem cells. *Am J Physiol Heart Circ Physiol* **284**, H2114–H2123.

Baruscotti M, DiFrancesco D & Robinson RB (1996). A TTX-sensitive inward sodium current contributes to spontaneous activity in newborn rabbit sino-atrial node cells. *J Physiol* **492**, 21–30.

Bogdanov KY, Vinogradova TM & Lakatta EG (2001). Sinoatrial nodal cell ryanodine receptor and Na^+-Ca^{2+} exchanger: molecular partners in pacemaker regulation. *Circ Res* **88**, 1254–1258.

DiFrancesco D (1981). A study of the ionic nature of the pace-maker current in calf Purkinje fibres. *J Physiol* **314**, 377–393.

DiFrancesco D (1993). Pacemaker mechanisms in cardiac tissue. *Annu Rev Physiol* **55**, 455–472.

DiFrancesco D, Ferroni A, Mazzanti M & Tromba C (1986). Properties of the hyperpolarizing-activated current (i_f) in cells isolated from the rabbit sino-atrial node. *J Physiol* **377**, 61–88.

Hagiwara N, Irisawa H, Kasanuki H & Hosoda S (1992). Background current in sino-atrial node cells of the rabbit heart. *J Physiol* **448**, 53–72.

Herrmann S, Stieber J, Stockl G, Hofmann F & Ludwig A (2007). HCN4 provides a 'depolarization reserve' and is not required for heart rate acceleration in mice. *EMBO J* **26**, 4423–4432.

Irisawa H, Brown HF & Giles W (1993). Cardiac pacemaking in the sinoatrial node. *Physiol Rev* **73**, 197–227.

Klug MG, Soonpaa MH, Koh GY & Field LJ (1996). Genetically selected cardiomyocytes from differentiating embronic stem cells form stable intracardiac grafts. *J Clin Invest* **98**, 216–224.

Kolossov E, Lu Z, Drobinskaya I, Gassanov N, Duan Y, Sauer H, Manzke O, Bloch W, Bohlen H, Hescheler J & Fleischmann BK (2005). Identification and characterization of embryonic stem cell-derived pacemaker and atrial cardiomyocytes. *Faseb J* **19**, 577–579.

Kuwahara K, Saito Y, Takano M, Arai Y, Yasuno S, Nakagawa Y *et al.* (2003). NRSF regulates the fetal cardiac gene program and maintains normal cardiac structure and function. *EMBO J* **22**, 6310–6321.

Macri V & Accili EA (2004). Structural elements of instantaneous and slow gating in hyperpolarization-activated cyclic nucleotide-gated channels. *J Biol Chem* **279**, 16832–16846.

Macri V, Proenza C, Agranovich E, Angoli D & Accili EA (2002). Separable gating mechanisms in a Mammalian pacemaker channel. *J Biol Chem* **277**, 35939–35946.

Maltsev VA, Rohwedel J, Hescheler J & Wobus AM (1993). Embryonic stem cells differentiate in vitro into cardiomyocytes representing sinusnodal, atrial and ventricular cell types. *Mech Dev* **44**, 41–50.

Maltsev VA, Vinogradova TM & Lakatta EG (2006). The emergence of a general theory of the initiation and strength of the heartbeat. *J Pharmacol Sci* **100**, 338–369.

Maltsev VA, Wobus AM, Rohwedel J, Bader M & Hescheler J (1994). Cardiomyocytes differentiated in vitro from embryonic stem cells developmentally express cardiac-specific genes and ionic currents. *Circ Res* **75**, 233–244.

Mery A, Aimond F, Menard C, Mikoshiba K, Michalak M & Puceat M (2005). Initiation of embryonic cardiac pacemaker activity by inositol 1,4,5-trisphosphate-dependent calcium signaling. *Mol Biol Cell* **16**, 2414–2423.

Mistrik P, Mader R, Michalakis S, Weidinger M, Pfeifer A & Biel M (2005). The murine HCN3 gene encodes a hyperpolarization-activated cation channel with slow kinetics and unique response to cyclic nucleotides. *J Biol Chem* **280**, 27056–27061.

Nagy A, Rossant J, Nagy R, Abramow-Newerly W & Roder JC (1993). Derivation of completely cell culture-derived mice from early-passage embryonic stem cells. *Proc Natl Acad Sci U S A* **90**, 8424–8428.

Noble D, Denyer JC, Brown HF & DiFrancesco D (1992). Reciprocal role of the inward currents $i_{b,}$ Na and i_f in controlling and stabilizing pacemaker frequency of rabbit sino-atrial node cells. *Proc Biol Sci* **250**, 199–207.

Porter GA Jr & Rivkees SA (2001). Ontogeny of humoral heart rate regulation in the embryonic mouse. *Am J Physiol Regul Integr Comp Physiol* **281**, R401–R407.

Proenza C, Angoli D, Agranovich E, Macri V & Accili EA (2002). Pacemaker channels produce an instantaneous current. *J Biol Chem* **277**, 5101–5109.

Robbins J, Gulick J, Sanchez A, Howles P & Doetschman T (1990). Mouse embryonic stem cells express the cardiac myosin heavy chain genes during development in vitro. *J Biol Chem* **265**, 11905–11909.

Robinson RB & Siegelbaum SA (2003). Hyperpolarization-activated cation currents: from molecules to physiological function. *Annu Rev Physiol* **65**, 453–480.

Santoro B, Chen S, Luthi A, Pavlidis P, Shumyatsky GP, Tibbs GR & Siegelbaum SA (2000). Molecular and functional heterogeneity of hyperpolarization-activated pacemaker channels in the mouse CNS. *J Neurosci* **20**, 5264–5275.

Sartiani L, Bettiol E, Stillitano F, Mugelli A, Cerbai E & Jaconi ME (2007). Developmental changes in cardiomyocytes differentiated from human embryonic stem cells: a molecular and electrophysiological approach. *Stem Cells* **25**, 1136–1144.

Stieber J, Herrmann S, Feil S, Loster J, Feil R, Biel M, Hofmann F & Ludwig A (2003). The hyperpolarization-activated channel HCN4 is required for the generation of pacemaker action potentials in the embryonic heart. *Proc Natl Acad Sci U S A* **100**, 15235–15240.

Viatchenko-Karpinski S, Fleischmann BK, Liu Q, Sauer H, Gryshchenko O, Ji GJ & Hescheler J (1999). Intracellular Ca^{2+} oscillations drive spontaneous contractions in cardiomyocytes during early development. *Proc Natl Acad Sci U S A* **96**, 8259–8264.

Wang K, Xue T, Tsang SY, Van Huizen R, Wong CW, Lai KW *et al.* (2005). Electrophysiological properties of pluripotent human and mouse embryonic stem cells. *Stem Cells* **23**, 1526–1534.

Whitaker GM, Angoli D, Nazzari H, Shigemoto R & Accili EA (2007). HCN2 and HCN4 isoforms self-assemble and co-assemble with equal preference to form functional pacemaker channels. *J Biol Chem* **282**, 22900–22909.

White SM & Claycomb WC (2005). Embryonic stem cells form an organized, functional cardiac conduction system in vitro. *Am J Physiol Heart Circ Physiol* **288**, H670–H679.

Wobus AM, Wallukat G & Hescheler J (1991). Pluripotent mouse embryonic stem cells are able to differentiate into cardiomyocytes expressing chronotropic responses to adrenergic and cholinergic agents and Ca^{2+} channel blockers. *Differentiation* **48**, 173–182.

Yasui K, Liu W, Opthof T, Kada K, Lee JK, Kamiya K & Kodama I (2001). I_f current and spontaneous activity in mouse embryonic ventricular myocytes. *Circ Res* **88**, 536–542.

Zhang YM, Hartzell C, Narlow M & Dudley SC Jr (2002). Stem cell-derived cardiomyocytes demonstrate arrhythmic potential. *Circulation* **106**, 1294–1299.

Zhang YM, Shang L, Hartzell C, Narlow M, Cribbs L & Dudley SC Jr (2003). Characterization and regulation of T-type Ca^{2+} channels in embryonic stem cell-derived cardiomyocytes. *Am J Physiol Heart Circ Physiol* **285**, H2770–H2779.

Acknowledgements

The authors are grateful for the input of Dr Pamela Hoodless in the early phases of this work. These studies were generously supported by an operating grant from Canadian Institutes of Health Research (G.F.T. and E.A.A.), a Grant-in-Aid from the Heart and Stroke Foundation of British Columbia and the Yukon (E.A.A.), and a postdoctoral fellowship from the Heart and Stroke Foundation of Canada (Y.Q.). L.H.-M. is a recipient of a 'Ramon y Cajal' grant from the Spanish Ministry of Science and Technology and E.A.A. and G.F.T. are the recipients of Tier II and Tier I Canada Research Chairs, respectively. The gift of HCN2- and HCN3-specific antibodies from Ryuichi Shigemoto are gratefully acknowledged. We thank Dr S. X. Bamji (UBC) for the embryonic tissue. Finally, comments from anonymous reviewers were greatly appreciated.

APPENDIX B: USING BIOLUMINESCENCE RESONANCE ENERGY TRANSFER TO MEASURE ION CHANNEL ASSEMBLY [4]

[4] This chapter has been published. Whitaker GM, Accili EA. (2008) Using bioluminescence resonance energy transfer to measure ion channel assembly *Methods in Molecular Biology*. 491, 189-197

USING BIOLUMINESCENCE RESONANCE ENERGY TRANSFER (BRET) TO MEASURE ION CHANNEL ASSEMBLY

SUMMARY

Bioluminescence Resonance Energy Transfer (BRET) measures protein interactions within 10nm of each other. Aside from its ability to probe for interactions at high resolution, this technique operates in live, intact cells, and offers a high throughput method of detection. Thus far, BRET has been widely used in measuring G protein receptor dimerization. In this chapter, we describe the BRET methodology in detail and apply this technique to the measurement of ion channel assembly. In addition, we discuss how BRET can be used to compare the extent of homomeric and heteromeric channel assembly.

Key Words: Bioluminescence Resonance Energy Transfer; ion channel assembly; protein-protein interactions; heteromer; homomer; tetramer; subunit.

1. INTRODUCTION

It is widely accepted that the majority of potassium channels assemble as tetramers to form functional channels. Channels can self-assemble from four identical subunits to form homomers, or can form heteromers by co-assembly of structurally homologous subunits. Functional co-assembly is traditionally addressed by electrophysiology, which can also provide information on subunit stoichiometry (1, 2). Physical assembly of ion channel subunits has been directly examined by crystal structure analysis, which has perhaps provided the clearest picture of channel structure thus far (3, 4). Nevertheless, the ability to crystallize ion channels has proven to be extremely difficult and thus these studies are few and far between. More commonly, indirect measurements using techniques such as *in vitro* translation or co-immunoprecipitation are used to measure interactions between subunits (5). However, the rigorous biochemical manipulation involved in such techniques, as well as removal of channels from their membrane environment, can alter the native channel structure as well as putative intersubunit interactions. In addition, these techniques cannot easily distinguish between direct and indirect protein interactions within larger complexes. One can circumvent some typical issues associated with traditional biochemical techniques by using Fluorescence Resonance Energy Transfer (FRET) (6, 7). FRET measures protein interactions at a high resolution, within 10nm, whilst in their membrane environment, resulting in precise information pertaining to the subcellular location of interaction. Nonetheless, FRET measurements can be difficult to interpret since the assay requires initial excitation by an external light source which can result in photobleaching, autofluorescence, or direct excitation of the acceptor molecule, thereby producing erroneous signals or high signal-to-background ratios.

Similarly to FRET, Bioluminescence Resonance Energy Transfer (BRET) also measures energy transfer in live cells, between proteins of interest located less than 10nm

from one another. To measure BRET, two putatively-interacting proteins of interest are fused with either Renilla-Luciferase (R-Luc, a bioluminescent donor molecule) or Green Fluorescence Protein (GFP, the acceptor molecule) and co-expressed in a heterologous expression system. A substrate (coelenterazine), which is added to the cells, is oxidized by R-Luc, which in turn emits bioluminescent energy at a wavelength of 395nm. GFP is excited at this wavelength, thereby emitting fluorescence at 510nm provided that interacting partners are in close enough proximity (**Figure 1**). The efficiency of energy transfer can then be quantified as a BRET ratio of emission intensity at 510nm to that at 395nm. The magnitude of a BRET signal varies inversely with the 6^{th} power of distance up to 10nm, thus providing high resolution for measuring interacting proteins (8). By using the coelenterazine substrate rather than an external light source to excite the donor molecule, the issues associated with fluorescence excitation can be avoided. Further, BRET measurements are taken on large populations of cells, thus providing a high throughput method of detection of protein interactions.

BRET is widely used to measure dimerization of G protein-coupled receptors (GPCR) as well as dynamic changes in GPCR interactions, and has also been used to quantify the extent of homo- and hetero-dimerization of GPCRs (9, 10). We have recently adapted this technique to measure self- versus co-assembly of different Hyperpolarization-activated Cyclic Nucleotide-modulated (HCN) channel subunit isoforms (HCN2 and HCN4) (11). In this chapter, we elaborate on how BRET can be used to measure and compare homomeric and heteromeric ion channel assembly in live Chinese Hamster Ovary (CHO) cells.

2. MATERIALS

2.1 Cell Culture and Transfection

1. Fusion protein expression vectors: $pGFP^2$-N, $pGFP^2$-C, pRLuc-N and pRLuc-C (Perkin Elmer)
2. cDNA encoding ion channel subunits of interest
3. Chinese Hamster Ovary (CHO) cells (American Type Culture Collection) (*see* **Note 1**)
4. Cell culture medium: F12 Nutrient Mixture (1X) containing L-glutamine, supplemented with 5% fetal bovine serum (FBS) and 0.25% Penicillin-Streptomycin (Invitrogen Canada Inc.)
5. FuGENE 6 Transfection Reagent (Roche Diagnostics Canada)
6. Transfection Media: F12 Nutrient Mixture (1X) containing L-glutamine, supplemented with 5% FBS (Invitrogen Canada Inc.)
7. 60mm cell culture-treated dishes

2.2 BRET Assay

1. Dulbecco's-Phosphate-Buffered Saline (D-PBS): 0.1g/L $CaCl_2$, 0.1g/L $MgCl_2$*6H2O, 1g/L D-glucose (Invitrogen Canada Inc.)
2. 0.05%Trypsin with EDTA-4Na (1X) (Invitrogen Canada Inc.)
3. F12 Nutrient Mixture (1X) containing L-glutamine, supplemented with 5% FBS (Invitrogen Canada Inc.)
4. BRET buffer: D-PBS supplemented with 2ug/ml of aprotinin
5. DeepBlueC coelenterazine substrate (PerkinElmer Inc.) reconstituted to 1mM in absolute ethanol and diluted to 15uM in BRET buffer just prior to use (*see* **Note 2**)
6. 96-well white optiplates (PerkinElmer Inc.)
7. Victor V Plate Reader (PerkinElmer Inc.) including the following additions:

    - Optical Excitation filter: 405/5 nm (for GFP fluorescence quantification)
    - Optical Emission filters: 410/80 nm and 515/30 nm
    - 1-3 channel injectors
    - Wallac 1420 workstation software

3. METHODS

3.1. Cell Culture and Transfection

1. Make cDNA fusion constructs of interest using standard subcloning techniques such that each cDNA partner is tagged with GFP or RLuc at either the N- or C-termini (*see* **Note 3 and Note 4**).
2. Culture CHO cells in Cell Culture Media, in 60mm cell culture-treated dishes at 37°C with 5% CO_2 injection until they are approximately 50% confluent. Include one dish as an untransfected background control.
3. In 1.5mL eppendorf tubes, mix cDNA (either RLuc-tagged construct alone, or optimized combinations of RLuc- and GFP-tagged constructs, (*see* **Note 5 and Note 6**) with 100µl of F12 media (without antibiotics) and FuGENE 6. transfection reagent. Use a 3:1 ratio of FuGENE 6 Transfection Reagent to total cDNA amount added. Incubate tubes at room temperature for 30 minutes.
4. Replace Cell Culture Media from cultured cells with Transfection Media, then add transfection mixture from eppendorf tubes to cells. Agitate gently, then incubate for 24 hours at 37°C with 5% CO_2 injection.

3.2. BRET Assay

3.2.1. Cell Preparation

1. Twenty-four hours post-transfection, wash cells twice with 3mL of D-PBS at room temperature.
2. Add 1mL of 0.05%Trypsin-EDTA and incubate cells for 5 minutes with occasional agitation.
3. Add 3mL of Transfection Media to inactivate the 0.05%trypsin-EDTA, then collect the cell mixture in appropriate centrifuge tubes.
4. Centrifuge cells at 500-700g for 5 minutes.
5. Remove supernatant and resuspend cells in 100ul of BRET buffer
6. Add 50ul of well-mixed cells (approximately 100,000 cells) in duplicate to individual wells of a 96 well white Optiplate.
7. Incubate cells for 30 minutes at room temperature in the dark.
8. Just prior to proceeding with BRET measurements, prepare a sufficient amount of 15uM DeepBlueC in BRET buffer and keep it on ice in the dark.

3.2.2. Measurement of GFP Fluorescence

1. Place the 96-well plate into the Victor V plate reader
2. Set up and run the protocol for measurement of GFP fluorescence using the Wallac 1420 workstation software (*see* **Note 7**)
    a. Shake the entire plate for 5 seconds at medium speed
    b. Use the 405/5 nm excitation filter and 515/30 nm emission filter to measure relative GFP fluorescence units for each well that contains cells
3. Calculate the fold over background of GFP fluorescence according to the following equation, where background is the relative fluorescence units from the well containing untransfected cells.

$$\frac{\text{Relative Fluorescence Units at 510nm of well } x}{\text{Relative Fluorescence Units at 510nm of background}}$$

3.2.3. Measurement of BRET

Design a protocol for BRET using the Wallac 1420 workstation software as follows, such that machine runs through the entire protocol for each well before proceeding to subsequent wells.

1. Add 25µL of 15µM DeepBlueC in BRET buffer to the first well using the injector installed on the Victor V plate reader, such that the final concentration of DeepBlueC in the well is 5µM.
2. Shake the Optiplate for 5 seconds at medium speed in the plate reader.

3. Immediately measure emission intensity at 395nm (relative luminescence units) followed by emission intensity at 510nm (relative fluorescent units) in the first well.
4. Repeat steps 1 through 3 for subsequent wells until all wells are read.

3.3.4. BRET Analysis

1. Use the following equation to calculate BRET ratios for each well (*see* **Note 8**)

$$\frac{\text{(Emission at 510nm – Emission at 510nm of control well)}}{\text{(Emission at 395nm – Emission at 395nm of control well)}}$$

2. Determine the mean BRET values from duplicate wells.
3. Repeat the experiment and plot 'n' number of duplicates as a bar graph of BRET ratios including standard error. Compare the test pairs to negative and positive controls using one-way ANOVA followed by a post test to compare all pairs (*see* **Figure 2** and **Note 9**).

4. NOTES

1. The cell culture and transfection protocol and reagents described in this chapter have been optimized for a CHO cell heterologous expression system. However, other mammalian expression systems and transfection reagents would also be appropriate and have been used for BRET assays (12, 13).

2. DeepBlueC is air and light sensitive, thus store vial tightly sealed in the dark at -20°C and allow it to equilibrate to room temperature prior to opening.

3. In our experiments, the following cDNA constructs were made: HCN2-GFPN and HCN2-GFPC, as well as HCN2-RLucN and HCN2-RLucC such that HCN2 is expressed on the N- and C- terminal ends respectively, of either GFP or RLuc. These constructs were also made using HCN4 (HCN4-GFPN, HCN4-GFPC, HCN4-RLucN and HCN4-RLucC). We also made a construct in which Kv1.5 is expressed on the C- terminal end of the RLuc tag, to be used as a negative control (*see* **Note 6**). All tagged combinations (both N and C) should be made in order to determine the optimal combination for efficient energy transfer. Once the optimal Rluc- and GFP- tagged combination is determined, this should be kept constant across all compared partners and controls in order to accurately compare BRET ratios.

4. Once constructs are made, it is important to verify that folding, assembly or trafficking of the channel is not inhibited by the fused protein tags. In our case, we used patch-clamp electrophysiology to measure currents of expressing constructs in CHO cells, ensuring that the tagged constructs produced currents similar to their wild type counterparts.

5. The magnitude of BRET increases with increasing GFP-expression to a saturating level if the expressing RLuc- and GFP-tagged constructs are interacting within 10nm. Thus, in order to obtain optimal BRET ratios, it is important to transfect variable amounts of GFP-tagged cDNA with a constant and optimized amount of RLuc-tagged cDNA. For our experiments, we transfected 0.5ug of Rluc-tagged cDNA in all conditions. For GFP-tagged constructs, we transfected the following amounts: 0.5µg, 1.0µg, 1.5µg, 2.0µg and 2.5µg. Expression levels are measured as "fold-over-background" of relative luminescence and fluorescence units, using the plate reader (*see* **Note 6**).

6. When analyzing BRET data, it is important to compare the results to appropriate controls. In our case, we felt it important to choose a negative control which is similar in structure and function to, but does not co-assemble with, HCN2 or HCN4 subunits. Thus we co-expressed RLuc-tagged Kv1.5 (Kv1.5-RLuc) with either HCN2-GFP or HCN4-GFP as our negative control. In addition, we transfected Kv1.5-RLuc alone, as a control for background BRET levels. For positive controls, we co-transfected differently-tagged homomeric combinations: HCN2-Rluc with HCN2-GFP, or HCN4-Rluc with HCN4-GFP, since HCN2 and HCN4 channels form functional homotetrameric channels (14).

7. Direct measurement of GFP fluorescence (by exciting GFP at the correct wavelength) gives information about the level of GFP-tagged protein expression. With increasing GFP expression (while maintaining RLuc expression constant), BRET values consequently increase to eventually saturating levels if the protein interaction is specific. This can be plotted as a graph of BRET ratio vs. GFP/RLuc fold over background and fit with a saturation curve. However, in our experiments, GFP-tagged protein expression levels remained relatively constant despite increasing the amount of transfected GFP-tagged cDNA. Thus, in our case we used a bar graph to accurately compare BRET values.

8. The emission from control wells is the background luminescence and resulting fluorescence either from untransfected cells (as performed in our experiments) or from cells that have only been transfected with Rluc-tagged construct.

9. In our experiments, we compared homomeric Rluc- and GFP-tagged HCN2 and HCN4 combinations (our positive control) with co-expression of differently tagged HCN2 and HCN4 subunits. Within the limits of BRET sensitivity, the magnitudes of BRET ratios were not significantly different between all homomeric and heteromeric combinations of HCN2 and HCN4. Thus, we concluded that HCN2 and HCN4 subunit isoforms are able to self-assemble and co-assemble with equal preference in CHO cells (**Figure 2**).

5. REFERENCES

1. Isacoff, E.Y., Jan, Y.N., Jan, L.Y. (1990) Evidence for the formation of heteromultimeric potassium channels in xenopus oocytes. *Nature.* **345**, 530--534

2. MacKinnon, R. (1991). Determination of the subunit stoichiometry of a voltage-activated potassium channel. *Nature.* **350**, 232--235

3. Doyle, D.A., Morais Cabral, J., Pfuetzner, R.A., Kuo, A., Gulbis, J.M., Cohen, S.L., Chait, B.T., MacKinnon, R. (1998) The structure of the potassium channel: Molecular basis of K+ conduction and selectivity. *Science.* **280**, 69--77

4. Long, S.B., Campbell, E.B., Mackinnon, R. (2005) Crystal structure of a mammalian voltage-dependent shaker family K+ channel. *Science.* **309**, 897--903

5. Babila, T., Moscucci, A., Wang, H., Weaver, F.E., Koren, G. (1994) Assembly of mammalian voltage-gated potassium channels: Evidence for an important role of the first transmembrane segment. *Neuron.* **12**, 615--626

6. Zheng, J., Zagotta, W.N. (2004) Stoichiometry and assembly of olfactory cyclic nucleotide-gated channels. *Neuron.* **42**, 411--421

7. Jares-Erijman, E.A., Jovin, T.M. (2006) Imaging molecular interactions in living cells by FRET microscopy. *Curr. Opin. Chem. Biol.* **10**, 409--416

8. Wu, P., Brand, L. (1994) Resonance energy transfer: Methods and applications. *Anal. Biochem.* **218**, 1--13

9. Gales, C., Van Durm, J.J., Schaak, S., Pontier, S., Percherancier, Y., Audet, M., Paris, H., Bouvier, M. (2006) Probing the activation-promoted structural rearrangements in preassembled receptor-G protein complexes. *Nat. Struct. Mol. Biol.* **13**, 778--786

10. Goin, J.C., Nathanson, N.M. (2006) Quantitative analysis of muscarinic acetylcholine receptor homo- and heterodimerization in live cells: Regulation of receptor down-regulation by heterodimerization. *J. Biol. Chem.* **281**, 5416--5425

11. Whitaker, G.M., Angoli, D., Nazzari, H., Shigemoto, R., Accili, E.A. (2007) HCN2 and HCN4 isoforms self-assemble and co-assemble with equal preference to form functional pacemaker channels. *J. Biol. Chem.* **282**, 22900--22909

12. Lisenbee, C.S., Miller, L.J. (2006) Secretin receptor oligomers form intracellularly during maturation through receptor core domains. *Biochemistry.* **45**, 8216--8226

13. Lavoie, C., Mercier, J.F., Salahpour, A., Umapathy, D., Breit, A., Villeneuve, L.R., Zhu, W.Z., Xiao, R.P., Lakatta, E.G., Bouvier, M., Hebert, T.E. (2002) Beta 1/beta 2-adrenergic receptor heterodimerization regulates beta 2-adrenergic receptor internalization and ERK signaling efficacy. *J. Biol. Chem.* **277**, 35402--35410

14. Ludwig, A., Zong, X., Stieber, J., Hullin, R., Hofmann, F., Biel, M. (1999) Two pacemaker channels from human heart with profoundly different activation kinetics. *EMBO J.* **18**, 2323--2329

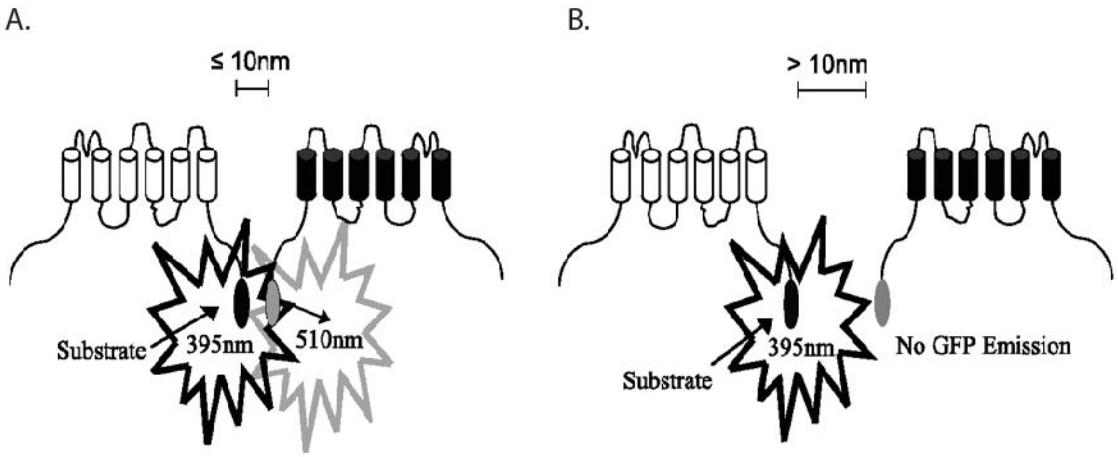

Figure 1 BRET measures protein interactions within less than 10nm apart.

A, Upon degradation of its substrate (DeepBlueC coelenterazine), Rluc emits light at 395nm.Emission at this wavelength will excite GFP if it is located within 10 nm of the Rluc protein. The GFP will then emit light at 510 nm. The intensity of GFP emission depends on the proximity of GFP to Rluc. B, If Rluc and GFP are greater than 10 nm from each other, the emission from Rluc will not excite GFP, and the calculated BRET ratio will be low. BRET ratios are calculated by dividing the recorded GFP emission (relative fluorescent units) by Rluc emission (relative luminescent units). (Reproduced from **ref. 11** with permission from the American Society for Biochemistry and Molecular Biology, Inc).

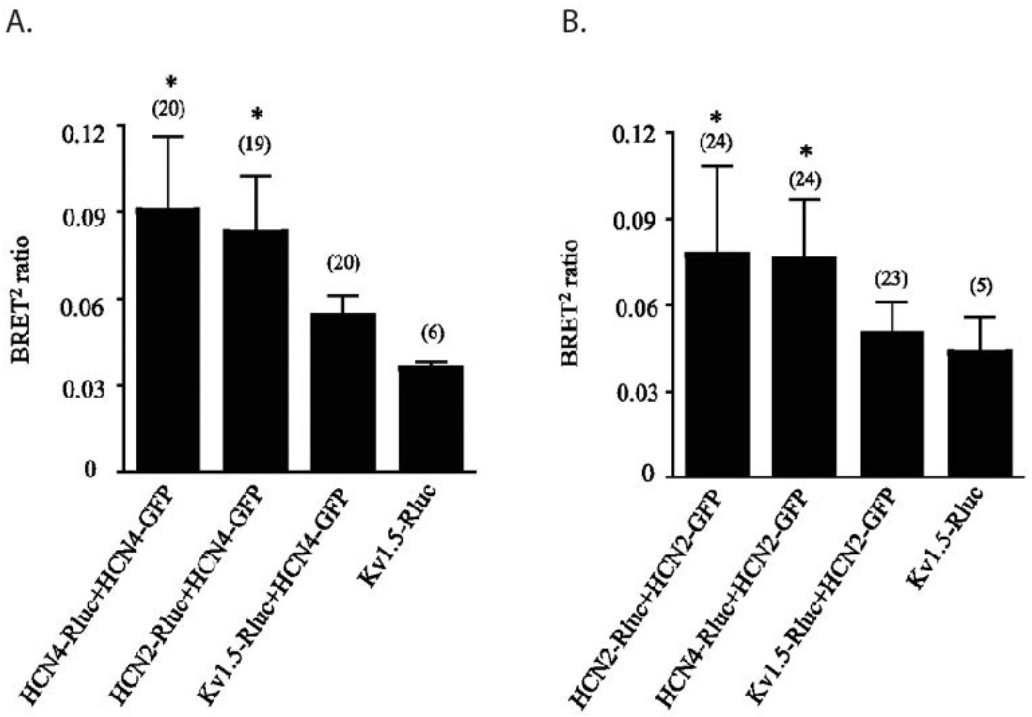

Figure 2 BRET ratios support similar levels of self-assembly and co-assembly of HCN2 and HCN4 isoforms in live CHO cells.

A,B. Bar graphs of BRET values determined from cells co-transfected with different channel construct combinations. Values represent means ± S.D. for each set of constructs, and (n) values depict number of cell populations used to determine mean values over 3-6 independent transfections. Experiments were performed in duplicate at four different Rluc/GFP cDNA ratios. Statistical comparisons carried out using a one-way analysis of variance followed by Bonferroni's multiple comparison post-test comparing all pairs. The asterisks indicate significant differences from the BRET ratios produced by co-transfection of Kv1.5-Rluc and HCN2-GFP or HCN4-GFP or Kv1.5-Rluc transfected alone. All combinations of HCN isoforms are significantly greater than negative controls ($p < 0.01$) but are not different from each other ($p > 0.05$). Kv1.5-Rluc + HCN2-GFP and Kv1.5-Rluc + HCN4-GFP BRET ratios are not significantly greater than the Kv1.5-RLuc background BRET ratio ($p > 0.05$). (Reproduced from **ref. 11** with permission from the American Society for Biochemistry and Molecular Biology, Inc).

APPENDIX C: BIOHAZARD APPROVAL CERTIFICATE

The University of British Columbia

Biohazard Approval Certificate

PROTOCOL NUMBER: **B09-0277**

INVESTIGATOR OR COURSE DIRECTOR: **Eric Accili**

DEPARTMENT: **Cellular & Physiological Sc.**

PROJECT OR COURSE TITLE: **Pacemaker Lab**

APPROVAL DATE: **February 18, 2010** START DATE: **November 18, 2009**

APPROVED CONTAINMENT LEVEL: **2**

FUNDING TITLE: **Molecular regulation of pacemaker channel function**
FUNDING AGENCY: **Heart and Stroke Foundation of British Columbia and Yukon**

FUNDING TITLE: **Comparative studies of pacemaker channels**
FUNDING AGENCY: **Natural Sciences and Engineering Research Council of Canada (NSERC)**

UNFUNDED TITLE: **N/A**

The Principal Investigator/Course Director is responsible for ensuring that all research or course work involving biological hazards is conducted in accordance with the University of British Columbia Policies and Procedures, Biosafety Practices and Public Health Agency of Canada guidelines.

This certificate is valid for one year from the above start or approval date (whichever is later) provided there are no changes. Annual review is required.

A copy of this certificate must be displayed in your facility.

Office of Research Services
102, 6190 Agronomy Road, Vancouver, V6T 1Z3
Phone: 604-827-5111 FAX: 604-822-5093